UNIVERSITY OF SOUTHAMPTON

FACULTY OF ENGINEERING AND THE ENVIRONMENT

Electro-Mechanical Group

Droplets Generation And Sampling On Demand With Peristaltic Pumping Systems

by

Yu Zhang

Thesis for Ph.D.

March 2016

UNIVERSITY OF SOUTHAMPTON

ABSTRACT

FACULTY OF ENGINEERING AND ENVIRONMENT

Thesis for Ph.D

DROPLETS GENERATION AND SAMPLING ON DEMAND WITH PERISTALTIC PUMPING SYSTEMS

YU ZHANG

In the last few decades, droplet microfluidics has been developed as a new area of microfluidics, where samples are compartmentalised in another immiscible phase. With these micro-droplets, Taylor dispersion can be minimised between samples and thorough mixing is easy and fast within the droplets themselves. Moreover, the sample consumptions are comparatively low as the samples are limited within nano-litre, pico-litre or even smaller droplets. Due to these attractive features, droplet microfluidics has been widely used as a platform to study various phenomena in chemistry, biology and physics. Droplets are normally generated in a T-junction or flow-focusing with syringe pumps or other pressure sources. An alternative way to generate droplets is to sequentially aspirate aqueous samples and carrier oil under negative pressures. Both of the typical T-junction methods and the current aspiration methods, have limitations in freely introducing/collecting samples into designed droplets, such as continuous sampling where introduction of samples does not affect the droplet generation, and *in-situ* sampling where samples from environment can be directly introduced into droplets. This '*sample in'* problem is still a challenge in droplet microfluidics.

This thesis addresses the two droplets sampling issues in droplet microfluidics: continuous droplet sampling, and *in-situ* droplet sampling. To solve the first issue, a novel microfluidic platform was engineered which includes aspiration droplet generators, a peristaltic pumping system and a feedback system which is used to synchronise droplet generation with pulsations of flowrates from the peristaltic pump. The demonstration of this platform successfully shows the capability of continuously generating and pumping droplets. To solve the second

issue, a micro peristaltic pump was engineered to realise a robust droplet generation method and a direct sample introduction from ‘out-world’ to chip. The results show that this device is capable of generating droplets *in-situ*.

Table of Contents

List of tables

List of figures

DECLARATION OF AUTHORSHIP

I, Yu Zhang, declare that this thesis and the work presented in it are my own and has been generated by me as the result of my own original research.

DROPLET GENERATION ON DEMAND WITH PERISTATLIC PUMPING SYSTEM

I confirm that:

1. This work was done wholly or mainly while in candidature for a research degree at this University;
2. Where any part of this thesis has previously been submitted for a degree or any other qualification at this University or any other institution, this has been clearly stated;
3. Where I have consulted the published work of others, this is always clearly attributed;
4. Where I have quoted from the work of others, the source is always given. With the exception of such quotations, this thesis is entirely my own work;
5. I have acknowledged all main sources of help;
6. Where the thesis is based on work done by myself jointly with others, I have made clear exactly what was done by others and what I have contributed myself;
7. The work in in chapter 3 and chapter 4 is being submitted as a journal paper to Biomicrofluidics: **Yu Zhang**, Martyn Hill, Xize Niu, Continuous droplet generation and pumping with a peristaltic pump.
8. The work in Chapter 5 in together with clinical test result will also be submitted as journal paper,

Signed:.....

Date:.....

Acknowledgements

Firstly, I would like to express my appreciation to my supervisors, Dr. Xize Niu and Professor. Martyn Hill for their support and guidance throughout this thesis. Thanks Dr. Xize Niu for providing me the studentship. His expertise in droplet microfluidics has extended my view and guided me to enjoy these fascinating Lilliputian droplets. I would also thank him for his patient supervision and useful suggestions during this researching process. Thanks Professor Martyn Hill for motivating and encouraging me during the up and downs in research. I have learnt a lot from him on how to think about research and how to do research.

I would like to show my appreciation to Dr. Peter Glynne-Jones for his suggestion on choosing the model of sensors and on other daily helps in the lab. I would also thank Dr. Adrian Nightingale for his suggestions on paper and thesis writing.

In Section 5.2 of Chapter 5, the first version of the peristaltic pump was jointly finished with MSc student Zhengkai Xu. The design of pump and the chips were jointly finished. The video recording and test was done by Zhengkai Xu. The experimental set-up and methodology of testing were designed, and data analysis performed by Yu Zhang. In section 5.4.6 of Chapter 5, the measurement of glucose was collected by MSc student Han Luo and analysed by Yu Zhang. Thanks for Zhengkai Xu and Han Luo.

I would also thank my colleagues Sammer-ul Hassan, Yan Zhao, Junjun Lei, Robert Zmijan, Dario Carugo and Adam Lewis for the knowledge and experience shared with me. Special thanks go to Sammer-ul Hassan for the preparation of the glucose assay.

Finally, I would like to express my love and thanks to my family and friends for their tremendous support over the years.

1. Introduction and motivations

1.1. Introduction

Microfluidics is the science and technology that studies fluids in channels with dimensions of a few micrometres to hundreds of micrometres [1]. It has shown many advantages and is being applied in many areas. In chemical analysis, microfluidic analysis has revolutionized traditional bulky chemical analysis with new techniques that can achieve high throughput analysis, consume much less sample and provide higher sensitivity, multiple functional analysis or called '*Lab-on-a-chip*'[1].

In the early stage, microfluidics mainly focused on studying continuous fluids with fundamental achievements on fluidic mixing, micro-valve and pump [2] and chemical biological applications such as Polymerase Chain Reaction (PCR), separation, cell analysis etc. However, continuous microfluidics has several limitations in fluidic transportation and manipulation. Taylor dispersion is significantly high in microfluidic channels, which can blur the chemical signals the fluids carry. Besides, the Reynolds number *Re* in continuous microfluidics is generally below 100, as a consequence mixing is extremely slow.

In recent years, droplet microfluidics has been studied as a new method of microfluidics, where aqueous samples are compartmentalised in an immiscible oil phase or vice versa. Using micro droplets, Taylor dispersion can be minimised between samples and thorough mixing is easy and fast. Moreover, the sample consumptions are comparably low as the samples are limited within nano-litre, pico-litre or even smaller droplets. There are less chances for sample loss or contamination on the channel walls. Due to these attractive features, droplet microfluidics has been widely used as a platform to study phenomena in chemistry, biology and interfacial physics.

1.2. Challenges in droplet microfluidics

A microfluidic system normally requires components such as: a method of introducing reagents and samples; and a method to handle the fluids in the chip [1]. In droplet microfluidics, reagents and samples are encapsulated into droplets with a process of droplet generation. These droplets normally are generated in chip with a T-junction or flow-focusing geometry with syringe pumps [3] as positive pressure. With external assistance, such as valves [4, 5] or electro-forces [6], on-demand control of these droplets can be realised. Because of easy designs and fabrication procedures of these geometries and good accessibilities of syringe pumps, these typical devices have dominated the research in droplet generation and pumping. An alternative method of droplet generation is to sequentially introduce oil and aqueous samples with negative pressure provided by a syringe pump or a vacuum pump [7-10].

Both of the typical in-chip generation methods and the current aspiration methods, have limitations in freely introducing/collecting samples into designed droplets, such as continuous sampling where introduction of samples does not affect the droplet generator status and *in-situ* sampling where samples from environment can be directly introduced into droplets [11]. This '*sample in*' problem is still a challenge in droplet microfluidics.

1.3. Objectives and aims

To solve this '*sample in*' problem in droplet microfluidics, new droplet sampling methods are developed in this thesis, with a novel and critical part of a peristaltic pumping system coupled with an appropriate droplet generation method. The targets of this thesis are to develop, to engineer, to demonstrate, and to study these droplet sampling methods, and to apply these methods in chemical screening as an example application.

The first aim of this thesis is to develop a continuous droplet sampling method. To achieve that, a novel hybrid platform was proposed, engineered, and studied which integrates a peristaltic pump with aspiration droplet generators, as shown in Figure 1.1. This hybrid platform was further expanded to drive multiple parallel channel flows, to achieve parallel synchronisation of droplets, which is extremely important in merging of droplets and performing assays with droplets.

The second aim of this thesis is to develop an *in-situ* droplet sampling method. To realise this, a robust droplet generation method is proposed. A micro peristaltic pump is to engineered and to be developed which is capable of alternatively introduce the dispersed phases and oil phase into a T-junction based on the flowrate pulsations, as shown in Figure 1.2.

1.4. Thesis structure and contributions

The thesis is structured into one literature review chapter, three research chapters and one conclusion chapter, with contributions listed in the research chapters, briefly:

- In Chapter 2, the state-of-the-art of droplet microfluidics research is reviewed, especially droplet generation methods, operations of droplets and dynamics of droplet microfluidics. The fundamentals of droplets and related interfacial science are briefly reviewed. The engineering of peristaltic pumps is also reviewed.
- In Chapter 3, a novel continuous droplet sampling platform is proposed, engineered, demonstrated and studied. This platform interfaces a peristaltic pumping system and an aspiration droplet generator via a feedback control system to achieve in-phase generation of droplets with flow rate pulsation from the peristaltic pump. Detailed engineering and calibration demonstrate that this platform is able to continuously generate and deliver droplets.
- Chapter 4 expands the continuous sampling platform to drive multiple channel flows and study parallel synchronisation of droplets. With the new platform, the synchronisation of droplet was achieved at different fluidic conditions for various flow rates and droplet sizes. With this synchronisation method, droplet merging can be easily achieved. The integrated platform is applied for a glucose assay as an example application for chemical screening and it can be further applied to multiple-stage reaction. Besides, the stable introduction of air bubble is demonstrated, which is useful to regulate the merging of droplets.
- In Chapter 5, an in-situ droplet sampling method is developed and studied. A screw-driven micro-peristaltic pump and related microfluidics were

engineered. The novelty of this sampling method lies in the robust droplet generation and intrinsic introduction of samples. This micro-pumping device can easily regulate the generation of droplets and realise intermittent droplet generation. With this device, calibration of concentration of glucose was also implemented and synchronisation of droplets was demonstrated.

- Chapter 6 concludes the work.

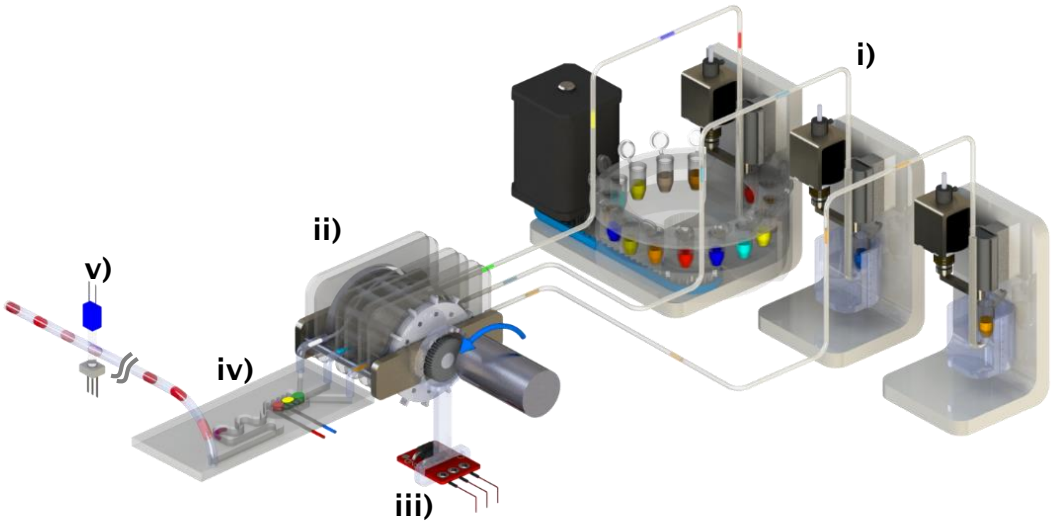

Figure 1.1 Overview of multiple parallel channels integrated platform. It contains a carousel aspiration generator that is capable of housing 15 different aqueous samples and two linear aspiration droplet generators each of which houses one independent aqueous sample i), a modified peristaltic pumping system in which 12 micro-fabricated pillars are mounted and the cassette was fabricated to be transparent ii), with feedback system iii), a PMMA pillar-induced merging chamber with electrodes iv), a droplet detection flow cell consisted by a pair of LED and photodiode v).

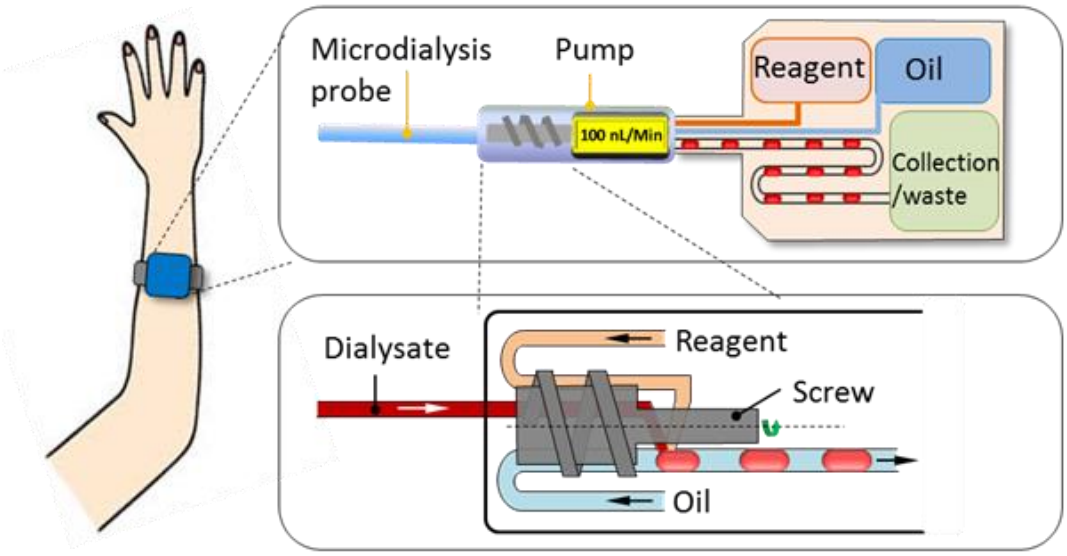

Figure 1.2 Overview of the miniaturised peristatlic pump. The flow rate of oil phase and that of aqueous phase are in anti-phase poistion.

Reference List

1. Whitesides, G.M., *The origins and the future of microfluidics.* Nature, 2006. **442**(7101): p. 368-373.

2. Unger, M.A., et al., *Monolithic microfabricated valves and pumps by multilayer soft lithography.* Science, 2000. **288**(5463): p. 113-116.

3. Thorsen, T., et al., *Dynamic pattern formation in a vesicle-generating microfluidic device.* Physical Review Letters, 2001. **86**(18): p. 4163-4166.

4. Churski, K., J. Michalski, and P. Garstecki, *Droplet on demand system utilizing a computer controlled microvalve integrated into a stiff polymeric microfluidic device.* Lab on a Chip, 2010. **10**(4): p. 512-518.

5. Zeng, S.J., et al., *Microvalve-actuated precise control of individual droplets in microfluidic devices.* Lab on a Chip, 2009. **9**(10): p. 1340-1343.

6. Tan, S.H., B. Semin, and J.C. Baret, *Microfluidic flow-focusing in ac electric fields.* Lab on a Chip, 2014. **14**(6): p. 1099-1106.

7. Chabert, M., et al., *Automated microdroplet platform for sample manipulation and polymerase chain reaction.* Analytical Chemistry, 2006. **78**(22): p. 7722-7728.

8. Du, W.B., et al., *Automated Microfluidic Screening Assay Platform Based on Drop Lab.* Analytical Chemistry, 2010. **82**(23): p. 9941-9947.

9. Gielen, F., et al., *A Fully Unsupervised Compartment-on-Demand Platform for Precise Nanoliter Assays of Time-Dependent Steady-State Enzyme Kinetics and Inhibition.* Analytical Chemistry, 2013. **85**(9): p. 4761-4769.

10. Wu, J.B., et al., *Multiple and High-Throughput Droplet Reactions via Combination of Microsampling Technique and Microfluidic Chip.* Analytical Chemistry, 2012. **84**(22): p. 9689-9693.

11. Slaney, T.R., et al., *Push-Pull Perfusion Sampling with Segmented Flow for High Temporal and Spatial Resolution in Vivo Chemical Monitoring.* Analytical Chemistry, 2011. **83**(13): p. 5207-5213.

2. Literature review

This chapter reviews fundamental of micro droplets and the related interfacial science, the state of the art of engineering droplet microfluidics, particularly those associated with droplet sampling and droplet generation according to the research motivations, and peristaltic pumping method.

2.1. Fundamentals of micro droplets and related interfacial science

Interfacial science lays the scientific background for the understanding and designing of droplet microfluidic. In water-oil boundary, this interface [1] can be treated as zero thickness for simplification. Surface tension, γ is the measurement of surface energy loss, whose unit is J/m^2 or N/m.

$$\boldsymbol{\gamma \approx \frac{U}{2\delta^2}} \qquad \textbf{Equation 2.1}$$

Where U is the total cohesive energy per molecule, and δ is the characteristic molecular dimension. Surface tension increases as the intermolecular attraction increases and the molecular size decreases. Surface tension of oil-gas is normally from 20~30 mN/m and that of pure water-gas is around 70 mN/m. Surface tension can be modified by temperature (T), as shown in Equation 2.2, with the measured reference value (γ_o, T_o), and critical temperature constant β,

$$\boldsymbol{\gamma \approx \gamma_o(1 + \beta(T - T_o))} \qquad \textbf{Equation 2.2}$$

When an interface is curved, there is a pressure difference between regions inside and outside the interface, which is defined as Laplace pressure or pressure jump. This can be calculated by Laplace's law (Equation 2.3), the product of the surface tension and the local curvature, κ.

$$\boldsymbol{\Delta P_L = \gamma \cdot \kappa} \qquad \textbf{Equation 2.3}$$

Generally, the curvature is evaluated by the principle curvatures (maximum $1/R_1$ and minimum $1/R_2$, where R is radius), as expressed in Equation 2.4. Noticeably, a curvature has a direction which is expressed by negative or positive. The

analysis of Laplace pressure is important in droplet microfluidics. For example, Baroud et al [2] utilised a special geometry to increase the curvature that apressure can be induced which can help to generate droplets.

$$\kappa = \frac{1}{2}\left(\frac{1}{R1} + \frac{1}{R2}\right) \qquad \textbf{Equation 2.4}$$

When a drop of water spreads on a plate, if the contact angle with the plate is less than 90°, the contact is said to be hydrophilic. If it is bigger than 90°, the contact is said to be hydrophobic. The surface tensions of the solid-gas, solid-liquid and liquid-gas interfaces, follow a relationship described by the Young's Law.

$$\boldsymbol{\theta = arccos\frac{\gamma_{SG}-\gamma_{SL}}{\gamma_{LG}}} \qquad \textbf{Equation 2.5}$$

Where θ is contact angle, $\gamma_{SG}, \gamma_{SL}, r_{LG}$ are the surface tensions of solid-gas, solid-liquid and liquid gas interfaces respectively.

For a droplet or interface confined in a capillary, the force related to surface tension is called capillary force. Capillary force can rise a certain height of liquid in a tube, *h*, if the liquid can wet the surface of the tube. The relationship is described by Jurin's law [1],

$$\boldsymbol{h = \frac{2\gamma - cos\theta}{\rho g r}} \qquad \textbf{Equation 2.6}$$

where $\rho, g\ and\ r$ is the density of liquids, gravitational acceleration and radius of the tube respectively. Capillary forces are important in microscopic scales where r is small. For example, capillary pump exploits capillary force to deliver liquids in microfluidics [3], and this is widely used in lateral flow devices [4] such as pregnancy test stripe.

Surfactants also play an important role in droplet microfluidics. Surfactant is a term short for *surface active agent* [5], and is normally added to stabilise water-oil interface, and to prevent coalescence of the droplets or sticking of droplets to the solid walls. Surfactants used in droplet microfluidics are formed of amphiphilic molecules with an amphiphilic head to water, and hydrophilic tail to attract oil as sketched in Figure 2.1.

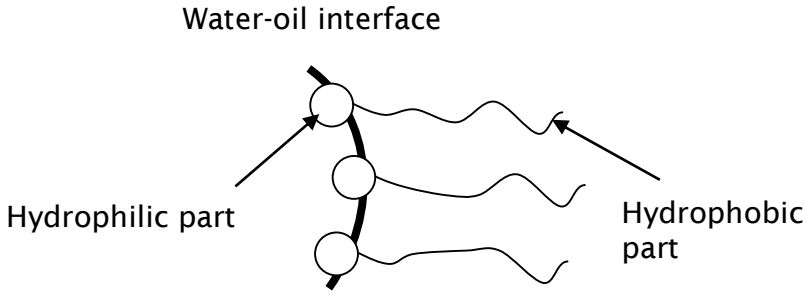

Figure 2.1 Schematic of amphiphilic molecules of surfactant. The molecule has one hydrophilic head and one hydrophobic tail. The head is attached to water and tail is attached to oil part.

The presence of surfactant at the interface can change its surface tension. The relationship is described by Gibbs adsorption isotherm [6]

$$\Gamma = -\frac{C}{R_c T_c} \cdot \frac{d\gamma}{dC} \qquad \textbf{Equation 2.7}$$

where Γ is surface concentration of the interface, c, R_c and T_c are the surfactant bulk concentration, gas constant and temperature constant.

Baret et al [6] have made a thorough review on the current development of surfactant in droplet microfluidics.

2.2. Droplet microfluidics

This section reviews state of the art in generation/sampling of droplets, the essential operations of droplets in microfluidic devices and dynamics of droplets transportation.

2.2.1. Introduction of droplet microfluidics

In continuous microfluidics (or single phase flow), Taylor dispersion often occurs [7]. In the channel, a parabolic profile velocity is established from the side to centre of fluid, which means velocity close to the channel wall is nearly zero and velocity in centre is the highest. This generates a residence-time distribution which will cause broadening of the sample and smearing of the signals in the channels. Besides of Taylor dispersion, cross-contamination tends to occur in continuous microfluidics due to reagent absorption onto the microfluidic channel walls. Conversly, in droplet microfluidics, reagents are confined in droplets with size ranging from pico-litre to nano-litre. Because there are oil lubricant films to separate the aqueous droplets from touching the wall of channels, the aforementioned cross-contamination can be significantly eliminated. Figure 2.2 describes the difference between the continuous microfluidics and the droplet microfluidics [8].

Micro-droplets are highly monodispersed with standard deviation within 1% [9]. As a consequence, quantitative measurements are achievable in experiments. Microfluidic droplets are typically generated in femtoliter to nanoliter (10^{-15} L to 10^{-9} L), therefore only small amount of reagents is consumed, and thus the cost of micro-droplet assay can be much more economic, in comparison, in the other microfluidics formats. In most microfluidic labs, the droplet formation frequencies can be in the range of 0.1 to 2 KHz [10] with passive droplet generation, and thus controllable speed of experiment can be achieved.

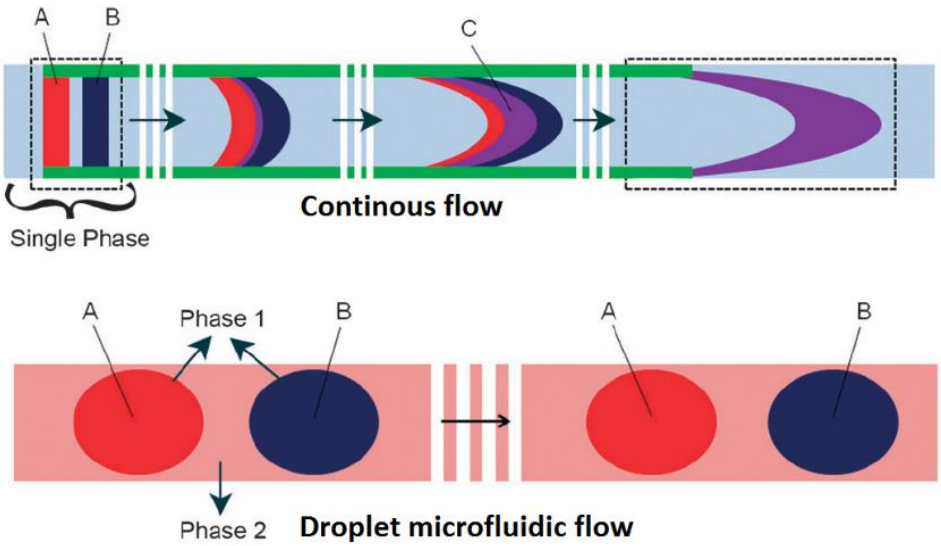

Figure 2.2. Comparison between continuous and droplet microfluidics. (A) Fluid A and Fluid B is dispersed in the channel to form c due to Taylor dispersion. (B) In droplet microfluidics, the aqueous samples are compartmentalized into droplets which creates an interface to avoid Taylor dispersion. *Copyright ©2011 Chem.Commun.*

2.2.2. Generation of droplets in microfluidic devices

Droplet generations can be categorised into two kinds: passive ones and active ones. In passive methods, the droplets are typically formed by a surface induced instability with different geometries depending on the required droplet frequency. The typical geometries used are, T-junction geometry, co-flowing geometry, flow-focusing geometry, and step geometry. The size of droplets relies on the dimension of the device geometries, flow rates and fluid physics. Active generation methods are those applied external components such as valves, electrical fields or to control the generation of droplets. Such active methods are normally applied to realise on-demand generation, at which sizes, frequencies or even fluidic contents can be controlled. Depending on the fluids pumping method, droplet generation methods can also be categorised into positive pressure ones, and negative pressure generation ones.

2.2.2.1. Generation of droplets with typical geometries

2.2.2.1.1. T-junction

A T-junction geometry was firstly applied to generate mono-dispersed droplets [11]. Due to the simple geometry and simple fabrication method, this geometry has been thoroughly demonstrated, and studied and understood. A typical T-junction geometry (Figure 2.3) has two channels, one main channel containing continuous phase and one side channel containing dispersed phase, which are perpendicularly intersected with each other. The two phases form an interface at the T-junction as the flow continues which is typically powered by a syringe pump. In the early stage [11], it was understood that shear force is the dominant reason for the break-up of droplets in T-junction. With further modelling [12] , simulations [13] and experiments [14-17], it was found three regimes distinguished by Ca=$\gamma u_c/\mu_c$, dripping regimes, squeezing regime, and jetting regimes.

In squeezing regime (Ca < 0.002), the break-up of droplets is arisen from hydraulic pressure due to the block of tip in the main channel. There are two stages defined. In the first stage, the tip attempts to block the channel while the shear force is not strong enough to shear it off. During this stage, the growth of the tip is ~w, which is approximated by the width of the main channel. At the end of this stage, there formed a neck with characteristic length, d, as defined in Figure 2.3 (A). In the second stage, the tip is squeezed by the arising hydraulic pressure. The squeezing rate is approximated with speed of carrier phase (u_c). During this stage, the growth of tip is product of the growing rate and its time, $u_d \times (d/u_c)$. With the analysis of squeezing regime, Garstecki *et al* [12] estimates the length of droplet with a scaling law as shown in Equation 2.8. This scaling law is further agreed with numerical models [13] and other experimental works [14-16, 18].

$$\frac{L}{W} = 1 + \alpha \frac{Q_d}{Q_c} \qquad \textbf{Equation 2.8}$$

Where L is the length of droplets in the main channel, α is the geometry constant.

In dripping regime (0.01< Ca <0.03), the aqueous tip normally could not block the main channel before it is sheared off, during which the shear force is dominating against the interfacial force. The size of droplets in spherical format can be scaled as $r \sim 1/Ca$, where r is the diameter of the spherical droplet [11, 14, 19]. In dripping regime, size of droplets is almost independent of flowrate of dispersed phase.

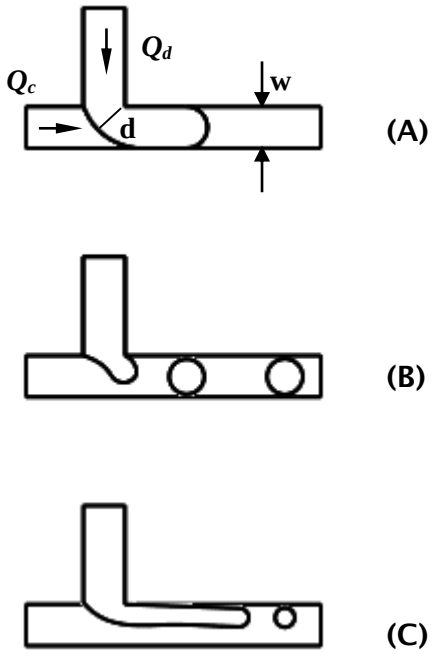

Figure 2.3 schematic of generation of droplets in three different regime. (A) Squeezing regime. d is the characteristic length, w is width of the main channel (B) dripping regime (C) jetting regime.

2.2.2.1.2. Co-flowing

In co-flowing geometry, dispersed phase is introduced into carrier phase via a dual tube and the dispersed phase eventually decays into droplets caused by Rayleigh-Plateau instability, as schematised in Figure 2.4. Generating droplets with co-flowing geometry in microfluidics was firstly applied by Cramer *et al* [20]. During the demonstration, two distinct regimes can be found: dripping regime and jetting regime, which depends on the critical flowrate of carrier phase, Q_c, .This flow rate could also be affected by viscosity ratio and surface tension.

Further observation [21] summarises that the transition from dripping to jetting regime is determined by *Ca*. This conclusion is further agreed with other analysis [22-24].

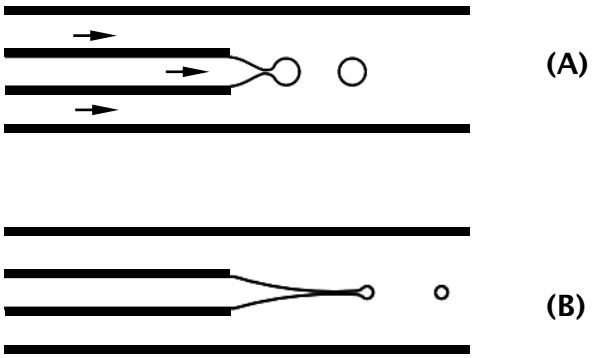

Figure 2.4 Schematic of generation of droplets in co-flowing geometries. (A) Dripping regime. (B) Jetting regime.

2.2.2.1.3. Flow-focusing and modified geometries

Flow-focusing is another effective and simple geometry to generate droplets where the dispersed phases are pushed by counter-stream flows of continuous phases shown in Figure 2.5. This geometry was firstly introduced into microfluidics by Anna *et al* [25]. It applies the geometry to create the taming saddle point where break-up starts [25-29]. As it was reviewed [30], 4 main regimes can be found: squeezing, dripping, jetting and thread formation. Due to the complex variations in the geometry, there is no scaling law to directly predict the size of droplets. However, in squeezing regime, it was reported by Funfschilling et al [29], that once the advancing finger blocks the orifice, hydraulic pressure difference is arisen to squeeze the fingers which is similar to the process in squeezing stage in T-junction. It was further reported by Lee et al [31], in squeezing/dripping regime, generation of droplets merely relies on

geometry and flow fields in upstream of flow-focusing rather than on those in downstream.

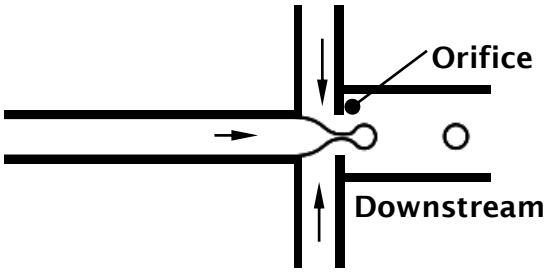

Figure 2.5 Generation of droplets in flow-focusing geometry.

In general, the design and fabrication processes in co-flowing and flow-focusing is more complicated than those in T-junction. However, as reviewed in [32], co-flowing and flow-focusing offers wider ranges of flexibility in varying sizes of droplets. These three typical geometries can be easily modified to generate droplets with different purpose. For example, in [33], Shui *et al* investigated the generation in a head-on microfluidic device operated with two identical channels as shown in Figure 2.6 (A). The break-up of droplets is due to the global capillary instability. It was found that at low Ca (10^{-5} or less), the sizes of droplets equal to the volume of constriction channel. In squeezing regime, as demonstrated by Shui et al [34] the generation of droplets follow the processes of that in a typical T-junction. The geometry can also be modified to realise step-emulsification [35], as shown in Figure 2.6 (B). It was found that the growth of droplets in the step geometry leads the thinning of the neck. This geometry was further modified and explained by Dangla et al [2]. By introducing a non-parallel bottom and top walls, a gradient is created to increase the curvature to assist the generation. This device is able to generate droplets with uniform sizes even though surface tension is different. Besides, Steijn et al [36] engineered a geometry to fix volumes of droplets as shown in Figure 2.6 (C). Once the aqueous tip blocks the

port of main channel, break-up occurs. Thus, the volume of droplets always equals to that of the chamber.

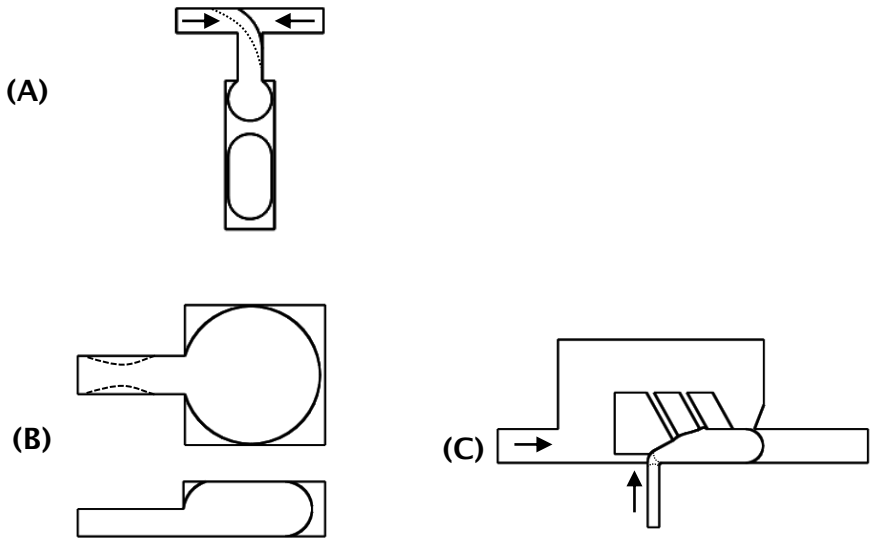

Figure 2.6 Schematic of modified geometries. (A) Head-on generation in T-junction. (B) Step emulsification geometry (C) Block-and-break geometry. Dimension is not in scale. *Reprint © 2013 Biomicrofluidics*.

2.2.2.1.4. On-demand generation of droplets in geometries

To realise controllable or on-demand generation of droplets in the typical geometries, there are four methods summarised in this section: regulating flowrates of carrier phase and (or) dispersed phase, controlling geometry, controlling physics properties of fluids, and employ external force.

Regulation of flowrates is normally realised by valve-based system with pressure sources or a programmed displacement pump. The valves can be pneumatic valves and mechanical valves. Branksy et al [37] used a piezoelectric actuator as valves to control generation of droplets in a T-junction. During this demonstration, it was found pressure source which is realised by positioning fluids to a certain height, can provide better generation of droplets on sizes over a positive syringe pump. Zeng et al [38] firstly demonstrated pneumatic valves with T-junction platform and negative pressure to realise on-demand generation of droplets. Correlation between calculation and experiment was found excellent. Flexibility is appreciated in this demonstration. Churski et al [39, 40] has demonstrated and studied the generation of droplets with solenoid valve pumped by positive pressure sources and a typical T-junction as shown in Figure 2.7 (A). With this method, an arbitrary of combinations of frequencies, sizes and

distances can be achieved. The reproducibly is found excellent. The valve was further developed with engineering a solenoid plunger system [41]. Besides, Lorenz et al [42] has programmed the flowrate of oil phase to pull and push the droplets. Thus, simultaneous formation of droplets can be realised with applying a step geometry.

Instead of regulating flowrates, controllable generation of droplets can also be realised by adjusting the geometry of T-junction or flow-focusing. Abate et al [43] utilised membrane valve to control the geometries of flow-focusing in PDMS chips, as shown in Figure 2.7 (B). In this demonstration, two versions of valves have been designed. The first version is designed to control the orifice so that the size of droplets can be adjusted. The second version was designed to control the width of channel for aqueous phase so that the generation frequency can be controlled. It was reported that real-time control on sizes of droplets and generation frequency can be realised. Lee et al [44] and Hsiung et al [45] has demonstrated a similar function with moving wall in T-junction by. Lee et al [44] also further demonstrated generation of double emulsions in the same device.

In non-squeezing regimes of generation in T-junction, generation of droplets is significantly related with surface tension. Varying surface tension or viscosity in T-junction or flow-focusing can be used to control generation of droplets. Nguyen et al [46] reported a low temperature heater (25~70 °C) to both vary surface tension and viscosity in dripping regime generation with a flow-focusing geometry. It was found that the change on viscosity is faster than that on surface tension. This difference induces a change on the volume of droplets: increasing temperature can increase the volume of droplets. Due to low temperature applied in the heater, this device can be used widely in biological fields. This method has been further studied by Murshed et al [47] and Stan et al [48] and similar phenomenon was observed. Slightly different from this approach, a laser heater was applied by Baroud *et al* [49, 50]. Due to the rapid temperature change, Marangoni flows are produced to block aqueous phases. With this laser heater, controllable generation and sorting can be realised.

Besides the aforementioned methods, external forces can also be applied to assist the break-up of droplets, such as electro-forces [51] and acoustic forces [52, 53], as shown in Figure 2.7(D).

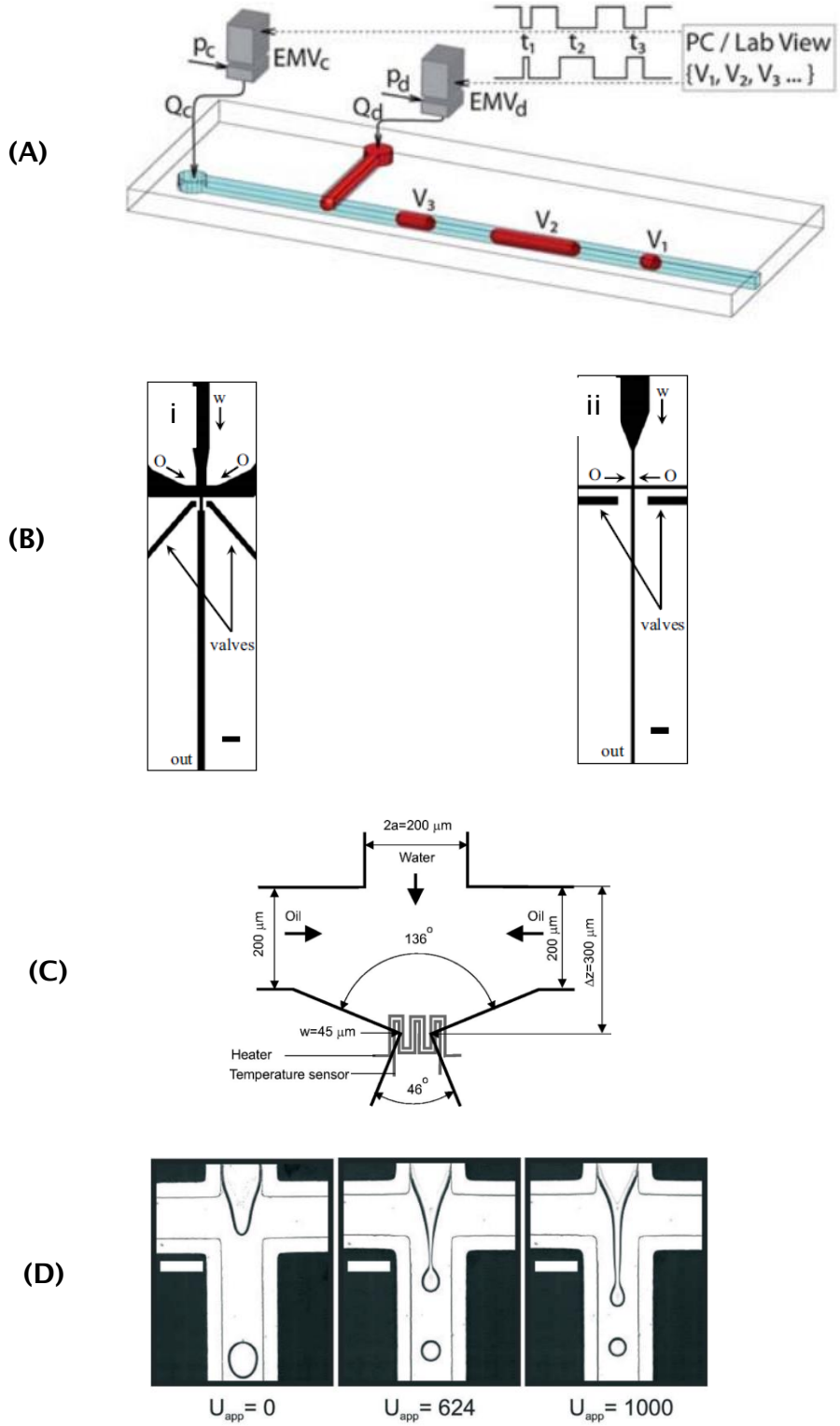

Figure 2.7 Schematics of devices that can realize on-demand generation based on the passive generation method. (A)Droplet-on-demand realized by controlling valve. *Copyright © 2010 Lab on a Chip*. (B) Controlling sizes of droplets by adjusting the geometry. *Copyright © 2008. JOURNAL OF MICROELECTROMECHANICAL SYSTEMS* (C) controlling the temperature to vary surface tension and viscosity. *Copyright © 2007 Applied physics letter*. (D) Controlling sizes of droplets by adjusting the electrical field. *Copyright © 2014 Lab on a Chip*.

2.2.2.2. Generation of droplets with aspiration technique

This part reviews the droplet generation method in aspiration format. This format of generation of droplets allows the system to directly arrange samples in open environment. In the early stage, to realise a simple and fast liquid delivery method, Linder et al [54] has developed a cartridge to aspirate reagent with air-bubble as spacers, as shown in Figure 2.8 (A). This fluid delivery is simple and eliminates the requirements of syringe pumps or vacuum sources, especially in the absence of electricity and computers. By adding three washing buffers and surface treatment, cross-contamination can be minimised. This system can also be interfaced with vacuum sources controlled by valves to present isolated parallel manners, as shown in Figure 2.8 (B). To avoid any cross contamination in the system, Chen et al [55] has used carrier oil as spacer by coating surface hydrophobic. The demonstration has successfully shown its purpose.

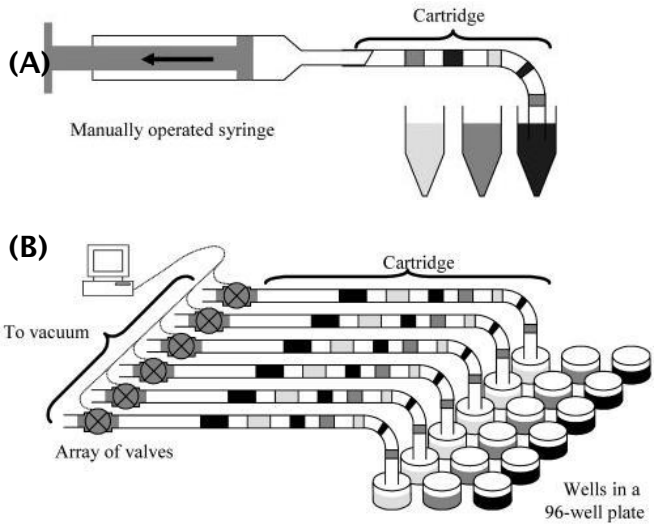

Figure 2.8 Delivery of fluids with negative pressure and a cartridge. (A) A manually operated format. (B) Vacuum source operated format. Cross-contamination can be effectively avoided by adding three washing buffers and surface treatment. *Copyright © Anal. Chem. 2005*.

This cartridge fluid delivery method was further adopted and applied to generate controllable droplets. This technique is termed as aspiration droplet generation in this review. Chabert et al [56] firstly modified the cartridge fluid delivery method to generate droplets. Their platform uses pull-push architecture of fluids delivering method to sequentially aspirate oil and aqueous phase, as shown in

in (A) of Figure 2.9 (i). With programmed protocols, the volume fractions between oil and aqueous phase can be well defined. The designed architecture includes two syringe pumps, two valves and two buffer channels in parallel. When pump 1 is working at negative status to aspirate fluids from well plate, pump 2 is working at positive status to push the preformed droplets in buffer channel 2 to downstream. The two working systems are sequentially insulated by the two valves and thus pressure cross-talking in the two channels can be avoided. During this process, the oil and aqueous samples are stored in a prepared microliter plate with three layers: aqueous layer, carrier oil layer and cleaning solutions. This platform was successfully applied in reagent mixing and performing polymerase chain reaction (PCR). Du et al [57, 58] applied a tapered capillary to sequentially aspirate aqueous fluids or oil fluids which are stored in independent containers (Figure 2.9 (ii). With a liquid presenting platform, the liquids can be aspirated by a syringe pump with picoliter precision. In this device, droplets can be mixed during the generation process without an external droplet merging module. Du's device accentuates liquid handling method and individual droplet generation. Du's device has been further used to demonstrate single cell analysis [58]. However, cross-contamination may be a challenge in this device. Zhu et al [59] further covered an oil layer to eliminate the concerns of cross-contamination. With precise control of liquid handling, generation of droplets, sampling droplets, mixing droplets, depositing droplets and merging droplets can be realised whose functions are similar to EWOD. Wu et al [60] automated the process of generating droplets in the aspirating platform with applying a motor to sequentially aspirate the oil and aqueous phase stored in a well-plate. The aqueous phase is covered by oil phase in a well plate. The aspiration of fluids is realised by a vacuum source. Gielen et al [61] further simplified this aspiration droplet generation technique, and provided a more convenient and direct method to load samples with aqueous phase sitting on the top of oil, as shown in Figure 2.9 (ii-(B)). A carousel liquid presenting system and a solenoid actuation system were engineered. Different from Wu's device, Gielen utilised negative syringe pump and this may increase the precision of generation over these with vacuum source. These aspirating platforms have a generic capability in common: sequentially introduce fluids with negative pressure. Similarly, Zeng's valve based platform [38] at which oil fluids and aqueous fluids are sequentially aspirated with vacuum source, can present the same functions.

(i)

(ii)

(iii)

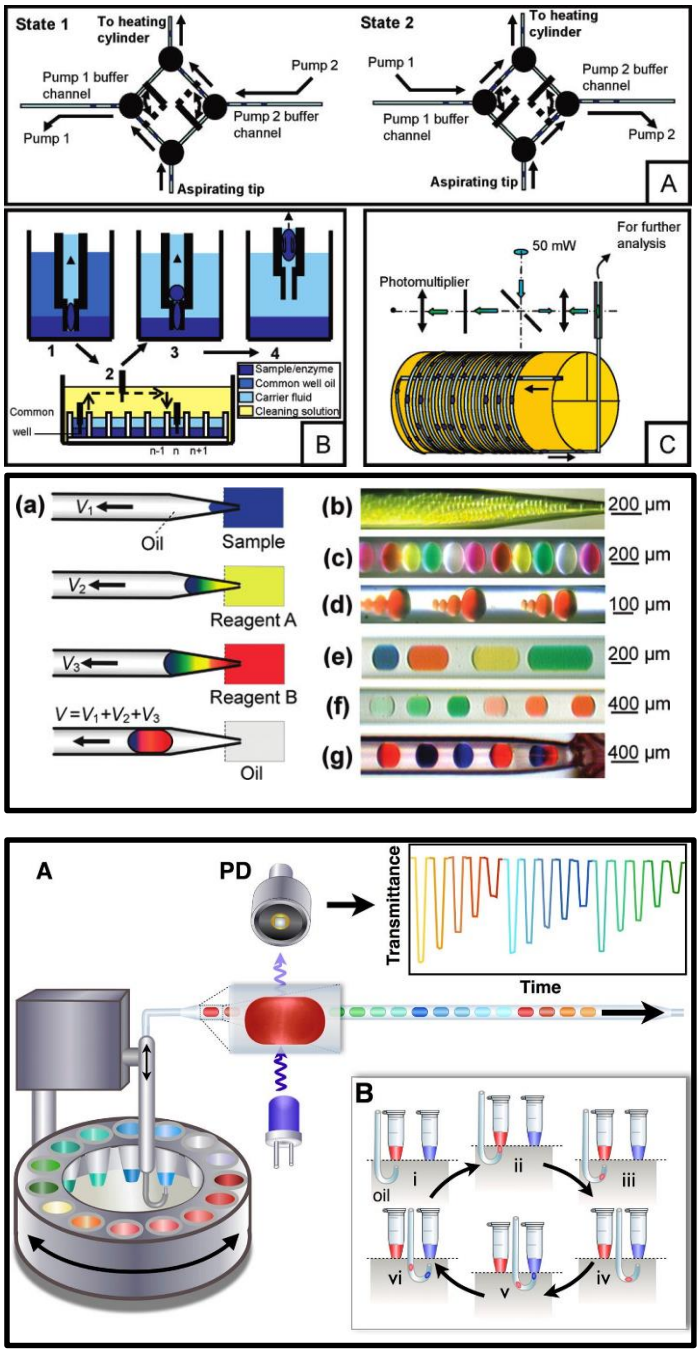

Figure 2.9 (i) Combination of sequential injection with continuous flow using a two state loop with two syringe pumps each connected to a three-way pinch valve. State 1: pump 1 sequentially forms samples from the aspirating tip while pump 2 pushes the droplets formed in state 2 of the last cycle to the heating cylinder. State 2: pump 1 pushes the droplets formed from state 1, while pump 2 forms a new train of droplets. *Copyright © 2006 Anal. Chem.* (ii) Droplab. (a) Principles for assembling a 3-component droplet. (b-g) examples of generating droplets. *Copyright © 2010 Anal.Chem.* (iii). Samples are sitting on the top of oil inside of enpendorf tube with bottom cut. The tip is sequentially aspirating oil and aqueous samples. *Copyright © 2013 Anal. Chem.*

Different from the aforementioned platforms, Rane et al [62] utilised positive pressure to press the fluids, as shown in Figure 2.10. The pressing is realised by a special designed adaptor which is used to seal liquid container when the positive pressure is working. With the positive pressure, aqueous samples and carrier phase are sequentially introduced. It is feasible to free then end of the downstream system to enable further operations such as collecting sample droplets. It was found the system can provide a precise on control on sizes of droplets. However, Rane's platform disables the direct sampling loading chances as the capillary adapter covers sample containers especially when the system is at working status.

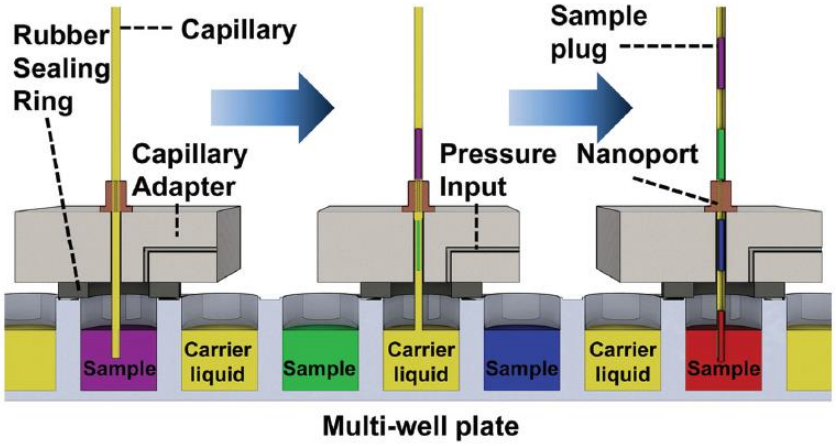

Figure 2.10 Generation of droplets with positive pressure and a sequence control. The capillary is sequentially moved to wells to deliver either samples or fluids. *Copyright © by Society for Laboratory Automation and Screening*

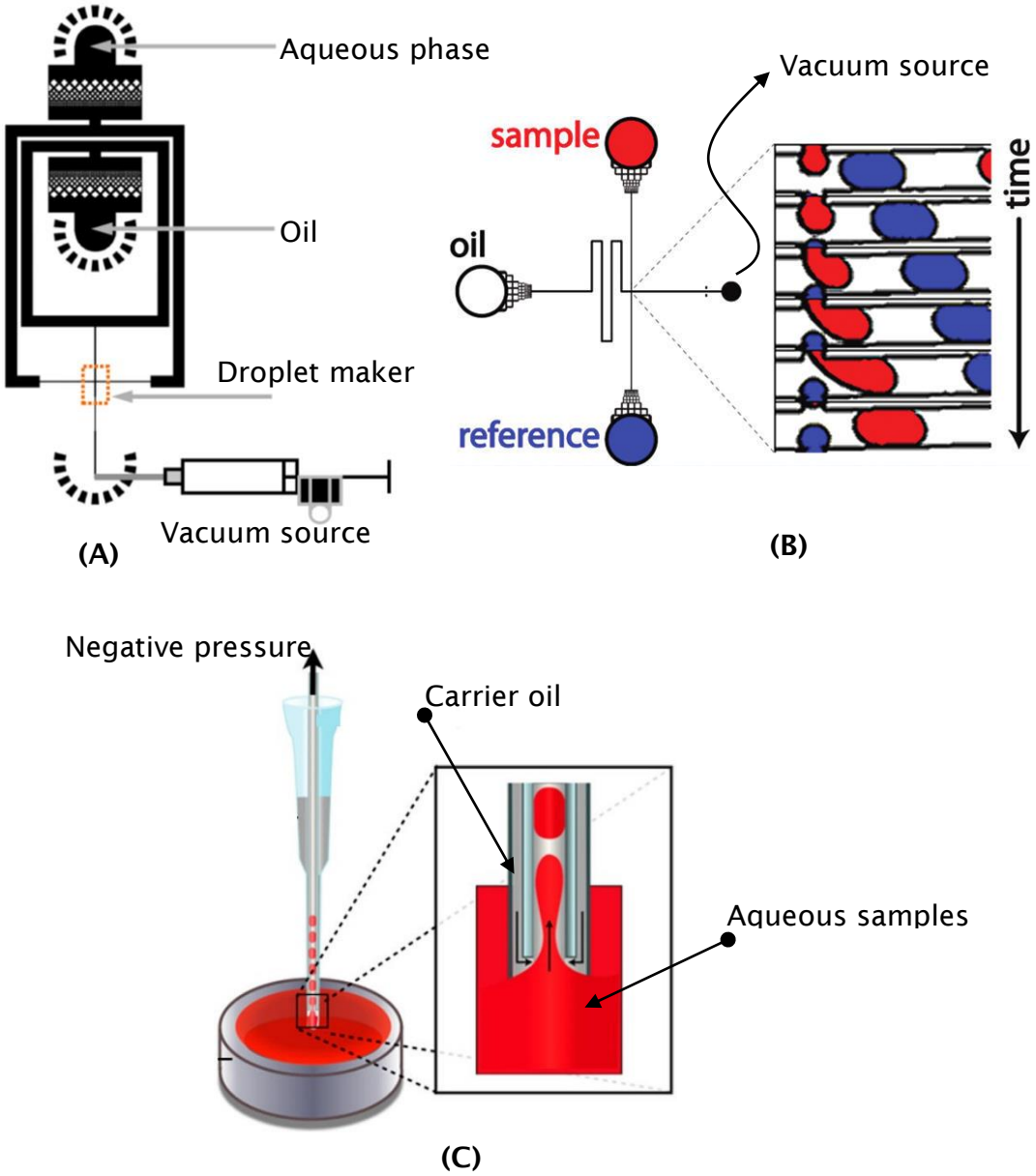

Figure 2.11 Directly aspirating samples into a droplet generator with no sequence control on volume fractions between that of samples and oil. (A) Syringe-vacuum microfluidics. *Copyright © 2011 Biomicrofluidics.* (B) Self-regulated and droplet-based sample chopper. *Copyright © 2012 Anal. Chem.* (C) A sampler aspirated by negative pressure. *Copyright © 2015 Anal. Chem.*

Akin to these sequential introduction of fluids platforms with negative pressure, the droplet generator can also be replaced and simplified by utilising a geometry based generator. Abate et al [63] utilised a manual vacuum pump to aspirate fluids from a flow-focusing, as shown in Figure 2.11 (A). Relying on the resistance distribution between the two channels, droplets with a certain volume fractions between oil and aqueous phase, are generated. The size of droplets can be varied by changing the resistance in oil phase channel and aqueous phase channel. The whole device is simple, portable and low-cost. Two parallel aspirations of droplets has been demonstrated with a single aqueous contents. Similar function has been realised by Easley *et al* [64] and Godwin *et al* [65]. Based on these designs, Deal *et al* [66] has further introduced an opposite T-junctions as shown in Figure 2.11 (B). The droplets from the reference channel are working as a chopper to regulate the generation in sample channel. Therefore, an automatic manner is presented. Gielen *et al* [67] adopted this technique by applying a duo tube one of which for aqueous phase and the other one for oil, as shown in Figure 2.11 (C). This geometry can be regarded as a modified flow-focusing. To vary sizes of droplets, the impressing depth can be changed. These devices eliminate the requirement of registering samples in well plates or special containers and makes the sampling more direct. Besides, the generators are usually simple geometry chips which are portable. However, as the volume fractions between oil and aqueous phase rely on the resistance distributions, generation of droplets is difficult to be on-demand manner, particular in real environment where the aqueous contents can be various. Introductions of multiple contents may be challenge. To help reduce the reliability on resistance, Stanley *et al* [68] utilised push-pull scheme to generate

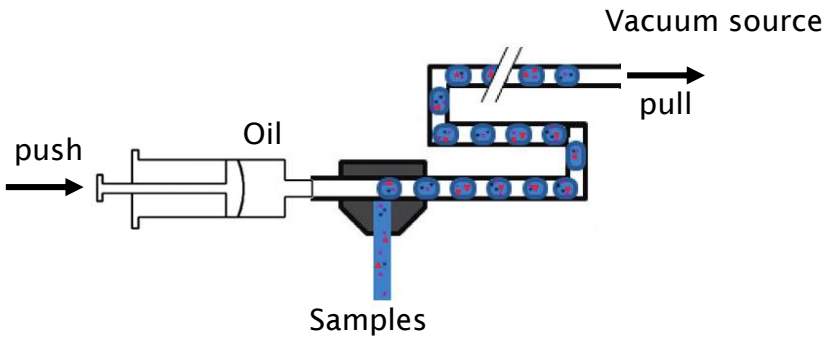

Figure 2.12 Push-pull scheme to generate droplets. The system consists a syringe pump, a T-junction and vacuum source. The vacuum source is aspirating samples from microdialysis probe and carrier oil is pulled by syringe pump. *Copyright © 2008 Anal. Chem.*

droplets from microdialysis probes, at which the aqueous contents can be various, as shown in Figure 2.12.

2.2.2.3. Other methods to generate droplets

There are also some other unconventional methods of generating droplets, such as slip-chip based and electrowetting on dielectric (EWOD).

Du *et al* [69] engineered a slipchip to generate multiplexed droplets without pumps or valves. In EWOD, as electric field is applied upon the electrodes, the interfacial energy which can affect the contact angle between a fluid and the surface. For example, the electrical field can be used to decrease the contact angle and causes the fluid to 'wet' the surface. Insulating layers are typically deposited on the top of electrodes. Besides that, another layer will be coated on the insulation layers to make the layers hydrophobic. Advantages of EWOD over passive methods are summarized by Wheeler A.R. such as samples are addressed individually and flexible operation. However, rendering and controlling the right surface properties is a challenge for EWOD approach, on top of the complicated device fabrications [70].

2.2.2.4. Summary

In this section, droplet generation methods are thoroughly reviewed: droplet generation in typical geometries and the following modified geometries, generating droplets in aspirating devices. Some other methods such as slipchip and EWOD, were mentioned.

In typical geometries, droplet generation is normally driven by syringe pumps in positive status or positive pressure sources. Droplet on demand manners can be realised by regulating flowrates of aqueous phases and (or) oil phases, controlling the dimensions of geometries, controlling the physics properties of fluids, and applying external forces. The procedures of operating generation of droplets are summarised as: loading aqueous samples and carrier phases into syringe pumps or wells, preparing pumping system and calibrating flowrates such as driving air bubbles in the pumping system, stabilising generation of droplets because of compliance effects in the system. This operation and preparation is tedious and less continuous.

In aspirating devices as reviewed in section 2.2.2.2, the generation of droplets is realised by introducing aqueous samples and oils with a protocol of controlling volume fractions between aqueous samples and oil phases under negative pressures. The volume fraction control can be realised by sequential control such as DropLab, which shows strong on-demand feature, i.e. multiple contents introduction and controllable sizes of droplets. It can also be realise by merely relying on the resistance distribution, which shows weak on-demand control. The pumping system is usually syringe based pumping systems or vacuum pumping system.

2.2.3. Operations of droplets

Operations of droplets are important procedures in droplet microfluidic circuits. The two important operations of droplets are reviewed: one is accelerating mixing inside droplets and other one is adding samples into droplets.

2.2.3.1. Droplets mixing

Mixing of reagents [71] is important in achieving a homogenous reactive environment. Mixing in droplets is easy to achieve by the internal circulating flows caused by the wall friction when the droplet is moving. However, when the droplets flow in a straight channel [72], the circulating flows are symmetric which is shown in Figure 2.13 (A) and the mixing efficiency is low.

To promote the efficiency of droplets mixing, a few schemes have been invented. The serpentine channel can be added to induce chaotic advections inside the droplets with *friction induced motion* methods. Such chaotic advections can make the axis of the two circulating flow unparalleled to direction of the flow, thus enhances the internal mixing [73], as schematically shown in Figure 2.13 (B) [32]. Bumpy channels can also be used to increase the frictions. The *non-friction induced* methods are those involved with external tools to motivate the droplets mixing, such as the laser spot [74] which can provide local temperature variations inside a droplet, or manipulating of super paramagnetic beads [75].

(A)

(B)

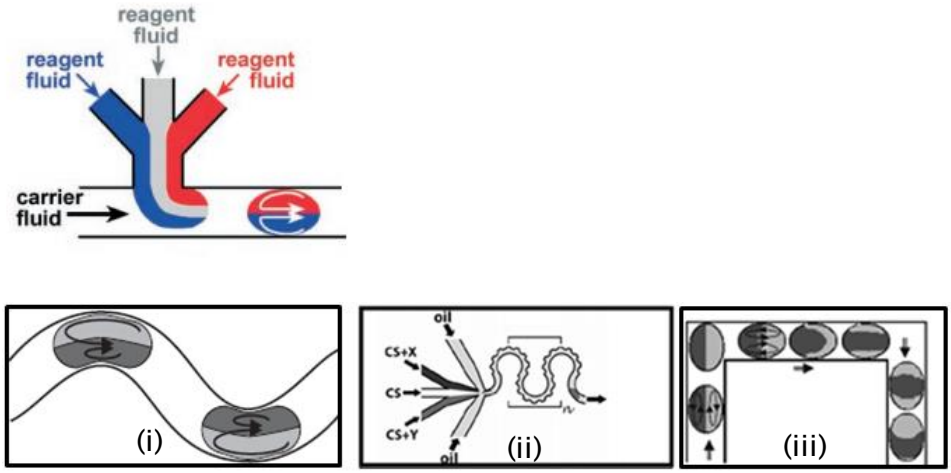

Figure 2.13 (A) Schematic of the straight channel: the two parts of the internal circulating flow are symmetrical. *Copyright © 2006 Angewandte Chemie-International Edition.* **(B). Serpentine channel to accelerate mixing efficiency.** *Copyright © Angewandte Chemie-International Edition.*

2.2.3.2. Adding samples into droplets

Additions of samples or reagents into droplets is a fundamental process in operating droplets in microfluidics. This operation has significant meaning in droplet microfluidics such as triggering a certain reactions, accurately dosing contents in bio-applications. The addition operations can be realised by either direct injecting samples into droplets or merged the designed droplets.

2.2.3.2.1. Injecting samples into droplets

Injecting samples into pre-formed droplets was firstly applied by Shestopalov *et al* [76]. In this system, the droplets were generated with a T-junction. These pre-formed droplets were delivered downstream to encounter another continuous aqueous sampling via a second T-junction, as shown in Figure 2.14 (A). The pre-formed droplets are joined by the continuous samples if merging successfully occurs. However, the merging step has strict requirement on the fluids properties, such as flowrate fractions between aqueous phase and oil phase and the presence of surfactants, which may make merging difficult to occur. Besides, cross-contamination has been observed [77]. Ismagilov's group [55, 78] then applied air bubbles to regulate success rate of merging in absence of surfactant, as shown in Figure 2.14 (B). Nightingale et al [79] further quantified that air bubbles can improve success rate of injection at T-junction.

To solve presence of surfactants in injection, Abate et al [80] developed picoinjector which is realised by a pressurised orifice and electro-fields, as shown in Figure 2.14 (C). When the preformed droplets surrounded by surfactants pass through the orifice with electrodes 'ON', the water-oil interface is raptured due to electrically induced thin-film instability. At that moment, the injecting samples are pressed into the droplet. Eventually, break-up of the new droplet occurs whose breaking mechanism is similar to that in T-junction. The volume of samples injected can be controlled via velocity of preformed droplets and pressure applied on the samples. As the picoinjector is sensitive to pressure difference between main channel and pressurised channel, Rhee et al [81] has further engineered a pressure stabiliser to tune the pressure, and thus a more controllable manner can be achieved.

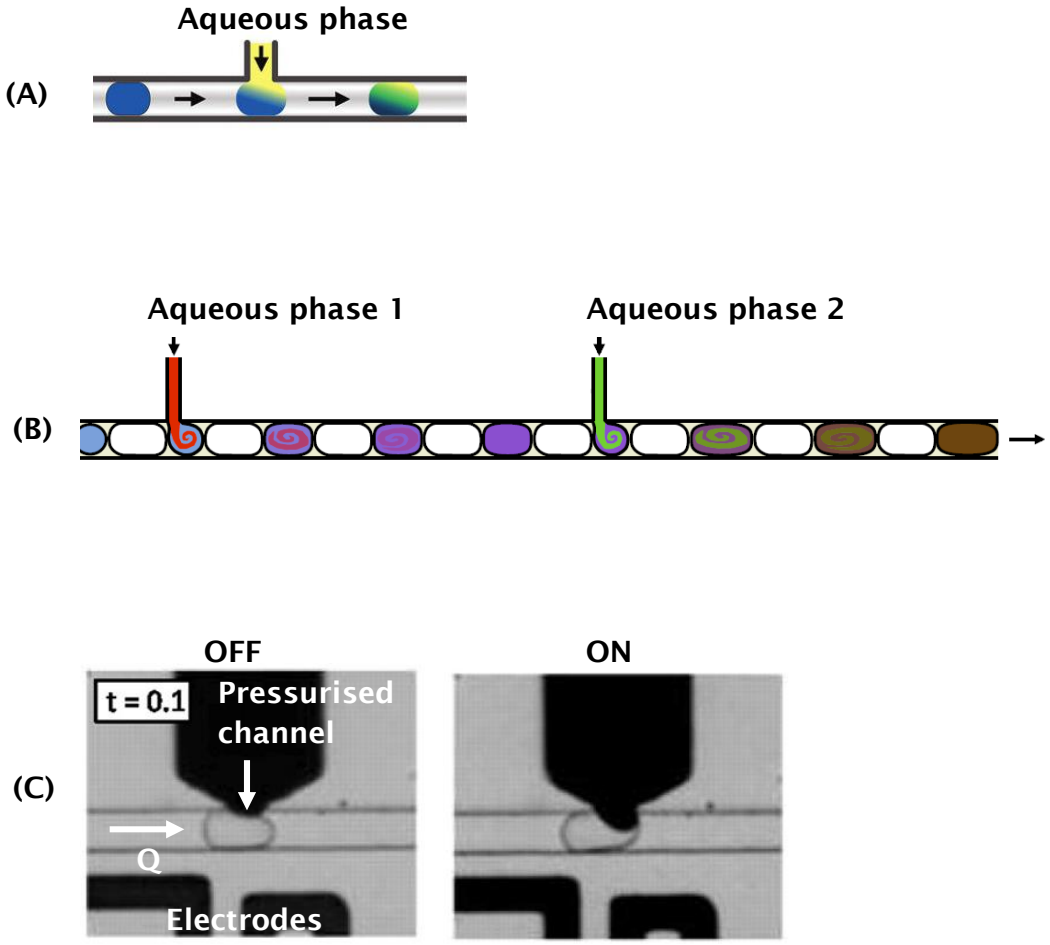

Figure 2.14 Injecting samples into pre-formed droplets. (A) Directly injecting aqueous into droplets. *Copyright ©2010 by Anal. Chem.* (B) Injecting samples with assistance from air-bbubels. *Copyright © 2014 by Nature Communications.* (C) Picoinjector. *Copyright ©2010 by National Academy of Sciences*

2.2.3.2.2. Merging droplets

Droplet merging module can also be used to add samples into droplets if droplets are controlled in synchronised manner [ref]. The generic process of merging droplets [82, 83] is that interfaces of two droplets approach closely to each other during which the thin film drains until they are able to interact with each other through van der Waals forces. The forces [84] can accelerate film drainage and amplify thermal fluctuations of the two interfaces. This leads the two droplets to form a localised liquid bridge which will unzip the interfaces. The unzipping time is related with the magnitude of the pressure decrease and the resistance to flow [30]. Figure 2.15 depicts the merging processes. To ensure droplets merging, an essential operation is to bring interfaces close enough.

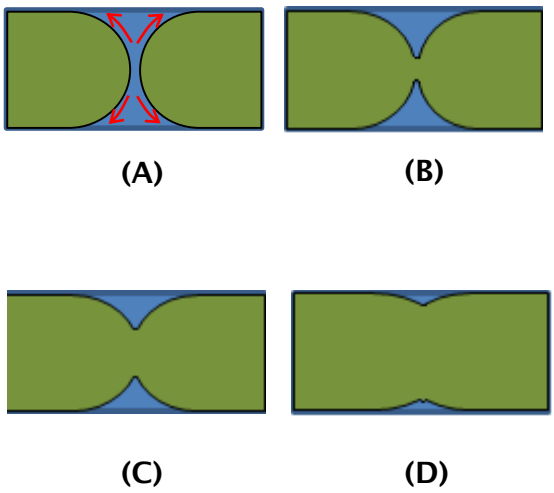

Figure 2.15. The processes of merging two droplets. (A). Two droplets get adjacent and contact with each other. (B) A bridge is formed and interface begins to be unzipped. (C) Unzipping continues and. (D) the two droplets are almost fully merged.

Several geometries have been developed to realise this merging function. One of the exploited geometries is the narrow channel which can be used to slow

down the leading droplets to wait for the subsequent droplets to touch it, as shown in Figure 2.16 (A) [85-87]. The second typical geometry is that an enlargement of the channels is applied to trap and to stop the droplets schematically [87]. The subsequent droplets are coming to meet with the trapped droplets, and be merged. Another similar trapping geometry is pillar induced droplet merging developed by Niu *et al* [88]. The innovations of such geometry are from the pillars which can stop the droplets and only permit continuous phase going through as shown in Figure 2.17 (B). There are two rows of pillars implanted inside enlargement of the channel to divide it into three separated channels. When droplets enter the merging chamber, they are distributed into the middle channel automatically. The first droplet is trapped by the pillars to wait for the next droplets to be merged. Besides, trapping droplets can be also realised by modifying the surface property of micro channels [89], as shown in Figure 2.16 (D)

Counterintuitively, separation of droplets can assist the coalescence as shown in Figure 2.16 (C). This phenomenon has been reported by Bremond et al [82]. An abrupt separation between two close droplets, can create a facing nipple to bring the interfaces closely enough, as shown in inset picture in Figure 2.16 (C). This phenomenon is also found in simulations [90] and experiment [91]. Niu *et al* [88] also observed this in the pillar-induced merging chamber. This phenomenon has been theoretically explained by Lai *et al* [92].

Generally, to prevent merging during transportation and storing of droplets, surfactants are added into droplets flows. This structure [30] makes the interfaces retard each other and it slows down the drainage rate by improving surface viscosity [83, 93, 94]. In presence of surfactants, electric field can be applied to assist coalescence of droplets. The electric field destabilises a range of thermal fluctuations on the interfaces of droplets, and thus leads the interfaces to form liquid bridge. Besides, electric field may also increase the temperature around interfaces and this can induce surfactant depletion. The practical application of merging two single droplets was demonstrated firstly [95] by Chabert *et al*. Niu *et al* [96] further applies electrical fields on the pillar-induced merging chamber [88] to trigger merging.

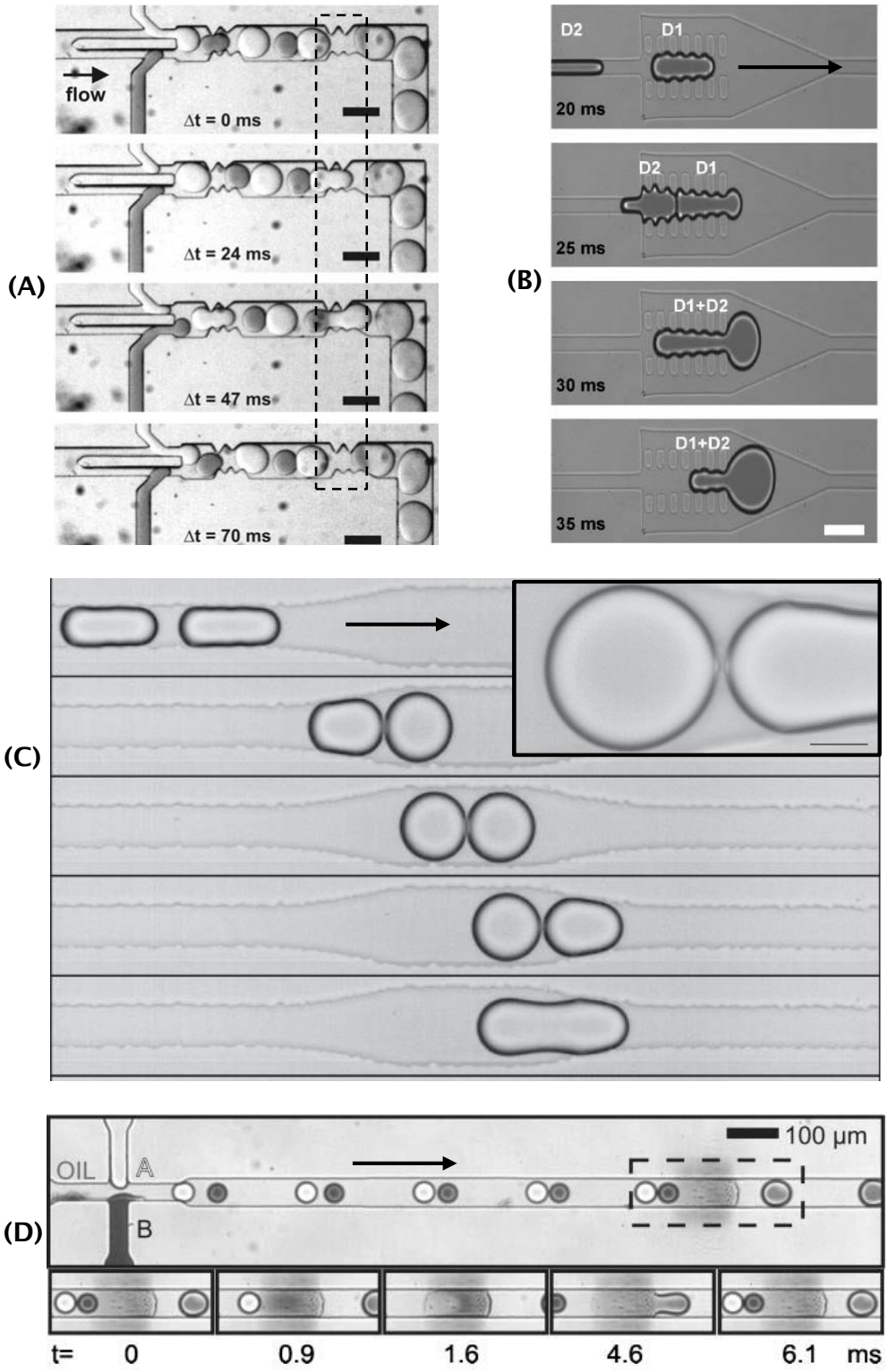

Figure 2.16 Droplet merging modules. (A)Narrow geometry to slow down droplets. *Copyright © 2010 Lab on a Chip.* (B) Pillar induced merging chamber. *Copyright © 2008 Lab on a Chip.* (C) Decompressing favors droplet merging. The inset picture shows facing nipples to bring the two interfaces close. *Copyright © 2008 Physical review letters.* (D)Modifying surface property to trap droplets *Copyright © 2007 Lab on a Chip.*

2.2.3.2.3. Other operations of droplets

Other operations of droplet include splitting droplets, sorting droplets and diluting droplets. Splitting can scale up the experimental capacity easily by increasing the number of the droplets. One of the mostly used geometries is T-junction. When droplets flow out from the middle channel, the resistance created from the channel wall will change the direction of droplets. The continuous flow pushes droplets to move forward. With the cooperation of the two forces, droplets splitting occurs and droplets will move into two side channels. Sorting droplets can be realised by sensing sizes of droplets [97, 98] and contents of droplets [97]. Diluting contents in droplets, has been demonstrated and studied by Niu et al [99] and further applied by Korcyyk *et al* [100].

2.2.4. Dynamics of transportation of droplets in microfluidic devices

This section reviews the dynamics of transportation of droplets microchannel. The dynamics review paper [30] in droplet microfluidics is thoroughly cited in this section.

The droplets flow in micro channels can be categorised into two groups: the first one is the bubbly flows where diameters of droplets are smaller than those of the microchannel schematically shown in Figure 2.17 (A), and second one is slug flows where droplet size is comparable or bigger than the channel widths schematically shown in Figure 2.17 (B). Droplets in bubbly flows are usually assumed to flow at the local velocity of the continuous flow. In this case, the droplets in the centreline of the channel will move faster than droplets near the channel walls. Droplets in slug flows are dominated by capillary effects and by the deformability of the droplets surface. In such case, a few physical

phenomenon are concerned, including *lubrication films and droplet velocity*, *pressure drop and the mean velocity*, and *flow fields*.

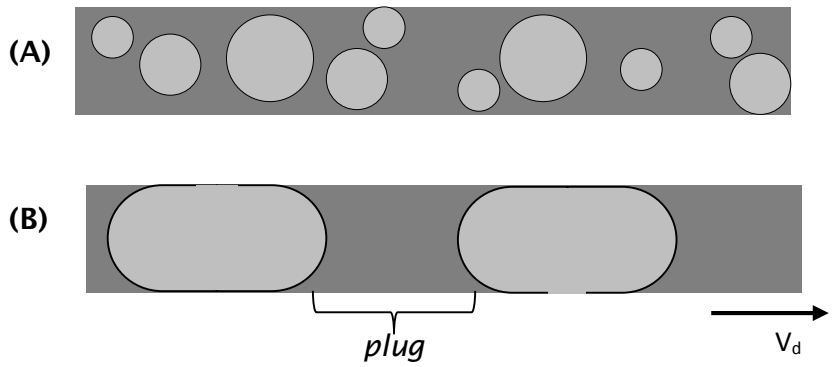

Figure 2.17 Schematically depicts of the two different droplets flow. (A) Bubbly flows where diameters of droplets are smaller than those of the microchannels. (B) Slug flows where droplets dominate spatially in the channel. *Reprint from 2010 Lab on a Chip*

2.2.4.1. Velocities of droplets in micro-channels

Lubrication films are always present in the slug flows, which are deposited between the droplets and the walls of the microchannel. Lubrications films can prevent contamination from the droplet samples to the walls. The thickness *e* of the lubrication films can be evaluated by viscous drag and capillary pressure. It is found that a nonlinear law for *e* with small capillary number in a circular tube of diameter *H* [101]:

$$\frac{e}{H} \propto Ca_d^{2/3} \qquad \textbf{Equation 2.9}$$

This relationship has been theoretically [102-104] and experimentally [105] studied.

It is observed that the thickness of the films is on the order of 1% to 5% of the channel's half height, with low *Ca* (*Ca*<0.01).

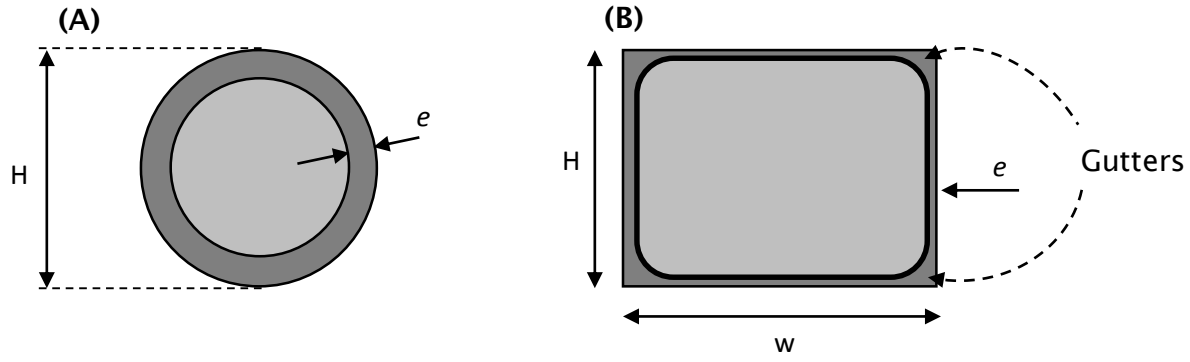

Figure 2.18. Schematic of the thickness of the film coating in between droplet and wall of channel. (A-B) The lubrication film between droplets and channel walls. *Reprint from 2010 Lab on a Chip*

To analyse the dynamics of the droplet flows, frame of droplet is set as reference. It is found that a flux of continuous flow Q_e can be evaluated by the velocity of droplet V_d and the mean velocity of the continuous flow V_{ext}. In circular microchannel schematically shown in Figure 2.18 (A), the film is evenly spaced around the wall whose velocity is $-V_d$, such that the drop sees a net flux of the external phase, of magnitude Q_e, which scales with the film thickness: $Q_e \propto -Ca_d^{2/3} SV_d$ [105]. As it was reviewed by Baroud et al [30], in this case, the droplet is faster than the films by an amount

$$\frac{V_d - V_{ext}}{V_d} = Ca_d^{2/3} \qquad \textbf{Equation 2.10}$$

For rectangular microchannel schematically shown in Figure 2.18 (B), the droplets do not completely fill the channel and there will be gutters around the corners where continuous fluid can flow. The velocity relation was found by Wong:

$$\frac{V_d - V_{ext}}{V_d} \propto -Ca_d^{-1/3} \qquad \textbf{Equation 2.11}$$

This equation is experimentally measured by Fuerstman *et al* [106]. It was also understood that surfactants can reduce velocity of droplet up to 50 % in some cases.

2.2.4.2. Pressure drop and flow fields

In single-phase microfluidics, the pressure drop along the microchannel can be evaluated as:

$$\triangle P = RLV = a\frac{\mu}{WH}LV \qquad \textbf{Equation 2.12}$$

Where *R* is the fluidic resistivity, *L* is the length of the microchannel; *V* is the mean velocity; *a* is a dimensionless constant [107]; *W* is the width of the microchannel; *H* is the height of the microchannel

In droplet microfluidics, there are three kinds of pressure drops. They are plug pressure drop ΔP_{plug} , droplets pressure drop $\Delta P_{droplet}$ and the droplet cap pressure drop ΔP_{cap}. To evaluate the plug drops along the microchannel, it can be assumed that continuous flow is single phase without considering droplets. In this case, the plugs pressure drops can be evaluated as

$$\triangle P_{plug} = a\frac{\mu_f}{WH}L_{plugs}V_{ext} \qquad \textbf{Equation 2.13}$$

where L_{plugs} is length of all the plugs. The pressure drops inside the droplets can be evaluated with the same equation,

$$\triangle P_{droplets} = b\frac{\mu_{in}}{WH}L_{droplets}V_d \qquad \textbf{Equation 2.14}$$

where $L_{droplets}$ is length of all the droplets, *b* is another dimensionless number. The pressure drop across the droplets is

$$\triangle P_{caps} = n_d c\frac{\gamma}{H}Ca_d^{2/3} \qquad \textbf{Equation 2.15}$$

where n_d is the number of droplets in the channel and *c* is a dimensionless number which depends on the geometry. In this case, the total pressure drop can be calculated,

$$\Delta P = \Delta P_{plug} + \Delta P_{droplets} + \Delta P_{cap} \qquad \textbf{Equation 2.16}$$

A sketch of pressure drop in microdroplet flow is schematically shown in Figure 2.19. In the real situation, droplets inside the microchannel travel with a velocity which is smaller than that of the continuous flow. The liquid particles inside the continuous phase will catch up with droplets. The flow direction of these particles will be affected by the droplets and vortexes inside and outside of the droplets exist. A topology of the flow fields inside and outside droplets is given by Hodges *et al* [102].

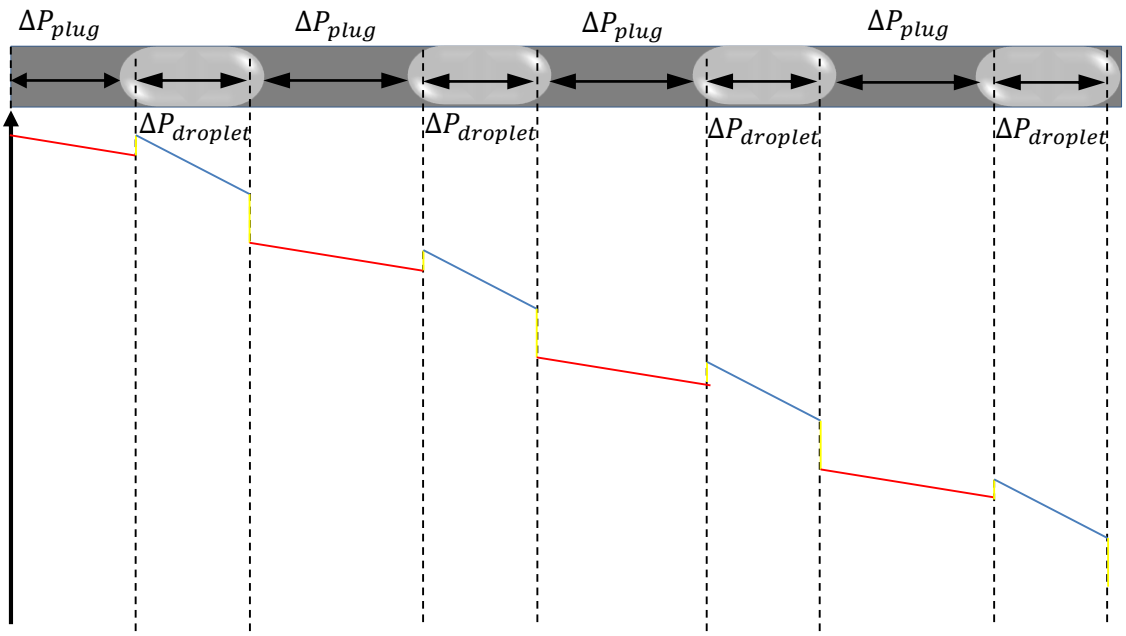

Figure 2.19 Pressure drop along the microchannel: The red lines in the plot represents the plug pressure drop, the blue line in the plot represents the droplets pressure drop, and the yellow line in the plot represents the cap pressure drop. *Reprint from 2010 Lab on a Chip*

2.3. Peristaltic pumping method

Fluids delivering and pumping is a key process in microfluidic devices. Syringe pumps, vacuum/pressure source and peristaltic pumps are the most commonly used pumping system in biological labs. This section specifically reviews the engineering of peristaltic pumps.

A peristaltic pump applies rollers or other mechanisms to squeeze the elastic tubing in the inlet and release it in the outlet. In the inlet, the spontaneous restitution of the squeezed parts of the tubing occurs as the rollers move forwards. This generates vacuum to aspirate fluids. In outlet, the rollers or other mechanisms force the fluids forward [108]. This process is termed as peristalsis, which is widely applied nature, such as digesting system. A peristaltic pump is a combination of a displacement pump with controllable compliance and check valves. Besides, it can pump fluids without any limitations on the volumes [109], which is different from syringe pumps.

The first category of peristaltic pump is these applied special mechanism to continuously deliver fluids. The mechanism can be rollers or screws. For example, Kock et al [110] applied miniaturised rollers, PDMS channels and a micro motor to miniaturise the conventional bench peristaltic pump. It was found the flowrate and back pressures are highly controllable. Instead of applying rollers, Rhie et al [111] utilised a screw to continuously compress PDMS channels. This pump is highly compacted, low cost and precise. It is also demonstrated that pulsation issue can be solved by anti-phasing fluids in opposite positions. Zhang et al [112] applied a cam and a spring to engineer a linear chip-based peristaltic pump. This design significantly simplifies the engineering processes.

The second category of peristaltic pumps apply valves to discretely pump fluids. The valve can be actuated by solenoids, pressure, shape memory alloys and etc. Unger et al [113] designed a multilayer valves which can sequentially work to pump fluids, as shown in Figure 2.20 (C). Sassa et al [114] has applied shape memory alloy (Ti-Ni) to sequentially control 3 valves by applying pulses of electric power. However, as it was reported, the response of shape memory alloys is slow compared to other mechanisms.

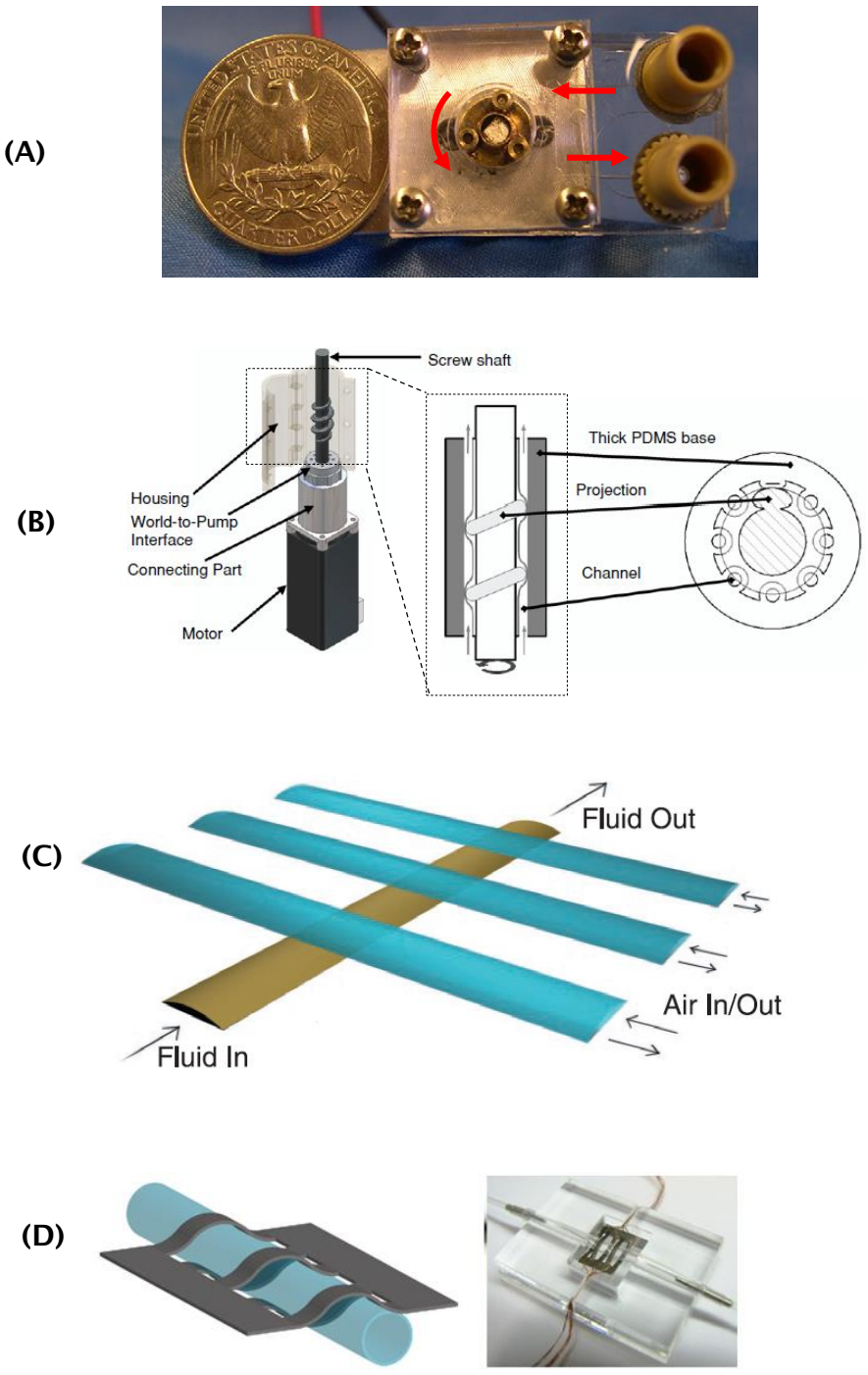

Figure 2.20 (A) Roller mechanism peristaltic pump. *Copyright © 2009 Sensors and Actuators B.* (B) Screw mechanism peristaltic pump. *Copyright ©2010 J. Micromech. Microeng* (C) Multi-layer pressure mechanism. Copyright © 2000 Science. (D) Shape memory alloy mechanism. *Copyright © 2012 by Sensors and Actuators B.*

2.4. Conclusions

This chapter has reviewed fundamental of micro droplets and the related interfacial science, the state of the art of engineering droplet microfluidics, particularly those associated with droplet sampling and droplet generation, and peristaltic pumping method.

Firstly, this chapter has introduced droplet microfluidics and related interfacial science, which is useful to understand generation and operation of droplets in microfluidics.

Secondly, the features and advantages of droplets microfluidics have been listed.

Thirdly, droplet generation methods are thoroughly reviewed and can be categorised into three groups: droplet droplets in typical geometries and their modifications, generating droplets in aspirating devices, and some other methods such as slipchip and EWOD. In the first groups, droplet generation normally is pumped by syringe pumps at positive status or positive pressure pumps. In the second group, droplets generation normally is pumped by negative pressure pumps. The aspirating technique can be further developed to directly aspirate samples.

Fourthly, the important processes in operating droplets in microfluidic devices are reviewed, which are mixing in droplets and adding samples into droplets. Mixing can be accelerated by adding serpentine channels or by external tools such as laser spot. Adding samples into droplets can be realised by direct injecting samples into pre-formed droplets or by merging droplets with merging modules. In merging droplets, one essential procedure is to present droplets in synchronised manners.

Fifthly, the dynamics of transportation of droplets in micro-channels have been reviewed. This dynamics is important in engineering microfluidic devices which is capable of generating droplets, pumping droplets or operating droplets.

Finally, the engineering of peristaltic pumps, which is going to be introduced in droplet microfluidics, was reviewed. Two groups of peristaltic pumps are categorised: continuous peristaltic pump and discrete peristaltic pump.

Reference List

1. Berthier, J., *Micro-Drops and Digital Microfluidics*. Micro and Nano Technologies. Vol. 541. 2013: Elservier Inc.
2. Dangla, R., S.C. Kayi, and C.N. Baroud, *Droplet microfluidics driven by gradients of confinement.* Proceedings of the National Academy of Sciences of the United States of America, 2013. **110**(3): p. 853-858.
3. Lynn, N.S. and D.S. Dandy, *Passive microfluidic pumping using coupled capillary/evaporation effects.* Lab on a Chip, 2009. **9**(23): p. 3422-3429.
4. Yetisen, A.K., M.S. Akram, and C.R. Lowe, *Paper-based microfluidic point-of-care diagnostic devices.* Lab on a Chip, 2013. **13**(12): p. 2210-2251.
5. Rosen, M.J., *Surfactants and Interfacial phenomenon.* 2004: John Wiley & Sons, Inc.
6. Baret, J.C., *Surfactants in droplet-based microfluidics.* Lab on a Chip, 2012. **12**(3): p. 422-433.
7. deMello, A.J., *Control and detection of chemical reactions in microfluidic systems.* Nature, 2006. **442**(7101): p. 394-402.
8. Huebner, A., et al., *Microdroplets: A sea of applications?* Lab on a Chip, 2008. **8**(8): p. 1244-1254.
9. Christopher, G.F. and S.L. Anna, *Microfluidic methods for generating continuous droplet streams.* Journal of Physics D-Applied Physics, 2007. **40**(19): p. R319-R336.
10. Theberge, A.B., et al., *Microdroplets in Microfluidics: An Evolving Platform for Discoveries in Chemistry and Biology.* Angewandte Chemie-International Edition, 2010. **49**(34): p. 5846-5868.
11. Thorsen, T., et al., *Dynamic pattern formation in a vesicle-generating microfluidic device.* Physical Review Letters, 2001. **86**(18): p. 4163-4166.
12. Garstecki, P., et al., *Formation of droplets and bubbles in a microfluidic T-junction - scaling and mechanism of break-up.* Lab on a Chip, 2006. **6**(3): p. 437-446.
13. De Menech, M., et al., *Transition from squeezing to dripping in a microfluidic T-shaped junction.* Journal of Fluid Mechanics, 2008. **595**: p. 141-161.
14. Xu, J.H., et al., *Correlations of droplet formation in T-junction microfluidic devices: from squeezing to dripping.* Microfluidics and Nanofluidics, 2008. **5**(6): p. 711-717.

15. van Steijn, V., M.T. Kreutzer, and C.R. Kleijn, *mu-PIV study of the formation of segmented flow in microfluidic T-junctions.* Chemical Engineering Science, 2007. **62**(24): p. 7505-7514.

16. Christopher, G.F., et al., *Experimental observations of the squeezing-to-dripping transition in T-shaped microfluidic junctions.* Physical Review E, 2008. **78**(3).

17. van Steijn, V., C.R. Kleijn, and M.T. Kreutzer, *Flows around Confined Bubbles and Their Importance in Triggering Pinch-Off.* Physical Review Letters, 2009. **103**(21).

18. van Steijn, V., C.R. Kleijn, and M.T. Kreutzer, *Predictive model for the size of bubbles and droplets created in microfluidic T-junctions.* Lab on a Chip, 2010. **10**(19): p. 2513-2518.

19. Tice, J.D., A.D. Lyon, and R.F. Ismagilov, *Effects of viscosity on droplet formation and mixing in microfluidic channels.* Analytica Chimica Acta, 2004. **507**(1): p. 73-77.

20. Cramer, C., P. Fischer, and E.J. Windhab, *Drop formation in a co-flowing ambient fluid.* Chemical Engineering Science, 2004. **59**(15): p. 3045-3058.

21. Guillot, P., et al., *Stability of a jet in confined pressure-driven biphasic flows at low reynolds numbers.* Physical Review Letters, 2007. **99**(10).

22. Utada, A.S., et al., *Absolute instability of a liquid jet in a coflowing stream.* Physical Review Letters, 2008. **100**(1).

23. Guillot, P., A. Colin, and A. Ajdari, *Stability of a jet in confined pressure-driven biphasic flows at low Reynolds number in various geometries.* Physical Review E, 2008. **78**(1).

24. Utada, A.S., et al., *Dripping to jetting transitions in coflowing liquid streams.* Physical Review Letters, 2007. **99**(9).

25. Anna, S.L., N. Bontoux, and H.A. Stone, *Formation of dispersions using "flow focusing" in microchannels.* Applied Physics Letters, 2003. **82**(3): p. 364-366.

26. Ward, T., et al., *Microfluidic flow focusing: Drop size and scaling in pressure versus flow-rate-driven pumping.* Electrophoresis, 2005. **26**(19): p. 3716-3724.

27. Tan, Y.C., V. Cristini, and A.P. Lee, *Monodispersed microfluidic droplet generation by shear focusing microfluidic device.* Sensors and Actuators B-Chemical, 2006. **114**(1): p. 350-356.

28. Nie, Z.H., et al., *Emulsification in a microfluidic flow-focusing device: effect of the viscosities of the liquids.* Microfluidics and Nanofluidics, 2008. **5**(5): p. 585-594.

29. Funfschilling, D., et al., *Flow-field dynamics during droplet formation by dripping in hydrodynamic-focusing microfluidics.* Physical Review E, 2009. **80**(1).

30. Baroud, C.N., F. Gallaire, and R. Dangla, *Dynamics of microfluidic droplets.* Lab on a Chip, 2010. **10**(16): p. 2032-2045.

31. Lee, W., L.M. Walker, and S.L. Anna, *Role of geometry and fluid properties in droplet and thread formation processes in planar flow focusing.* Physics of Fluids, 2009. **21**(3).

32. Seemann, R., et al., *Droplet based microfluidics.* Reports on Progress in Physics, 2012. **75**(1).

33. Shui, L.L., et al., *Geometry-controlled droplet generation in head-on microfluidic devices.* Applied Physics Letters, 2008. **93**(15).

34. Shui, L.L., A. van den Berg, and J.C.T. Eijkel, *Capillary instability, squeezing, and shearing in head-on microfluidic devices.* Journal of Applied Physics, 2009. **106**(12).

35. Dangla, R., et al., *The physical mechanisms of step emulsification.* Journal of Physics D-Applied Physics, 2013. **46**(11).

36. van Steijn, V., et al., *Block-and-break generation of microdroplets with fixed volume.* Biomicrofluidics, 2013. **7**(2).

37. Bransky, A., et al., *A microfluidic droplet generator based on a piezoelectric actuator.* Lab on a Chip, 2009. **9**(4): p. 516-520.

38. Zeng, S.J., et al., *Microvalve-actuated precise control of individual droplets in microfluidic devices.* Lab on a Chip, 2009. **9**(10): p. 1340-1343.

39. Churski, K., J. Michalski, and P. Garstecki, *Droplet on demand system utilizing a computer controlled microvalve integrated into a stiff polymeric microfluidic device.* Lab on a Chip, 2010. **10**(4): p. 512-518.

40. Churski, K., P. Korczyk, and P. Garstecki, *High-throughput automated droplet microfluidic system for screening of reaction conditions.* Lab on a Chip, 2010. **10**(7): p. 816-818.

41. Churski, K., et al., *Simple modular systems for generation of droplets on demand.* Lab on a Chip, 2013. **13**(18): p. 3689-3697.

42. Lorenz, R.M., et al., *Simultaneous generation of multiple aqueous droplets in a microfluidic device.* Analytica Chimica Acta, 2008. **630**(2): p. 124-130.

43. Abate, A.R., et al., *Valve-based flow focusing for drop formation.* Applied Physics Letters, 2009. **94**(2).

44. Lee, C.Y., Y.H. Lin, and G.B. Lee, *A droplet-based microfluidic system capable of droplet formation and manipulation.* Microfluidics and Nanofluidics, 2009. **6**(5): p. 599-610.

45. Hsiung, S.K., C.T. Chen, and G.B. Lee, *Micro-droplet formation utilizing microfluidic flow focusing and controllable moving-wall chopping techniques.* Journal of Micromechanics and Microengineering, 2006. **16**(11): p. 2403-2410.

46. Nguyen, N.T., et al., *Thermally mediated droplet formation in microchannels.* Applied Physics Letters, 2007. **91**(8).

47. Murshed, S.M.S., et al., *Microdroplet formation of water and nanofluids in heat-induced microfluidic T-junction.* Microfluidics and Nanofluidics, 2009. **6**(2): p. 253-259.

48. Stan, C.A., S.K.Y. Tang, and G.M. Whitesides, *Independent Control of Drop Size and Velocity in Microfluidic Flow-Focusing Generators Using Variable Temperature and Flow Rate.* Analytical Chemistry, 2009. **81**(6): p. 2399-2402.

49. Baroud, C.N., et al., *Thermocapillary valve for droplet production and sorting.* Physical Review E, 2007. **75**(4).

50. Baroud, C.N., M.R. de Saint Vincent, and J.P. Delville, *An optical toolbox for total control of droplet microfluidics.* Lab on a Chip, 2007. **7**(8): p. 1029-1033.

51. Tan, S.H., B. Semin, and J.C. Baret, *Microfluidic flow-focusing in ac electric fields.* Lab on a Chip, 2014. **14**(6): p. 1099-1106.

52. Schmid, L. and T. Franke, *Acoustic modulation of droplet size in a T-junction.* Applied Physics Letters, 2014. **104**(13).

53. Schmid, L. and T. Franke, *SAW-controlled drop size for flow focusing.* Lab on a Chip, 2013. **13**(9): p. 1691-1694.

54. Linder, V., S.K. Sia, and G.M. Whitesides, *Reagent-loaded cartridges for valveless and automated fluid delivery in microfluidic devices.* Analytical Chemistry, 2005. **77**(1): p. 64-71.

55. Chen, D.L. and R.F. Ismagilov, *Microfluidic cartridges preloaded with nanoliter plugs of reagents: an alternative to 96-well plates for screening.* Current Opinion in Chemical Biology, 2006. **10**(3): p. 226-231.

56. Chabert, M., et al., *Automated microdroplet platform for sample manipulation and polymerase chain reaction.* Analytical Chemistry, 2006. **78**(22): p. 7722-7728.

57. Du, W.B., et al., *Automated Microfluidic Screening Assay Platform Based on Drop Lab.* Analytical Chemistry, 2010. **82**(23): p. 9941-9947.

58. Gu, S.Q., et al., *Multifunctional Picoliter Droplet Manipulation Platform and Its Application in Single Cell Analysis.* Analytical Chemistry, 2011. **83**(19): p. 7570-7576.

59. Zhu, Y., et al., *Sequential Operation Droplet Array: An Automated Microfluidic Platform for Picoliter-Scale Liquid Handling, Analysis, and Screening.* Analytical Chemistry, 2013. **85**(14): p. 6723-6731.

60. Wu, J.B., et al., *Multiple and High-Throughput Droplet Reactions via Combination of Microsampling Technique and Microfluidic Chip.* Analytical Chemistry, 2012. **84**(22): p. 9689-9693.

61. Gielen, F., et al., *A Fully Unsupervised Compartment-on-Demand Platform for Precise Nanoliter Assays of Time-Dependent Steady-State Enzyme Kinetics and Inhibition.* Analytical Chemistry, 2013. **85**(9): p. 4761-4769.

62. Rane, T.D., H.C. Zec, and T.H. Wang, *A Serial Sample Loading System: Interfacing Multiwell Plates with Microfluidic Devices.* Jala, 2012. **17**(5): p. 370-377.

63. Abate, A.R. and D.A. Weitz, *Syringe-vacuum microfluidics: A portable technique to create monodisperse emulsions.* Biomicrofluidics, 2011. **5**(1).

64. Easley, C.J., et al., *Quantitative Measurement of Zinc Secretion from Pancreatic Islets with High Temporal Resolution Using Droplet-Based Microfluidics.* Analytical Chemistry, 2009. **81**(21): p. 9086-9095.

65. Godwin, L.A., et al., *Passively Operated Microfluidic Device for Stimulation and Secretion Sampling of Single Pancreatic Islets.* Analytical Chemistry, 2011. **83**(18): p. 7166-7172.

66. Deal, K.S. and C.J. Easley, *Self-Regulated, Droplet-Based Sample Chopper for Microfluidic Absorbance Detection.* Analytical Chemistry, 2012. **84**(3): p. 1510-1516.

67. Gielen, F., et al., *Interfacing Microwells with Nanoliter Compartments: A Sampler Generating High-Resolution Concentration Gradients for Quantitative Biochemical Analyses in Droplets.* Analytical Chemistry, 2015. **87**(1): p. 624-632.

68. Slaney, T.R., et al., *Push-Pull Perfusion Sampling with Segmented Flow for High Temporal and Spatial Resolution in Vivo Chemical Monitoring.* Analytical Chemistry, 2011. **83**(13): p. 5207-5213.

69. Du, W.B., et al., *SlipChip.* Lab on a Chip, 2009. **9**(16): p. 2286-2292.

70. Abdelgawad, M. and A.R. Wheeler, *The Digital Revolution: A New Paradigm for Microfluidics.* Advanced Materials, 2009. **21**(8): p. 920-925.

71. Solvas, X.C.I. and A. deMello, *Droplet microfluidics: recent developments and future applications.* Chemical Communications, 2011. **47**(7): p. 1936-1942.

72. Song, H., D.L. Chen, and R.F. Ismagilov, *Reactions in droplets in microflulidic channels.* Angewandte Chemie-International Edition, 2006. **45**(44): p. 7336-7356.

73. Bringer, M.R., et al., *Microfluidic systems for chemical kinetics that rely on chaotic mixing in droplets.* Philosophical Transactions of the Royal Society of London Series a-Mathematical Physical and Engineering Sciences, 2004. **362**(1818): p. 1087-1104.

74. Cordero, M.L., et al., *Mixing via thermocapillary generation of flow patterns inside a microfluidic drop.* New Journal of Physics, 2009. **11**.

75. Roy, T., et al., *Magnetic microsphere-based mixers for microdroplets.* Physics of Fluids, 2009. **21**(2).

76. Shestopalov, I., J.D. Tice, and R.F. Ismagilov, *Multi-step synthesis of nanoparticles performed on millisecond time scale in a microfluidic droplet-based system.* Lab on a Chip, 2004. **4**(4): p. 316-321.

77. Song, H., et al., *On-chip titration of an anticoagulant argatroban and determination of the clotting time within whole blood or plasma using a plug-based microfluidic system.* Analytical Chemistry, 2006. **78**(14): p. 4839-4849.

78. Zheng, B. and R.F. Ismagilov, *A microfluidic approach for screening submicroliter volumes against multiple reagents by using preformed arrays of nanoliter plugs in a three-phase liquid/liquid/gas flow.* Angewandte Chemie-International Edition, 2005. **44**(17): p. 2520-2523.

79. Nightingale, A.M., et al., *Controlled multistep synthesis in a three-phase droplet reactor.* Nature Communications, 2014. **5**.

80. Abate, A.R., et al., *High-throughput injection with microfluidics using picoinjectors.* Proceedings of the National Academy of Sciences of the United States of America, 2010. **107**(45): p. 19163-19166.

81. Rhee, M., et al., *Pressure stabilizer for reproducible picoinjection in droplet microfluidic systems.* Lab on a Chip, 2014. **14**(23): p. 4533-4539.

82. Bremond, N., A.R. Thiam, and J. Bibette, *Decompressing emulsion droplets favors coalescence.* Physical Review Letters, 2008. **100**(2).

83. Chesters, A.K., *The Modeling of Coalescence Processes in Fluid Liquid Dispersions - a Review of Current Understanding.* Chemical Engineering Research & Design, 1991. **69**(4): p. 259-270.

84. Aarts, D.G.A.L., M. Schmidt, and H.N.W. Lekkerkerker, *Direct visual observation of thermal capillary waves.* Science, 2004. **304**(5672): p. 847-850.

85. Chokkalingam, V., et al., *Optimized droplet-based microfluidics scheme for sol-gel reactions.* Lab on a Chip, 2010. **10**(13): p. 1700-1705.

86. Chokkalingam, V., et al., *Template-free Preparation of Mesoporous Silica Spheres through Optimized Microfluidics.* Chemphyschem, 2010. **11**(10): p. 2091-2095.

87. Kohler, J.M., et al., *Digital reaction technology by micro segmented flow - components, concepts and applications.* Chemical Engineering Journal, 2004. **101**(1-3): p. 201-216.

88. Niu, X., et al., *Pillar-induced droplet merging in microfluidic circuits.* Lab on a Chip, 2008. **8**(11): p. 1837-1841.

89. Fidalgo, L.M., C. Abell, and W.T.S. Huck, *Surface-induced droplet fusion in microfluidic devices.* Lab on a Chip, 2007. **7**(8): p. 984-986.

90. Yoon, Y., et al., *Coalescence of two equal-sized deformable drops in an axisymmetric flow.* Physics of Fluids, 2007. **19**(10).

91. Manica, R., et al., *Transient responses of a wetting film to mechanical and electrical perturbations.* Langmuir, 2008. **24**(4): p. 1381-1390.

92. Lai, A., N. Bremond, and H.A. Stone, *Separation-driven coalescence of droplets: an analytical criterion for the approach to contact.* Journal of Fluid Mechanics, 2009. **632**: p. 97-107.

93. Amarouchene, Y., G. Cristobal, and H. Kellay, *Noncoalescing drops.* Physical Review Letters, 2001. **87**(20).

94. Bibette, J., et al., *Stability-Criteria for Emulsions.* Physical Review Letters, 1992. **69**(16): p. 2439-2442.

95. Chabert, M., K.D. Dorfman, and J.L. Viovy, *Droplet fusion by alternating current (AC) field electrocoalescence in microchannels.* Electrophoresis, 2005. **26**(19): p. 3706-3715.

96. Niu, X.Z., et al., *Electro-Coalescence of Digitally Controlled Droplets.* Analytical Chemistry, 2009. **81**(17): p. 7321-7325.

97. Niu, X.Z., et al., *Real-time detection, control, and sorting of microfluidic droplets.* Biomicrofluidics, 2007. **1**(4).

98. Tan, Y.C., Y.L. Ho, and A.P. Lee, *Microfluidic sorting of droplets by size.* Microfluidics and Nanofluidics, 2008. **4**(4): p. 343-348.

99. Niu, X.Z., et al., *A microdroplet dilutor for high-throughput screening.* Nature Chemistry, 2011. **3**(6): p. 437-442.

100. Korczyk, P.M., et al., *Microfluidic traps for hard-wired operations on droplets.* Lab on a Chip, 2013. **13**(20): p. 4096-4102.

101. Bretherton, F.P., *The motion of long bubbles in tubes.* J.Fluid.Mech, 1961. **10**: p. 166-188.

102. Hodges, S.R., O.E. Jensen, and J.M. Rallison, *The motion of a viscous drop through a cylindrical tube.* Journal of Fluid Mechanics, 2004. **501**: p. 279-301.

103. Wong, H., C.J. Radke, and S. Morris, *The Motion of Long Bubbles in Polygonal Capillaries .1. Thin-Films.* Journal of Fluid Mechanics, 1995. **292**: p. 71-94.

104. Wong, H., C.J. Radke, and S. Morris, *The Motion of Long Bubbles in Polygonal Capillaries .2. Drag, Fluid Pressure and Fluid-Flow.* Journal of Fluid Mechanics, 1995. **292**: p. 95-110.

105. Schwartz, L.W., H.M. Princen, and A.D. Kiss, *On the Motion of Bubbles in Capillary Tubes.* Journal of Fluid Mechanics, 1986. **172**: p. 259-275.

106. Sarrazin, F., et al., *Hydrodynamic structures of droplets engineered in rectangular micro-channels.* Microfluidics and Nanofluidics, 2008. **5**(1): p. 131-137.

107. Fuerstman, M.J., et al., *The pressure drop along rectangular microchannels containing bubbles.* Lab on a Chip, 2007. **7**(11): p. 1479-1489.

108. *How do peristaltic dosing pumps work?* ; Available from: http://www.verderflex.com/en/how-do-peristaltic-pumps-work/.

109. *Features and benefits of peristaltic pumps*. Available from: http://www.verderflex.com/en/features-and-benefits/.

110. Koch, C., V. Remcho, and J. Ingle, *PDMS and tubing-based peristaltic micropumps with direct actuation.* Sensors and Actuators B-Chemical, 2009. **135**(2): p. 664-670.

111. Rhie, W. and T. Higuchi, *Design and fabrication of a screw-driven multi-channel peristaltic pump for portable microfluidic devices.* Journal of Micromechanics and Microengineering, 2010. **20**(8).

112. Zhang, X.N., Z.T. Chen, and Y.Y. Huang, *A valve-less microfluidic peristaltic pumping method.* Biomicrofluidics, 2015. **9**(1).

113. Unger, M.A., et al., *Monolithic microfabricated valves and pumps by multilayer soft lithography.* Science, 2000. **288**(5463): p. 113-116.

114. Sassa, F., et al., *Miniaturized shape memory alloy pumps for stepping microfluidic transport.* Sensors and Actuators B-Chemical, 2012. **165**(1): p. 157-163.

3. Continuously generating and pumping droplets with a peristaltic pumping system

3.1. Introduction

In recent years, the field of droplet microfluidics has been continuously growing because of its attractive features as introduced in Chapter 2, *e.g.* small sample consumption, fast mixing, and digitalisation which can avoid cross-contamination between different samples. One important operation of droplet microfluidics is sampling droplets, during which samples are collected, digitalised into droplets and delivered for further operations. Almost exclusively, droplets are generated with on-chip methods including T-junction geometry, flow focusing geometry or co-flowing geometry driven by syringe pumps. With these methods, the polydispersity, which is the measurement of droplet size variation, is low and the set-up can be easily built up with a microfluidic chip and syringe pumps for driving oil and aqueous samples. As a result, these generation methods have been intensively used and studied experimentally and numerically in the last ten years [1-5]. However, T-junction or flow focusing generation with syringe pumping or pressure pumping gives only poor control of an individual droplet and is not able to achieve *droplet on demand* generation. The poor individual local control comes from the compliance in the pumping system, such as air bubbles trapped in syringe pumping system or the soft channels and tubing. Consequently, the fluidic system needs a long time (a few minutes or even longer) to stabilise the flow rate to produce droplets with uniform sizes. Garstecki *et al* has demonstrated that external valves can be used to control both oil and aqueous channels [6], and droplet on demand can be realised. However, the droplets produced from those platforms are large in size, normally at about ~100 nL. Besides the limitation in control of the sizes of droplets, it is tedious to collect/load samples into syringes and to frequently change syringes. This limits the operation of direct loading samples into system and thus makes the *loading-generation* processes less continuous.

Unlike on-chip generation, aspiration of samples as a droplet generation method [7-11] can partially circumvent the aforementioned problems. This method exploits negative pressure to sequentially aspirate oil and aqueous samples

which are registered in a well or container, with pre-programmed protocols, and the negative pressure can be provided by a syringe pump [11] or a vacuum source [10]. Chaber *et al* [11] first utilised this method in polymerse chain reactions with a push-pull valve method. After that, this method was further adopted in a variety of applications [8-10]. Gielen et al [7] further simplified this method by eliminating the pre-programmed protocols. In this aspiration generation method, these droplets are generally stored in a tubing for further operations and analysis. However, that length of tubing and the limited volume of the syringe pumps does not allow for continuous droplet generation, and makes the collection of the droplets difficult to realise. More importantly, the stepwise behaviour of the introduction of droplets and those from the droplet operations such as merging and splitting can vary the flow resistance dramatically [12]; therefore the flow rate can be variable, thus making droplet size poorly controlled.

To solve the aforementioned issues, a peristaltic pumping system is proposed to realise more stable continuous droplet sampling. In contrast to other pumping methods, such as centrifuge pumps, syringe pumps or impedance pumps, a peristaltic pump benefits from low dead volume, less contamination, low fluidic compliance and ultimate pumping displacement. In this chapter, the peristaltic pumping system is integrated with the aspiration droplet generator to generate and deliver droplets. To interface these two systems, a synchronisation feedback system was engineered to synchronise the generation and delivery of droplets with the pulsation from the peristaltic pump. It was demonstrated that the whole integrated system is able to continuously generate and deliver droplets with high accuracy. It eliminates the long stabilising time of droplet generation in the aforementioned platforms and presents a quick set-up generation format.

3.2. Construction of an aspiration droplet generation platform

3.2.1. Introduction

An aspiration droplet generation method with a syringe pumping system or a vacuum pumping system has been described previously [7-9]. Depending on different applications, the procedures for aspirating aqueous samples and the oil phase can vary. For example, Du *et al* [8] introduced different aqueous samples into a system for mixing first and then introduced oil, while in [9], to avoid contaminations, each individual droplet is completed first and then introduced into the system. In the second method, Fluorinert™ FC oil is generally used as the carrier oil whose density is 1.855 g/cm^3. The difference between the two densities ensures that aqueous samples are sitting on the top of FC-40 in a reservoir to be exposed to the open environment. With this format, an interface is formed to separate aqueous samples from FC oil. To generate droplets (Figure 3.1), Polytetrafluoroethylene (PTFE) tubing shaped by a hook is actuated by a solenoid to be up or down to penetrate the interface to aspirate either aqueous samples or carrier oil. In this project, this procedure was applied to realise aspiration droplet generation. For a flowrate $Q(t)$, the droplet size is determined by the time when the PTFE tubing head is placed into the aqueous sample, t_{enter}, and the time when the PTFE tubing head exits the aqueous sample, t_{exit} . The procedures are schematically shown in Figure 3.1.(B). The relationship is expressed by Equation 3.1, where V_i is the volume size of the i-th droplet.

$$V_i = \int_{t_{enter}}^{t_{exit}} Q(t) \bullet dt \qquad \textbf{Equation 3.1}$$

3.2.2. Design and assembly of linear aspiration droplet generator

To demonstrate the continuous droplet sampling method with a peristaltic pump, an easily-assembled linear aspiration droplet generator was developed. The design is schematically shown in Figure 3.2. There are four major parts: the *x-y-z* stage, solenoid, solenoid-stage interface and PTFE tubing shaped by metal hook.

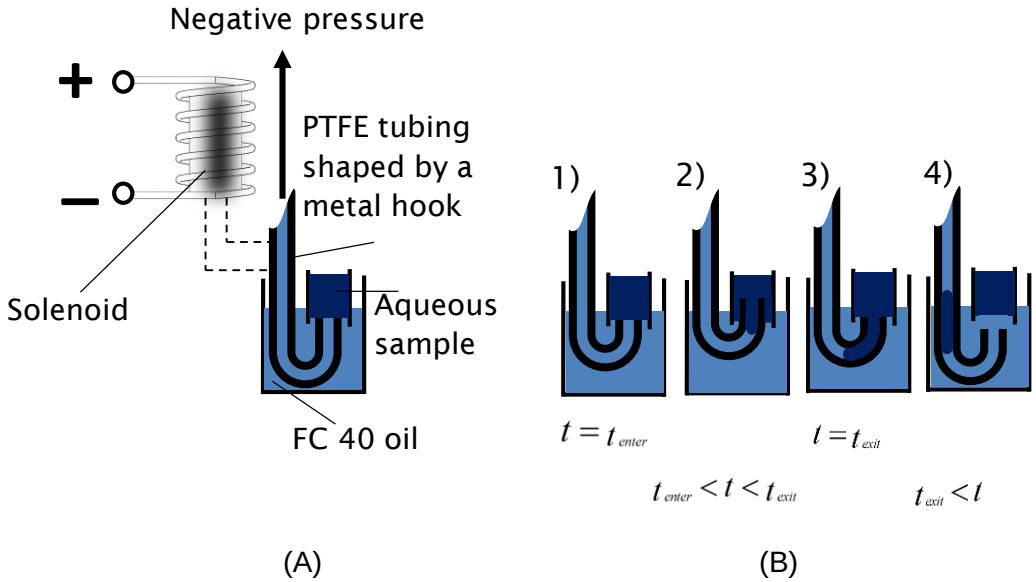

Figure 3.1 Aspiration droplet generation method. (A). Schematic of an aspiration droplet generator. The PTFE tubing inside the metal hook is actuated by a solenoid to be up or down to approach aqueous samples or FC 40 oil. Meanwhile, pumping system is providing negative pressure to aspirate fluids. (B).The schematic processes of forming one complete droplet. 1). At $t = t_{enter}$, PTFE tubing is penetrating the interface between FC40 oil and aqueous sample to enter aqueous sample. 2). during $t_{enter} < t < t_{exit}$, aqueous sample is introduced into PTFE tubing. 3). At $t = t_{exit}$, PTFE tubing is leaving the interface between FC40 oil and aqueous sample. 4).During $t_{exit} < t$, with FC40 oil introduced into PTFE tubing, one complete droplet is formed.

The metal tubing (Coopers Needle Works, Ltd) was carefully bent to be a hook shape with an inner diameter of ~10 mm and a length of ~60 mm to shape the soft PTFE tubing (PM-1214, Upchurch). The metal hook was fixed with the connector which was connected to the solenoid (300-2501280, RS). The connector was designed and fabricated from material (Veroclear™) with a high-resolution 3D printer. The hook was inserted into the connector and fixed by superglue (RS 473-455). The solenoid which is used to actuate the hook with PTFE tubing was attached to the solenoid-stage interface. The interface was also

designed and was fabricated from PMMA material (Acrylic Online) with a CNC mill (LPKF S100). A precise slide (BSP 1025 SL, I.K.O. Nippon Thompson™) was used to link the connector to the solenoid-stage interface. This slide ensures one degree of freedom of the metal hook along the *z* axis and a stroke range of 15 mm. The solenoid-stage interface was attached with the *x-y-z* stage (PT3, travel translation stages, THORLABS™) so that the PTFE tubing with the hook can be easily adjusted to approach the position as desired. The stage working area is 25 mm × 25 mm × 25 mm. The total weight of the whole system is ~2 kg which is light enough to be subject to vibration of the whole system because of the actuation of solenoids.

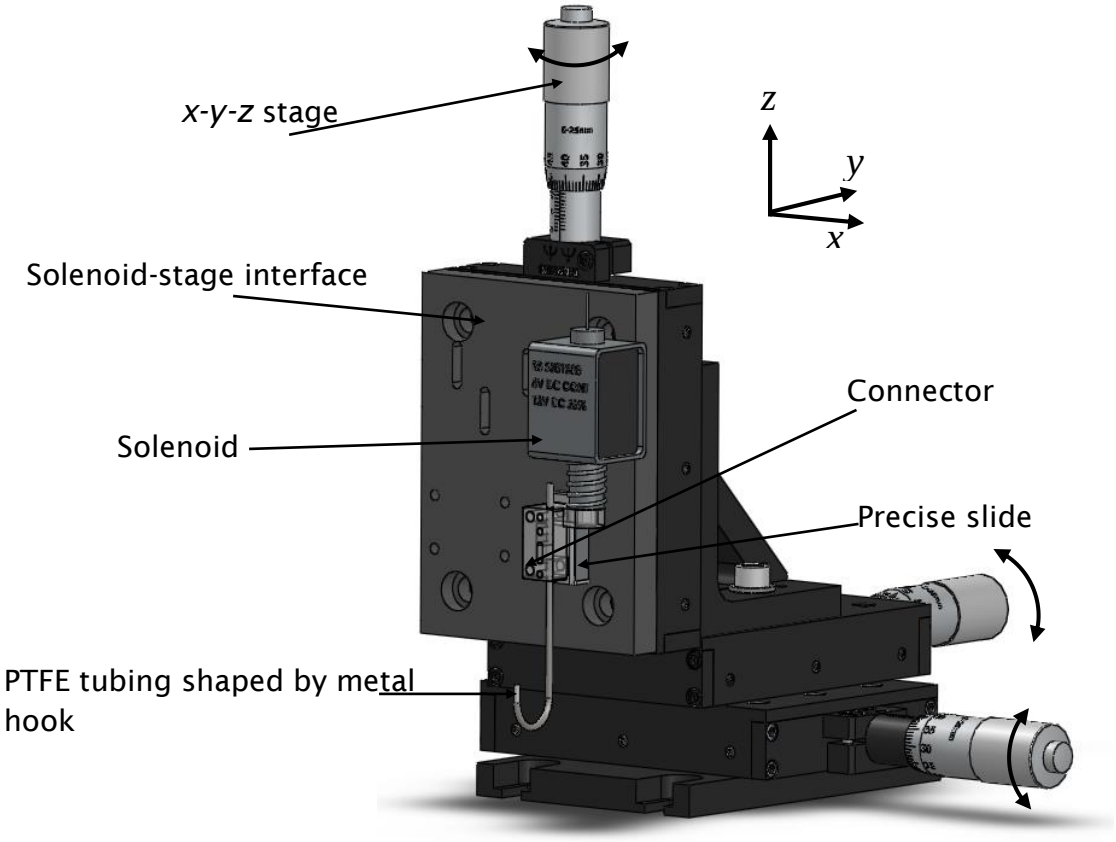

Figure 3. 2 Linear aspiration droplet generator. Four major parts: the x-y-z stage, solenoid, solenoid-stage interface and PTFE tubing shaped by metal hook.

The long hook tends to vibrate during the 'up and down' processes. It was observed during the process of generating droplets that strong vibration would cause the system to generate daughter droplets, as shown in Figure 3.3 (A). The

vibrated PTFE tubing may disturb the interface between the aqueous sample and FC-40 oil in the container and cause generation of daughter droplets. These daughter droplets tend to gather around the interface, especially in the situation where surfactants are present.

A practical method to reduce the daughter droplets accumulated is to frequently resupply the samples after a few generations of droplets. However, this would make the generation procedures less continuous and more importantly sample consuming. Another method is to control the hook vibration which is related with the striking force to stop the plunger. A solenoid is working with three pieces: a metal plunger, a coil wrapped in a solenoid metal, and a spring on the plunger, as shown in Figure 3.4. When the working voltage is ON, the plunger is accelerated upwards by magnetic force, and terminated by the solenoid metal spontaneously. This offers plunger a striking force which is the reason of vibration. In this situation, that striking force is determined by the stroke and the working voltage. Reducing the stroke and lowering working voltage can decrease the striking force and thus the vibration. Figure 3.3 (B) shows the case where low voltage and short stroke were applied. It obviously compares that fewer daughter droplets would be generated with low voltage and short stroke. In this platform, the voltage smaller than 6 V and the stroke ~3 mm were generally used.

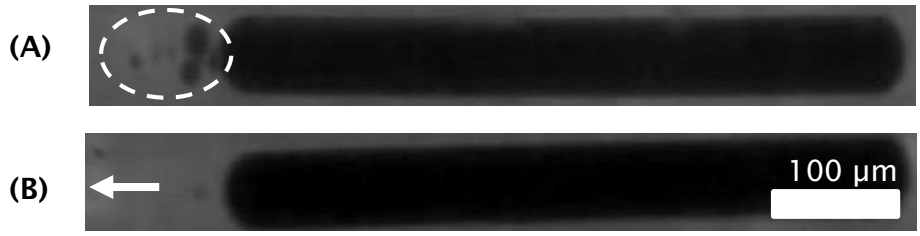

Figure 3.3 Comparisons of two cases. (A) Daughter droplets were observed with high voltage (8 V) and long stroke (~5 mm) after ~30 generation of droplets (B) Fewer daughter droplets were observed with low voltage (6 V) and short stroke (~3 mm). The brightness and contrast were tuned in ImageJ™

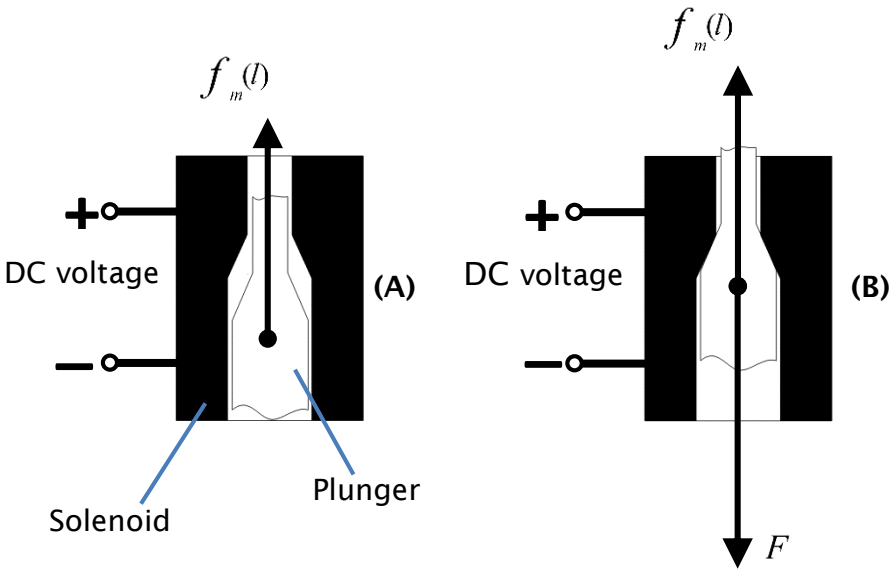

Figure 3.4 The schematic of processes of raising up of plunger in solenoid. (A). Before being stopped, the plunger is accelerated by the magnetic force $f_m(l)$. Both the momentum and are increasing. In this process, the gravity and elastic force is ignored as they are comparably small. (B). The plunger is stopped by the solenoid in a short period Δt . During this process, magnetic force and the striking force are applied on the plunger. The momentum of the plunger is decreasing to be 0 in Δt .

3.3. Generating droplets with a peristaltic pump and an aspiration droplet generator

In this section, the linear droplet generator was interfaced with a peristaltic pump to generate droplets. A peristaltic pump applies rollers or other mechanisms to squeeze the elastic tubing in the inlet and release it into the outlet. In the inlet, the spontaneous restitution of the squeezed parts of the tubing occurs as the rollers move forwards. This process generates a vacuum to aspirate fluids. The squeeze and release can make the flow rate pulsating in both the inlet and in the outlet. This pulsating flow rate can make the size of droplets difficult to control.

Therefore, sizes of droplets under the different combinations of generation frequencies and pulsation frequencies was investigated. Based on this investigation, a method to stabilise the generation of droplets was proposed,

investigated and verified. This method is based on phasing the droplet generation with peristaltic pumping pulsations.

3.3.1. Interfacing an aspiration droplet generator with a peristaltic pump

The pulsating flowrate of a peristaltic pump, *Q(t)*, can be modelled as a periodic wave repeated with frequency f_p. From Equation 3.1, the droplet size is determined by local flow rate, and the immersing time (t_{exit} - t_{enter}). In this aspiration generation method [8], on-demand generation of droplet is often controlled by varying the immersing period. Due to the pulsating flowrate, controllable generation of droplets is difficult to achieve. With consideration of the normalised frequency f_p/f_g (f_g is frequency of droplet generation), there are two cases to be considered: (i) f_p/f_g is a non-integer; (ii) f_p/f_g is an integer. In the *non-integer* case, the flowrate to aspirate aqueous phase and oil phase is different due to the fact that the phase (position) of the flowrate is shifted, and thus the periodically variable sizes of droplets can be observed. It is stated, in this period the number of samples equals to the denominator of the simple fraction format of f_p/f_g. For example, if the generation frequency is 0.15 Hz and the pulsation frequency is 0.2 Hz, one period contains 3 (0.2/0.15=4/3) droplets with variable sizes and the repetition frequency is 0.45 Hz. In the *integer* case, as the aspiration droplet generator is aliasing with the pulsating flowrate which makes the aspiration droplet generator is sampling droplet in the same phase (position) of the flowrate each time, and thus all of the droplets generated are theoretically equal. For example, if f_p=3f_g, the normalised frequency, f_p/f_g, is 3 and sizes of droplets are equal.

To stabilise the droplets generated with a peristaltic pump, one method is to realise the *integer* case by manipulating the generation frequency to be equal to the pulsation frequency. In this section, the generation of droplets in the *non-integer* case and the *integer* case was investigated, compared and verified by characterising the sizes. In the experiment, f_p and f_g were manually pre-calculated and controlled to achieve the required ratio. To improve the generation frequency with fixed pulsation frequency which is related to the flowrate, the integer is normally defined as 1 (f_p= f_g) to synchronise droplet generation with pulsation of peristaltic pump in this project.

3.3.2. Methodology and experimental set-up

A programme was written in MatLab to measure the droplet sizes and to characterise the droplets. To quantify the characterisation, polydispersity of sizes of droplets was introduced, as shown in Equation 3.2, where a is the measured volumetric sizes of a group of droplets.

$$Polydispersity = \frac{s.t.d.(a)}{mean(a)} \qquad \textbf{Equation 3.2}$$

The programme is represented in a flowchart in Figure 3.5.

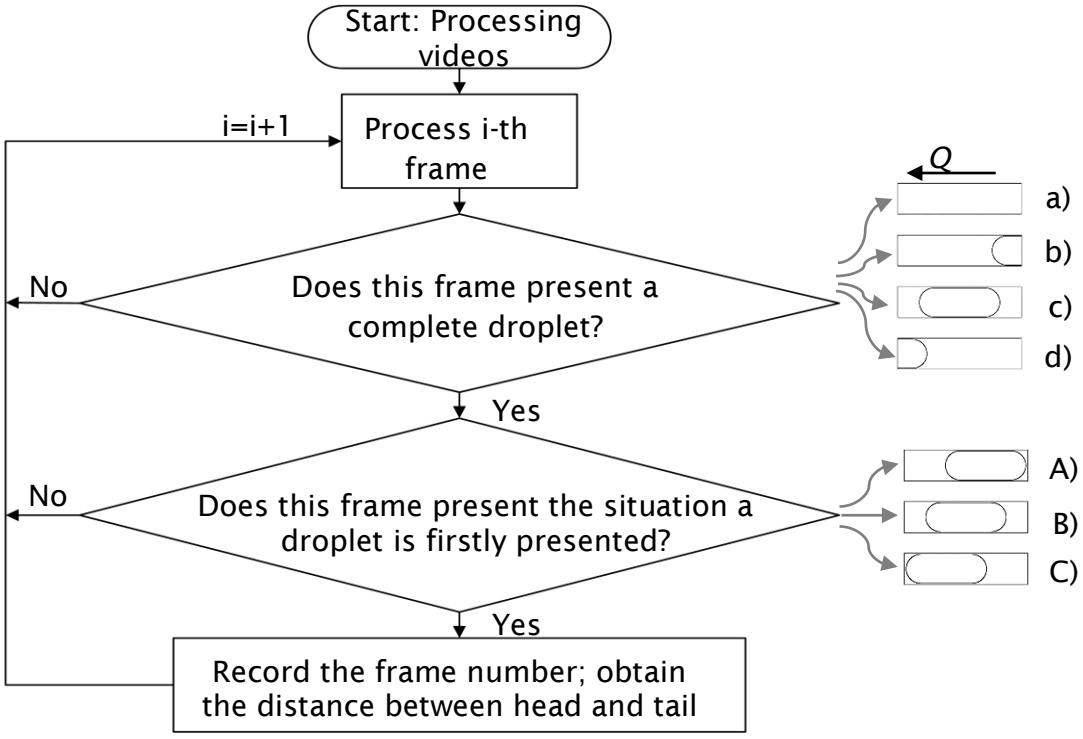

Figure 3.5 Flowchart of the algorithms to calculate sizes of droplets. a) no droplet captured, b) head of droplet captured, c) one complete droplet captured, d) tail of droplet captured. A) Droplet firstly entering the cropping area, B) droplet in between first frame and last frame, C) droplet lastly exiting the cropping area.

It relies on two important algorithms: (i) to track those frames of videos which present a complete droplet as shown in Figure 3.5 c), rather than those which present a half droplet or present no droplet, as shown in Figure 3.5 a), b) and d); (ii) to identify the tracked frame which saw the moment when the complete

droplet is firstly introduced into the area, as shown in Figure 3.5 (A). Prior to exploiting this programme, the recorded videos need to be cropped with ImageJ™ which is java-based imaging processing software, to ensure no more than one complete droplet appears in one single frame. Besides, the cropping areas should be chosen at the places where the positive flow-rate of the droplets is present, and this can effectively avoid the case where one single droplet is identified twice because of that droplet is moving out and back into frame.

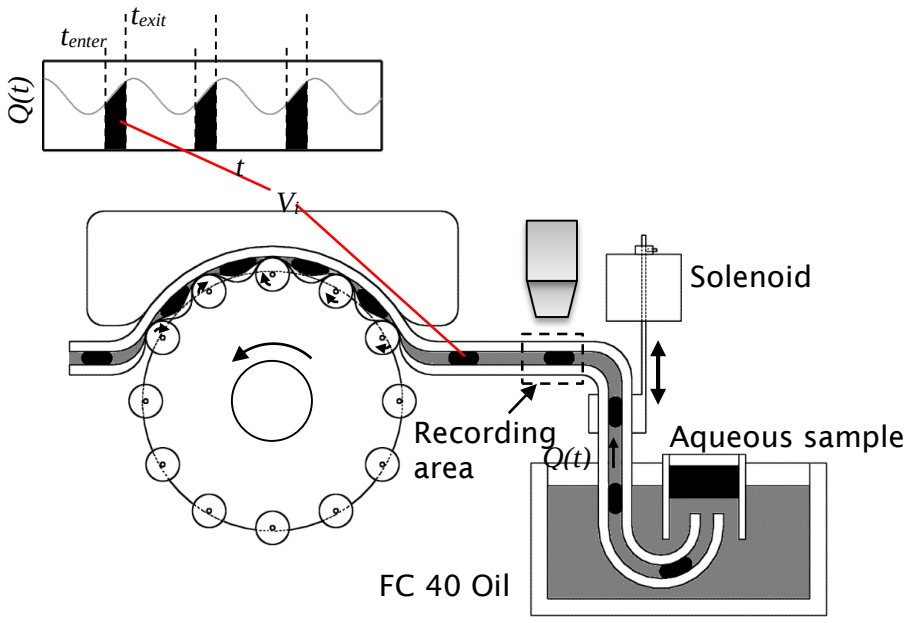

Figure 3.6 Schematic of the experimental set-up of characterizing sizes of droplets. The linear aspiration droplet generator was directly interfaced to the peristaltic pump via PTFE tubing. A high-speed camera mounted on micro-scope with X4 lens.

The experimental set-up was assembled as shown in Figure 3.6. The peristaltic pump (ISM 597, REGLO, ISMATEC) in this experiment was able to have its rotation speed controlled by a built-in speed sensor. To squeeze the peristaltic pump tubing, a commercial cassette which was used to press the tubing was non-transparent making observation of droplets underneath the cassette impossible. The elastic tubing used in this experiment was PVC tubing (PVC Manifold tubing, Watson, Marlow) with I.D. of 0.25 mm. PTFE tubing from the aspiration generator was carefully inserted into PVC tubing to interface aspiration droplet generation into the peristaltic pump. To insert the PTFE tubing, the PVC tubing was first

expanded with metal bar (O.D.0.7 mm). After PTFE tubing was inserted into the PVC tubing, it could be tightly sealed because of the elasticity of the PVC tubing. To reduce the fluidic compliance and fluidic resistance in the system, the length of PVC tubing extended from the pump was around ~30 mm and the PTFE tubing was set to be ~300mm by the restriction of the dimensions of the linear aspiration droplet generator and the peristaltic pump. The high speed camera (Genie™, Teledyne, DALSA) was mounted on the microscope (Hund, Wetzlar) to record droplets in PTFE tubing.

To improve the accuracy of measurement, high-resolution recording of the droplets was required. In this experiment, the objective was X4 and the resolution of the camera set was 640×100. During the experiment, the pulsating flow-rate of peristaltic pump was measured, which was useful to analyse the droplet size change. The measurement of flow rate was based on tracking the boundaries of a droplet. The linear aspiration droplet generator was controlled by a pre-programmed platform based on LabView™ [9]. The resolution of the generation frequency is 0.01 Hz. The pumping pulsation frequency was manually calculated by counting the rollers. The low accuracy of this calculation may cause an error between the empirical results and theoretical results.

3.3.3. Results and discussion

In this experiment, to achieve the *non-integer* conditions, the pulsation frequency was fixed at 0.2 Hz by manual calculation and the generation frequency was changed between 0.19 Hz, 0.15 Hz and 0.13 Hz. In each measurement, the volume of samples and oil was kept the same. Each measurement contained at least 100 droplets and was repeated 3 times.

Figure 3.7 illustrates examples of the volumetric sizes of droplet with the three frequencies. In the droplet generation with frequency 0.19 Hz (Figure 3.7 (A)), the mean droplet size was ~20 nL, the biggest droplet size was ~31 nL and the smallest droplet size is ~9 nL. The volumetric droplet sizes showed a periodic pattern as highlighted with *dashed lines*. In each period, there were 19 droplets. This parameter shows an agreement with the statement in *non-integer* case: the number of droplets in each period equals to the denominator of the simple fraction format of f_p/f_g (0.2 Hz/0.19 Hz= 20/19).

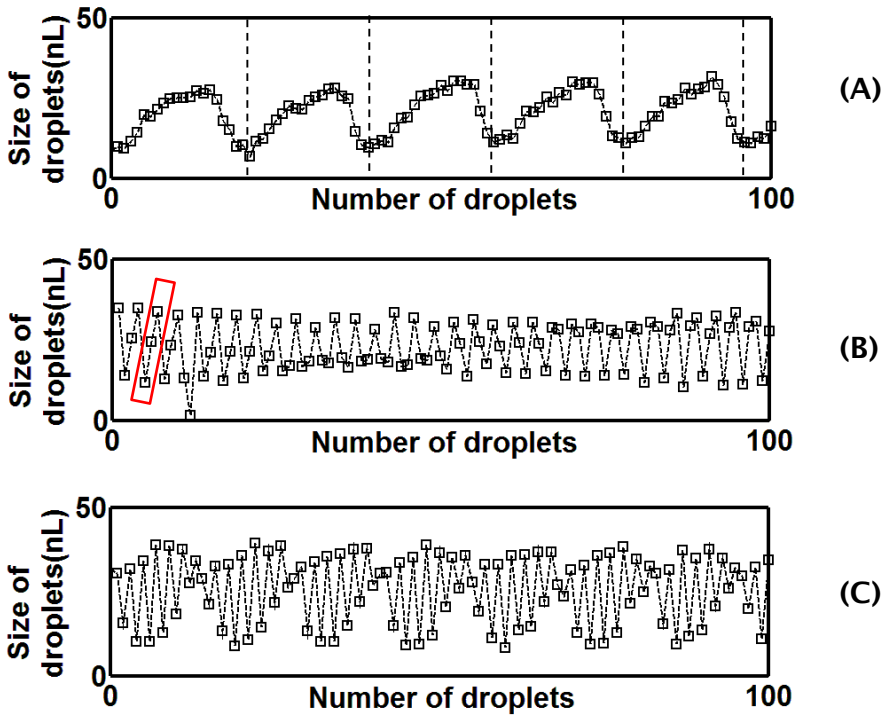

Figure 3.7 The volumetric droplet sizes with different droplet generation and a fixed pulsation frequency 0.2 Hz. (A). The volumetric droplet sizes with generation frequency 0.19 Hz. Periodic pattern was observed which contained 19 droplets. (B).The volumetric droplet sizes with generation frequency 0.15 Hz. (C). The volumetric droplet sizes with generation frequency 0.13 Hz. The approximated same droplet sizes were repeated in every ~13 droplets.

Figure 3.7 (B) presents the results of droplet sizes with a generation frequency of 0.15 Hz. The mean droplet size was ~25 nL. At this frequency, the periodic pattern was clearly observed in the first 20 droplets. Each period contains 3 droplets with the small size in the first position, medium size in the second position and big size in the third position, which are highlighted with a *red rectangle*. After ~40 droplets had been generated, the second droplet in each period became the smallest while the first droplet in the period has the medium size among the three droplets. This change may be arisen from the error between calculated frequency and experimental frequency which is different from 0.15 Hz. However, the third droplet size did not comparably change much as the first one and second one did. The third droplet changed its size from ~36 nL to ~34 nL while the first one and the second one change their sizes from ~13 nL to ~35 nL and from 25 nL to 11 nL respectively. To further understand this, the pulsating flow rate of the peristaltic pump was measured, and the pulsation wave was analysed and shown in Figure 3.8. In one period, flow rate took 1.38

seconds from the peak to the bottom and 3.62 seconds from the bottom to the peak. On the left side and the right side of the bottom, the pattern was comparably sharp. The left side of the peak showed a comparably smooth pattern. From the observation where the first droplet and the second droplet size dramatically changed and the third droplets comparably changed less, it was analysed that phases of the first droplet and the second droplet were around the bottom and the third droplet was around the peak. From the observation where the first droplet and the third droplet were increasing and the second droplet was decreasing, it could be deduced that: (i) the phase of first droplet was located on the left side of the bottom and was shifted to the left in the next period (Figure 3.8); (ii) the phase of second droplet was located on the right side of the bottom and was shifted to the left in the next period; (iii) the phase of the third droplet was located on the left side of the peak and was shifted to the left in the next period. As the phase of generation tent to shift to the left in next generation of droplet, the pulsation frequency used in the experiment was slightly smaller than 0.2 Hz.

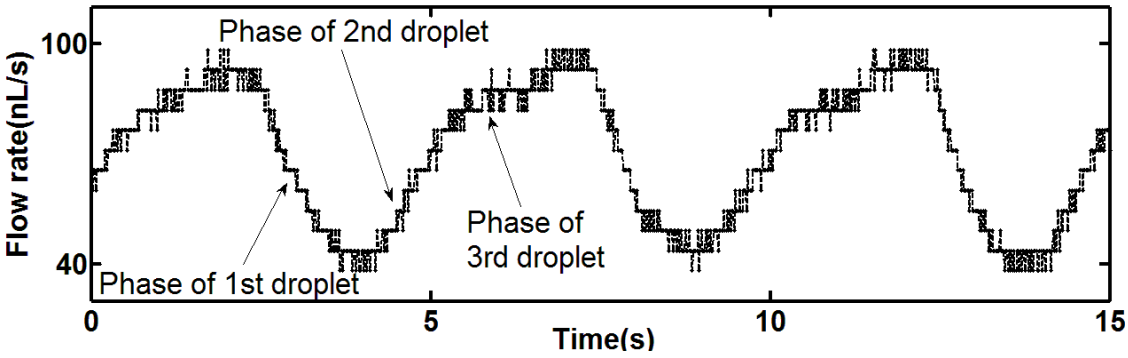

Figure 3.8 Volumetric flow rate of fluids in the inlet part of peristaltic pumping system. Combining the analyses of the change of droplets in Figure 3.6 (B), the approximate position of the phases of the three droplets were marked with arrows.

Figure 3.7 (C) demonstrates the size of droplets generated with frequency 0.13 Hz. The mean droplet size is ~25 nL, the biggest droplet size is ~40 nL and the smallest one is ~8 nL. The plot also shows periodic patterns which contains 13 droplets. Due to phase shift caused by the calculation error, it is observed that the first droplet size in each period was decreasing, while the size of second droplet was increasing in each period. This error made the droplet size not exactly repeated in every 13 droplets.

Figure 3.9 demonstrates the result of the size of droplets generated with 0.2 Hz, which is in *integer* case where pulsation frequency equals generation frequency. The measurement was performed 3 times with at least 100 droplets. Among 100 droplets, periodic change of droplets was not observed. The droplet size was comparably uniform with those observed in generation frequency 0.13 Hz, 0.15 Hz and 0.19 Hz. However, the decreasing trend and increasing trend were observed which was coming from the phase shift due to the error calculated as observed before. The polydispersity of the size of those droplets generated with 0.13 Hz, 0.15 Hz, 0.19 Hz and 0.2 Hz was presented in Figure 3.10. The droplets generated with 0.13 Hz had the biggest polydispersity 41% while the droplets generated with 0.2 Hz had the smallest polydispersity 21%. With the generation frequency approaching the pulsation frequency ~0.2 Hz (which should be modified), the polydispersity was decreasing. This verifies the proposed method in the integer case where the generation frequency equals the pulsation frequency, the droplet sizes are theoretically the same. However, technically, the generation frequency cannot equal the pulsation frequency from this less-accurate frequency calculation method. This suggests that an accurate calculation method of pulsation frequency is necessary in decreasing the

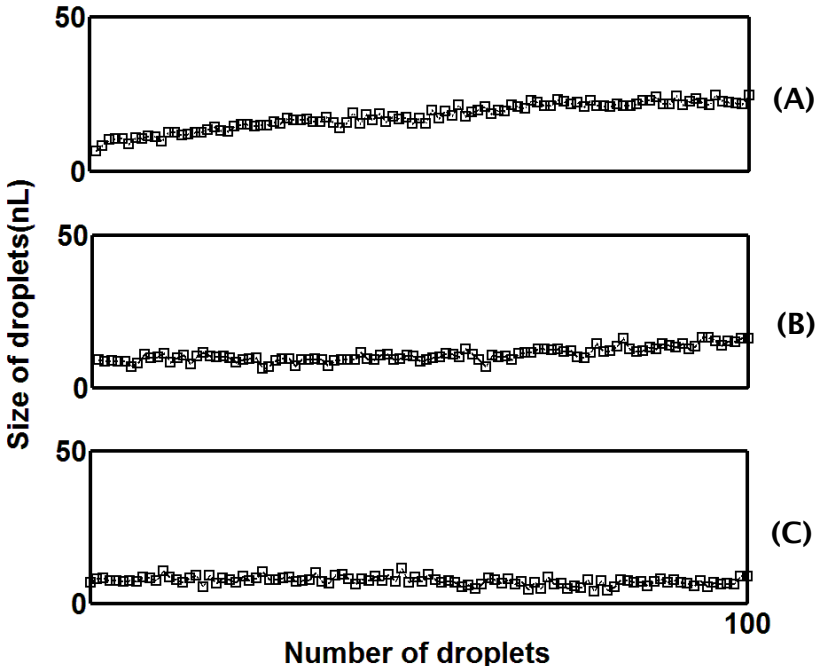

Figure 3.9 The volumetric droplet sizes with generation frequency 0.2 Hz and pulsation frequency 0.2 Hz. Periodic pattern was not observed within 100 droplets, but an increasing trend and a decreasing trend were observed in (A), (B) and (C) respectively.

polydispersity of sizes of the droplets.

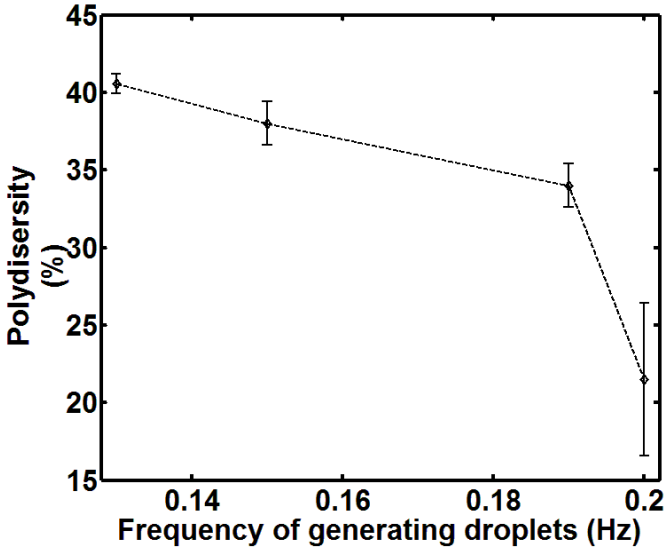

Figure 3.10 Polydispersity of sizes of droplets generated in different frequencies, 0.13 Hz, 0.15 Hz, 0.19 Hz and 0.2 Hz, with fixed pulsation frequency ~0.2 Hz.

3.3.4. Summary

In this section, the two cases: f_p/f_g is a non-integer; f_p/f_g is an integer, were investigated. Through the investigation, a method of stabilising sizes of droplets was proposed and verified. To characterise sizes of droplets, methodologies of measuring volumetric sizes of droplets and volumetric flow rate were established. The methodologies will be useful in further measurement.

In the non-integer case, periodic patterns were observed. Each period contains the calculated droplets which shows an agreement with the statement. In the integer case, the periodic pattern was not observed and the polydispersity of droplet sizes was dramatically smaller than the experimental results in non-integer case, although a decreasing trend or an increasing trend was observed. However, during the experiment, the error from calculation of frequencies would affect this method and increased the polydispersity of the size of generated droplets. Moreover, the calculation of pulsation frequencies is laborious. Based on the observation and results, it was suggested that a more accurate-practical

frequency calculation method was necessary to further decrease the polydispersity of sizes of droplets.

3.4 Investigation of the percentage of survived droplets after peristaltic pump

3.4.1. Introduction

Along with dynamics of droplet aspiration investigated in section 3.3, another key consideration in the proposed continuous sampling method with a peristaltic pumping system is that the droplets might be squashed by the rollers when the preformed droplets are introduced into the peristaltic pump.

This section specifically investigates and quantifies the possibility of droplet survival when they are introduced into a peristaltic pump. This preliminary investigation provides evidence of the importance of devising a method to safely pass droplets through the peristaltic pump.

3.4.2. Methodology and experimental set-up

The possibility of droplet survival is characterised by calculating the percentage of those with complete integrity at the outlet of the peristaltic pump against the total number generated. To realise a systematic investigation, a series of droplets with a range of sizes and distances between two adjacent droplets (DBTAD) were required. As the droplets from the aspiration droplet generator are less controllable because of frequency calculation errors in the peristaltic pumping as shown in last section, a T-junction generation platform with two syringe pumps was applied (Figure 3.11). Different sizes of droplets and different DBTADs were achieved by adjusting the ratios between the flow-rate of the aqueous phases and that of the oil phases. There are three key parts in the experimental set-up: a droplet generation system to provide defined droplets which includes a PDMS T-junction chip and two syringe pumps, a peristaltic pump (ISM 597, REGLO, ISMATEC), and a vertical connection adaptor. The adaptor is used to adapt the flowrate difference between peristaltic pump and the syringe pumps. The connection adaptor is made from a piece with 50 mm length of PVC tubing whose inner diameter is 0.25 mm. The connection adaptor was connected with three parts: the peristaltic pump, syringe pumping system and the open atmosphere via the oil phases. It is vertically oriented to ensure

that droplets are moving upwards into the chamber with the assistance of the density difference between aqueous phases and oil phases, rather than into side channel, especially in the case when the peristaltic pumping flow-rate is smaller than that of syringe pumping system. The width ratio of T-junction chip was

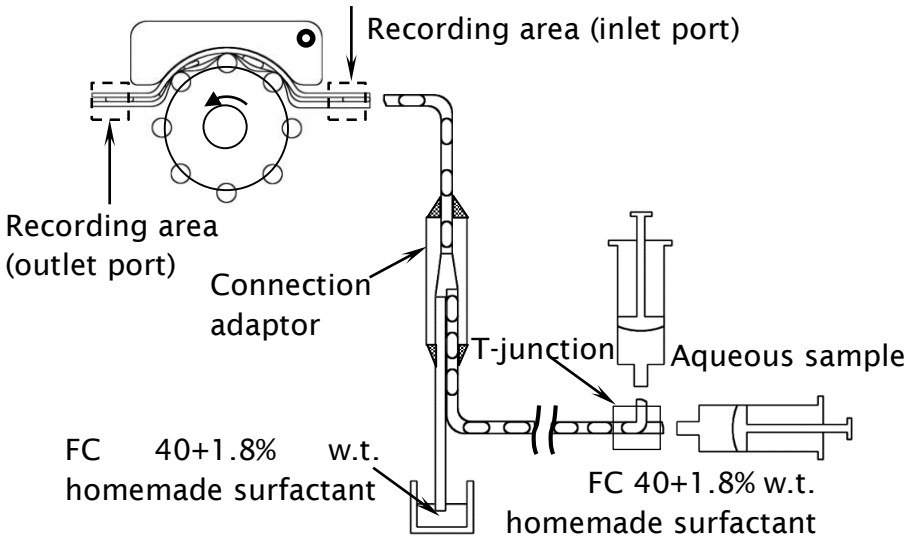

Figure 3. 11 Experimental set-up which includes three key parts. Droplets are generated with a T-junction, which are driven by two syringe pumps with one for aqueous sample and the other for oil phase. These droplets are further delivered to the peristaltic pumping system through a connection adaptor which is interfaced with atmosphere via oil phases

fixed to be 1:2 with the width of channel for aqueous phases 0.2 mm and that for oil phases 0.4 mm, and the chip was made of PDMS following the procedures shown in Figure 3.12.

As the later discussion in Section 3.5.3, a better surface property of PVC tubing can be obtained by adding 1.8 w.t % homemade surfactant / FC 40 oil. To

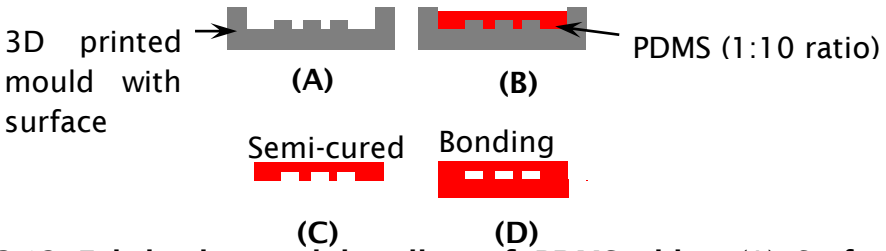

Figure 3.12 Fabrication and bonding of PDMS chips (A) Surface treatment is applied to make the surface of the 3D printed mold hydrophobic with Duxback (Duxcoat™). (B) Mixing PDMS reagent and base at 1:10 ratio and pouring the thoroughly mixed PDMS into 3D printed mold. Desiccating the PDMS. (C) Curing the PDMS chip for 30 minutes at 65 °C to make it semi-cured (D) Bonding the semi-cured chips with another semi-cure flat PDMS and curing them for 2 hours at 65 °C.

measure the sizes of droplets, the videos of droplets in the inlet and outlet were recorded respectively with a micro-camera (Figure 3.11).

3.4.3. Results

During the experiment, the flow-rates of the peristaltic pump and that of the syringe pumps were varied following table 3.1. Three mean droplet sizes were obtained 50 nL, 80 nL and 100 nL under three different flow-rate ratios, (20 µL/ min : 2.5 µL/ min), (20 µL/ min : 5.5 µL/ min) and (20 µL/ min : 8.5 µL/ min).

Table 3.1 Table of flowrates for peristaltic pumping system and syringe pumping system

Mean flow-rate of peristaltic pump	Flow-rate ratio (oil phase : aqueous phase)
15 µL/ min	20 µL/ min : 2.5 µL/ min 20 µL/ min : 5.5 µL/ min 20 µL/ min : 8.5 µL/ min
20 µL/ min	
25 µL/ min	
30 µL/ min	
35 µL/ min	

Figure 3.13 presents an example of the comparison of sizes of droplets before they were introduced into the peristaltic pump and after they exited from the peristaltic pump, with different DBTADs ranging from~1.7 mm to 5.7 mm. In this comparison, the desired droplet size was 80 nL and each test contained 100 droplets. Three statuses of droplets were observed: droplets safely passed, droplets were split and droplets were merged. The split of droplets was arisen from that the squash of peristaltic rollers while merging of droplets was induced by the inference of pulsations particularly in the case where droplets are close

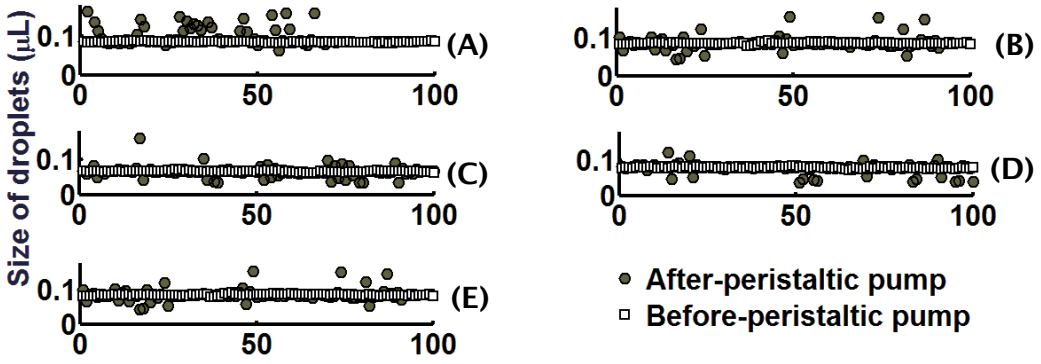

Figure 3.13 Comparison of sizes 80nL of droplets before the peristaltic pump and after peristaltic pump, with different droplet distances, (A) ~1.7 mm, (B) ~2.7 mm, (C) ~3.7 mm, (D) ~4.7 mm, and (E) ~5.7 mm.

to each other. It was observed that the number of merged and split droplets decreased with the increase of DBTADs while survived droplets was increasing with the increase of DBTADs.

Figure 3.14 shows survival possibility of droplets with a series of sizes, 50 nL, 80 nL and 100 nL. It quantified the relationships between the possibility of survived droplets, DBTAD, and sizes of droplets. It also shows that the smaller droplets has higher possibility of survival than those with bigger sizes. This is due to the fact that a droplet of this kind has less chance of being involved with the area of the PVC tubing that is pressed by the peristaltic pump rollers.

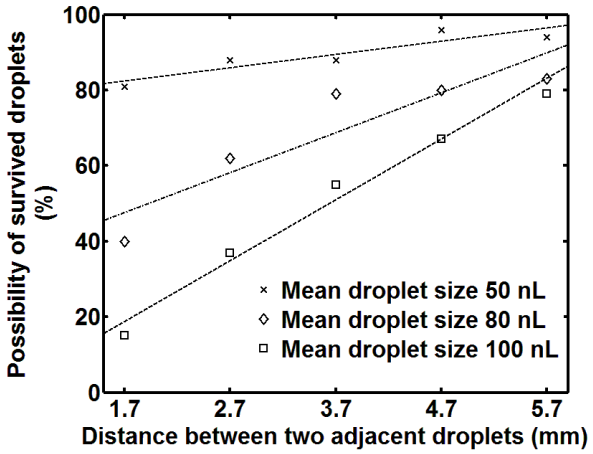

Figure 3.14 Percentage of possibility of survived droplets.

3.4.4. Discussions and summary

In this section, an experiment was designed to preliminarily investigate droplets passing the peristaltic pump. To perform the experiment, a controllable experimental set-up was built. The investigation showed that droplets with smaller sizes and bigger DBTADs tended to have higher possibilities of survival, but it is difficult to achieve 100 % survival. This investigation suggests the necessity to develop a method to guarantee 100 % survival. To realise this, a function or method to accurately position these droplets in between the rollers to avoid squashing, and to control DBTAD to avoid merging, is necessary.

Interestingly, the method synchronising generation of the aspiration droplet generator with the pulsation can also control size of oil plugs between droplets, as it was investigated in the *integer case* in section 3.3. Besides, if the phase change of droplets from the aspiration droplet generator to inlet of peristaltic

pump can be tolerated, this method may also be able to synchronise delivery of droplets with the squashing whose phase is the same with that of pulsation. With alignment of the two phases, these droplets can accurately be positioned in the gap between the peristaltic pump rollers. Instead of squashing aqueous droplets, the rollers squash the oil plugs. This operation is similar to that of a synchronisation gear [13] for synchronising triggering of machine gun with the rotation of the propeller in an aircraft to avoid bullets striking the propeller.

3.5. A Feedback system to synchronise droplet generation with pumping pulsations

In section 3.3 and section 3.4, it was shown that pulsating flows can affect generation of droplets from the aspiration generator and the integrities of droplets are challenged in peristaltic pumping system. It was suggested to achieve *non-integer* case to stabilise the generation and secure the integrities of droplets. This section engineered a digital feedback control system to directly synchronise the droplet generation with the pumping pulsations with a phase alignment structure, and thus ensures the generation remains in phase with the pulsation. With the engineered system, this section demonstrated and verified that this method is able to both stabilise the sizes of droplets and secure survival of droplets passing through the pump. The results show that this system can achieve the two functions, and thus eliminates the need for laborious calculations of generation frequency and pulsation frequency.

3.5.1. Design of the synchronisation system

The overview of the feedback control system integrated with the pumping and generating system is schematically shown in Figure 3.15 (A). The feedback system contains an electrical circuit, pillars mounted on the peristaltic pump and sensor frame which is used to tune the alignment of generation phase with pulsation phase. Figure 3.15 (B) describes the schematic processes of signal transforming. Based on this, an electrical system was built up as shown in Figure 3.16 (A) which includes an Arduino™ UNO controller, coded with sketch™ platform which is based on the C++ language, an infrared sensor and the solenoid for the aspiration droplet generator. Data transfer with a computer was realised through serial communication.

The working principle is that: once the pillars (12 pillars) which are rotating with the peristaltic pump head passes the infrared sensor, a pulse is sent to the microcontroller spontaneously and a pulse with width, $\Delta t_{d,l}$, is outputted to trigger the aspiration droplet generator to complete a droplet. In this way, the generation is synchronised with the pulsation and the volumetric sizes of droplets can be on-demanded by varying the output width, $\Delta t_{d,l}$,. The alignment of phase of generation with that of pulsation was tuned by rotating the relative position of the infrared sensor to the pillars, which is scaled by the relative angle A°, as shown in Figure 3.15 (B). The algorithm of generating N_d droplets with size $V_l \sim \Delta t_{d,l}$, is shown in Figure 3.16 (B).

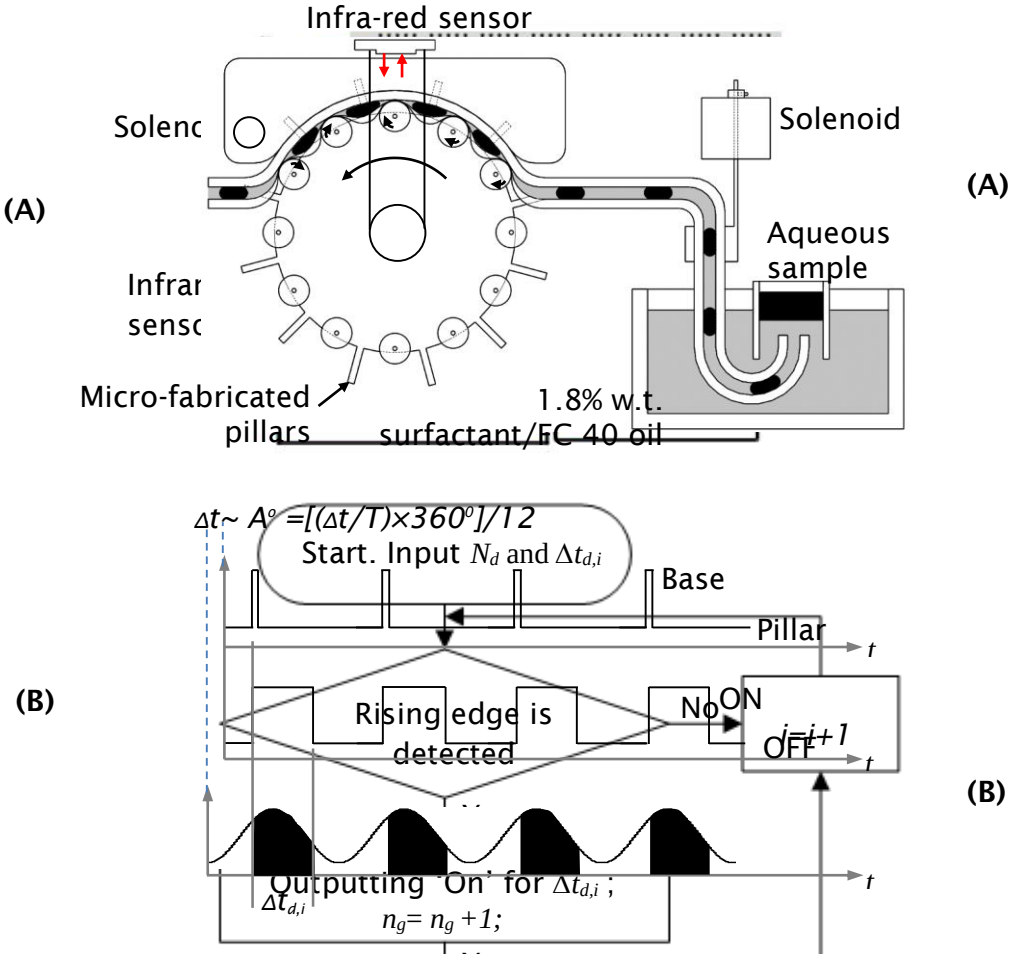

Figure 3.15 Design of feedback system to in-phase generation with pulsation (A) Schematic of the feedback system integrated with aspiration droplet generator. There are 12 pillars evenly mounted on the peristaltic pump head. (B) Schematic of processes of signals transforming. (i) The infra-red sensor detects pillars and base. (ii) Output signal for the linear aspiration generator. The starting of 'ON' is directly in phase with the pillar detection and duration is $\Delta t_{d,i}$.(iii) schematic of pulsating flow-rate in inlet of a peristaltic pump. (i) and (ii) are in the same phase. (iii) and (ii) are in the phase with a difference $\Delta t/T$, where T is the pulsation period.

Figure 3.16 (A) Electrical circuit of the feedback control system, which includes a microcontroller, an infrared sensor, a solenoid from aspiration droplet generator, a transistor array to amplify voltage and power supply. (B) Flowchart of algorithm to digital feedback system.

A sensor with precise resolution should is necessary to improve phase accuracy. The sensor selected here was an infrared sensor (QTR-1RC, Pololu™) in terms of its small size, low cost, easy mounting and high sensitivity. A comparison of sensors is listed in Table 3.2. This infrared sensor is sensitive to rough surface. Here, non-transparent red PMMA materials were used to make the pillars mounted on the peristaltic pump. There were 12 pillars in total and the key

dimension is shown in Figure 3.17 (A). The pillars were fabricated with a CNC micromill (ProtoMat, LPKF™).

Table 3. 2 Comparisons between hall-effect sensor and infrared sensor

Sensors	Sensitivity	Voltage	Size (mm^3)	Sensing objects	Cost
Hall effect sensor	High precision	2.7 ~18 V	4×1.5×3.3	Magnetic obstacles	£0.856 (SSO-3)
Infrared sensor	High precision	5 V	7×12×2.5	Non-transparent obstacles	£1.99 (OTR-1RC)

To measure the accuracy of fabrication and mounting, the pillars fixed on the peristaltic pump were calibrated with the infrared sensor by measuring the output signal. The infrared sensor was mounted with a distance of ~2 mm from the pillars. The data was collected through the serial communication port. The results were calculated with this equation: $[t_m(i)- t_{trend}(i)]\times100\%/T$, where $t_m(i)- t_{trend}(i)$ denotes the residual between the measured time of i^{th} pillar and i^{th} point on the

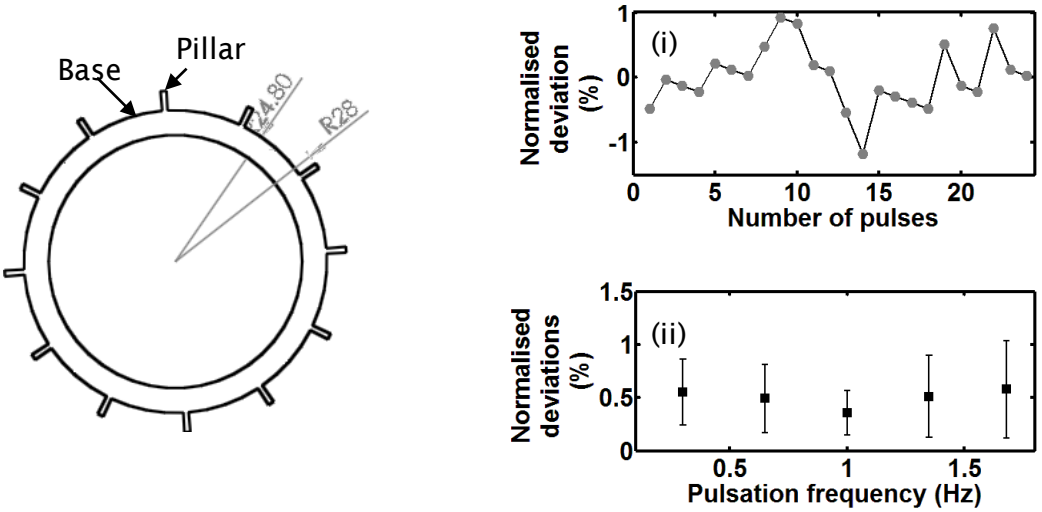

Figure 3.17 (A) The design of pillars with non-transparent PMMA. The height of the pillar is 3.2 mm. This height would ensure that the sensor was able to detect the difference between the pillars and the other parts. **(B) The results to show the measurement of signal from the pillars.** (i) Details the results from the pulsation with frequency of 0.65 Hz. (ii) quantifies the normalized deviation of fabrication with a series of different pulsation frequency 0.3 Hz, 0.65 Hz, 1 Hz, 1.38 Hz and 1.68 Hz

linear trend of total time, and T denotes the period. Figure 3.17 (B) presents the result that the difference was less than 0.7 % which was acceptable for this platform.

3.5.3. Fabrication of cassettes and assembly of the integrated system

To observe and monitor the delivery of droplets inside the peristaltic pump, a transparent cassette was designed and fabricated. Besides the transparency, the cassette was also designed to provide high pressure to compress the PVC tubing. This integrated platform may be used for multiple-channel droplet generation. With these considerations, a sandwich structure with three channels was designed (Figure 3.18). The design was composed of two key components: the inner part and the frame. The inner part was sandwiched by the frame as whole component which was fixed with the peristaltic pump. In the inner part, three tubing guiders were designed to guide the PVC tubing in a direction perpendicular to rollers of the peristaltic pump. The frame was designed to hold

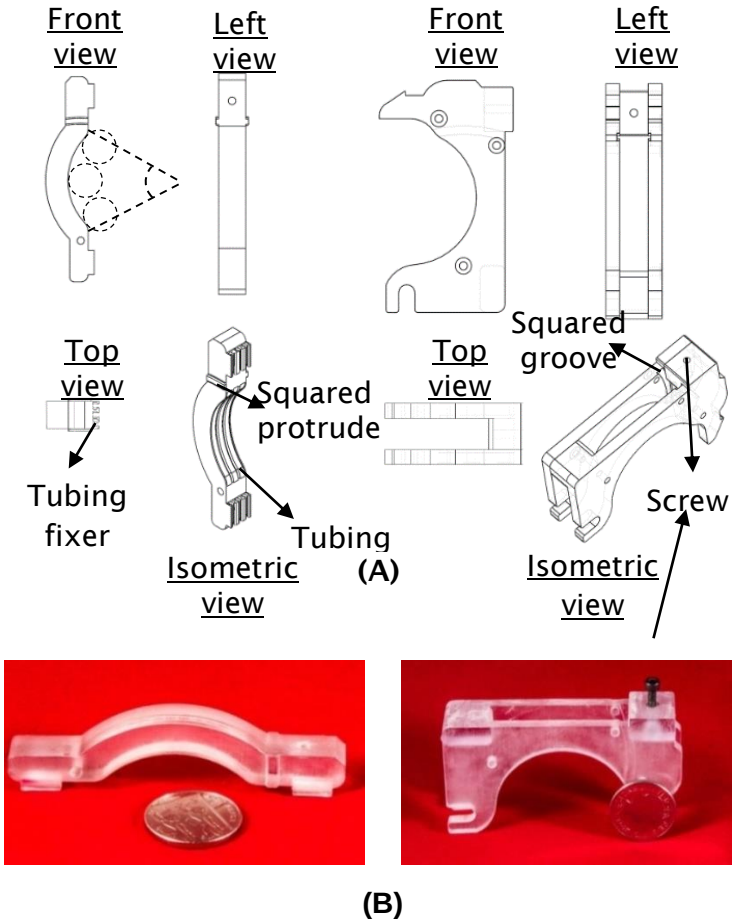

Figure 3.18 Design and fabrication of the transparent and multiple-channel cassette. (A) The design of inner part and the frame. (B) 3D printed inner part and frame.

the inner part tightly and to balance the inner part to be parallel to the peristaltic pump rollers. This was realised with the design of a square-protrude groove structure highlighted in Figure 3.19 to force inner part to be perpendicular to the frame. The squeezing pressure applied on the PVC tubing was able to be tuned by an adjustable screw on the frame. The inner part and frame were fabricated from Veroclear™ material with a 3D printer. This material is transparent. After the 3D printing, the inner part was polished with *wet and dry* sanding paper to ensure a better transparency. The total assembly is shown in Figure 3.19.

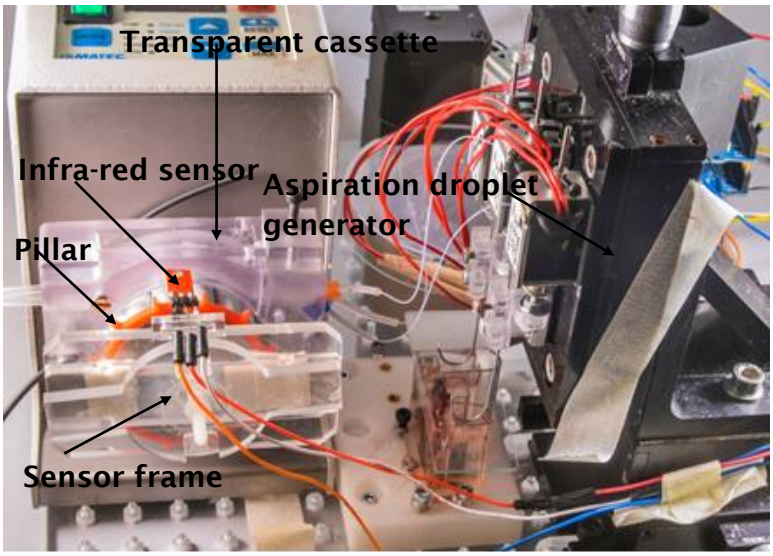

Figure 3.19 The overview of the feedback system installed on the peristaltic pump. Key parts: peristaltic pump, pillars mounted on the head, sensor frame, transparent cassette, and linear aspiration droplet generator.

3.5.4. Characterising the size of droplets

With the feedback system to synchronise the generation with pulsation, the polydispersity of volumetric sizes of droplets was measured to characterise the stabilisation. Droplets were generated at different frequencies, ~0.3 Hz, ~0.65 Hz, ~1 Hz, ~1.38 Hz and ~1.68 Hz. At each frequency, the measurement was performed 3 times and each measurement contained at least 150 droplets. Notably, the maximum size of droplets generated is ~200 nL. This is limited by the volume of fluids occluded between the adjacent rollers. A droplet with a size smaller than that volume could avoid being squashed by the rollers with proper adjustment of the phase difference. The size of droplets generated in this experiment was controlled between 20 nL and 30 nL by varying the immersing

period. Thus, the volume of oil plugs is at least ~150 nL. To block the back flow of peristaltic pumping, the cassette was tightly pressed with adjustment of the tuneable screws. Figure 3.20 presents the results of volumetric droplet sizes. Compared with trend of the sizes of droplet in Figure 3.9, the trend of sizes of droplets in the feedback system was more stable, as shown in the top-left of plots in Figure 3.20. This shows the feedback control system was able to accurately synchronise droplet generation phase with peristaltic pump pulsation phase, without laborious calculation of frequencies.

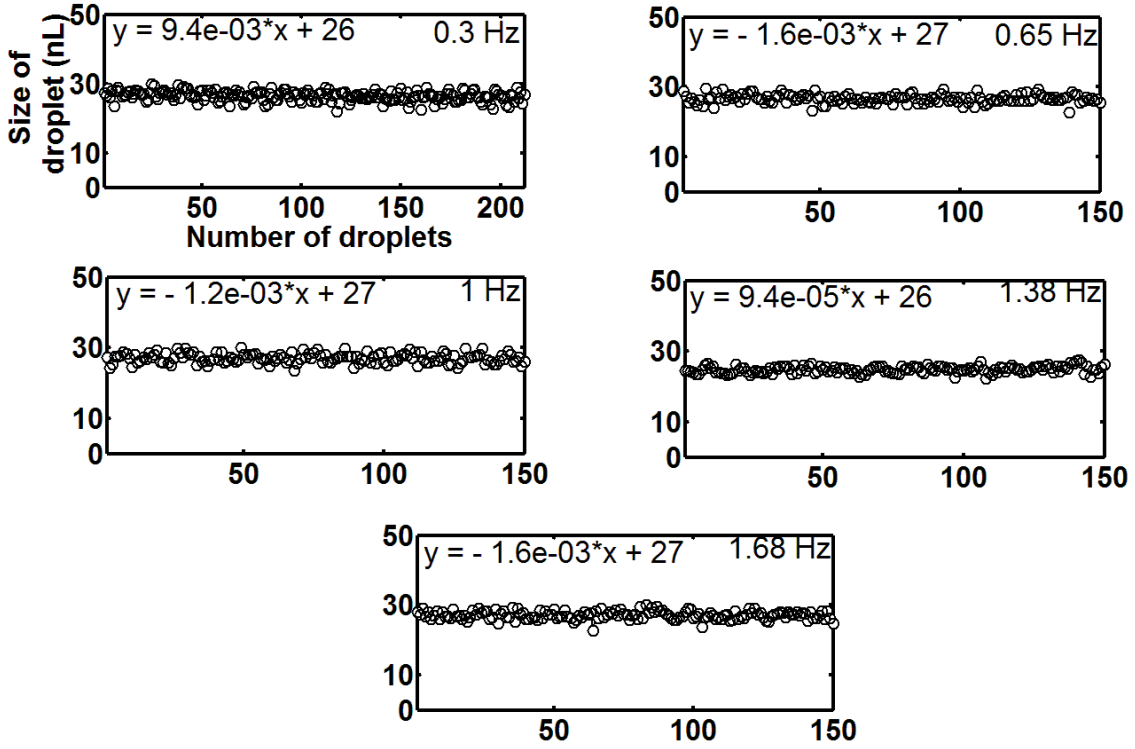

Figure 3.20 Volumetric droplet sizes at 0.3 Hz, 0.65 Hz, 1 Hz, 1.38 Hz and 1.68 Hz. The 1st linear trend of sizes of droplets (nL) to number of droplets, was given at the top-left corner to show stable trend of the droplet sizes.

Figure 3.21 (A) presents the relationship between generation frequency and polydispersity of droplet sizes. The biggest polydispersity was 6.3 % while the smallest polydispersity was 4.1 %. The polydispersity was decreasing while the generation frequency was increasing. During the experiment, stepwise variations in the speed of the peristaltic pump were observed. This stepwise speed variation may come from the low resolution of the speed sensor or the low fractions of the gear box, whose frequencies are higher than that of pulsation. It affected the speed of rollers and further made the pumping flow rate noisy. The noisy flow rate could affect droplet generation and induce variations of droplet sizes. This decreasing-increasing relationship was believed

to be due to the noisy flow rate. At higher frequency, the noise in the flowrate would be attenuated and this can decrease the polydispersity because of the compliance effect.

As expected, the polydispersity of these droplets generated with the feedback system was dramatically reduced compared with that of those generated without a feedback system. Figure 3.21 (B) detailed the improvement from the aforementioned system with manual calculations in section 3.3 to the feedback system.

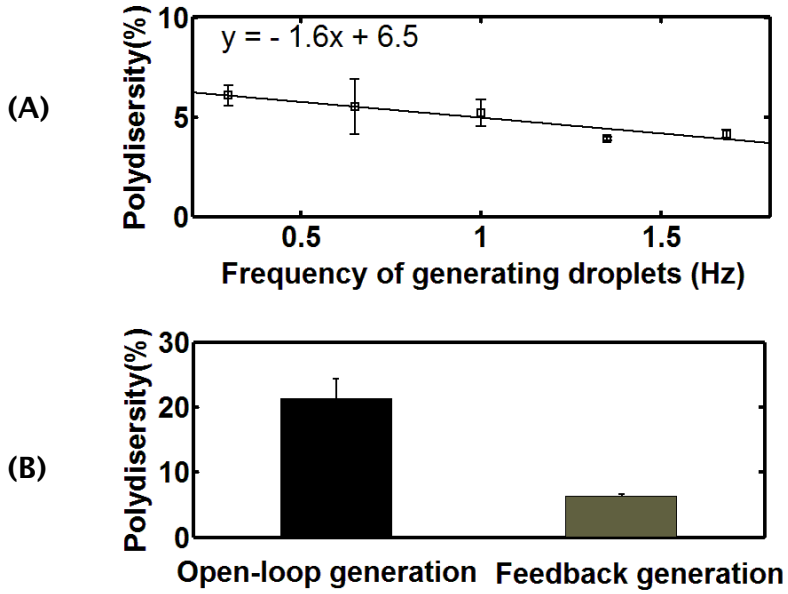

Figure 3.21 (A) The polydispersity of droplet sizes generated at different frequencies is less than 6.3 %. The frequencies are 0.3 Hz, 0.65 Hz, 1 Hz, 1.38 Hz, and 1.68 Hz. The trend is 1st order linear. (B) Comparison between the best measurement of polydispersity in non-feedback generation and the worst measurement of that in feedback generation.

3.5.5. Droplets passing though the rollers of peristaltic pump

When the droplets were introduced into the peristaltic pump, it was observed that the aqueous droplets would stick on the surface of the PVC tubing and break up after they entered the peristaltic pump. This break-up of droplets was due to the poor surface property of the PVC tubing. To improve the hydrophobicity of PVC tubing, Duxback™ was used to coat the surface. With the coated PVC tubing, it was observed that the droplets would keep the integrity in the beginning part of PVC tubing which was not squeezed by the rollers but broke up again in the

squeezed part. This indicates the squeeze from the rollers may destroy the coating and further made the surface less hydrophobic. Instead of employing hydrophobic surface, here surfactant is added into the oil phase. The surfactant molecules have one hydrophilic end to attach to phase, and one hydrophobic end that can hold oil molecules. This ensure a thin film is coated around the aqueous droplets to prevent the contact with PVC surface.

To ensure a series of droplets pass the peristaltic pump, the alignment of phase of delivery of droplets with that of pulsation is needed. Figure 3.23 presents the protocols to generate and to deliver a series of droplets. It was noticed later on changing the distance between peristaltic pump and the aspiration generator can also be used to align the phases.

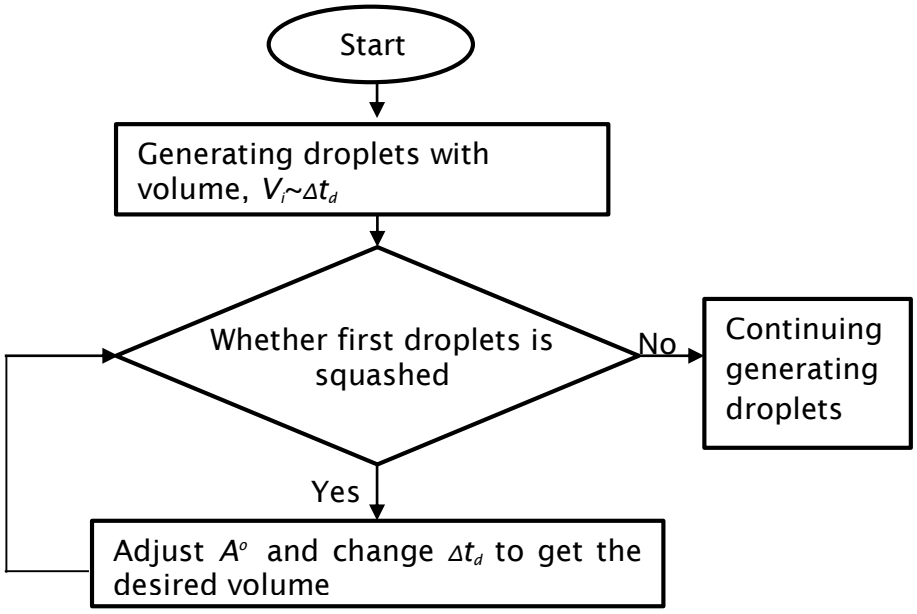

Figure 3.22 Protocols of generating droplets and delivering droplets.

To observe the droplets passing the peristaltic pump, an experimental set-up was built up as shown in Figure 3.23. A high-resolution camera (Nikon™ D800 camera (1920×1080)) was used to obtain wide overview and high resolutions. The surfactant used in this experiment was w.t. 1.8 % homemade surfactant/FC 40 oil [14].

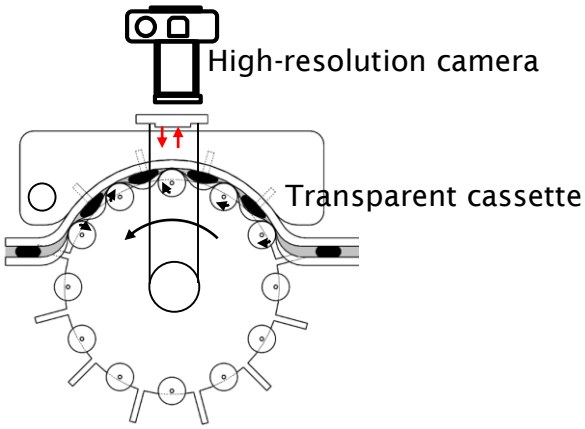

Figure 3.23 Experimental set-up of observing droplets passing the peristaltic pump. The high-resolution camera was fixed close to the transparent cassette.

In the experiment, droplets were generated with *small-medium-big* sizes. The generation frequency was 0.4 Hz. It was observed that the droplets would keep their integrity inside the PVC tubing. With alignment of the phases, the droplets can be accurately positioned in between the two adjacent rollers (Figure 3.25), and safely delivered. The moving speed of the positioned droplet was observed to be approximately the same as that of the rollers. When the droplets were approaching the outlet of the pump, the droplet would be suddenly slowed down or pulled back due to fact that the roller was abruptly releasing the tubing. After that, the droplet progressively moved forward. Video 3.1 clearly shows all of the droplets could pass the peristaltic pump without being squashed. Figure 3.24 demonstrates 24 droplets in 8 groups passing the peristaltic pump. The sizes of droplets kept the sequence: small-medium and big, and no daughter droplets were detected.

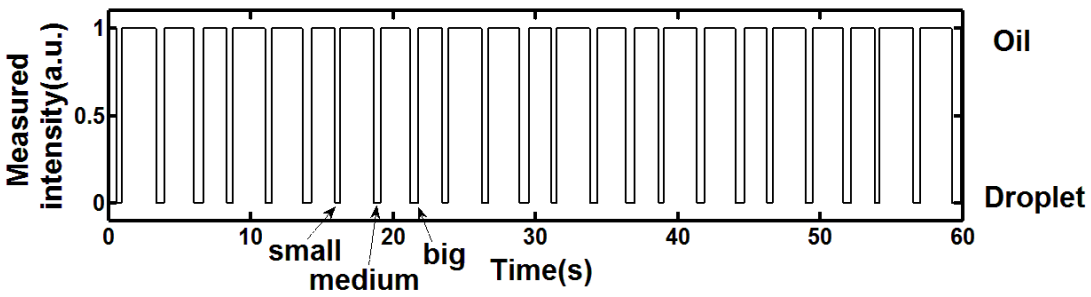

Figure 3.24 24 droplets in 8 groups passing the peristaltic pump without being squashed.

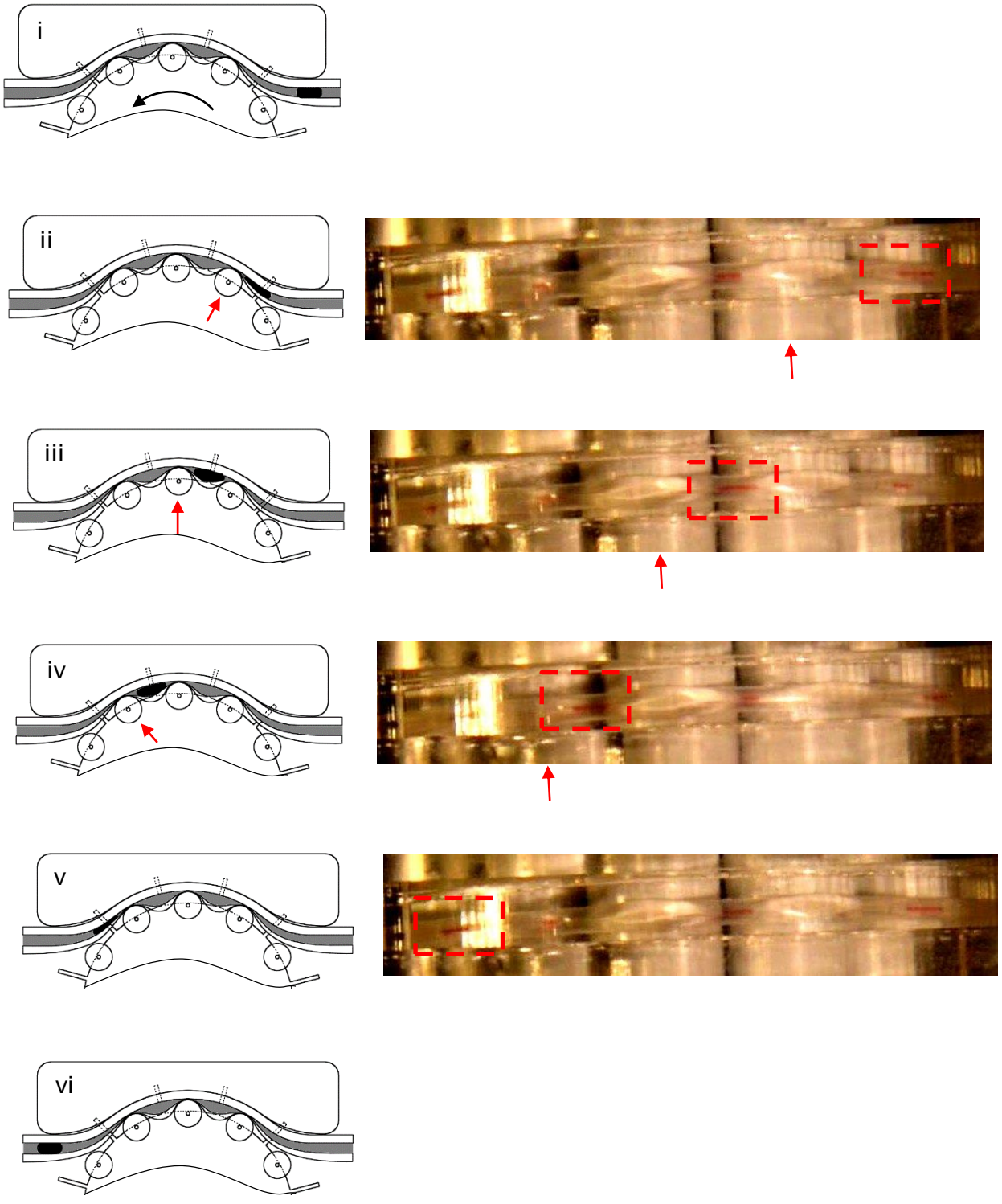

Figure 3.25 Snapshots of one droplet passing the peristaltic pump. The schematics shows the rough positions of droplets with reference of roller which is highlighted with red arrow. Contrast was tuned to show clear snapshots.

3.5.6. Discussions and summary

Based on the suggestions from section 3.3 and section 3.4, this section proposed, designed and engineered a synchronisation system to generate and deliver droplets. This synchronisation system eliminates the laborious calculation of pulsation frequencies and generation frequencies and accurately synchronises the generation with pulsation. It was shown that the trend of sizes of droplets was stabilised with 150 droplets. The polydispersity was dramatically reduced to 6.3 % from ~22 % in the non-feedback system. It was also found that the polydispersity was reduced with the increase of its generation frequency in this platform. This was believed because of the stepwise variation of speed in this peristaltic pump making the size of droplets noisy. With the synchronisation system, droplets can successfully pass through the peristaltic pump. Two functions of the synchronisation system demonstrate its success: accurate generation of droplets and successful delivery of droplets.

With the synchronisation system, the quick set-up generation format makes this peristaltic pumping system superior to the aforementioned pumping system [8-11] in aspiration droplet generators, which requires the droplets to fill a long tube. It is speculated that the peristaltic pumping system can be widely interfaced with any other frequency-controlled generation methods, such as the valve-based generation method [6]. Besides, the whole integrated system can be used to deliver two-phase flows and those squeezing vulnerable fluids in biological labs and hospitals, such as those which contain cells and blood which can be compartmentalised in droplets for delivery.

3.6. Continuous pumping of droplet flows

3.6.1. Introduction

Continuous sampling capability is limited by the volumetric sizes of syringes [8, 10]. For example, if the displacement of syringe is used up, the generation process in the aspirating platforms has to be stopped to recharge the displacement of syringe or to replace the syringe. Fundamentally different from syringe pumping, a peristaltic pump is capable of unlimitedly delivering fluids and this enables the integrated system to generate and pump droplets continuously.

Firstly, this section speculated and observed that the level of water-oil interface in the container can affect the sizes of droplets and further designed a simple method to keep the level of interface to stabilise generation of droplets by using the intrinsic feature of peristaltic pumps. Secondly, this section demonstrated this integrated system is able to generate and pump droplets unlimitedly and thus proves its continuous capability.

3.6.2. Results and discussion

The level of water-oil interface inside sample container of the linear aspiration droplet generator may affect the sizes of droplets. This can be explained as shown in Figure 3.26. During the generation of droplets, the immersing time is pre-programmed to be, t_s, which is the time difference between point when the solenoid starts to be *ON* and the point when it starts to be *OFF*. The real immersing time, t_h, should be considered with the time for solenoid to be up-down, which is different from the pre-programmed time t_h. Changing the positon of interface can bring different immersing time ($P_h > P_l$ induces $t_h < t_l$), and thus different sizes of droplets. A continuous sampling which unlimitedly aspirates oil and aqueous samples can bring different level of water-oil interface and may vary sizes of droplets. The measurement of 500 droplets in system, is presented in Figure 3.28 (A). In the beginning, the size of the droplets was ~0.031 μL. It was stable at this stage and contained ~270 droplets. The size would drop down abruptly to ~0.025 μL and this stage saw a decreasing trend. The measurement was repeated 3 times and similar phenomenon was observed. This abrupt drop may be related with the wetting process inside sample container. Treating the inner surface of container to be hydrophobic may extend the beginning stable regions.

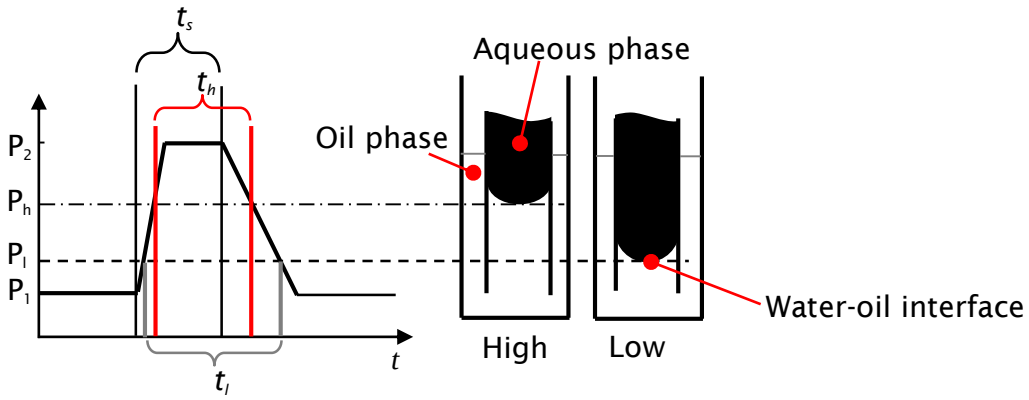

Figure 3.26 Schematic of interface between aqueous samples and carrier oil in container. The pre-programmed immersing time is t_s, and the immersing time for position is t_h and the immersing time for position is t_l. ($t_h < t_l$)

Hence, stabilisation of the level of interface is important in the accuracy of this continuous droplet sampling method. To realise this, a method to circulate the oil and to feed the samples is designed as shown in Figure 3.27. Benefitting from the intrinsic pumping characters of a peristaltic pump, it is practically feasible to collect the waste from the downstream of the system. This collected waste which includes the waste aqueous droplets and oil are introduced into the circulating system, as highlighted by dot-dashed lines in Figure 3.27. The circulating system is able to separate the aqueous droplets from the oil according to their density difference, and to deliver the waste aqueous sample to the waste container and to keep the oil in the main container. In this way, the level of oil is fixed, P_f. In the meanwhile, benefitting from open feature of the sample container, the aqueous samples can be directly fed into the sample container. With these two operations, the water-oil interface is expected to be fixed. In this stabilising scheme, the oil is always circulating so that oil can be saved, particularly in the case where expensive surfactants are applied, which is different from Dropix's approach [15] where dual syringe pumps are applied to both feed oil and samples.

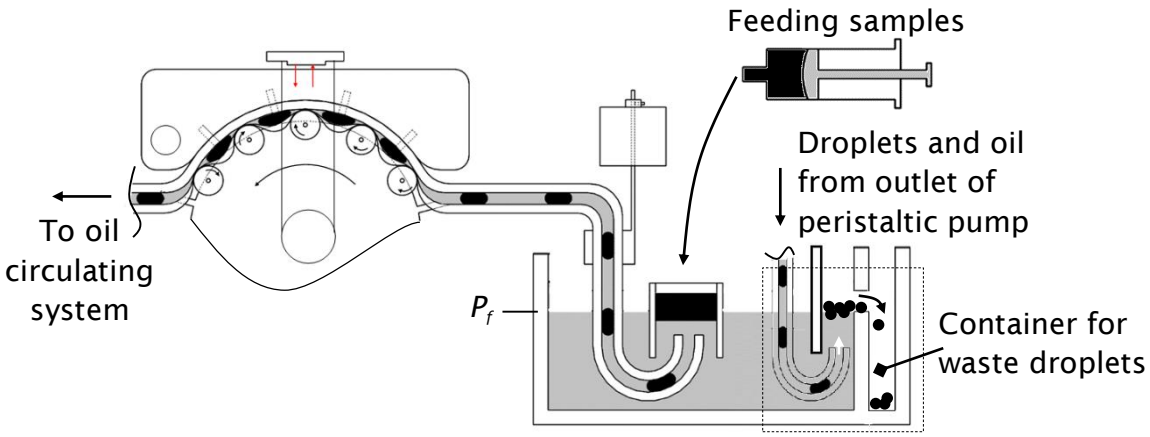

Figure 3.27 Experimental set-up to stabilize aqueous-oil interface. An oil circulating is highlighted by *dot-dashed* line: to separate aqueous droplets from oil to keep the level of oil, fixed. Another channel pumped by syringe to feed aqueous samples into the aqueous sample container.

Figure 3.28 (B) describes the results of the droplet sizes in the system with the stabilising system. It can be observed that the droplet size was stabilised at least 500 droplets. In the repeated experiments, a similar trend was observed. Figure 3.29 presents a comparison of polydispersity and the trend of droplet sizes between non-stabilising and stabilising. The polydispersity was dramatically reduced from 39 % to 4.3 %. The trend was characterised by the 1st order linear trend. It showed better trend from -20×10^{-6} to 0.51×10^{-6}. With supplying oil and aqueous samples, the platform can unlimitedly generated and pump droplets with high accuracy.

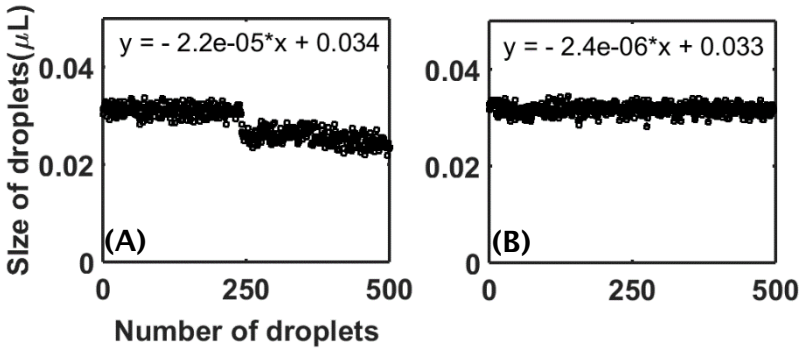

Figure 3.28 (A). The volumetric sizes of 500 droplets generated without any interface stabilising method. The 1st order trend was on the top left corner. (B) The volumetric sizes of 500 droplets generated with stabilising scheme.

3.6.3. Summary

This section demonstrated an intrinsic continuous sampling method for droplets with a method to stabilise the water-oil interface in the linear aspiration droplet generator. The results show at least 500 droplets can be accurately generated. This integrated system samples droplets without the issue of stopping the system to provide enough displacement for the pump, and offers a continuous sampling style. Notably, if this continuous droplet sampling method coupled with other frequency controlled droplet generator, such as Zeng's valve platform [6], the level of interface issue can be easily circumvented.

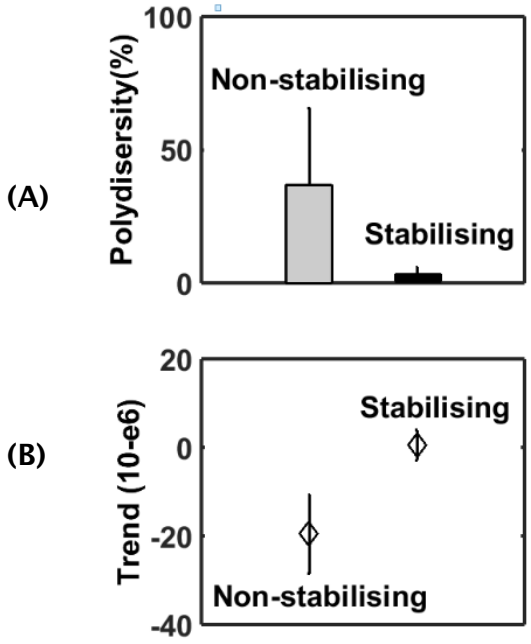

Figure 3.29 A comparison of polydispersity and trend of droplets between non-stabilising and stabilising (A) The polydispersity of droplets were reduced from 39% to 4.3% with stabilising scheme. (B) The linear trend of the sizes of 500 droplets was stabilized from -20×10^{-6} to 0.51×10^{-6}.

3.7. Conclusions

In this chapter, a linear aspiration droplet generator was developed based on a continuous sampling method. It was observed that reducing vibration of the hook could help to reduce the generation of tiny droplets in the system. To

minimise the nonlinearity effect of droplets and to realise continuous droplet generation, it was proposed to apply peristaltic pumping system to generate and to pump droplets with the integration of an aspiration droplet generator.

To solve the two challenges that droplets may be squashed by the peristaltic pump rollers and the pulsation of the flow rate will affect the generation of droplets, a method was proposed, detailed and investigated. To verify this method, a methodology of characterising the droplet sizes and the experimental set-up based on this methodology was built up. It was found the method could decrease the polydispersity of the sizes of droplets to be ~21 %, which was still comparably bigger than that of the droplets generated with traditional method such T-junction. It has been predicted and was analysed that the inaccurate calculation method increased the polydispersity. Besides that, this calculation was laborious and unpractical. To circumvent the low accurate frequency calculation method, a digital feedback control system was built up to further synchronise the droplet generation with pumping pulsation. With this feedback system, the polydispersity of the size of the droplets was reduced from ~21 % to 6.3 % and the trend of the size was stabilized. With proper adjustment of the phase difference between the droplet generation and the pumping pulsation, the droplets could find a safe position in between the two peristaltic rollers. To improve the surface property of PVC tubing, 1.8 % homemade surfactant/FC 40 oil was used. However, it was time-consuming to adjust the proper phase and to predict the desired size of droplets.

During the droplet generation, the interface between the oil and aqueous samples would change which may be related with contact angle hysteresis. The change of interface would significantly affect sizes of droplets. To stabilise the interface, a scheme of circulating oil and feeding samples to compensate for their consumption was used. With this scheme, the system could generate unlimitedly with high reproducibility.

To the best of my knowledge, the platform which was pumping and generating droplets with a peristaltic pump and an aspiration droplet generator was the first of its kind. This platform has versatility in regulating droplet generation frequency and size and in continuous droplet sampling capability. This continuous sampling method can be easily couple with any other frequency controlled droplet generators.

Reference list

1. Dangla, R., S.C. Kayi, and C.N. Baroud, *Droplet microfluidics driven by gradients of confinement.* Proceedings of the National Academy of Sciences of the United States of America, 2013. **110**(3): p. 853-858.

2. De Menech, M., et al., *Transition from squeezing to dripping in a microfluidic T-shaped junction.* Journal of Fluid Mechanics, 2008. **595**: p. 141-161.

3. Garstecki, P., *Formation of Droplets and Bubbles in Microfluidic Systems.* Microfluidics Based Microsystems: Fundamentals and Applications, 2010: p. 163-181.

4. Garstecki, P., et al., *Formation of droplets and bubbles in a microfluidic T-junction - scaling and mechanism of break-up.* Lab on a Chip, 2006. **6**(3): p. 437-446.

5. Xu, J.H., et al., *Correlations of droplet formation in T-junction microfluidic devices: from squeezing to dripping.* Microfluidics and Nanofluidics, 2008. **5**(6): p. 711-717.

6. Churski, K., J. Michalski, and P. Garstecki, *Droplet on demand system utilizing a computer controlled microvalve integrated into a stiff polymeric microfluidic device.* Lab on a Chip, 2010. **10**(4): p. 512-518.

7. Gielen, F., et al., *Interfacing Microwells with Nanoliter Compartments: A Sampler Generating High-Resolution Concentration Gradients for Quantitative Biochemical Analyses in Droplets.* Analytical Chemistry, 2015. **87**(1): p. 624-632.

8. Gielen, F., et al., *A Fully Unsupervised Compartment-on-Demand Platform for Precise Nanoliter Assays of Time-Dependent Steady-State Enzyme Kinetics and Inhibition.* Analytical Chemistry, 2013. **85**(9): p. 4761-4769.

9. Wu, J.B., et al., *Multiple and High-Throughput Droplet Reactions via Combination of Microsampling Technique and Microfluidic Chip.* Analytical Chemistry, 2012. **84**(22): p. 9689-9693.

10. Du, W.B., et al., *Automated Microfluidic Screening Assay Platform Based on Drop Lab.* Analytical Chemistry, 2010. **82**(23): p. 9941-9947.

11. Chabert, M., et al., *Automated microdroplet platform for sample manipulation and polymerase chain reaction.* Analytical Chemistry, 2006. **78**(22): p. 7722-7728.

12. Fuerstman, M.J., P. Garstecki, and G.M. Whitesides, *Coding/decoding and reversibility of droplet trains in microfluidic networks.* Science, 2007. **315**(5813): p. 828-832.

13. Barnes, C.H., *Bristol Aircraft Since 1910*. 1988: Putnam Aeronautical.

14. Draper, M.C., et al., *Compartmentalization of Electrophoretically Separated Analytes in a Multiphase Microfluidic Platform.* Analytical Chemistry, 2012. **84**(13): p. 5801-5808.

15. Ltd, T.D.C. *Mitos Dropix*. Available from: http://www.dolomite-microfluidics.co.uk/webshop/mitos_dropix_system.

4. Parallel aspirations of droplets with a peristaltic pumping system

4.1. Introduction

In high-throughput screenings, one target sample must be tested against a large number of different reaction conditions, such as different sample and reagent concentrations or reaction times. In droplet microfluidics, this normally needs a generic and flexible mechanism for introducing reagents into droplets. One way of introducing reagents is realised by injecting samples directly into the pre-generated droplets [1, 2]. For example, Zheng *et al* introduced aqueous samples into the pre-formed droplets via a T-junction with an air bubble to control the break-up of injection. However, cross-contamination has been observed between droplets although it was reported to be minimal [3]. Additionally, the injected volume is difficult to control, and relies on uniform spacing of the pre-generated droplets coming to the injection points [4]. Other methods of introducing reagents are realised by synchronising and merging droplets. There are three categories of methods of synchronising droplets summarised.

The first method utilizes a parallel ladder to synchronise droplets that have slightly different phase, which was pioneered by Prakash *et al* [5] for synchronisation of air bubbles, and further studied and used for synchronising aqueous droplets [6, 7]. This passive method is only suitable to minimise the phase difference of the generated droplets, but not capable of synchronising large numbers of droplets especially handling droplets in more than two channels. In the second method [8-11] droplets were pre-formed and stored in parallel containers, and then further injected into a Y-junction with coupling two parallel T-junctions/flow-focusing. However, this method is incapable of indexing the droplets because it is difficult to control the injected droplets as desired although barcoding these droplets [12] can improve the capability of indexing. The third method exploits regulating methods to control the generation of droplets in synchronised manner. For instance, Guzowski *et al* [13] used valves to regulate the droplet generation in parallel channels with careful calculation so that these generated droplets arrive at the merging chamber with

the same frequency and at approximately the same time. In aspiration droplet generation, this synchronisation of droplets has been demonstrated [14-16] in serial format. However, this serial introduction and synchronisation of droplets significantly slows down the processes of screening because these droplets are processed in one-by-one serial format. Besides, it makes many meaningful investigations problematic, such as multiple-stage reactions [17-19] which requires parallel operations of droplets.

This chapter develops a parallel droplet aspiration platform to investigate droplets in parallel format, with further engineering the continuous droplet sampling in chapter 3. Each group of synchronised droplets are further operated upon, with actions such as merging where the reaction can be carried out. A pillar-induced merging chamber is used in this chapter and glucose enzymatic assay is exploited as an example application of this integrated system. The results demonstrate that this system is successful as designed and has the potential to be used in various screening applications.

4.2. Overview of the integrated platform

The overview of the proposed integrated platform is shown schematically in Figure 4.1. The design and development of this integrated platform are based on the investigations and suggestions in section 4.3 to section 4.5. Briefly, the platform includes five major components: three independently controlled aspiration droplet generators, a modified peristaltic pump from chapter 3, a digital feedback control system from chapter 3, a PMMA pillar-induced merging chamber with electrodes, and a droplet detection flow cell. One of the three robotic samplers was adopted from a carousel platform which is capable of sample selections from 15 different samples [15]. The other two aspiration droplet generators have single sample reservoir. Droplets produced from these 3 aspiration droplet generators samplers are introduced into the inlets of peristaltic pump via 3 parallel tubing. With proper adjustment of phases of the generation in parallel, after the peristaltic pump, those droplets are guided into a pillar-induced merging chamber with electrodes embedded. An optical detection flow cell was designed for detecting micro-droplets after colorimetric assays via absorption detection.

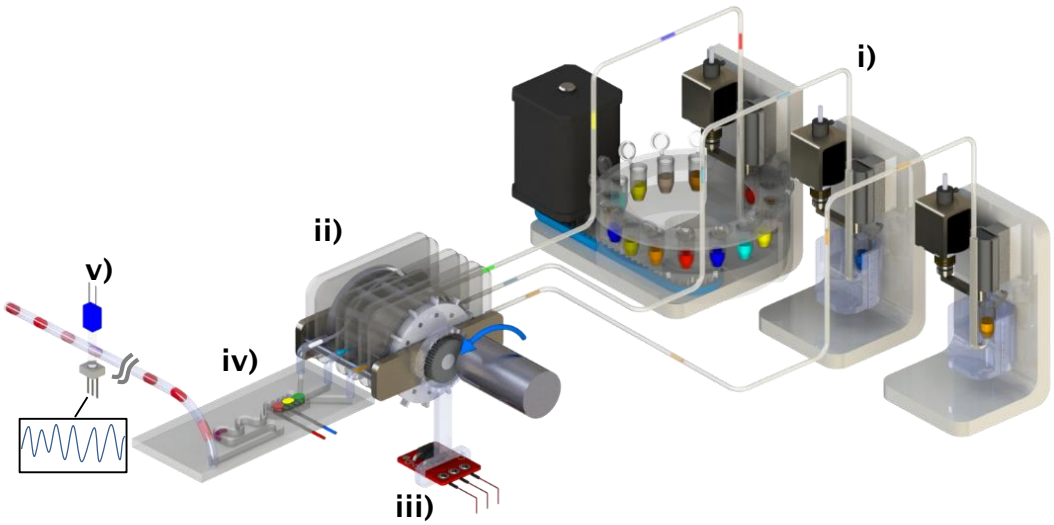

Figure 4.1 Overview of multiple parallel channels integrated platform. i) a carousel aspiration generator that is capable of housing 15 different aqueous samples and two linear aspiration droplet generators each of which houses one independent aqueous sample, ii) a modified peristaltic pumping system in which 12 micro-fabricated pillars are mounted and the cassette was fabricated to be transparent, with iii) a feedback system, iv) a PMMA pillar-induced merging chamber with electrodes, and v) a droplet detection flow cell consisted by a pair of LED and photodiode.

4.3. Parallel synchronisation of droplets

4.3.1. Introduction

Generations and operations of droplets in interconnected parallel channels are intrinsically problematic [20]. Due to pressure cross talk [4, 21], the generation of droplets is less controllable in terms of droplet sizes, generation frequency which can reduce the synchronisation efficiency of these droplets and makes further operations of droplets uncontrollable such as merging.

In the typical on-chip droplet generation and operations, a long channel is normally applied to increase the fluidic resistance and compliance between the operations modules and droplet generators (normally T-junction or flow-focusing) and this can effectively reduce the influence of droplet operations on

the generations [4]. In the parallel formats, a few methods have been applied to improve the controllability of generation in parallel. Chokkalingam *et al* [22] has developed a system with two parallel channels and two stepwise generators which can effectively reduce the influence of flow-rates of carrier phase on generation of droplets. Alternating generation [23-25] can also be applied to realise robust generation in parallel although it takes time to stabilise generation. Besides, the application of valve-based generation provides solutions to the generation of droplets in parallel [26-31]. Churski *et al* [30] has already successfully demonstrated fusion of droplets with different sizes from parallel channels with exploitation of valves and pressure pumps in parallel T-junctions.

However, among aspiration droplet generations, this pressure cross talk and parallel synchronisation of droplets has yet to be addressed. Firstly, this section designed an approach to synchronise parallel droplets with the intrinsic feature of peristaltic pump which is able to insulate pressure from out to inlet. Based on this approach, a parallel aspiration platform is engineered based on the continuous sampling platform in chapter 3. Secondly, to verify this approach in the capability of synchronising droplets, two series of experiment were designed to investigate the synchronising efficiency of parallel droplets: (i) generating parallel droplets with various sizes, (ii) generating parallel droplets with various flowrates. The results show that the parallel droplets can be effectively synchronised subject to a tolerable phase change.

4.3.2. Development of parallel synchronisation system

Interestingly, in avoiding pressure cross talk in parallel channels, the location of the pump (peristaltic pumps or syringe pumps) can make a fundamental difference. If those parallel channels are sharing one singe pumping source which is located at the end of the system (Figure 4.2(A)), pressure cross talk between parallel channels occurs. In contrast, if a peristaltic pump with multiple channels is located in between an aspiration droplet generator and pressure junction to pump each channel independently, as shown in Figure 4.2 (B), pressure cross-talk is less likely to occur, because the occlusion generated by a peristaltic pump can eliminate pressure talking between its inlet and outlet. With this arrangement of location of pumps, it is expected that droplet generations

in parallel channels are not affected by each other and a good synchronisation efficiency can be achieved.

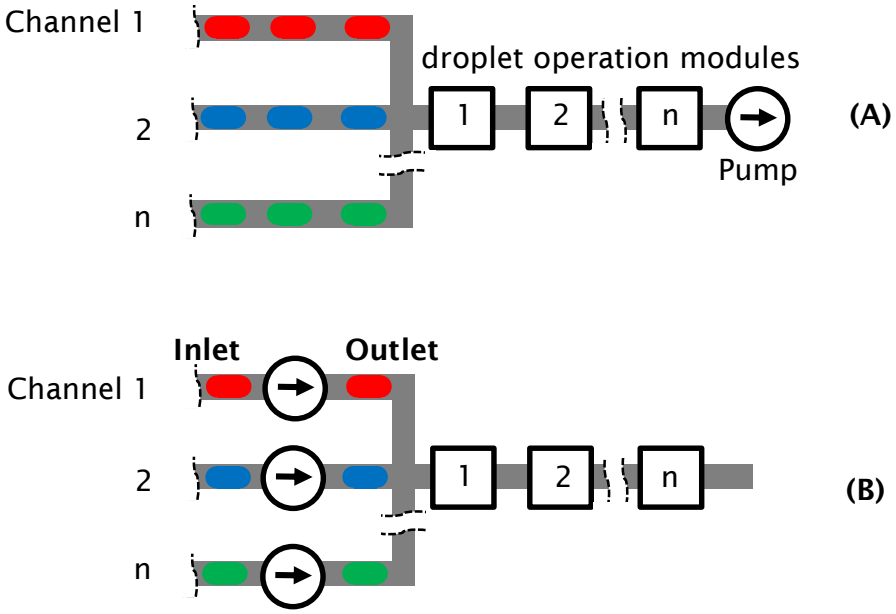

Figure 4.2 Comparisons of two approaches. (A) One single pump is allocated in the upend of the system with n parallel channels joining together before droplet operation modules, such as droplet merging modules, droplet diluting and etc. (B) n independent pumps are allocated in each channel followed by the joint and n droplet operation modules.

Following this approach, a parallel synchronisation system with three channels was integrated, and the system includes two linear independent aspiration droplet generators and one carousel aspiration droplet generator. All the lengths of PTFE tubing in between the peristaltic pump and the generators were approximately the same in the three channels, and were restricted to be as short as possible for the current setup, ~30 cm. The operating protocols of generating 3 parallel droplets and delivering them the same as that in Figure 3.22. It may be expected to introduce multiple samples from carousel aspiration droplet generator in further. This operation protocols is as follows:

- Calibration of phase of droplets (Figure 3.22);
- Inputting the number of droplets N_d, the number of samples in carousel aspiration droplet generator N_s, and the droplet size which is related with the immersing time $\Delta t_{d,i}$

- After generating N_d droplets in one sample, the carousel aspiration generator rotates its tank to select next sample till finishing all of the samples.

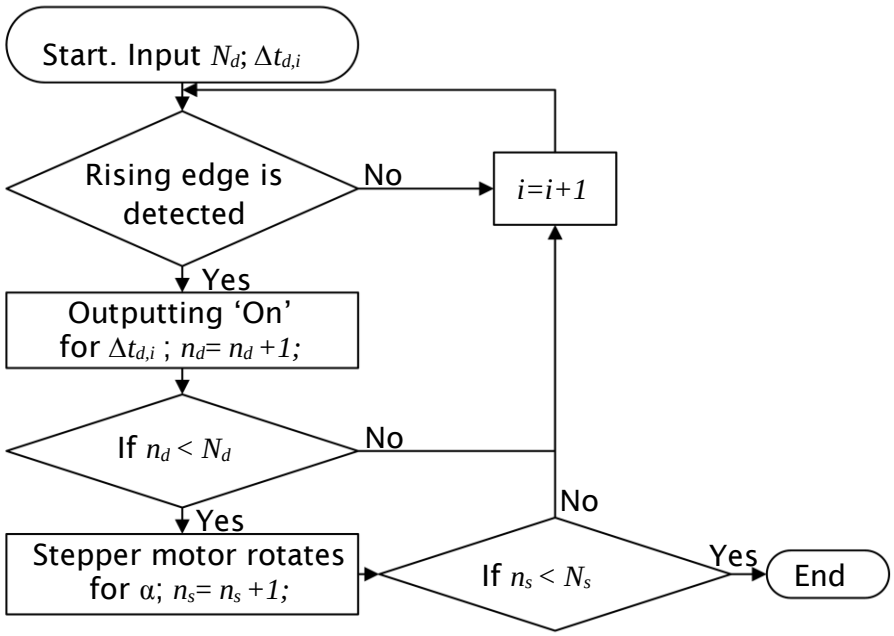

Figure 4.3 Flowchart of algorithm to generate parallel droplets with different samples.

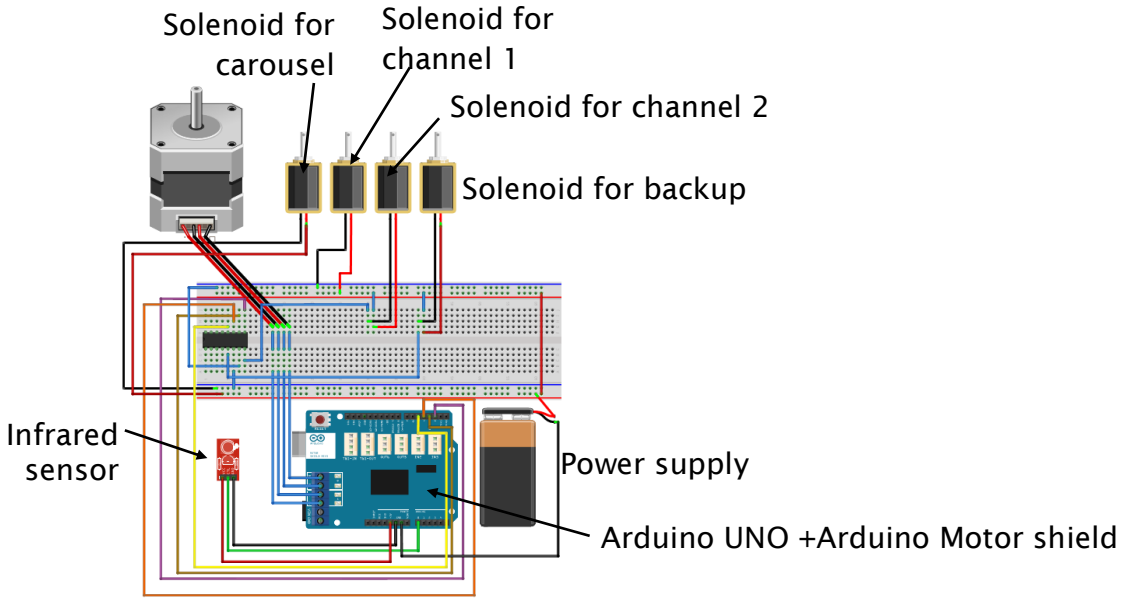

Figure 4.4 The electrical circuit of the integrated system. The electrical system includes an infrared sensor, an Arduino UNO control board with a stepper motor shield, a transistor array to amply the signal, four solenoids, a stepper motor and a power supply.

Based on this protocol, the program (Figure 3.16(A)) was further modified ton control more channels and function selections of different samples in carousel aspiration droplet generator, as shown in Figure 4.3. The electrical circuit (Figure 3.16 (B)) was also further modified to control at least 3 aspiration droplet generators, as shown in Figure 4.4. The circuit includes the synchronisation of the pumping pulsation with the droplet generation which was developed in Chapter 3 and an electrical circuit capable of controlling the stepper motor (RS 53550401) of the carousel robot and two more solenoids for another two channels. To control the stepper motor, a motor shield (Arduino™) was applied. During the rotation of the tank, the speed of rotation of the stepper motor was limited to control the vibrations of the oil. In this project, the speed was normally controlled within 7.5° per second.

All of the components of the system including the linear aspiration droplet generators, a carousel aspiration droplet generator, the peristaltic pump and the digital circuit board, were integrated on a home-made optical stage which could ensure easy transportation of the system (Figure 4.5). The total dimension of the whole integrated system was 35 cm× 30 cm.

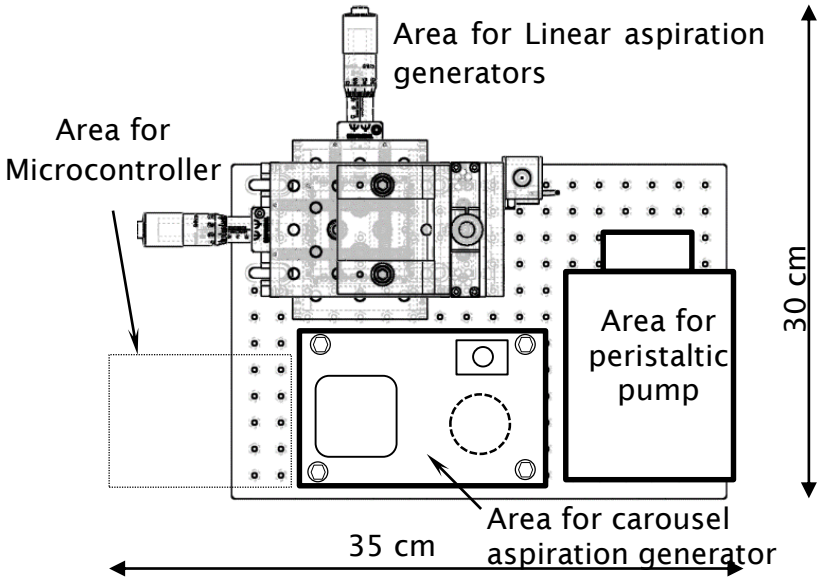

Figure 4.5 The compact system which includes linear aspiration droplet generators, a carousel aspiration droplet generator, microcontroller modules, a peristaltic pump. Its dimension is 35 cm × 30 cm.

To investigate the efficiency of synchronisation of droplets in three parallel channels, i.e. the phases of droplets and sizes of droplets, two series of experiments were performed. The purpose of the first experiment is to investigate whether the dynamical sizes of droplets in one of the parallel channels can affect phases and sizes of droplets in the other parallel channels. The purpose of the second experiment is to investigate whether different flowrates of droplets in parallel can affect phase and sizes of droplets with each other. Section 4.4.3 performed the first series of experiment, while section 4.3.4 performed the second series of experiment.

4.3.3. Synchronisation of droplets with different sizes in parallel channels

4.3.3.1. Methodology and experimental set-up

The experimental set-up is detailed in Figure 4.6. A group of three sets of PVC tubing was placed in parallel on the peristaltic pump with inlets connecting three aspiration droplet generators, and with outlets connected via a Y-junction. The cassette of the peristaltic pump was tightly compressed. Here, in channel 1, the sizes of droplets were intentionally controlled to be *small, medium* and *big* to generate a dynamic situation, while in channel 2 and channel 3 the droplets were generated with constant sizes. A high-resolution camera (Nikon™ D800) was mounted on microscope, to record the PTFE tubing at the outlet of the peristaltic pump. There were 5 groups of experiments with different droplet generation frequencies, 0.2 Hz, 0.23 Hz, 0.27 Hz, 0.4 Hz and 0.5 Hz. In each group, 30 droplets or more were recorded, which are enough for a complete set of screening application by providing at least 10 repeats.

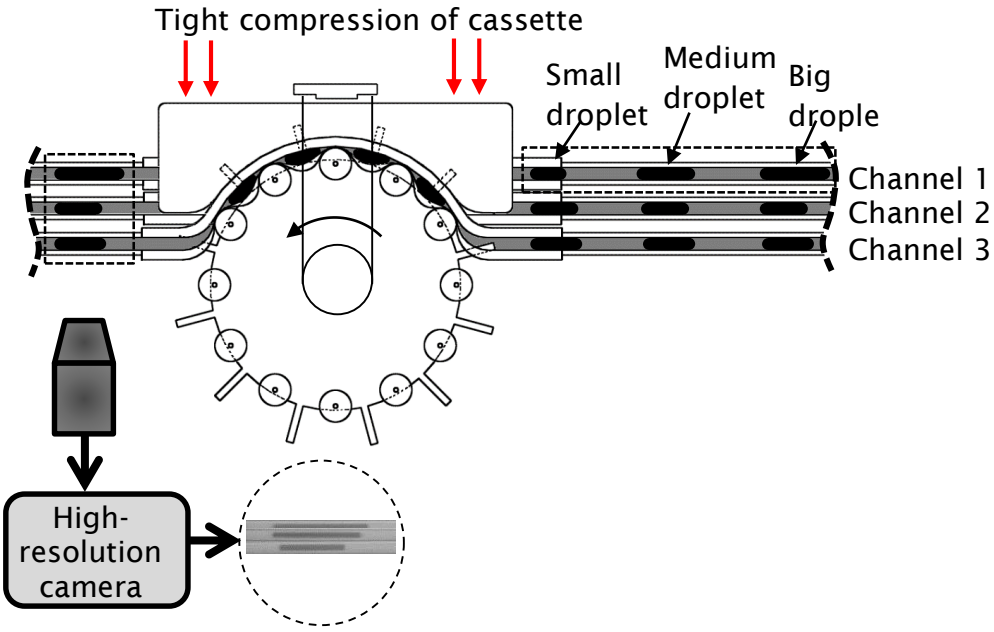

Figure 4.6 Experimental set-up investigating the synchronization of droplets in three channels. In the first channel, the sizes of droplets were controlled as small, medium and big. In the second channel and the third channel, the sizes of droplets were controlled to be constant.

During the test, it was difficult to produce exactly the same length of the tubing in the three parallel channels, due to practical issues such as inserting the PTFE tubing into the PVC tubing and the stretching of PVC tubing by the peristaltic pump rollers. This difference in tubing length could cause a time difference, Δt, for the droplets arriving at the detecting point. To deduce this difference which is termed as phase shift, the normalised *phase difference* is applied as shown in Equation 4.1, which is calculated by comparing the phase in the examined channel to that in reference channel.

$$PhaseDifference_{channel}(i) = \frac{t_{channel}(i) - t_{reference}(i) - \Delta t}{T} \times 100\% \qquad \textbf{Equation 4.1}$$

Here, $t_{channel}\ (i)$ and $t_{reference}\ (i)$ are the phase of the i^{th} droplets in the examined channel and reference channel respectively. T is the generation period.

4.3.3.2. Results and discussion

The sizes of droplets in channel 1 had *small, medium* and *big* pattern as desired (Figure 4.7 (A)) with a polydispersity of 22 % among 30 droplets, which is bigger than the characterised results (<6.3 %) shown in Section 3.5.2. Figure 4.7 (B) quantified the polydispersities of sizes of droplets in channel 2 and channel 3 with generation frequencies from 0.2 Hz to 0.5 Hz. The polydispersities of droplets in channel 2 was generally smaller than 7 % which was close to the characterised results (<6.3 %), while the polydispersities of sizes of droplets in channel 3 was also generally smaller than 7 %. The generation frequencies in three parallel channels are equal as all of them were generated according to the pulsation frequency via the digital feedback system. The good polydispersities of sizes of droplets in channel 2 and channel 3, confirms that the dynamic behaviours of droplets in channel 1 did not affect the generation of droplets (sizes and generation frequency) in channel 2 and channel 3.

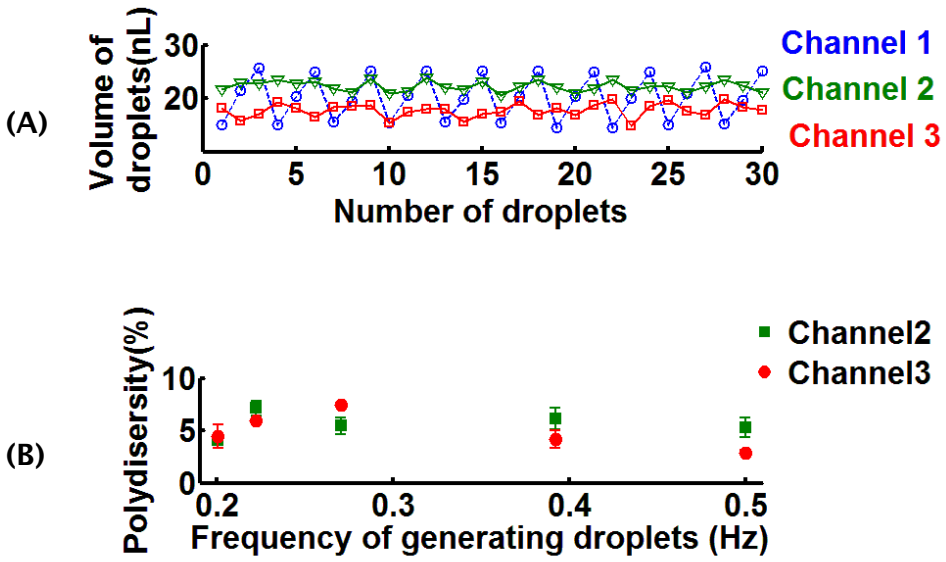

Figure 4.7 (A) an example of the sizes of droplets in the three parallel channels. The generation frequency was ~0.2Hz. The sizes of droplet in channel 1 were controlled to be small, medium and big. Those in channel 2 and channel 3 were controlled to be constant. (B) The polydispersity of sizes of droplets in channel 2 and the channel 3. The generation frequencies are 0.2 Hz, 0.23 Hz, 0.27 Hz, 0.4 Hz, and 0.5 Hz.

In this investigation, the phase of droplets in channel 1 and channel 3 were examined and the phase of droplets in channel 2 was chosen as reference. Figure 4.8 (A) described an example of local phase difference of each droplets in channel 1 and channel 3 with a generation frequency of 0.2 Hz, compared with that in channel 2. In channel 3, phase difference was ranging from -2 % to 2 %. The quantified mean phase differences (■ Figure 4.8 (B)) were ranging from -1 % to 1%, with generation frequencies from 0.2 Hz to 0.5 Hz. Generally, the volume fraction which is volumetric size of droplets divided by the total volume of fluids delivered by peristaltic pump in one period, is from 10 % to 50 %. Under this volume fraction, this phase difference can ensure droplets in parallel touch each after entering the junctions, given that the phase shift arising from the practical operation was eliminated. This phase differences show that the variable droplet sizes in channel 1 did not affect the phases in channel 3 so that the droplets in channel 2 and channel 3 were well synchronised. Different from a smoother pattern in channel 3, phase differences in channel 1 (Figure 4.8 (A)), ranged from -0.1 % to 6 % and showed a *zig-zag* pattern which is correlated with droplet size (Figure 4.7(A)). In this pattern, the big droplets were always delayed compared to the smaller droplets. Due to this *zig-zag* pattern, the quantified mean phase differences of big droplets (◆ Figure 4.8 (B)) in channel 1 was bigger than that in channel 3. With this phase difference, the droplets in channel 1 and channel 2 can still touch each other at the Y-junction. However, it shows that the variable droplet sizes in channel 1 affected their own local phases in channel 1 and made the droplets in channel 1 less synchronised with those in channel 2.

The reason for this was unclear so that extra investigation was performed to understand this.

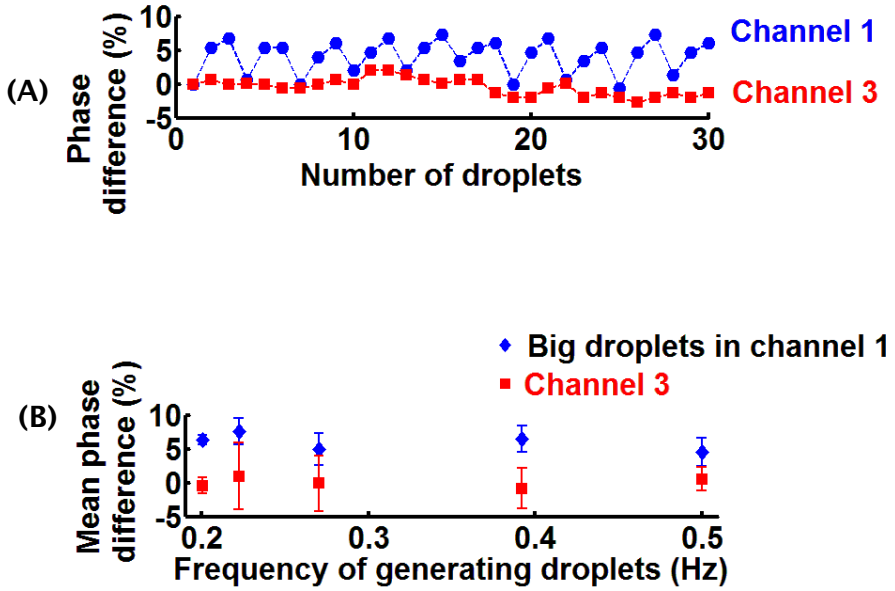

Figure 4.8 Phase differences in 5 groups of experiments with generation frequencies 0.2 Hz, 0.23 Hz, 0.27 Hz, 0.4 Hz and 0.5 Hz. (A) The example of local phase differences in channel 1 and channel 3 with those in channel 2 as reference (0.2 Hz). (B) Mean phase differences of droplets in channel 3 and mean phase differences of big droplets in channel 1, with that in channel 2 as reference. The frequencies are 0.2 Hz, 0.23 Hz, 0.27 Hz, 0.4 Hz, and 0.5 Hz.

4.3.3.3. Investigation of phase change

This section specifically investigates the phase change of droplets with variable sizes of droplets.

It was speculated that the phase of droplets with different sizes may be changed because of gutter flows in these areas shown in Figure 4.9:

- the PTFE tubing in the inlet part (area 1);
- the first connection to interface the PTFE tubing into PVC tubing (from area 1 to area 2);
- inside peristaltic pump (in between area 2 and area 3);

- the second connection to interface the PTFE tubing into PVC tubing (from area 3 to area 4); the PTFE tubing in the outlet part (area 4).

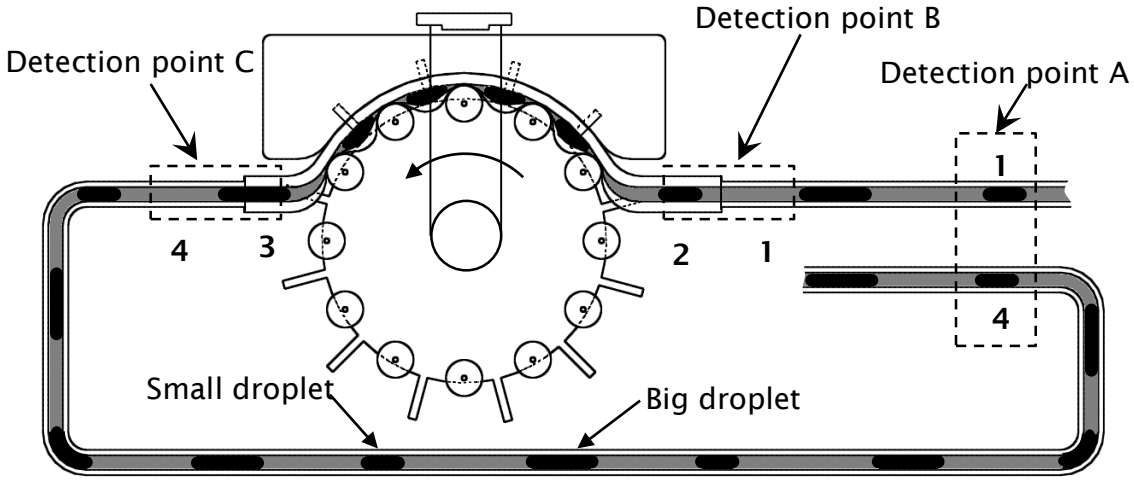

Figure 4.9 Schematic of peristaltic fluidic circuit. The key parts areas that may cause phase change of droplets with different droplet sizes and experimental set-up. The droplets were generated in small-big sizes.

In the experiment, the droplets were generated in a *zig-zag* pattern (small-big sizes) and introduced into a single channel in the peristaltic pumping system. As it was difficult to clearly cover the whole part of the system with a single camera, here, the investigations were separated into three detection points within three separate experiments, detection point A to compare droplets inlet and outlet, detection point B to compare droplets from area 1 to area 2, detection point C to compare droplets from area 3 to area 4.

To observe the phase change (delayed phenomenon and advanced phenomenon), histogram plots of sizes and phase difference were used to quantify the distributions of phase differences (phase of droplets after peristaltic pump with the reference of generation phase). For example, a comparison between these two cases was shown how to use the histogram plots: (A) droplets with constant size and (B) droplets with small-big size (*zig-zag* pattern), as show in Figure 4.10. Constant sizes of droplets presented a single regime in the distributions of sizes which was around 15 nL (Figure 4.10 (A)), while small-big sizes of droplet

presented two independent regimes (regime 1 is around 25 nL and regime 2 is around 37 nL) as shown in Figure 4.10 (B). Constant sizes of droplets presents a single regime (~0 %) in the phase difference distribution of droplets in outlet after peristaltic pump which indicates that no delayed or advanced regimes were observed in constant sizes. The phase difference distributions in *small-big* sizes of droplets presented double regimes. Regime 1 is around 0.2 % and regime 2 is around 11% and this indicates that regime 2 was delayed compared to regime 1, during which phase changes occur. The following investigations utilised this method to observe where the phase change occurs.

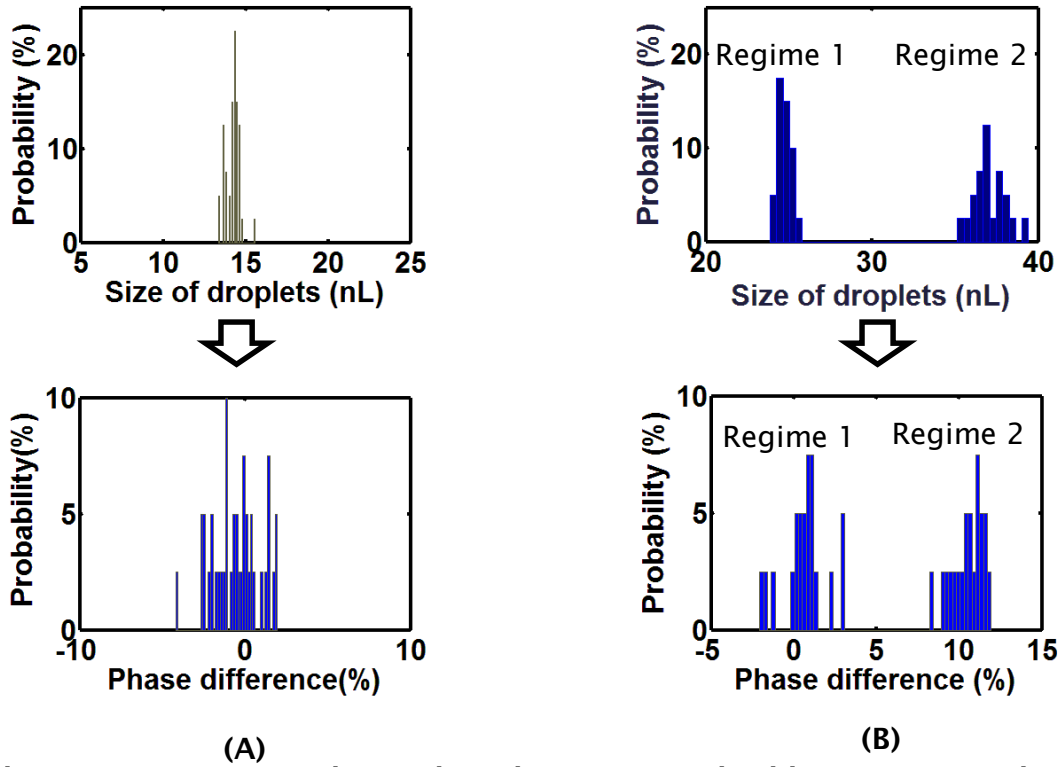

Figure 4.10 An example to show how to use the histograms to observe phase change: The correlations between size distribution and phase difference distribution Case (A): constant droplet size. Both of the size distribution and phase difference distribution had a single regime. Droplets contains one single regime. Case (B): small-big droplet size. Both of the size distribution and phase difference distribution had dual regimes.

Figure 4.11 presents the results of investigations of phase differences distributions in area 1, area 2, area 3 and area 4 for the *small-big* droplets. It shows that in detection point A, the single regime in phase difference distributions of droplets in area 1 was divided into two independent regimes in area 4. This indicates that the phase change did not occur in area 1 and may occur in one of the other positions: first connection, inside peristaltic pump, or second connection. Observation in detection point B manifests a single regime

(0 %) in areas 1 and 2. This indicates that phase did not change in first connection. Observation in detection point C describes two regimes (0 % and 6 %) respectively in area 3 and area 4. This indicates: (i) phase change has already happened in between area 2 and area 3 (ii) phase change did not happen in between area 3 and area 4. The three experiments shows that the phase change of droplets arise from the area inside peristaltic pump between area 2 and area 3. Gielen *et al* [15] observed that big droplets would catch small droplets in a sharp ascending flow-rate trend in a circular tubing, and this phenomenon was exploited to merge droplets in an abrupt accelerating flow rate. During the current experiment, a strong pull-back of flow was observed when the last roller was releasing the PVC tubing at the moment depicted in Figure 3.27 (v) and video 3.1. This strong pull back was due to the restitutions of the squashed tubing and of the stretched tubing. It is believed that this strong pull-back would generate different gutter flow depending on different droplet sizes, and this different gutter flow can shift the phase of droplets.

Combined with the results in section 4.3.3.2, it is concluded that: behaviours of droplets in parallel channels will not affect each other in terms of generation frequency which is always referred to the pulsation frequency, neither the size of droplets nor phase of droplets. Droplets with variable sizes would encounter phase change which happens inside the peristaltic pump which may be due to the strong pull-back of flow, and this phase change is tolerable. Subject to this tolerable phase change in variable droplet size case, this system can also easily realise different ratios of droplets in parallel by adjusting the generation frequency ratios, such as 1:2, 1:3 or 1: n, as demonstrated in [10, 11, 25]. To further reduce the phase change, it is important to reduce the pulsation of flow-rate in the releasing position of peristaltic pump, such as fixed the PVC tubing in the outlet of peristaltic pump and smoothening the sharp cassette.

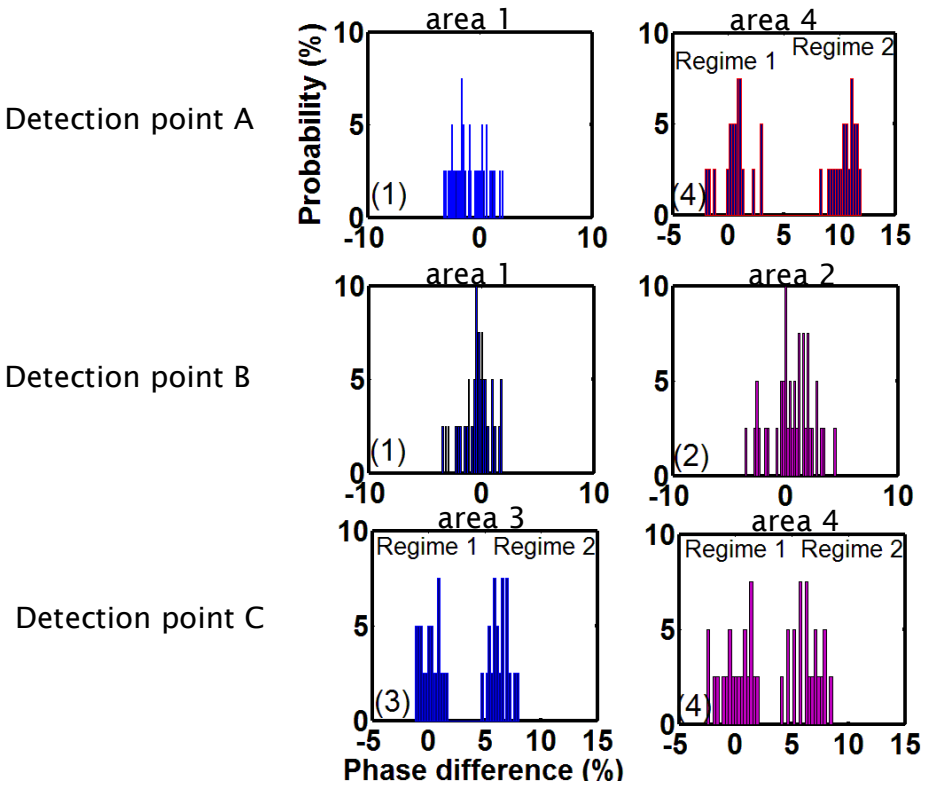

Figure 4.11 Phase differences in area 1, area 2, area 3 and area 4.

4.3.4. Synchronisation of droplets in parallel with different flow rates

This section performed the second series of experiment to investigate the synchronisation efficiency of parallel droplets with different flowrates. The results show that these parallel droplets can be effectively synchronised.

In this parallel system, different diameters of peristaltic pump PVC tubing were applied to realise different flow rates but the same frequencies. Here the first tubing has an I.D. of 0.19 mm and the second channel has an I.D. of 0.25 mm. The two channels were still interconnected via a Y-junction. The methodology of calculation of phase difference and experimental set-up is the same as used in the last section. The droplets were generated with constant sizes and there were 5 different frequencies, 0.2 Hz, 0.22 Hz, 0.27 Hz 0.4 Hz and 0.5 Hz. More than 30 droplets were produced in each frequency. The measurement of the flow rates in the outlet was shown in Figure 4.12 (A). It was observed that the flow rate in channel 1 has a more pronounced (-50 nL/s) negative pulsed flow than

that in channel 2. The quantified mean flow rate was plotted in Figure 4.12 (B) which shows a rough linear relationship with the pulsation frequencies.

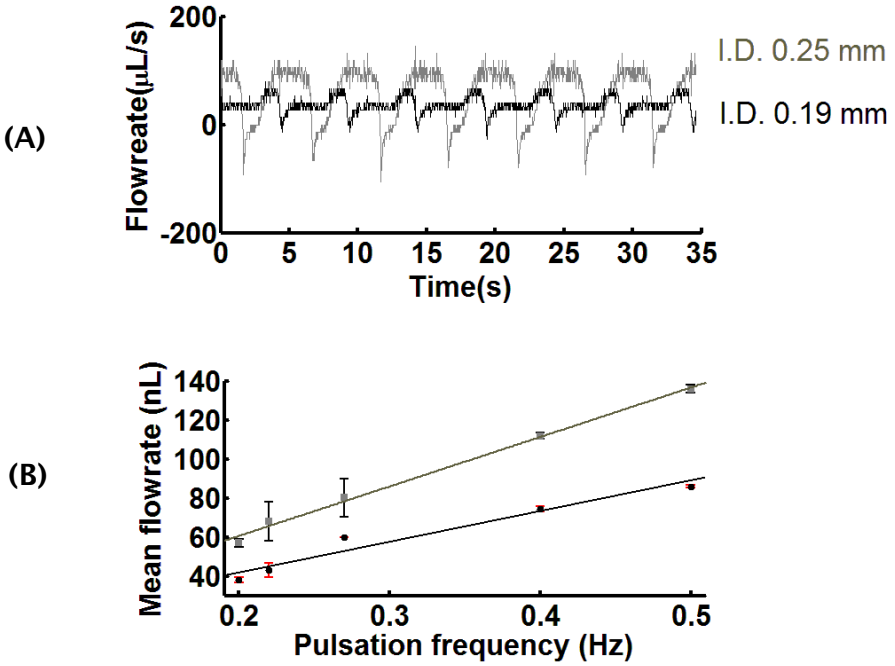

Figure 4.12 Mean flow rate of peristaltic pump with two inner diameters, 0.19 mm and 0.25 mm. (A) The flow rate of peristaltic pump at pulsation frequency of 0.2 Hz. (B) quantified mean flow rates

Figure 4.13 presents the quantified polydispersities of droplets in channel 1 and channel 2 which are smaller than 5.8 %, and smaller than 5.1 %, respectively. These quantified polydispersities are in the range of the characterised results in section 3.5.2 (<6.3 %). It shows that the behaviour of parallel droplets even with different flow-rates do not affect each other in term of droplet generation. The phase of droplets in channel 1 was further presented with droplets in channel 2 as references. Figure 4.14 (A) presents an example whose generation frequency is 0.5 Hz. The quantified phase difference was shown in Figure 4.14 (B). The smallest phase difference, 1 %, occurred at a frequency of 0.22 Hz, while the largest phase difference, -7 %, occurred at a frequency of 0.4 Hz. Compared with the volume fractions of droplets in one periodic volume (10 % to 50 %), this phase difference is able to ensure that the droplets in parallel channels can touch each other at junction part. These results show the droplets in parallel channels with different flowrate but with the same generation frequency can also be successfully synchronised with the designed synchronisation approach.

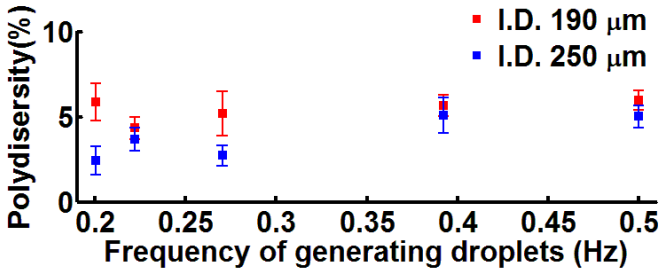

Figure 4.13 Quantified polydispersity in channel 1 (I.D. of PVC tubing 190 μm) and in channel 2 (I.D. of PVC tubing 250 μm) with generation frequencies, 0.2 Hz, 0.22 Hz, 0.27 Hz, 0.4 Hz and 0.5 Hz.

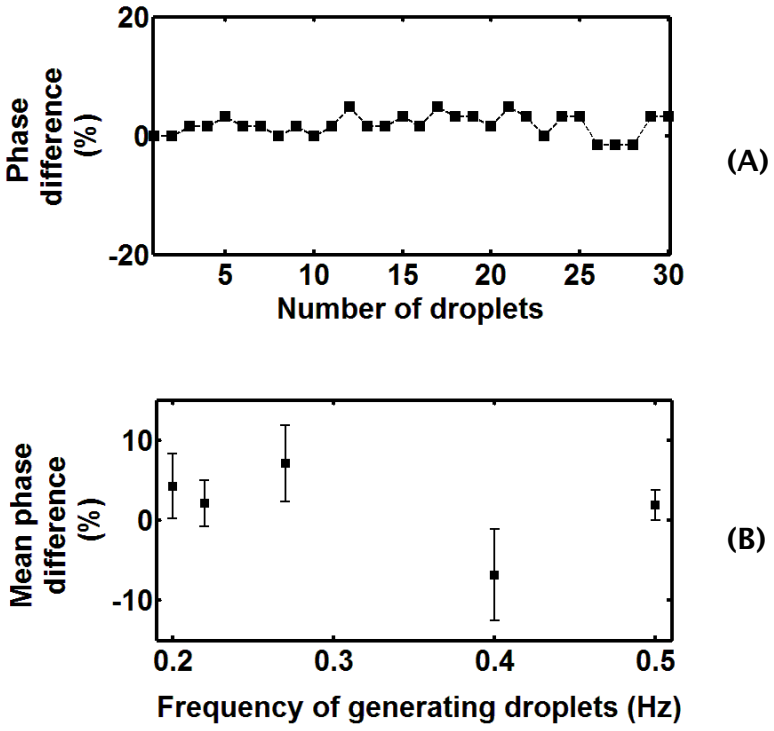

Figure 4.14 Phase differences of droplets in the second channel which has PVC tubing with I.D. 0.19 mm. (A) Phase difference of droplets in the second channel with frequency 0.5 Hz. (B) Maximum phase difference of droplets in different frequencies 0.2 Hz, 0.22 Hz, 0.27 Hz, 0.4 Hz and 0.5 Hz.

4.3.5. Summary

Droplets in parallel channels can affect each other due to pressure cross talk. This can significantly reduce the efficiency of synchronising droplets, which is an important process in operating droplets in droplet microfluidics. This section has designed a novel approach to synchronise droplets in parallel channels based on the characteristics of the peristaltic pump which is capable of avoiding pressure cross-talk between outlet and inlet. This approach can ensure that droplets in one parallel channel will not affect those in another one. The investigations have shown that pressure cross talk did not occur, although the variable sizes of droplets could induce a change in the local phase after the droplets pass through the peristaltic pump, which was believed to have been caused by the strong pulsation inside the peristaltic pump. Besides, parallel droplets with different flow rates can also be well synchronised. If desired, this approach can also realise the synchronisation of droplets in different generation frequencies [10, 11, 25].

The intrinsic design feature of the approach (avoiding pressure cross-talk from outlet to inlet due to occlusion of peristaltic pump) enables excellent synchronisation and control of droplets in parallel in different conditions. Such feature contrasts this synchronisation approach to other methods for pairing droplets or synchronising generation of droplets, especially those without regulation on generating frequencies and merely relying on dynamics of fluids in parallel channels [22, 24, 25].

4.4. Operations of the synchronised droplets in parallel: merging droplets

4.4.1. Introduction

Merging droplets is an important process in droplet microfluidics. In this section, the synchronised droplets from the integrated system were operated to demonstrate droplet merging. To demonstrate that, a droplet merging module was fabricated with a quick design-fabrication method. The successful demonstration suggested that this parallel aspiration platform can be applied in various operation modules. During the demonstration, some interesting

phenomenon were observed such as introducing air bubble can assist the merging.

4.4.2. Design and fabrication of merging chip

In merging droplets, there are different categories of merging schemes as reviewed in Chapter 2, such as decompressing scheme [32, 33] and compressing scheme. In this demonstration, the pillar-induced merging chamber [34, 35] was applied as it can effectively circumvent the phase difference. In this system, the scenario of merging is detailed as follows:

- The first droplet enters the middle channel of merging chamber and is trapped in the chamber to wait for the next two droplets;
- The second droplet enters the middle channel joining the first droplet to wait for the third droplet;
- The third droplet enters the middle channel. If the volume of the chamber is smaller than the total volume of the three droplet sizes, the merging chamber will be blocked by the third droplet. With the accumulation of the hydraulic pressure, the merged droplet is pushed forwards.
- As soon as the head of the merged droplets is pushed outside of the middle channel, the reminder of the merged droplets is accelerated due to Laplace pressure.

Notably, the merging chamber should be capable of (i) trapping the first droplet and the second droplet; and (ii) releasing the merged droplet. To design this merging chamber, it is of importance to consider the total flow rate and the volumetric size of droplets, which would effectively influence the trap of droplets inside the chamber. In this case, the chosen frequency of generation of droplets is 0.2 Hz during which the mean flow rate is ~55 nL/s, and the volumetric sizes of droplets are ~50 nL. In contrast to the experimental set-up in [34] where the pumping is realised by exploiting syringe pumps, the flow rate in this system is pulsatile. The combined flow rate of the three channels could range from -200 nL/s to 300 nL/s depending on the phases. Here, the volume of the merging chamber is chosen to be smaller than the total volume of droplet sizes to ensure the merged droplet can be pushed away from the chamber. From [34], it is known that the trapping of droplets is a competition between hydrodynamic forces and surface tension. If the first droplet has a small flow rate when it arrives at the merging chamber, the droplets will be stopped which is the desired case.

However, if the droplets are in the peak phase of the flow rate, the merging chamber should have appropriate dimensions to stop the droplets. Laplace's law and Poiseuille's law can be used to estimate the dimensions for trapping the first droplet and second droplet, following the derivation in [34] .The key dimensions are shown in Figure 4.15 (A). Considering the micro milling micro-fabrication

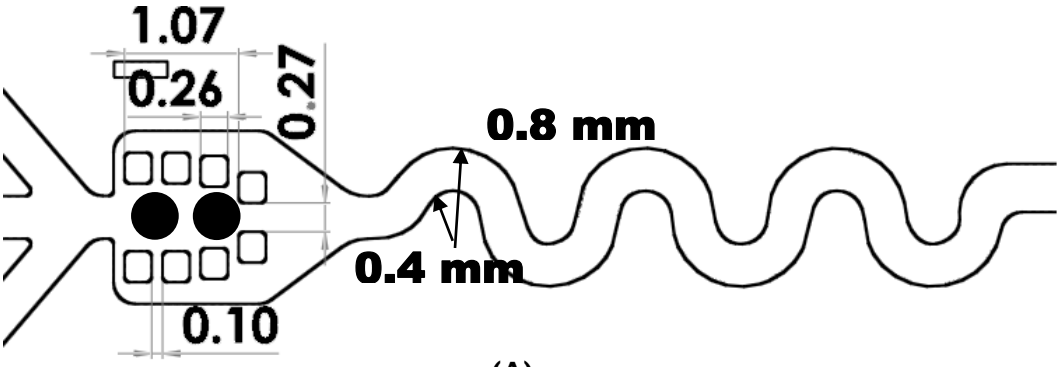

(A)

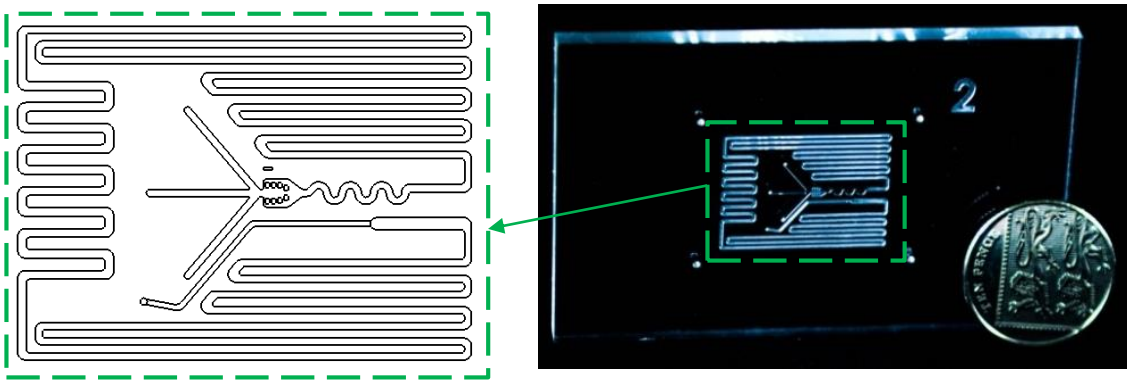

(B) (C)

Figure 4.15 Design and fabrication of pillar induced merging chamber. (A) The key dimension of the merging chamber is shown. There are four pairs of pillars in this merging chamber. The distance between two adjacent pillars is 0.1 with consideration of the micro-fabrication. There are six round winding channel. The inner diameter of the winding channel is designed to be equal to the channel width. This design will ensure a more efficient mixing. (B) The total length of the channel is 330 mm with section area 0.4×0.2 mm^2 (C) The merging chamber is fabricated from a CNC micromill (LPKF,S100).

technique which is used to provide a robust chip, the gap between two adjacent pillars was set to be at 0.1 mm. A smaller gap is difficult to fabricate.

Mixing is an important process for initiating reactions. Here, a winding channel was applied to further mix the merged samples, after the laminar-driven mixing and convection-driven mixing that was observed in the merging chamber [34].

The dimension is shown in Figure 4.15 (A). For a better observation of the merged droplets, here, the channel post the mixing channel is designed as shown in Figure 4.15 (B).

The chips were fabricated with PMMA (5 mm thickness) by a micro-mill (LPKF, S100) with a 100 μm diameter Endmill tool. Compared with photolithography, this method benefits from a quick design-to-fabrication procedure, no requirement for clean rooms and low cost. The fabricated merging chamber (Figure 4.15 C) was bonded with the other PMMA pieces. To align these two pieces, there are four alignment holes (1 mm) designed.

To effectively merge the droplets in the presence of surfactant, electrodes will be used. The electrodes are fabricated according to the following processes:

- Two designed holes (0.3 mm) were drilled;
- silver epoxy (1:1) was filled into the two holes;
- Using glass slide to remove the sliver epoxy remained on the surface and making sure the epoxy is completely filling the holes;
- Baking it in the oven (85°C) for 5 minutes.

To bond the two PMMA pieces, here, chloroform was used following the recipes in [36] with a simple rig. The bonding procedures (Figure 4.16) are as follows:

- Preparing the two bonded PMMA pieces: employ an ultrasonic bath for the two PMMA pieces for 7 minutes in 35°C; clean them with D.I. water and dry them with nitrogen gas.
- Exposing to chloroform: put the chloroform in the container and make sure the distance between the surface of the container and surface of the chloroform is ~1 cm; put the aligning bars (1 mm) into the aligning holes; put the PMMA pieces on the top of the containers and exposing chloroform for 3.5 minutes at room temperature.
- Aligning the two pieces: this process needs quick manual operations (<10 seconds)
- Pressing the two pieces: with the help of adjustable jars, press the two pieces. Put the pressed pieces in the oven with 65 °C for at least 5 hours.

After successful bonding, the channel was coated with Duxback™ to make the channel hydrophobic.

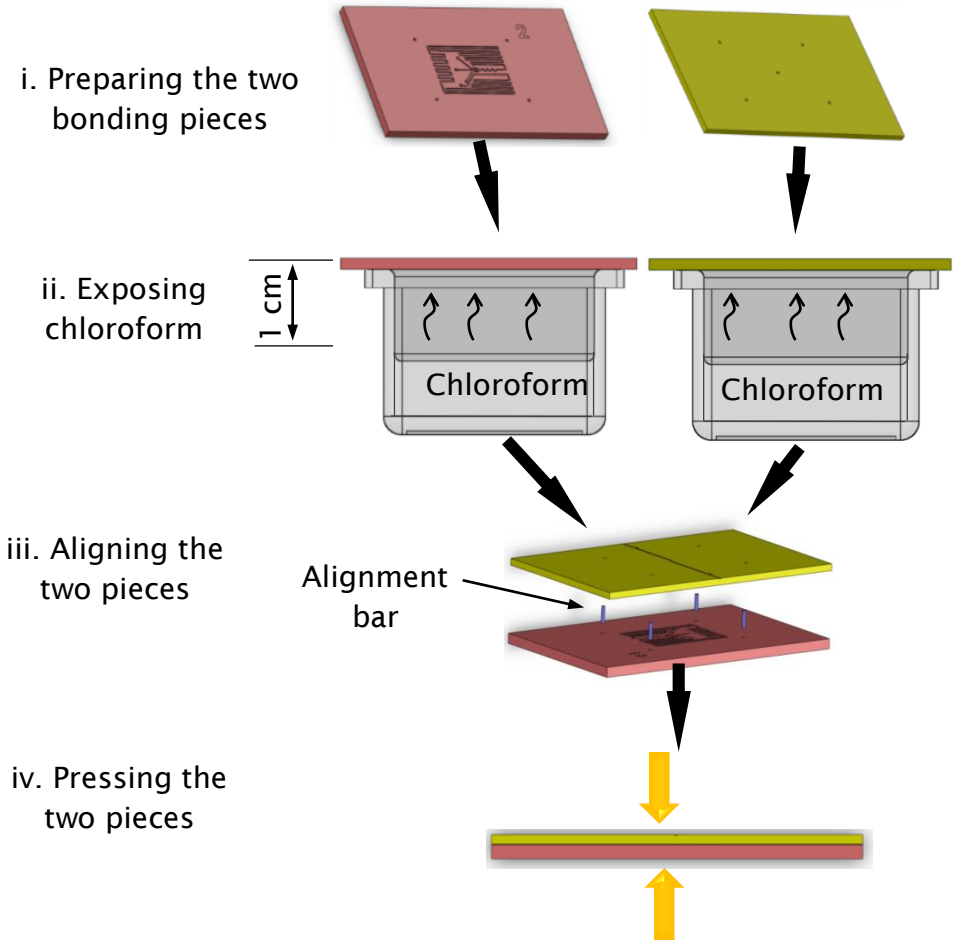

Figure 4.16 The processes of bonding PMMA chips with chloroform. (i) Preparing the two bonding pieces; (ii) exposing them to chloroform; (iii) aligning the two pieces; (iv) pressing the two pieces.

4.4.3. Results and discussion

Firstly, the electrodes are assessed whether they could effectively help the merging chamber to merge droplets. The merging chip is interfaced with the integrated system with epoxy glue. The oil phase still contains wt.1.8 % homemade surfactant/FC 40. The electrodes are connected with 6 DC V power source.

As shown in Figure 4.17 (A), it was found that the circular electrodes could not merge the trapped droplets even though the voltage was increased to 12 V, and there was no current going through the electrodes. It was observed the electrodes have a concave shape which is due to the shrinkage of silver epoxy during baking. The failure to merge droplets may arise from the fact that the droplets could not effectively touch the surface of the electrodes. This concave shape made it difficult for the droplets to approach the surface of the electrodes.

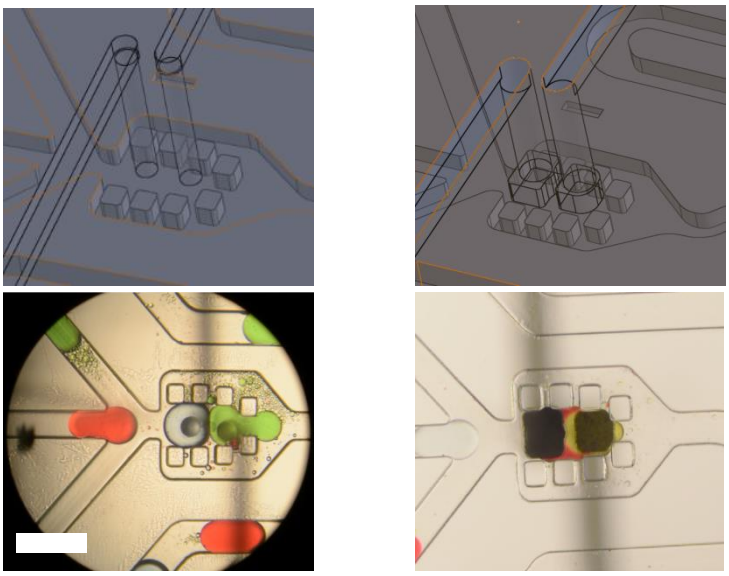

(A) (B)

Figure 4.17 The two designs of electrodes in the merging chamber. (A) Circular electrodes cannot effectively touch the droplets. The coalescence of droplets does not happen in this design. The scale bar is 1 mm. (B) the squared electrodes which increases its surface area to provide more chances to touch the droplets ensures coalesce of droplets happens.

This could be explained by Laplace's law and the mechanism is schematically shown in Figure 4.18 (A). To improve the chance of touching the droplets, the surface of the electrodes was increased as shown in Figure 4.17 (B) and the mechanism was shown in Figure 4.18 (B). By repeating the same assessment procedures, it was found the droplets could be effectively merged with the new design of electrodes with 6 DC V. The example of merged droplets is shown in Figure 4.17 (B).

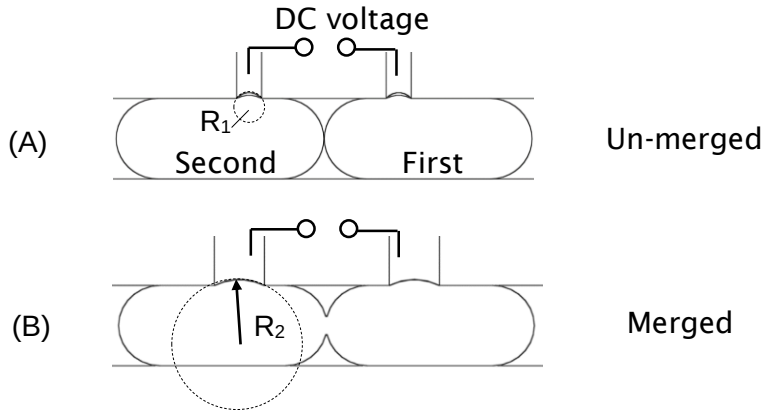

Figure 4.18 Schematic of the mechanisms of the droplets touching the electrodes. (A) *Un-merged* case. The Laplace pressure makes the droplets difficult to 'bend' its surface to touch the surface of electrodes. (B) *Merged* case. The bigger surface area of the electrodes provides chances for the droplets to easily touch the electrodes.

With the working electrodes, it was observed that the droplets (green ones) in the second channel entered the merging chamber first followed by the second droplets (blue ones) in the first channel and the third droplets (red ones) in the third channel, as shown in Figure 4.19 (A). After the first droplet arrived at the merging chamber, it was dramatically slowed down before it touched the pillars. This is because then flow rate of this droplet is smallest in that period. With entering the second droplets, the first droplet was pushed forward. As soon as the two droplets crossed over the two electrodes, the first droplet and the second droplet were merged directly with the help from electric field. This merged droplet was pushed forward until touching the pillars and was stopped by the pillars. After this, the third droplet entered the merging chamber to block the merging chamber. Due to the accumulation of the hydraulic pressure, the merged droplet and third droplet were pushed forward. During this process, the third droplet touched the merged droplet, and they would be merged as soon as the interfaces pass over the two electrodes. The complete merging processes are shown in Figure 4.19 (A). Figure 4.19 (B-C) shows the merging of more than 60 groups of droplets (video 4.1). All groups of the droplets kept the same sequence: the green droplets arrive at the merging chamber first followed by the clear droplets and the red droplets. This result compares this integrated system with the calibrated merging efficiency, 67 %, in [7].

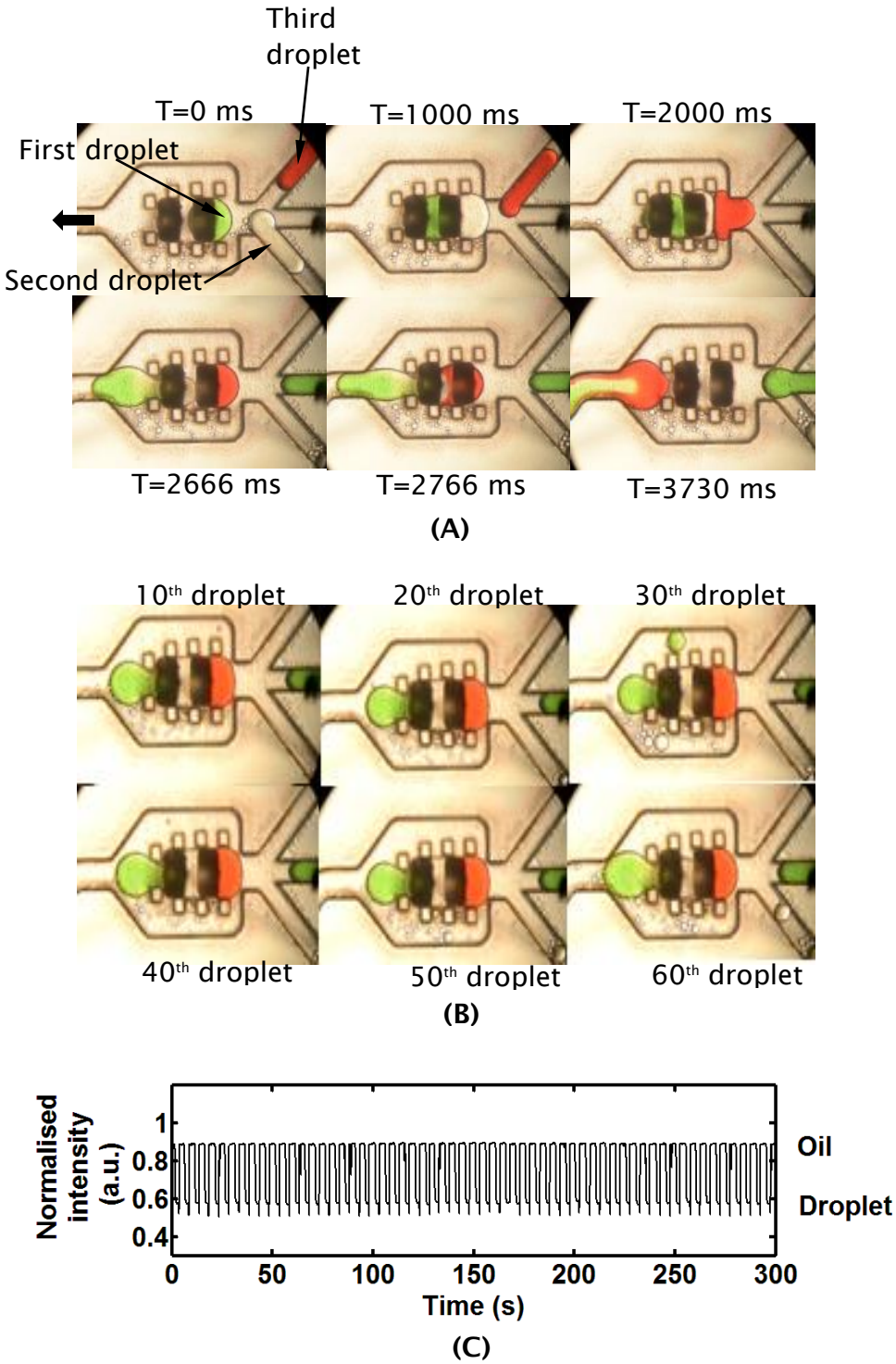

Figure 4.19 (A) the processes of merging droplets. (B) 60 droplets kept the same sequence: the green droplets arrived at the merging chamber firstly followed by the clear droplets and the red droplets. (C) Normalized intensity signal of 60 merged droplets.

To investigate the phase of merged droplets, the phase difference was calculated with Equation 4.1. Figure 4.20 (A) presents an example of the phase difference between phase of the merged droplet and phase of droplets in first channel (green) which shows a stable trend. Figure 4.20 (B) presents the quantified phase differences of the merged droplets with generation frequencies 0.2 Hz, 1.2 Hz and 3 Hz. The quantified mean phase difference ranges from to -5.3 % to 6.6 %. This small phase difference suggested the merged droplet could be further used for operations such as further introducing reagents into the merged droplets for multi-step reactions. To reduce the phase difference, it is important to apply circular channels in the fluidic system. Figure 4.21 (A) demonstrates droplets (as highlighted in grey circle) containing two kinds of candidate samples are synchronised with another parallel ones and are merged in merging chamber. It showed that the droplets with different contents can be effectively merged with another two droplets in parallel channels. (Video 4.2, video 4.3 and video 4.4 demonstrates various samples introduction and merging.)

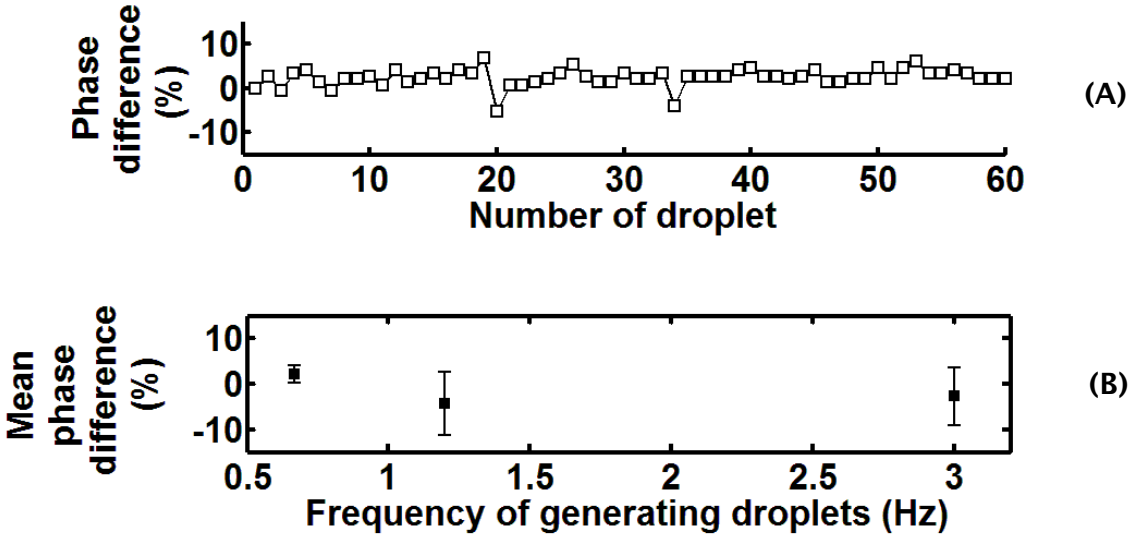

Figure 4.20 Phase difference between the merged droplets and the first droplet (green droplet). (A) The local phase difference of 3 merged droplets with reference of that in first channel (green droplets). (B) The quantified mean phase difference in a series of 3 different frequencies (0.2 Hz, 1.2 Hz and 3 Hz)

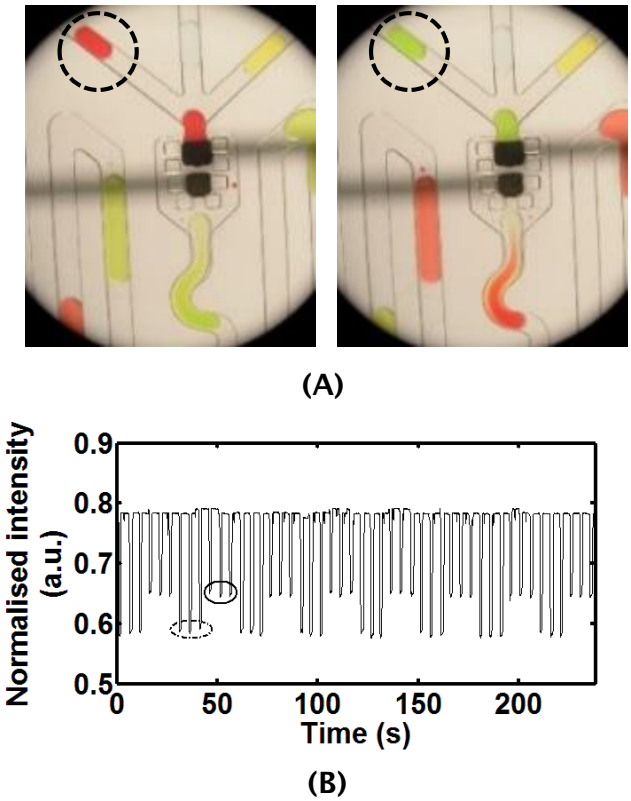

Figure 4.21 Introductions of variable samples into merging chamber (A) Snapshots. (B) Measured intensities of merged droplets with two different samples (red and green).

During the experiment, coalescence of droplets before the merging chamber was observed many times. Figure 4.22 detailed an example of this observation. In this example, the green droplet entered the merging chamber first and touched one or both of the electrodes. At a certain point, the droplet stopped completely because of the pulsation of the flow rate of this droplet. After that, the clear droplet arrived at the buffer area to approach the green droplet as shown at T=0 ms. With that the clear droplet getting closer to the green droplet at T=133 ms, the two droplets were merged. The merged droplet was still parking at the beginning of the merging chamber to wait for the red droplet to push forward. At T= 233 ms, the red droplet was getting closer to the merged droplet. At T= 300 ms, the red droplet was merged with the first merged droplet outside of the merging chamber. At T= 500 ms, a neck was formed in the red droplet because of the stretch of Laplace pressure and the hydraulic pressure from the first channel and the second channel. This neck elongated and

eventually the red droplet was split from the merged droplets at T= 500 ms. The merged droplets was stopped by the pillars in the merging chamber to wait for the remainder of the red droplet. With the push from the oil phase the split red droplet entered the merging chamber to block the merging chamber at T=1330 ms. The rest of the process was the same as described in Figure 4.19 (A). Here, coalescence of droplets was observed twice before those droplets entered the merging chamber to be compressed. Different from the observations in [35, 37] where the two droplets to be merged are crossing over the two electrodes when coalesce occurs, there was only one of the two droplets touching the electrodes in this observation.

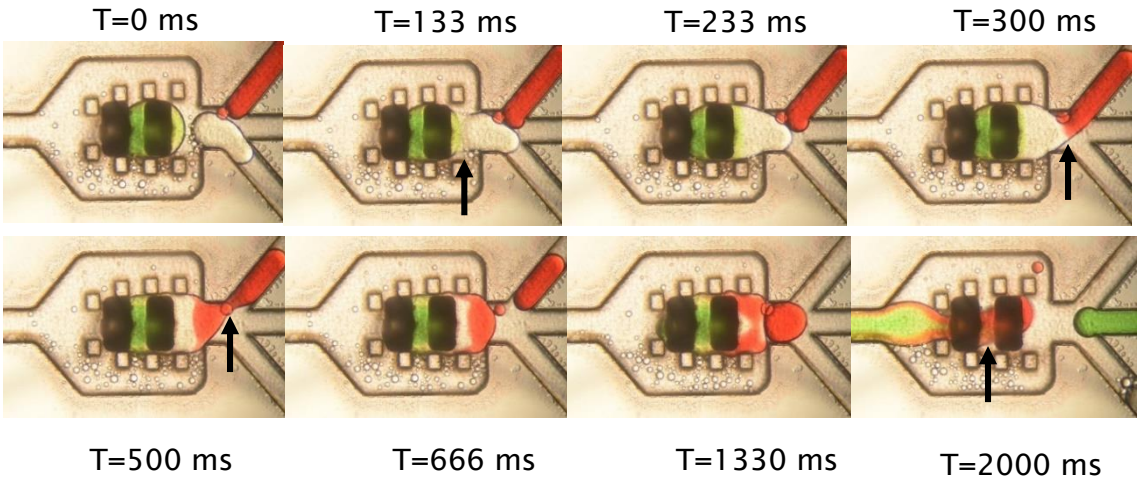

Figure 4.22 The coalescence of droplets before the merging chamber. At T=133 ms, the clear droplet was merged the green droplet as pointed with a black arrow. At T=300 ms, the red droplet was merged with first two droplets. At T=500 ms, a neck in the red droplet was formed and was elongated to split the red droplet. The detached red droplet would block the merging chamber to push all of the droplets forward at T=1330 ms.

4.4.4. Air bubble aided merging scheme

Interestingly, it was observed that air bubbles can be generated in a Y-junction and their generation was automatically synchronised with aspiration generation. Figure 4.23 (A) shows the processes of generating an air bubble and synchronising the droplets from aspiration generator. At T=0 ms, the head of the air bubble is seen above the buffer area. At T=500 ms, the head enters the buffer area. At T=1000 ms, it suddenly withdraws back due to the strong pulsation of flow rate in the second channel. This withdraw ensures that the droplet can freely enter the buffer area shown by the black arrow with dash bar at T=2000 ms. From T=2000 ms to T=3300 ms, the air bubble is re-entering buffer area and further pushing the droplet forwards. At T=4000 ms, a thin neck is formed. At T= 5000 ms, the generation of air bubble has been completed and is moving away from the merging chamber. Figure 4.23 (B) describes the phase

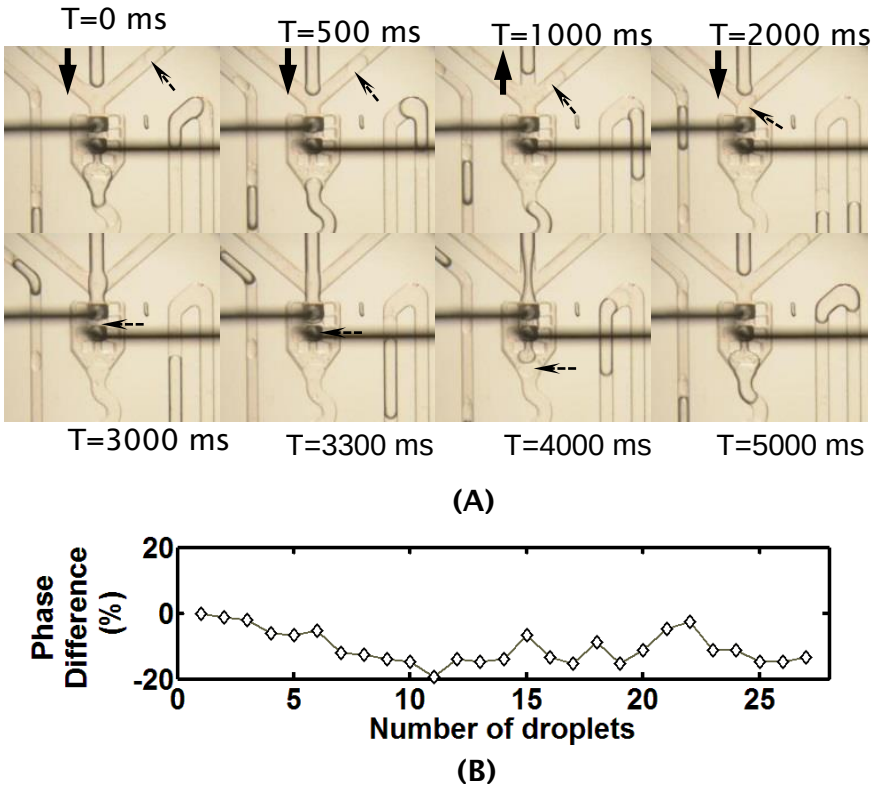

Figure 4.23 Investigation of generation frequencies of air bubbles and droplets. (A) The processes of generating an air bubble. (B) The phase difference between air bubble and the reference droplets.

differences of the air bubble with the phase of droplets as reference, which showed a perfect synchronisation (shown in Video 4.5_a).

In this integrated platform, the designed pillar-induced merging chamber could only merge droplets that have specific volume with fixed flow rate [34]. Lee,*et at* [11] have adjusted the flow rate to effectively tune the number of droplets merged. However, this method changes the phase of droplets and further makes the droplets less synchronised.

Different from these methods, here, it suggests an air bubble from the Y-junctions can be used to regulate the merging of droplets working as a piston to push the merged droplets away from the merging chamber. Nightingale *et al* [18] has intentionally introduced air bubbles to control the addition of reagents into the preformed droplets and Wang et al [38] further used air bubbles to regulate the generation of droplets. Besides of regulating the merging of droplets, the air bubble is expected to favour some certain reactions which is sensitive to gas such as the glucose reaction.

To investigate the influence of the generated air bubbles on merging, an experiment was designed. Figure 4.24 presents a comparison between the non-air bubble scheme and the air bubble scheme in merging droplets (video 4.5_b and video 4.5_c). In the first scheme, the designed merging chamber could merge 4 droplets which are delivered in two groups and each droplet size is ~30 nL. In the second scheme, this designed merging chamber could trap the first two droplets to wait for the air bubble to push them away. As shown in Figure 4.24 (A), the first two droplets arrived at the merging chamber at T=0 ms. At T=100 ms, the air bubble was entering the merging chamber. At T=1700 ms, the air bubble was detached and moving forwards to push the two merged droplets. It is shown that 10 droplets in channel 1 and channel 2 respectively were transformed into 5 droplets in the non-air scheme, while in air bubble scheme those droplets were effectively transformed into 10 droplets. This showed that the introduction of air bubble could effectively regulate the merging.

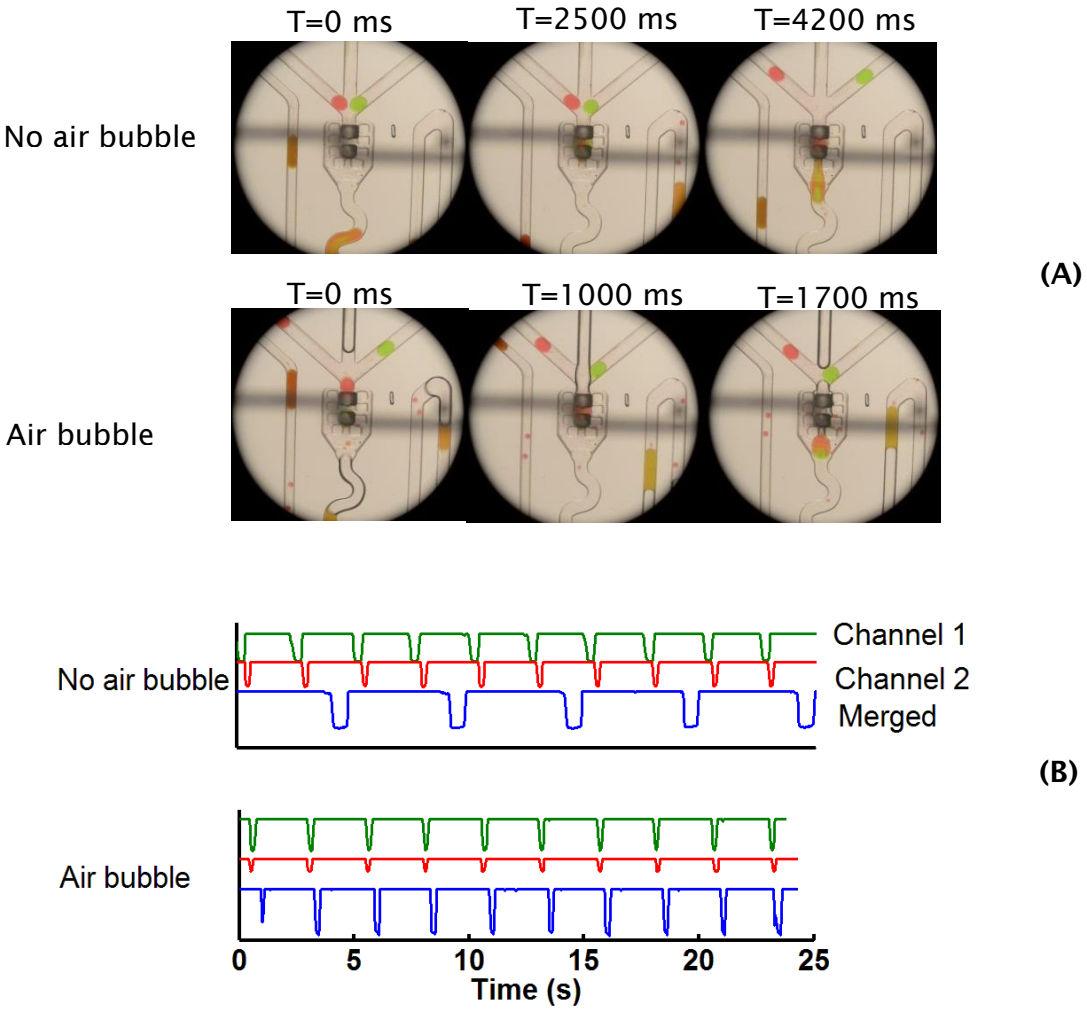

Figure 4.24 The comparison between *no air bubble* **merging and** *air bubble* **merging.** In the merging without air bubbles, the merging chamber could effectively merge four droplets which are contained in two groups. In the merging with air bubbles, the merging chamber could merge two droplets with the favor of an air bubble.

4.4.5. Summary and outlook

This section has designed and fabricated a merging chamber with working electrodes. The fabrication was realised by a CNC micro-mill that benefits from the quick design-fabrication procedures, lack of requirement for clean room and low cost. The bonding was realised by exploiting chloroform. Moreover, this

section successfully demonstrated the coalescence of parallel-synchronised droplets with a pillar-induced merging chamber. The coalescence of droplets before the merging chamber was observed. Interestingly, introduction of an air bubble into the merging chamber with the control of peristaltic pump can effectively regulate the number of droplets merged in merging chamber without affecting the phase of the droplets.

This integrated system is the first of its kind to synchronise droplets in parallel channels. Together with other characters, which are easy sample-loading [14, 15, 39, 40], continuous sampling and unlimited number of droplets delivering as demonstrated in last chapter, the versatilities compare this system with any other ones.

With these demonstrations, it is believed that the integrated system is capable of realising various combinations of droplet operations with different flow rates as shown in Figure 4.25, and can find a wide range of applications, such as example multi-step reactions [17-19].

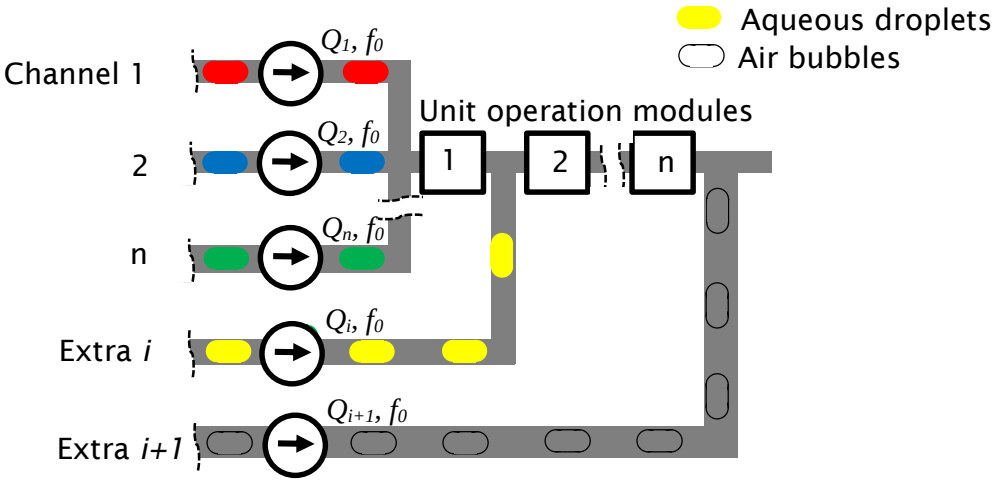

Figure 4.25 Various combinations of parallel modules.

4.5. Screening glucose with synchronised droplets

Hyperglycemia is a common disorder and is characterised by the high levels of glucose in human body. The measurement of glucose is of significance in

studying diabetes. In this section, the synchronisation system with merging scheme was proposed to be used in a glucose assay. It was found that droplets containing a glucose sample and glucose reagents could be successfully synchronised and merged, and easily present the calibrated results.

4.5.1. Methodology and experimental set-up

Here, a colorimetric enzyme-kinetic method based on Trinder's reaction [41], was applied to measure the concentration of glucose. The glucose is oxidized to gluconic acid and hydrogen peroxide. The hydrogen peroxide further reacts with 4-AAp and phenol to get the quinoneimine which shows violet colour. The colour change was detected a flow-cell which contain a pair of green LED and photodiode.

$$\text{glucose} + H_2O + O_2 \xrightarrow{\text{Glucose oxidase}} \text{gluconic acid} + H_2O_2$$

$$2H_2O_2 + \text{4-AAP} + \text{phenol} \xrightarrow{\text{Peroxidase}} \text{quinoneimine} + 4H_2O$$

The droplets in the two parallel channels were introduced into the merging chamber using the same procedures as in the last section. The working voltage for the electrodes was 6 V. The colour change was detected by a colorimetric flow cell specially designed for detecting a micro-droplet [15]. In brief, the flow cell was 3D printed with black PLA material inside of which a thin wall PTFE tubing (model) is mounted. The light from the LED can pass through a 0.3 mm wide slit perpendicular to the tubing and be received by the detector via another slit, as shown in Figure 4.26. A sequence of ~30 nL droplets containing 0 mg/dL, 100 mg/dL, 200 mg/dL, 300 mg/dL, and 400 mg/dL glucose (in PBS buffer) was introduced via in the first tubing. The reagent droplets contained glucose oxidase, 4-AAP, phenol, and peroxidase with ~30 nL in volume in second channel, were synchronised with the glucose droplets and was expected to be merged with the glucose droplets. Each group of these two droplets are merged in the merging chamber into one big droplet. After a reaction time of about 7 minutes in the winding channel, and then in the PTFE tubing, the merged droplets were detected. The signal from colorimetric flow cell detector was collected with an Arduino™ Nano chip (696-1667, R.S.) with a sampling rate of 100 Hz.

Prior to using this integrated system, the merging chip was tested for workability. The droplets which containing 400 mg/dL and glucose reagents, was introduced into the merging chamber to demonstrate the merging. Besides, the calibration of the flow cell detection device will be also performed with a series concentrations of colour dyes (vol. 10%, 20%, 30%, 40%, and 50 %).

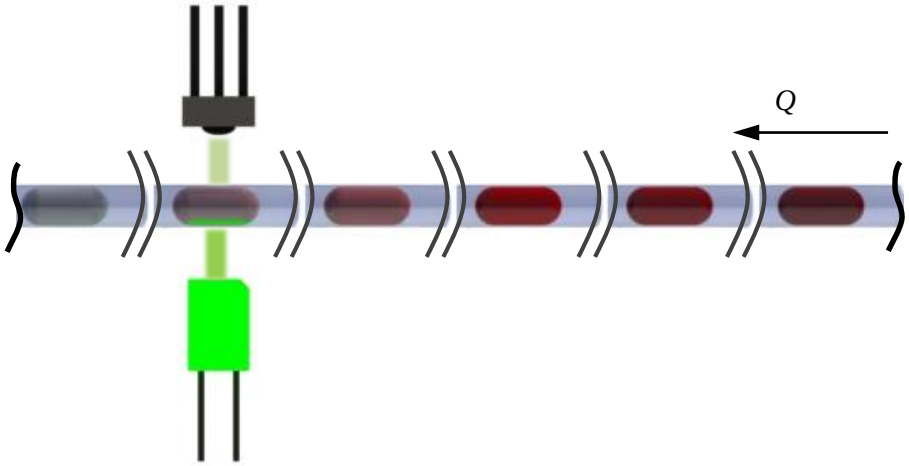

Figure 4.26 Flow cell detection device. It consists a pair of blue LED and photodiode. The droplets with red colour in the transparent PTFE tubing were examined with green light array, which attenuates differently due to the different strength of red colour.

4.5.2. Results and discussion

It was observed that droplets containing 400 mg/dL glucose in first channel can be effectively merged with the droplets containing glucose reagents in second channel, as shown in Figure 4.27 (A). However, these droplets containing glucose assays and glucose reagents experienced break-up in the following channel which would dramatically affect the accuracy of reaction and the measurement of colorimetric droplets. After the merged droplets exited from the mixing channel, they would be stretched by the viscous force, and thus the gutter flow was increased. Eventually, the droplets would break up. One of the example is given in Figure 4.27 (B). It may be because of the high viscosity of glucose assays or glucose reagents. The high viscous force competes with the capillary force to break the droplets. Instead of designing long winding channels in the merging chip, here a merging chamber was interfaced with a piece of PTFE

tubing (~50 cm) directly after the mixing channel and this can effectively avoid the break-up of droplets. The modified design is shown in Figure 4.28.

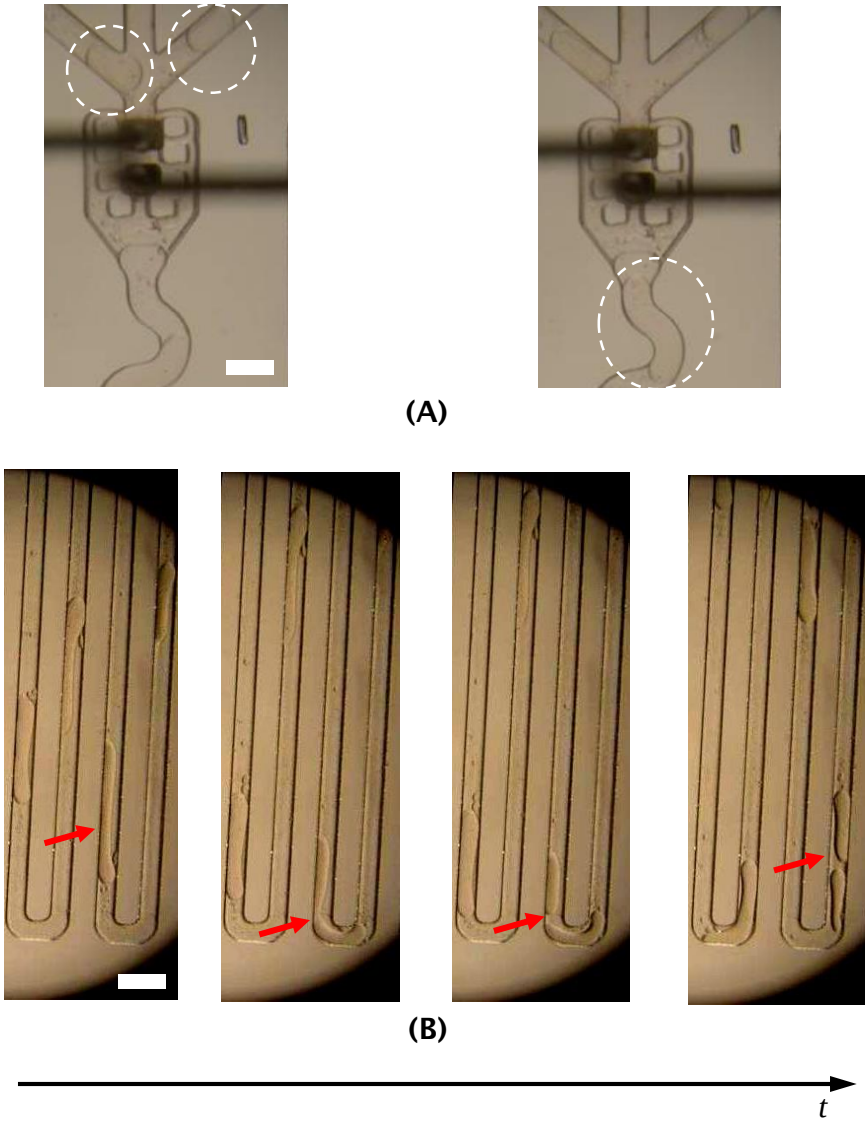

Figure 4.27 (A) An example of successful merging. (B) An example of break-up of droplets which contains glucose assays and glucose reagents. The viscous force is easily competing the capillary force to stretch the droplets. When the droplet goes through winding corner where high velocity could be generated, this high velocity further increased the viscous force and split the droplet by competing the capillary force. The scale bar is 1 mm. The brightness contrast has been tuned for better observation of the droplets.

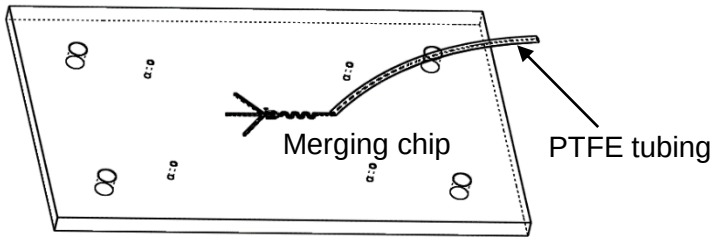

Figure 4.28 Modified design of merging chip. It consists a merging chip and a piece of PTFE tubing (~50 cm).

Figure 4.29 presents the calibration of colour dyes with the colorimetric flow cell device. Figure 4.29 (A) shows the measured intensity in which the low concentration is in left while the high concentration is in right. The intensity of droplets was picked in the central of a peak as highlighted. Interestingly, the two peak was not evenly placed, which is different from the observation in [15]. This may be due to the pulsatile movement of droplets. The quantified absorbance was plotted in Figure 4.29 (B). It was shown that the concentration of the colour dyes is linearly proportional to the absorbance, which shows an agreement with other calibration results [15].

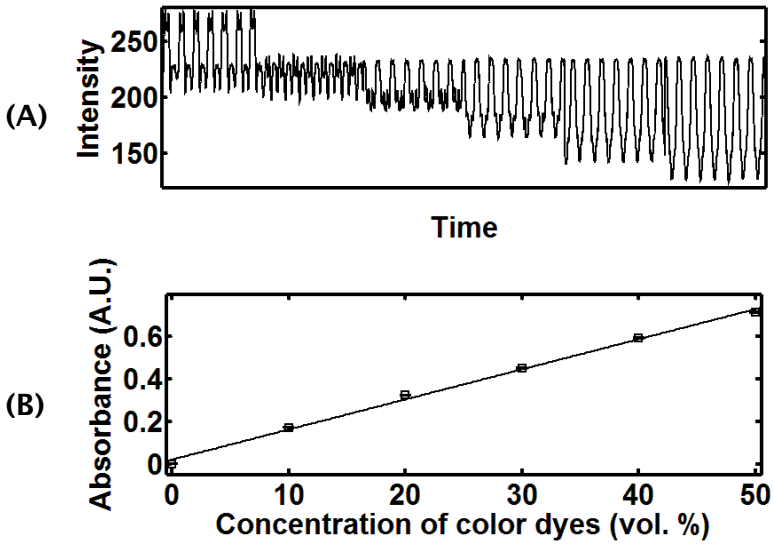

Figure 4.29 Calibration of colour dyes with different concentrations (vol. 0%, 10%, 20%, 30 %, 40% and 50%). (A) The measured signal which is ranging from 140 to 260. (B) The quantified absorbance. The concentration shows a linear relationship with the quantified absorbance.

Figure 4.30 shows the measured absorption versus the glucose concentration which shows a linear relationship. The merging-to-detection time could be reduced by further by optimising the reaction conditions for example the enzyme concentration and combination of the other reagents, or control of the oxygen environment by introducing an air bubble. But nevertheless, the example application shows the integrated system can be used in an automated enzymatic assay involving the mixing of three sample/reagents and sampling directly from a carousel robot or a well plate.

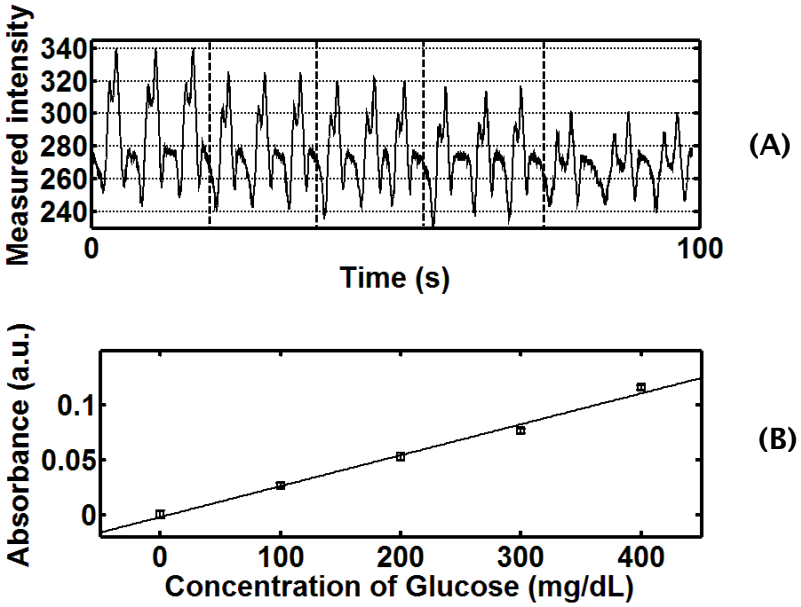

Figure 4. 30 Calibration of glucose (0 mg/dL, 100 mg/dL, 200 mg/dL, 300 mg/dL and 400 mg/dL). (A) The measured intensity for 5 different concentrations. Each concentration contains 3 repeat. From left to right, there are examined 0 mg/dL to 400 mg/dL. (B) Quantified absorbance.

4.5.3. Summary

This section applied the integrated system in screening of glucose and successfully demonstrated calibrating different glucose concentrations. This integrated system contrasts itself with other droplet screening platform especially on the easy operating procedures.

4.6. Conclusion

This chapter has developed three-parallel-channel peristaltic pumping and an integrated platform based on the results from Chapter 3. With this integrated platform, the synchronisation of droplets with different conditions, i.e. different sizes and different flow rates, has been investigated and implemented.

It was observed the quantified mean phase difference was generally smaller than 5%. The generation, size and phases of the droplets were not affected by each other even though a dynamic environment was created by generating variable sizes of droplets. However, the variable droplet sizes induce a phase change in the single channel. The investigation of the phase change of droplets in a single channel showed that droplets with a bigger size would be delayed while one with a smaller size would be advanced after they went through the peristaltic pump. It was believed that the strong pulsation caused the difference in the movement of droplets with different sizes. With the successful demonstration of synchronisation of droplets, the merging chamber could effectively trap and merge droplets. The coalescence of at least 60 groups of droplets has been demonstrated. Further, the coalescence of droplets with different samples was also demonstrated. This demonstration showed that the integrated system could realise the function proposed which is to inject different samples into the reagents. The interesting phenomenon of coalescence of droplets before merging was observed. It was also observed that the introduction of an air bubble could help to regulate the coalescence of droplets in the merging chamber. For example, with an air bubble generated in the Y-junction, 2 droplets could be effectively merged by the merging chamber that was designed for 4 droplets. Moreover, the introduction of air bubbles could help specific reactions that has high requirement of oxygen. The phase difference between the merged droplets and the droplets in one of the three parallel channels was generally smaller than 5%. This results suggested that further unit operations could be performed, such as further injecting reagents into the merged droplets for multi-step reactions. The screening of glucose with different concentration was carried out with the colorimetric detecting method. However, the droplets easily broke up in the channels of microfluidic chip. The break-up was analysed and believed to be due to the high capillary number. An alternative method was applied to introduce the merged droplets directly to the PTFE tubing and interrogated by the colorimetric flow cell device.

Reference list

1. Abate, A.R., et al., *High-throughput injection with microfluidics using picoinjectors.* Proceedings of the National Academy of Sciences of the United States of America, 2010. **107**(45): p. 19163-19166.

2. Zheng, B. and R.F. Ismagilov, *A microfluidic approach for screening submicroliter volumes against multiple reagents by using preformed arrays of nanoliter plugs in a three-phase liquid/liquid/gas flow.* Angewandte Chemie-International Edition, 2005. **44**(17): p. 2520-2523.

3. Song, H., et al., *On-chip titration of an anticoagulant argatroban and determination of the clotting time within whole blood or plasma using a plug-based microfluidic system.* Analytical Chemistry, 2006. **78**(14): p. 4839-4849.

4. Fuerstman, M.J., P. Garstecki, and G.M. Whitesides, *Coding/decoding and reversibility of droplet trains in microfluidic networks.* Science, 2007. **315**(5813): p. 828-832.

5. Prakash, M. and N. Gershenfeld, *Microfluidic bubble logic.* Science, 2007. **315**(5813): p. 832-835.

6. Ahn, B., et al., *Parallel synchronization of two trains of droplets using a railroad-like channel network.* Lab on a Chip, 2011. **11**(23): p. 3956-3962.

7. Xu, L.F., et al., *Fusion and sorting of two parallel trains of droplets using a railroad-like channel network and guiding tracks.* Lab on a Chip, 2012. **12**(20): p. 3936-3942.

8. Brouzes, E., et al., *Droplet microfluidic technology for single-cell high-throughput screening.* Proceedings of the National Academy of Sciences of the United States of America, 2009. **106**(34): p. 14195-14200.

9. Mazutis, L., J.C. Baret, and A.D. Griffiths, *A fast and efficient microfluidic system for highly selective one-to-one droplet fusion.* Lab on a Chip, 2009. **9**(18): p. 2665-2672.

10. Mazutis, L. and A.D. Griffiths, *Selective droplet coalescence using microfluidic systems.* Lab on a Chip, 2012. **12**(10): p. 1800-1806.

11. Lee, M., et al., *Synchronized reinjection and coalescence of droplets in microfluidics.* Lab on a Chip, 2014. **14**(3): p. 509-513.

12. Klein, A.M., et al., *Droplet Barcoding for Single-Cell Transcriptomics Applied to Embryonic Stem Cells.* Cell, 2015. **161**(5): p. 1187-1201.

13. Guzowski, J., et al., *Automated high-throughput generation of droplets.* Lab on a Chip, 2011. **11**(21): p. 3593-3595.

14. Du, W.B., et al., *Automated Microfluidic Screening Assay Platform Based on Drop Lab.* Analytical Chemistry, 2010. **82**(23): p. 9941-9947.

15. Gielen, F., et al., *A Fully Unsupervised Compartment-on-Demand Platform for Precise Nanoliter Assays of Time-Dependent Steady-State Enzyme Kinetics and Inhibition.* Analytical Chemistry, 2013. **85**(9): p. 4761-4769.

16. Wu, J.B., et al., *Multiple and High-Throughput Droplet Reactions via Combination of Microsampling Technique and Microfluidic Chip.* Analytical Chemistry, 2012. **84**(22): p. 9689-9693.

17. Pan, X.Y., et al., *Sequential microfluidic droplet processing for rapid DNA extraction.* Electrophoresis, 2011. **32**(23): p. 3399-3405.

18. Nightingale, A.M., et al., *Controlled multistep synthesis in a three-phase droplet reactor.* Nature Communications, 2014. **5**.

19. Shestopalov, I., J.D. Tice, and R.F. Ismagilov, *Multi-step synthesis of nanoparticles performed on millisecond time scale in a microfluidic droplet-based system.* Lab on a Chip, 2004. **4**(4): p. 316-321.

20. Barbier, V., et al., *Producing droplets in parallel microfluidic systems.* Physical Review E, 2006. **74**(4).

21. Adzima, B.J. and S.S. Velankar, *Pressure drops for droplet flows in microfluidic channels.* Journal of Micromechanics and Microengineering, 2006. **16**(8): p. 1504-1510.

22. Chokkalingam, V., S. Herminghaus, and R. Seemann, *Self-synchronizing pairwise production of monodisperse droplets by microfluidic step emulsification.* Applied Physics Letters, 2008. **93**(25).

23. Hong, J., et al., *Passive self-synchronized two-droplet generation.* Lab on a Chip, 2010. **10**(20): p. 2702-2709.

24. Hung, L.H., et al., *Alternating droplet generation and controlled dynamic droplet fusion in microfluidic device for CdS nanoparticle synthesis.* Lab on a Chip, 2006. **6**(2): p. 174-178.

25. Frenz, L., et al., *Microfluidic Production of Droplet Pairs.* Langmuir, 2008. **24**(20): p. 12073-12076.

26. Guo, F., et al., *Valve-based microfluidic device for droplet on-demand operation and static assay.* Applied Physics Letters, 2010. **97**(23).

27. Choi, J.H., et al., *Designed pneumatic valve actuators for controlled droplet breakup and generation.* Lab on a Chip, 2010. **10**(4): p. 456-461.

28. Churski, K., J. Michalski, and P. Garstecki, *Droplet on demand system utilizing a computer controlled microvalve integrated into a stiff polymeric microfluidic device.* Lab on a Chip, 2010. **10**(4): p. 512-518.

29. Churski, K., et al., *Rapid screening of antibiotic toxicity in an automated microdroplet system.* Lab on a Chip, 2012. **12**(9): p. 1629-1637.

30. Churski, K., P. Korczyk, and P. Garstecki, *High-throughput automated droplet microfluidic system for screening of reaction conditions.* Lab on a Chip, 2010. **10**(7): p. 816-818.

31. Zeng, S.J., et al., *Microvalve-actuated precise control of individual droplets in microfluidic devices.* Lab on a Chip, 2009. **9**(10): p. 1340-1343.

32. Bremond, N., A.R. Thiam, and J. Bibette, *Decompressing emulsion droplets favors coalescence.* Physical Review Letters, 2008. **100**(2).

33. Lai, A., N. Bremond, and H.A. Stone, *Separation-driven coalescence of droplets: an analytical criterion for the approach to contact.* Journal of Fluid Mechanics, 2009. **632**: p. 97-107.

34. Niu, X., et al., *Pillar-induced droplet merging in microfluidic circuits.* Lab on a Chip, 2008. **8**(11): p. 1837-1841.

35. Niu, X.Z., et al., *Electro-Coalescence of Digitally Controlled Droplets.* Analytical Chemistry, 2009. **81**(17): p. 7321-7325.

36. Ogilvie, I.R.G., et al., *Reduction of surface roughness for optical quality microfluidic devices in PMMA and COC.* Journal of Micromechanics and Microengineering, 2010. **20**(6).

37. Priest, C., S. Herminghaus, and R. Seemann, *Controlled electrocoalescence in microfluidics: Targeting a single lamella.* Applied Physics Letters, 2006. **89**(13).

38. Wang, K., et al., *Gas/liquid/liquid three-phase flow patterns and bubble/droplet size laws in a double T-junction microchannel.* Aiche Journal, 2015. **61**(5): p. 1722-1734.

39. Chabert, M., et al., *Automated microdroplet platform for sample manipulation and polymerase chain reaction.* Analytical Chemistry, 2006. **78**(22): p. 7722-7728.

40. Chen, Q.S., et al., *Qualitative and Quantitative Analysis of Tumor Cell Metabolism via Stable Isotope Labeling Assisted Microfluidic Chip Electrospray Ionization Mass Spectrometry.* Analytical Chemistry, 2012. **84**(3): p. 1695-1701.

41. Srinivasan, V., V.K. Pamula, and R.B. Fair, *Droplet-based microfluidic lab-on-a-chip for glucose detection.* Analytica Chimica Acta, 2004. **507**(1): p. 145-150.

5. *In-situ* droplet sampling

5.1. Background & introduction

In-situ sampling with microfluidics only removes small aliquot of target compounds, thus it can avoid disturbance to the normal balance of chemical compounds. It has become a method to investigate the complex and dynamical biological systems [3]. By taking less sample volume each time but more frequently, this method can significantly improve spatial-temporal resolution of the measured signals. Microdialysis is a successful demonstration of *in-situ* sampling, which is a technique for measuring extracellular concentrations of substances by means if a small probe equipped with a semi-permeable membrane. In contrast to biosensor techniques [3] where only a few well-known endogenous samples are applicable, e.g. glucose, electrolytes, and nitric oxide, microdialysis is suitable for more complex biological samples and can analyse a wider range of biomolecules. However, it is widely observed that Taylor dispersion from the sampling point to the detection point, during which samples are collected into vials with an auto sampler via a long tubing, is a big concern in microdaialysis [1].

To minimise the Taylor dispersion and to further increase the temporal resolution of sampling, Slaney *et al* [1] has demonstrated a droplet microfluidic system for monitoring *L*-glutamate in the striatum of anesthetized rats. The system utilizes droplets to digitalise the samples as soon as they are pumped out of the sampling point. The droplets are generated in a T-junction where the oil phase is pushed by a syringe pump and the aqueous phase is pulled by a vacuum pump. However, the generation of droplets is realised by a normal T-junction and poor local control of flow rates may decrease the accuracy of droplet generation. Besides, the cumbersome size of the total system because of the exploitation of syringe pumping limits this push-pull method from wider applications.

Different from this scheme, Chen et al [2] has developed a chemistrode in which pre-formed droplets are introduced into the specially designed ‘V’ chip with an opening at the bottom to interface with a substrate, for example a tissue sample. This special design ensures those droplets exchange contents with the substrate.

Molecules from the substrate are collected into those droplets, which are delivered downstream for analysis. In this scheme, droplets were generated with an aspiration device or T-junction and the whole system was pumped with syringe pumps or vacuum pumps. Yet again, this platform is cumbersome and difficult to have accurate control of droplets due to the syringe pumping and especially due the use of the 'V' chip. Besides, only substrate register-able contents can be applied in this scheme and this limits the range of applications.

Abate *et al* [4] applied a single syringe pump as a negative pressure source to suck both carrier phase and aqueous phase via flow-focusing which was termed as *drop maker*. Through this method, the aqueous phase can be collected directly from environment. Gielen *et al* [5] have further developed double tubes which are co-centralised to directly aspirate aqueous samples. However, as mentioned in the paper, robust control of droplets is impossible due to the difficulty in arranging fractions of aqueous phase and oil phase.

To solve the aforementioned issues and to widen the application of droplet microfluidics, this chapter proposes a novel and robust *in-situ* droplet sampling method with the exploitation of a single peristaltic pump. In this method, the pulsations from the peristaltic pump are intentionally employed to regulate the generation of droplets. This can effectively improve the accuracy of the droplet generation and thus eliminates the requirement of precise flow-rate control. To minimise the Taylor dispersion from the sampling point to the droplet generation point, a micro-screw peristaltic pump [6] was engineered to reduce the total device size so that it can be placed close to the sampling site, e.g. tissue. Upon droplet generation, target-specific chemical reagents can be added into the droplet to mix with the sample and initiate a reaction. A colorimetric detection device was integrated to monitor the droplets. Here, a glucose concentration calibration was demonstrated as an initial *in-situ* sampling application. It is believed that this *in-situ* droplet sampling method can find wide ranges of applications in environment monitoring, online healthcare and on-chip diagnosis, etc.

5.2. Proposed method to realise *in-situ* droplet sampling

Summarised from aforementioned work [1, 2], an *in-situ* droplet sampling platform incorporates three key modules (Figure 5.1): a sampling module which

is used to directly introduce samples into the system, a digitalisation module which digitalises the samples into droplets, and a detection module to monitor and examine the samples, or operation modules if necessary. The sampling module should be able to directly introduce samples into the system. For example, in the *push-pull* scheme [1], samples from the environment can be directly aspirated into a T-junction rather than being loaded into a syringe pump or being registered in a container. The digitalisation module should have the capability to generate droplets with high accuracy, particularly in the case where samples from environment are varied in terms of viscosities and surface tensions. The digitalisation module shall be closely connected to the sampling module and thus Taylor dispersion can be minimised.

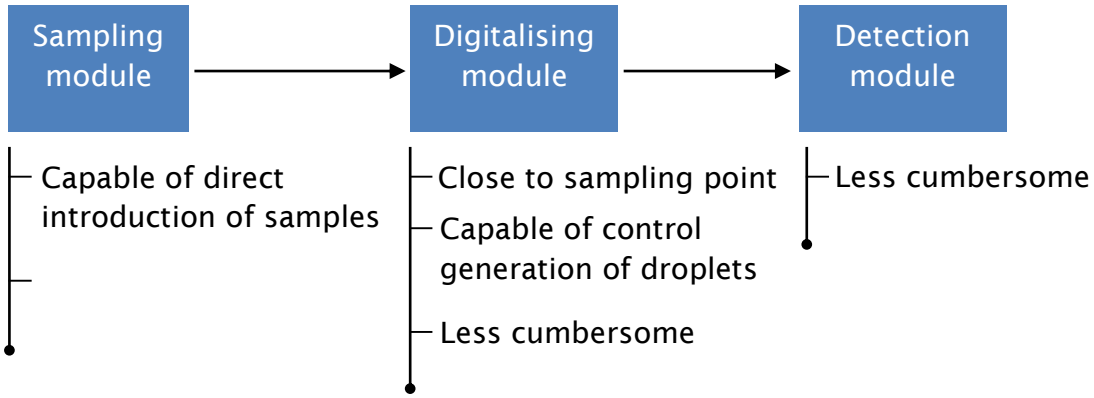

Figure 5.1 Key modules of *in-situ* droplet sampling platform which is summarized from the processes of in-situ sampling [1, 2]. Three key modules: sampling module, digitalising module and detection module. The descriptions in the bottom of each module are the requirement of designing the module.

These special requirements need an intrinsic fluid delivery method and a droplet generator to couple with. Here, a peristaltic pump is proposed to realise *in-situ* droplet sampling. Generally, a peristaltic pump applies shoes, rollers or other mechanisms to generate fixed occlusions to consistently deliver fluids, which provides a push-pull feature. With this feature, the pump can directly collect samples from environment and continuously deliver fluids. During this fluid delivery process, pulsation of flowrates inherently exists. This pulsation can be applied to regulate the generation of droplets with differentiating phase of oil phase and that of aqueous phase to be 180°. When these two streams with 180° phase difference are delivered into the same channel, e.g. via a T-junction, due to the pulsations of each flowrate and their phase difference, the introduction of the two fluids are alternating, as shown in Figure 5.2. Following this alternative pattern, the generation of droplets can occur at the T-junction or flow-focusing

junction and thus the generation can be regulated. Therefore a reliable droplet generation can be realised. Such generation is similar to the alternative introduction of fluids into a T-junction via a valve-controlled platform [7-9].

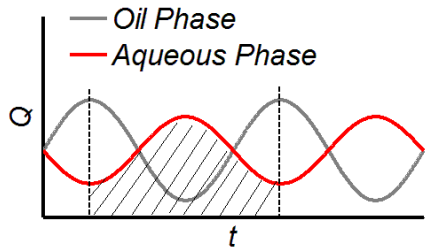

Figure 5.2 Schematic of flow-rate plot of oil phase and aqueous phase with 180° phase difference. The flow rate of the oil phase is highlighted in grey and that of aqueous phase is highlighted in red. The designed volume of a droplet is highlighted in grey shadow in a regulated format.

Based on this proposal, a preliminary design is sketched in Figure 5.3. Instead of using the classical roller peristaltic pump which has been demonstrated in Chapter 3 and Chapter 4, here, a screw-driven peristaltic pump which can be easily engineered was applied due to the fact it is easy to calibrate the phase of flow rates for oil phase and aqueous phases. Two of the channels which are used to deliver aqueous phase and oil phase are placed in opposite (180°) side of the screw, thus ensure an 180° phase difference for the two flows. As soon as the aqueous phase exits from the aqueous phase channel, it is introduced into a well-designed T-junction which is placed close to the screw. Following the

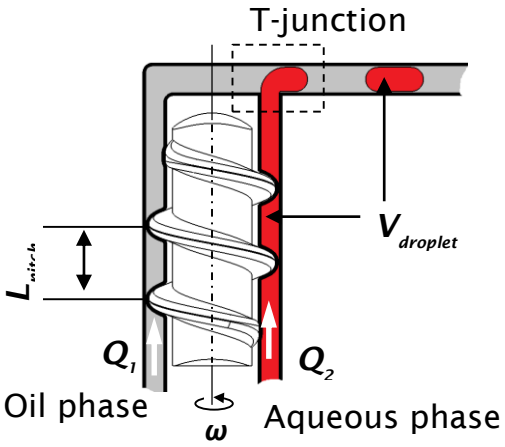

Figure 5.3 The proposed miniaturized peristaltic pump and droplet generation. The side-view of the peristaltic pump with two channels driven by a screw shaft.

designed alternative format, the volume of aqueous droplets equals that of the aqueous fluids delivered in one period. If the pumping efficiency is 100 %, the two volumes equal to that of occlusion between the adjacent pitches.

5.3. Preliminary engineering and demonstration of *in-situ* droplet sampling

5.3.1. Introduction

Based on the sketch in Figure 5.3, in this section, a miniaturised peristaltic pump with a screw-driven format was preliminarily designed, engineered and tested. With the device, the generation of droplets was demonstrated. The demonstrations show that such scheme is able to generate droplets stably and accurately. Together with the direct sampling introduction format, it is evident that this novel generation method is able to realise *in-situ* droplet sampling.

5.3.2. Design and fabrication of the miniaturised peristaltic pump

The screw shafts with pitches 5 mm were designed in Solidworks™, and fabricated with VeroClear™ material by a 3D printer (Objet, Connex 1). The screw shaft is driven by a micro-gear DC motor (gear ratio 298:1, medium power, Pololu Brushed DC motor) via a concentric tube fixed with two grub screws, as shown in Figure 5.4 (A). This high gear ratio (298:1) can ensures the shaft of the motor can sustain comparatively high torque. To compress the peristaltic tubing, a cassette with specific grooves that could hold 4 tubes was designed as shown in Fig. 5.4 (B). A motor shell was designed to contain the micro-gear motor, with the consideration that it should fit the cassette to link the two parts. Both the cassette and the motor shell were fabricated with a 3D printer.

To assemble the pump, two peristaltic pump tubes were inserted into the cassette, one of which was for the oil phase channel and the other was for the aqueous samples channel. After the insertion of the tubing, the screw shaft, connected to the micro-gear motor, was inserted into the cassette. To decrease the friction between the tubing and the screw shaft, lubricant was applied on the surface of the screw shaft. The peristaltic pump tubing used is commercialised Viton™ tubing with inner diameter 0.8 mm for the oil phase channel and PVC tubing with inner diameter 0.25 mm for the aqueous sample channel.

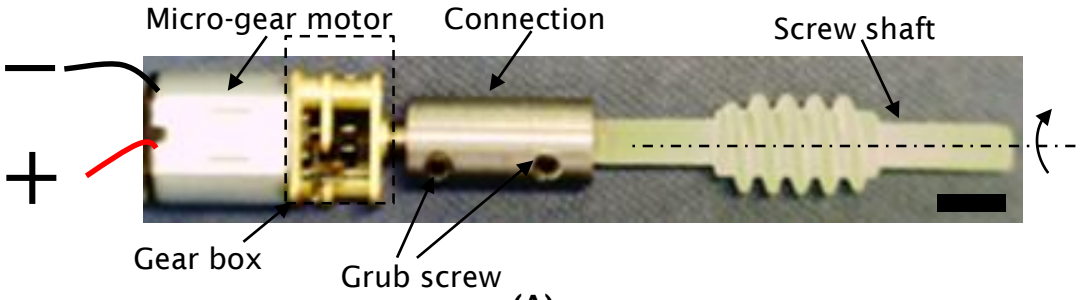

(A)

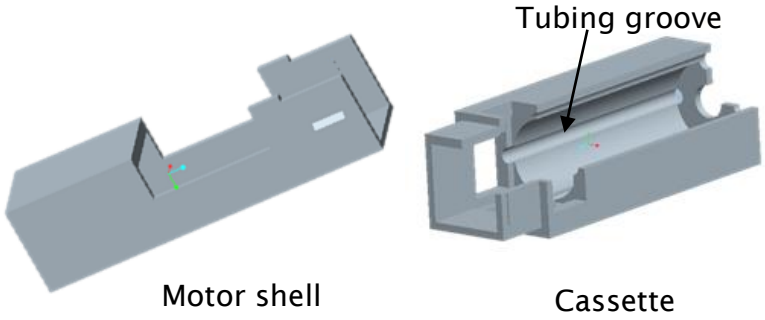

(B)

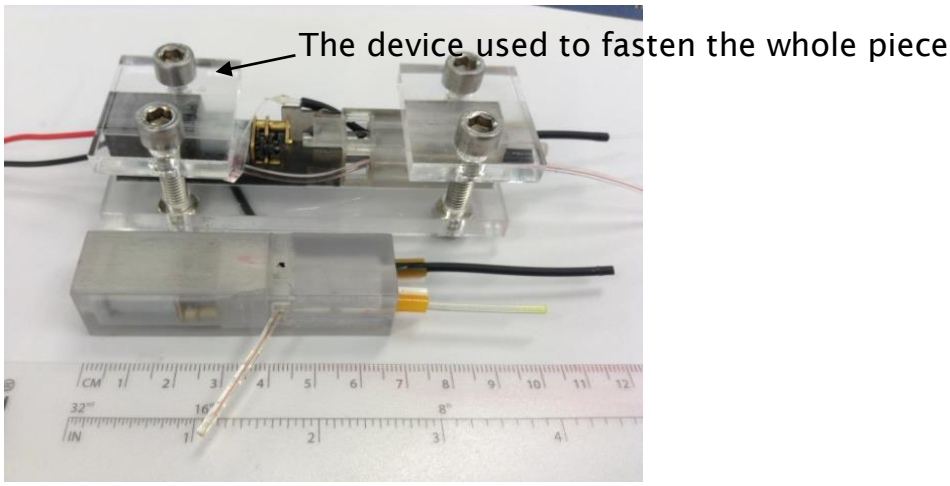

(C)

Figure 5.4 Design and assembly of the miniaturized peristaltic pump. (A)The assembly of screw shaft with micro-gear motor linked by concentric metal tube fixed by two grub screws. Scale bar: 1 cm. (B) The design of motor shell and cassette. (C) The assembly of the pump which was enhanced by a rig. The total dimension was 95 mm × 14 mm × 14 mm.

To test the assembly of the pump, 6 DC voltage was applied to the pump. It was observed the motor shell could not sustain high torque from the micro-gear motor. To solve this problem, a rig was added to hold the whole pump. The rig was fabricated with PMMA and fixed by four M5 screws. The total size of the assembly is 95 mm ×14 mm ×14 mm. Compared with the commercial peristaltic pump used in Chapter 3 and Chapter 4, the dimension is dramatically reduced and it is believed it can be further reduced with further engineering.

PDMS microfluidic chips were fabricated with T-junctions for droplet generation. The processes of replicating the T-junction pattern and bonding PDMS chips are schematically shown in Figure 5.5. The channel dimension is 0.2 mm: 0.2 mm in this application.

5.3.3. Results and discussion

Firstly the total flow rates of fluids in output, which contains the oil phase and the aqueous phase, was characterised using the same method as used in Section 4.3.4 in Chapter 4. In this experiment, droplets generated in the T-junction were used as indicators for calculation of the total flow rate after the T-junction. The DC voltage to power the pump was adjusted from 2.5 V to 6 V with 0.5 V increments, to realise different rotation frequencies, 0.18 Hz, 0.22 Hz, 0.26 Hz, 0.32 Hz, 0.36 Hz, 0.41 Hz, 0.46 Hz and 0.52 Hz.

Figure 5.6 presents the relationship between the mean value of total flow rate and the shaft rotation frequency. It was found the flow rate was linearly proportional to the rotation frequency. This linear relationship shows an agreement with the results in section 4.2, and other flow rate calibrations of peristaltic pumps. The insert plot in Figure 5.6 details the total flow rate against time. It can be seen that in each period there are two peaks and two troughs in one period such as marked in blue circles for peaks and red for troughs. Compared with the real-time video, it was found that the larger peak represents the moment when the oil flow- is dominant while the smaller one represents that of aqueous phase. This phenomenon is similar with that in [6]. The normalised time difference between peak 1 and peak 2, T_{pp}/T, was found to be 50 %, while that between trough 1 and trough 2, T_{bb}/T (as shown in Fig. 5.6), was also found to be 50 %. The two normalised time differences are identical to the 180° phase difference, as designed.

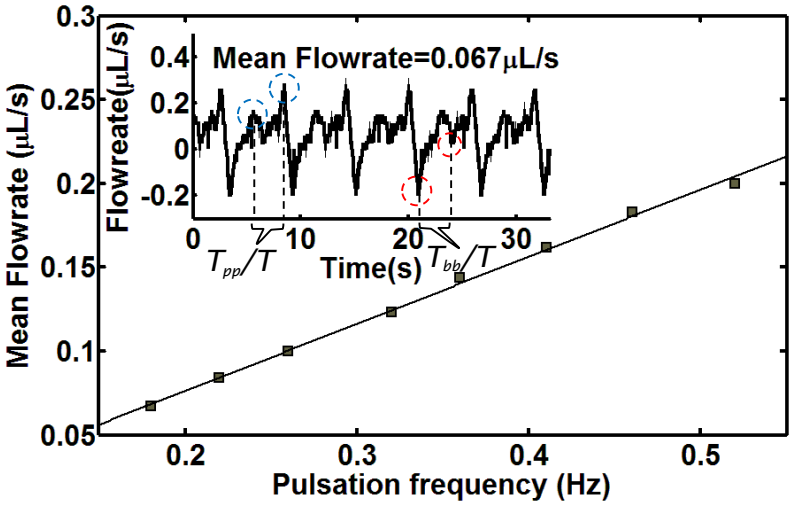

Figure 5.6 Measurement of flow rate at different rotation frequencies. The main plot: the pulsation frequency against the mean joint flow rate. Insert plot: an example of the joint flow rate at rotation frequency 0.18 Hz. The normalized time difference between the peak of oil phase and that of aqueous phase is defined a T_{pp}/T, while that between the troughs is defined as T_{bb}/T

To characterise the droplet generation, a series of measurements were performed with different motor rotation frequencies. The methodology of the measurement is the same as that used in Section 3.3.2 in Chapter 3, to capture key snapshots to measure the length of droplets in a fixed channel.

In the experiment the length of the tubing to interface the peristaltic pump into T-junction was reduced to be ~5 cm. It was found that with shorter tubing length which can contribute to reduced compliance and resistance in the pumping system, the pulsations in the flow is more prominent. This makes the alternative introduction more obvious. In all of the experiments, it was observed that droplet generation frequencies were always identical to the pulsation/rotation frequencies. It was found the polydispersity was generally in between 1 % and 2 %, as shown in Figure 5.7. Such small polydispersities in the method are comparable with the other traditional T-junction generations. The volumetric sizes of droplets generated at each frequency were equal with standard deviation 0.74% as shown in Figure 5.6. This result indicates that the sizes of droplets did not change with the total flow rates or generation frequencies. As the generation frequencies are identical to pulsation frequencies, the droplets sizes are identical to the fluids volume delivered in one period, which is merely determined by the designed parameters: pitches and I.D. of aqueous channels and the pumping efficiency which is normally 100 % with tight compression.

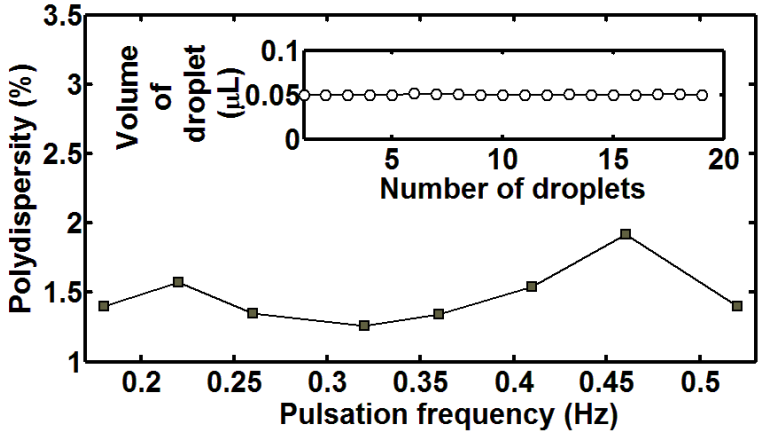

Figure 5.7 Polydispersities of droplets generated at different frequency. The pulsation frequency is ranging from 0.1 Hz to 0.6 Hz, which is identical to the frequency of generation. Each polydispersity is calculated from 20 droplets. Inset plot: an example of volumes of individual droplets with pulsation frequency 0.1 Hz.

In contrast to typical generation methods in a T-junction with syringe pumps, which is sensitive to flow-rates, this approach generates a single constant size of droplets: the size of droplets does not rely on the flow rate. This feature makes the precise control of flow-rate superfluous and demonstrates its capability on metering and fixing size of droplet, a function which was realised

by Steijn et al [10] and further applied by Korczyk et al [11]. Together with its direct sampling format, this generation method can be easily applied in point of care, diagnostic in emergency, and environment monitoring where fluidic conditions are diverse.

The resolution of this 3D printer (X-axis: 600 dpi; Y-axis: 600 dpi; Z-axis: 1600 dpi), is high compared with other traditional fabrication method such as milling. Therefore, friction was comparably strong so that the pump can only drive 2 tubes in total as tested. Additionally, a significant temperature rise was observed such that the plastic screw shaft can only run for limited periods and generate only a limited number (<50) of droplets. This temperature rise can make the life of screw shaft short. Due to the short life of screw shaft, it is difficult to consistently observe the generation of droplets and the robustness of this device is significantly restricted.

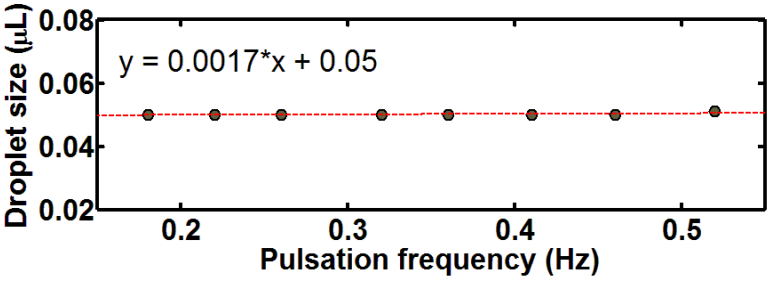

Figure 5.8 Mean value of sizes of droplets at different frequencies. The sizes are equal with standard deviation 0.37 nL which is small compared with the mean value 0.5 μL.

5.3.4. Summary

In this section, based on the preliminary design, a screw-driven peristaltic pump was designed and engineered to demonstrate a stable generation method with a direct sampling format. The polydispersity of the droplets is normally smaller than 2 %. It was observed that the sizes of droplets generated at different frequencies do not change with flow rates or the generation frequencies. It is evident this device can realise *in-situ* droplet sampling. However, the friction was still high due to improper compression and the 3D printed rough shaft.

5.4. Multiple-channel sampling with a peristaltic pump

In this section a modification of the screw-driven peristaltic pump is presented,

which is able to drive multiple channels, have high sustainability and have a long life time. A sandwich structure was adopted thus making uniform compression possible. With the device, droplet generation was systematically calibrated and the processes of droplet generation was observed. Such understanding of the processes of break-up of a droplet can be applied to realise intermittent generation of droplets which is useful in controlling the reaction time of the samples in the droplets. With the multiple-channel-driven capability, a glucose enzymatic assay was implemented as an example of application of *in-situ* sampling and analysis using the new system.

5.4.1. Design and fabrication

To drive multiple-channels, a sandwich structure was designed which is able to tune compression force, as schematised in Figure 5.9. The screw shaft is sandwiched in between two cassettes that have multiple embedded channel grooves to house tubing. The tubing for the oil phase channel is placed in the bottom while 3 tubing for different aqueous samples are placed on top. It should be noted that there are small phase difference (~5°) between the aqueous tubing. The centroid of the 3D printed cassettes can be modelled as a beam (Figure 5.9 (B)), which can bend in the initial design after a few minutes' usage, and the screw thread can no longer pump the PVC tubing. To solve this problem, a thicker cassette (~1cm) is designed to prevent deformation as shown in Figure 5.9 (C).

Based on this sketch, the pump was designed as shown in Figure 5.10. The screw shaft is suspended by the frame which can be plugged into the motor container. The motor container hosts the micro-gear motor. Cassette 1 could house 3 peristaltic pump tubes for aqueous phases while cassette 2 could house 1 peristaltic pump tube for the oil phase. 4 screws were used to fix the two cassettes on both side of the frame. By adjusting the screws, the sandwiching pressure could be tuned. It should be noted in this design the pressure may change in each assembly. The peristaltic tubing housed in the channel groove was pressed by the screw shafts and the cassettes. To easily add lubricant into the gear box of the motor and the screw shaft, lubricant holes are designed. Square windows on the motor shell are designed to lower the temperature generated by the micro gear motor. Rather than applying a concentric tube to link the screw shaft to the motor shaft as in last section, here, grub screws (M

1.5) were applied to hold them together.

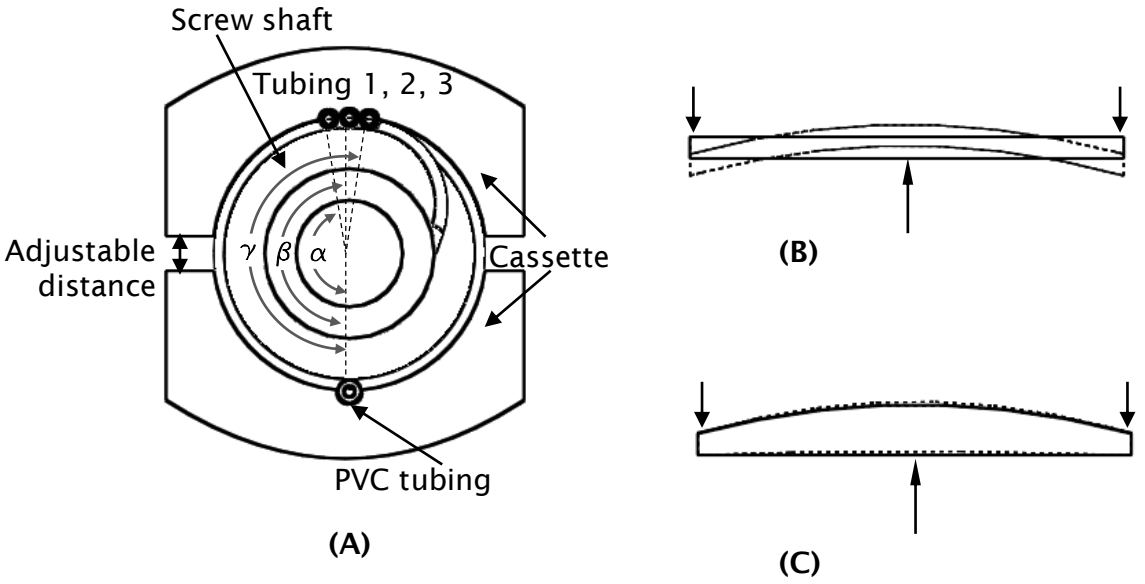

Figure 5.9 Modified design of the micro-peristaltic pump. (A) Sketch of the sandwich structure of the peristaltic pump. α ≈175°, β ≈180° and γ ≈185°. (B) Beam model of flat cassette (C) Beam model of cassette with thicker centroid.

The screw shaft was fabricated with aluminium on a lathe. Here, the screw shafts with a series of pitches (7 mm, 5.5 mm and 4 mm) were designed and fabricated. The key dimensions of the screw shafts are shown in Figure 5.11. After the aluminium shaft was machined, the surface was polished to reduce friction between the screw thread and peristaltic pump tubing. Side holes were drilled and taped so that the grub screw could directly fix the screw shaft to the micro gear motor shaft. The motor container, cassette 1, cassette 2 and frame were still fabricated with 3D printer. The screws to link cassette 1 and cassette 2 are M 3. All of the tubing applied in this version are PVC tubing (PVC Manifold tubing, Watson, Marlow). The tubing is restricted to be ~ 50 mm long. All the components are shown in Figure 5.12. The total dimension of the pump is 70 mm × 17 mm× 17 mm, which is significantly smaller than the design of the preliminary version in section 5.3.

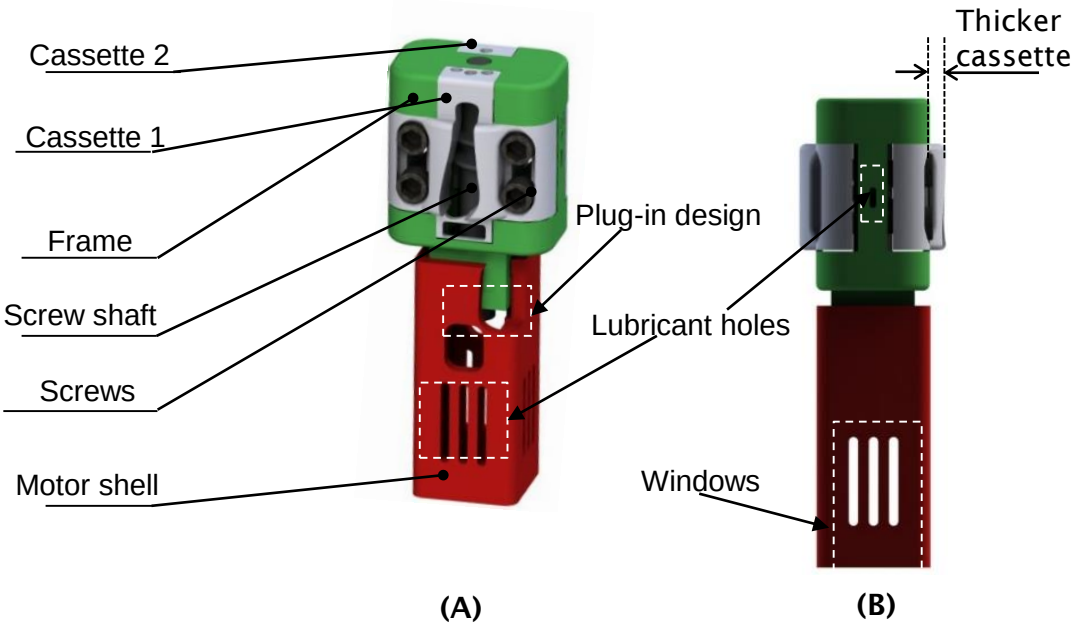

Figure 5.10 Design of the sandwich structure of the peristaltic pump. The design includes cassette 1 that hold three tubing, cassette 2 that hold one tubing, frame, screw shaft, screws to link cassette 1 and cassette 2, and motor shell which is used to contain the micro gear motor. (A) Front view (B) Right view.

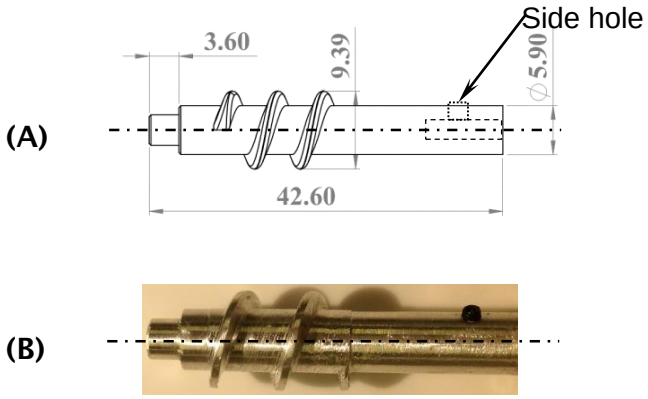

Figure 5.11 Fabrication of the aluminum screw shaft screw shaft. (A) Design of screw shat with pitch 7 mm. The key dimensions are highlighted. (B) Fabrication of the screw shaft.

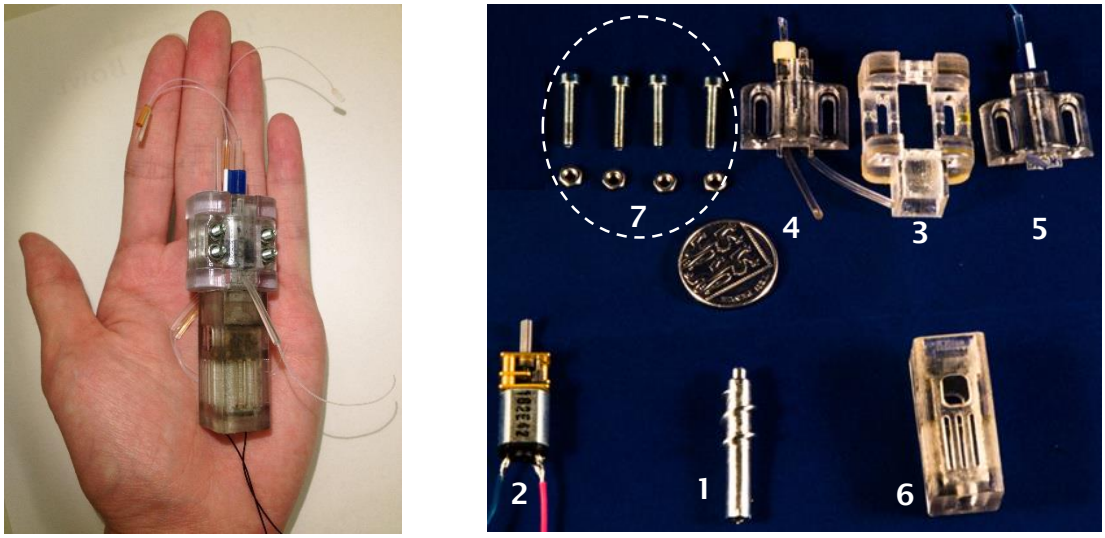

(A) (B)

Figure 5.12 Fabrication of the pump. (A) Assembly of the pump (B) Essential components of the pump. 1. Screw shaft; 2.Micro-gear motor; 3. Frame; 4. Cassette 1; 5. Cassette 2; 6. Motor shell; 7. 4 × M 3 screws and nuts.

5.4.2. Experimental set-up & rig

To characterise the pump, a rig was developed for easy transportation, quick set-up, and convenient arrangement. Similar to the design of the integrated system in Chapter 4, a miniaturised optical platform was made to compact all components together, as shown in Figure 5.13. The grid tapped holes are in M 3 with adjacent parallel distance 15 mm. The platform contains camera holder, sample container, pump holder that holds the pump, chip holder that holds the chips for some certain experiments. The pump is constrained by the pump holder which is screwed with the optical platform. With a chip holder, the microfluidic chips could approach the pump closely to reduce the distance between the pump and the chip. The chip holder could move along x axis ranging from 0 to 30 mm, which gives more flexibilities to the chips. The camera used in the experiment is micro-camera (Veho 20-400x Magnification Digital Microscope Camera). With the camera holder, the camera could easily approach the microfluidic chips. The design allows the camera to move along *x* axis with

range from 0 to 18 mm. The sample container is placed closely to the pump so that Taylor dispersion is expected to be minimised.

When designing the container, one may desire that the container will be capable of collecting the waste from the microfluidic chips, circulating the oil phase to save the oil, and adding extra samples during the experiment. Figure 5.13 (A) shows the design of this sample container. It could include 9 different samples. A guiding channel was designed to ensure the samples in the well did not exceed the maximum volume to contaminate the samples in other wells. As shown in Figure 5.13 (A) Front view, well 1 is designed to store the oil phase while well 2 is designed to collect the waste, and the two wells are connected via a channel. The waste that contains oil phase and aqueous phase will be separated in well 2 as the density of aqueous droplets is generally smaller than that of the oil phase. The aqueous phase is floating on the top while the oil phase is going to the bottom. With the accumulation of aqueous samples on the top, the extra waste samples that are separated will go to the waste well. This process ensures a generic circulation of oil phase. With this design, only ~300 µL FC 40 oil is needed in the experiment.

With this rig design, microfluidic chips were designed with standardised sizes that can be easily mounted on the chip holder. As shown in Figure 5.13 (B), the chips were made with PDMS, each contains 8 holes (2mm) for fixing. Here, a 3D printer was used to print the chip mould with Veroclear™ material. The mould was further cured at 60 °C overnight to remove the solvent, (which was found to affect the curing and bonding of PDMS chips). Two different widths were designed for the main channel of T-junctions (0.2 mm, and 0.3 mm) and all have a height 0.2 mm. As shown in Figure 5.13 (B), the three aqueous phase channels join an oil phase channel at a T-junction.

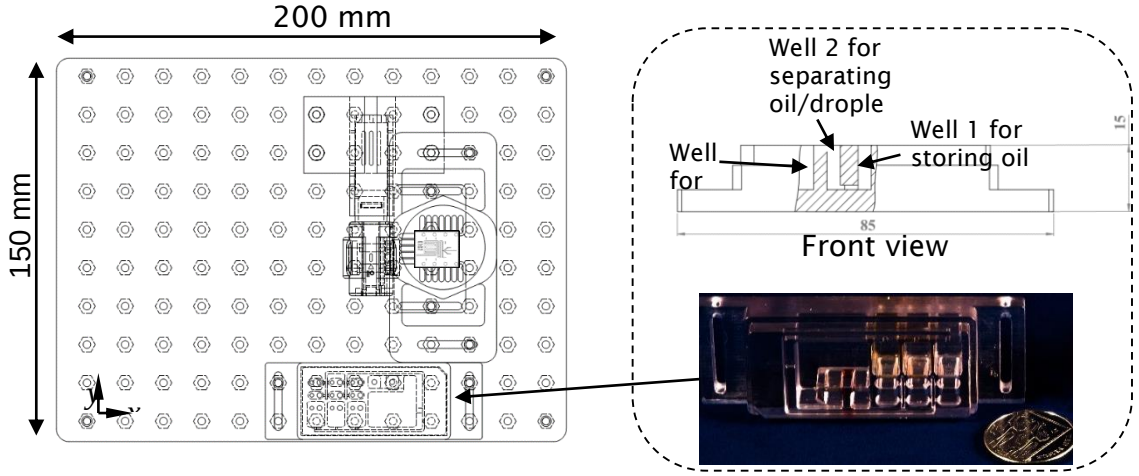

(A)

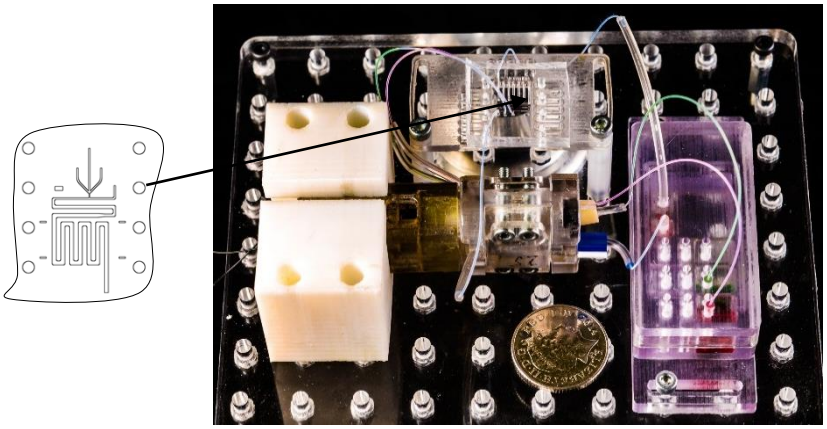

(B)

Figure 5.13 Design and assembly of the rig which compacts the pump, microfluidic chips, micro-camera holder and sample container together. The total dimension is 200 mm × 150 mm × 120 mm. (A) The Top view of the rig. (B) 3D design of the rig.

5.4.3. Investigation of generation of droplets

5.4.3.1. Introduction

Firstly, this section systematically characterises the generation of droplets with this new modified pump. Secondly, this section observes, interprets and understands the processes of break-up of droplets in different conditions. Such understanding formulates a generic process of generation of droplet with this

generation scheme and suggests the requirements of the generation.

The experiments were carried out with different combinations of screws with different pitches (7 mm, 5.5 mm and 4 mm) and PVC tubing (I.D. 0.19 mm and 0.13 mm. In the experiment, D.I. water mixed with food dyes as the aqueous phase, while the FC 40 oil with w.t. 1.8 % homemade surfactant [12] was used as carrier phase.

5.4.3.2. Results and discussion

Characterisation of generation of droplets

To stably generate droplets, the width of main channel in the T-junction was tested to choose the optimal dimensions. Table 5.1 details the selections of channel width of the T-junction for different combinations of PVC tubing and screw pitches. In each combination, there were ~1500 droplets (Figure 5.14 (A)) consistently generated and the pulsation frequencies were spontaneously changed, whose experimental conditions are different those in normal T-junction with syringe pumping system that needs a few minutes (>10 minutes) to stabilise the generation before measurement.

Table 5.1 The dimensions of the main channels for different combinations of oil phase channels and aqueous phase channels and pitches of screw shafts

I.D. of PVC tubing ×3	Pitch 7 mm	Pitch 5.5 mm	Pitch 4 mm
0.19 mm	0.3 mm	0.2 mm	0.2 mm
0.13 mm	0.3 mm	0.2 mm	0.2 mm

Figure 5.14 (B) presents the results of mean sizes of droplets generated among 6 combinations with frequencies from 0.8 Hz to 2.2 Hz. The biggest mean size of droplets was 0.22 μL, generated by the screw shaft with pitch 7 mm and the PVC tubing with inner diameter 0.19 mm, at a generation frequency 1.8 Hz. The smallest one was 0.052 μL, generated by the screw shaft with pitch 5 mm and the PVC tubing with inner diameter 0.13 mm at a generation frequency 1 Hz.

Standard deviation was used to characterise the droplet sizes at different generation frequencies. As shown in Figure 5.14 (C), the standard deviation was generally smaller than 2.33 %, which occurred at the combination of screw shaft 7 mm and PVC tubing with inner diameter 0.13 mm. The small deviation indicates that the sizes of droplets were constant at different generation frequencies and this further concludes that the size of generation does not change with the total flow rates or generation frequencies.

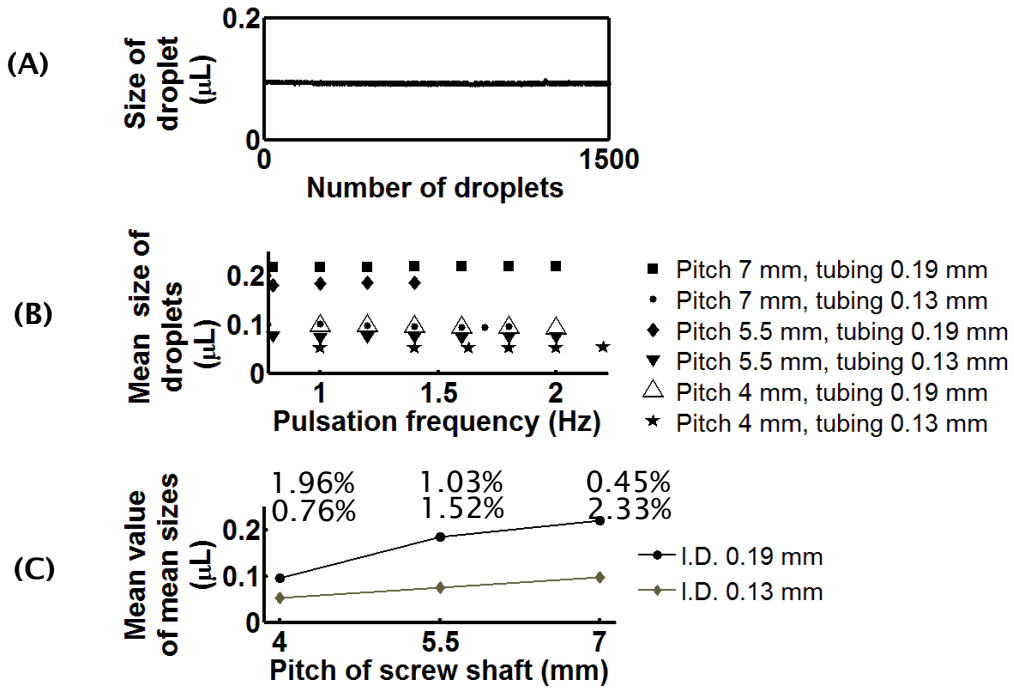

Figure 5.14 Characterization of generation of droplets in different combinations: screw pitches, inner diameters of PVC tubing for aqueous phases. (A) Shows an example of sizes of droplets generated by screw shaft with pitch 7 mm in the tubing with I.D. 0.13 mm, ranging from generation frequency of 1 Hz to 1.8 Hz. (B) Mean sizes of 100 droplets. The generation frequencies were ranging from 0.8 Hz to 2.2 Hz. (B) The mean value of mean sizes at each combination of tubing dimensions (I.D. 0.13 mm, I.D. 0.19 mm) and screw shafts (pitch 4 mm, 5.5 mm and 7 mm)

During each operations, the compression pressure on the PVC tubing was difficult to set constant. This difference can change the volume occluded in between the pitches and thus change the volume of fluids delivered during one period, thereby varied droplet sizes from different operations although the droplet sizes were uniform in one operation. Figure 5.15 shows the volume of the droplets can change by 10.87 % when the tubing was tightly compressed or loosely compressed.

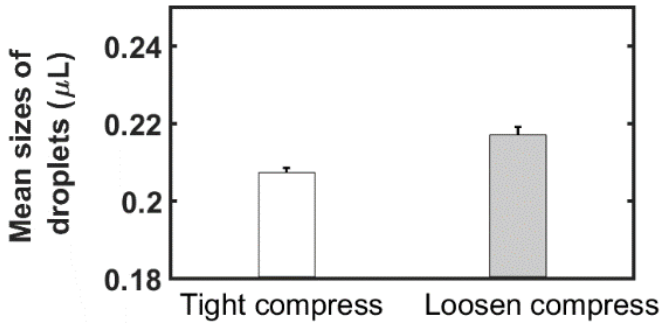

Figure 5.15 The comparison of sizes of droplets generated at different compress conditions. The droplets generated in tight compress conditions had mean size of 0.205 μL with polydispersity of 1.11%, while those generated in loosen compress conditions had mean size of 0.23 μL with polydispersity of 0.93 %.

Observation of the processes of break-up of droplets in T-junction

During the generation of droplets, it was observed that disturbance can occur near the boundary between the adjacent aqueous samples in the T-junction as shown in Figure 5.16. The aqueous contents (clear and red) in channel 2 and channel 3 were deflected to channel 1 due to pulsation of the flow-rate in first channel. This phenomenon sequentially occurs to aqueous phases in channel 2 and channel 3. It should be noted that this deflection may weaken the pulsation of the total flow rates of aqueous phases.

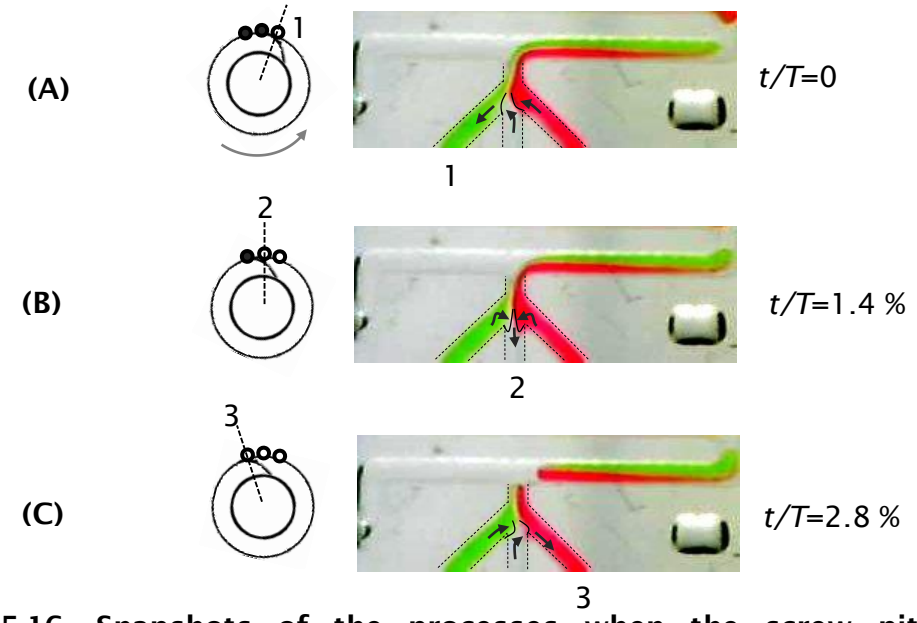

Figure 5.16. Snapshots of the processes when the screw pitches sequentially release the sample tubing. (A) The pitch is releasing the first tubing; green aqueous phase is withdrawing which pulls clear aqueous in channel 2 and red aqueous phase in channel 3 to channel 1 (B) The pitch is releasing the second tubing; (C) The pitch is releasing the third tubing

The total flow rate after the T-junction was measured as shown in Figure 5.17 with the screw pitch 7 mm, aqueous phase tubing with 0.13 mm i.d. and the oil phase tubing 0.25 mm i.d. It should be noted that this total flow cannot show details about the local flow rates at the T-junction, but it does indicate phase of pulsations in the aqueous channels and the oil channel from the observation. The measurement showed that there were two pulsatile troughs and one obvious pulsatile peaks in one duty period time T, and the total flow rate was ranging from 0.592 μL/s to -0.797 μL/s. T_{bb}/T was calculated to be 50%. As shown in inset plot in Figure 5.17, the first peak occurred at 123 ms while the two pulsatile troughs occurred at 300 ms and 928 ms respectively. The processes of break-up of droplets were interpreted by the optical micrographs which were depicted from the snapshots of the droplet. There identified six stages of formation of a droplet in one duty cycle. In **Stage 1** (snapshot I) t=30 ms, the tip of the aqueous phase entered into the main channel. In **Stage 2** (I~II), the aqueous phase was filled into the main channel and the tip attempted to block the main channel. This process lasted from t=30 ms to t=213 ms. The tip still did not detach from the main aqueous phase as the shear force upon the neck was not strong enough to shear it, which is related to the viscosity of the oil phase and local speed of oil phase [13]. Notably, to reduce the shear effect, the local speed of oil is constrained to be small given that the viscosity of oil is fixed. To realise that, in this stage, the width of the main channel was required to be bigger and the flow rate was required to be smaller to weaken the local speed. In **Stage 3** (II~III), the tip in the channel was suddenly directed upstream, which was due to the strong pulsation from the oil phase. In the meanwhile, the aqueous phase continued to fill the channel as the flow rate of aqueous phase was positive at this stage. Specifically, during this stage, the negative flow rate of oil attempted to squeeze the tip to detach from the main aqueous phase, which was not desired in the generation. The third stage lasted from 213 ms to 306 ms. In **Stage 4** (III~IV), which lasted 569 ms, the movement of the tip was towards downstream, and this movement would eventually make the tip bound in between the upper wall of the main channel and left wall of the side channel and start to stretch the interface. In this particular moment, the characteristic length is d, this follows the definition in Garstecki's model [13]. In this stage, the break-up cannot occur as the interface has not been stretched. In **Stage 5** (IV~V), the oil is squeezing the tip to thin the neck and the growth of the size of droplets was weakly going as the flow rate of aqueous phase was approaching zero. The squeezing makes

the bounded interface stretched. Eventually, the tip stops to grow. In **Stage 6** (V~VI), the tip was completely stopping to grow and the oil was continuing to thin the neck. This thinning could eventually bring the droplet to break-up in the end (t=1070 ms). The stage lasted for 129 ms and accounted for 13.1% in the whole duty period. All other observations of droplet generation show similar processes as shown in video 5.1_a and video 5.1_b.

The crucial step for droplet breakup is the thinning of the neck of aqueous tip occurred in **stage 5** and **stage 6**. In **stage 5**, the thinning of the neck of the tip was due to squeezing of the oil phase. In this stage, the process is similar to the typical squeezing mechanism as studied in [13-16]. According to Garstecki's model [13], the squeezing rate equals to the speed of oil in the squeezing area. In **stage 6**, the thinning is due to squeezing of the oil phase and the abrupt change of flow-rate of aqueous phase. In this generation scheme, the neck is always expected to be thinned off during one period. To achieve this, the oil phase should be able to compete the characteristic distance, *d*, with the assistance of abrupt flow rate change of aqueous phase. This compete could happen in **stage 5** (see video 5.2), such as the flowrate of oil is strong enough. If the conquer could not be finished in the end of **stage 6**, this generation needs more than one period, which is termed as *irregular generation*. This can be finished in one period is termed as *regular generation*.

Here, an irregular generation was demonstrated to further understand the processes of break-up of droplets. The irregular generation was realised by using the screw shaft with pitch 5.5 mm, oil phase tubing with I.D. 0.25 mm, aqueous phase tubing with I.D. 0.13 mm and a T-junction with main channel width 0.3 mm. The pulsation frequency of the pump ranging from 0.5 Hz to 4.2 Hz, was varied by changing the voltage. Figure 5.18 interprets the processes of break-up of droplets in one of the irregular generations. In this irregular generation, the complete break-up needs three duty periods when the pulsation frequencies was 1.5 Hz. The pattern of total flow rate of joint fluids after T-junction was similar to that in Figure 5.17, there were two pulsatile troughs and one obvious pulsatile peak. During these three duty periods, the characteristic length was gradually competed and eventually thinned off in **stage 6** of the third period. This forms such relationship: $d_T > d_{2T} > d_{3T,}$ where d_n denotes the characteristic lengths in the n^{th} period.

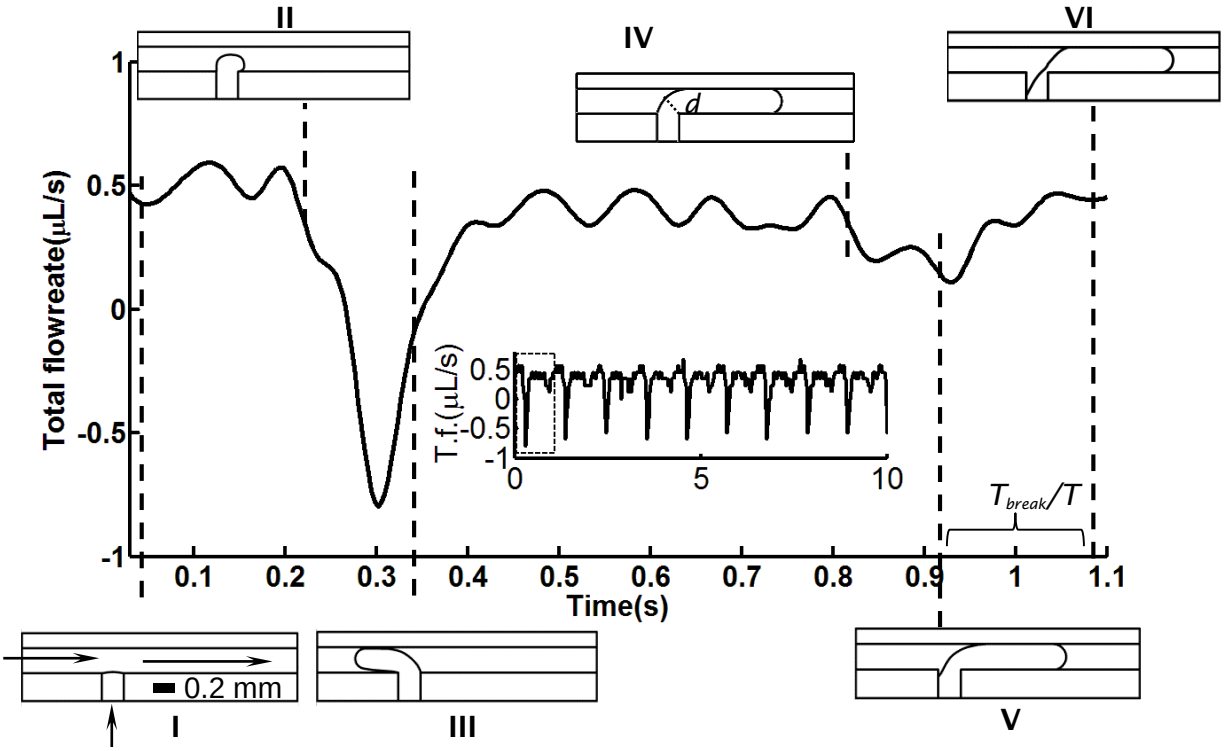

Figure 5.17 The processes of break-up of one droplet in one period. The oil phase tubing was 0.25 while the aqueous phase tubing was 0.13 mm. The pitch of screw shaft was 7 mm. In this observation, one duty period time was 1.13 s. The flow rate had two pulsatile troughs which occurred at t= 300 ms and t= 928 ms, and one pulsatile peak occurred at t= 123 ms. The processes were identified to have six stages. (I).The tip of aqueous phase entered into the main channel. (I~II) The aqueous phase was filled into the main channel and the tip attempted to block the main channel. This process lasted from t=30 ms to t=213 ms. (II~III) The tip in the main channel was suddenly directed upstream, which was due to the strong pulsation dominated by the oil phase channel. In the meanwhile, the aqueous tip was still growing to block the main channel. This stage lasted from 213 ms to 306 ms. (III~IV) The movement of the droplet was downstream and the aqueous tip was weakly growing. In the end of stage, the interface was stretched to form a characteristic length, d. This stage lasted for 569 ms. (IV~V) The growth of the size of droplets was almost terminating and the neck was thinned. This thinning eventually would bring the droplet to be broken up at stage (VI) (t=1070 ms).

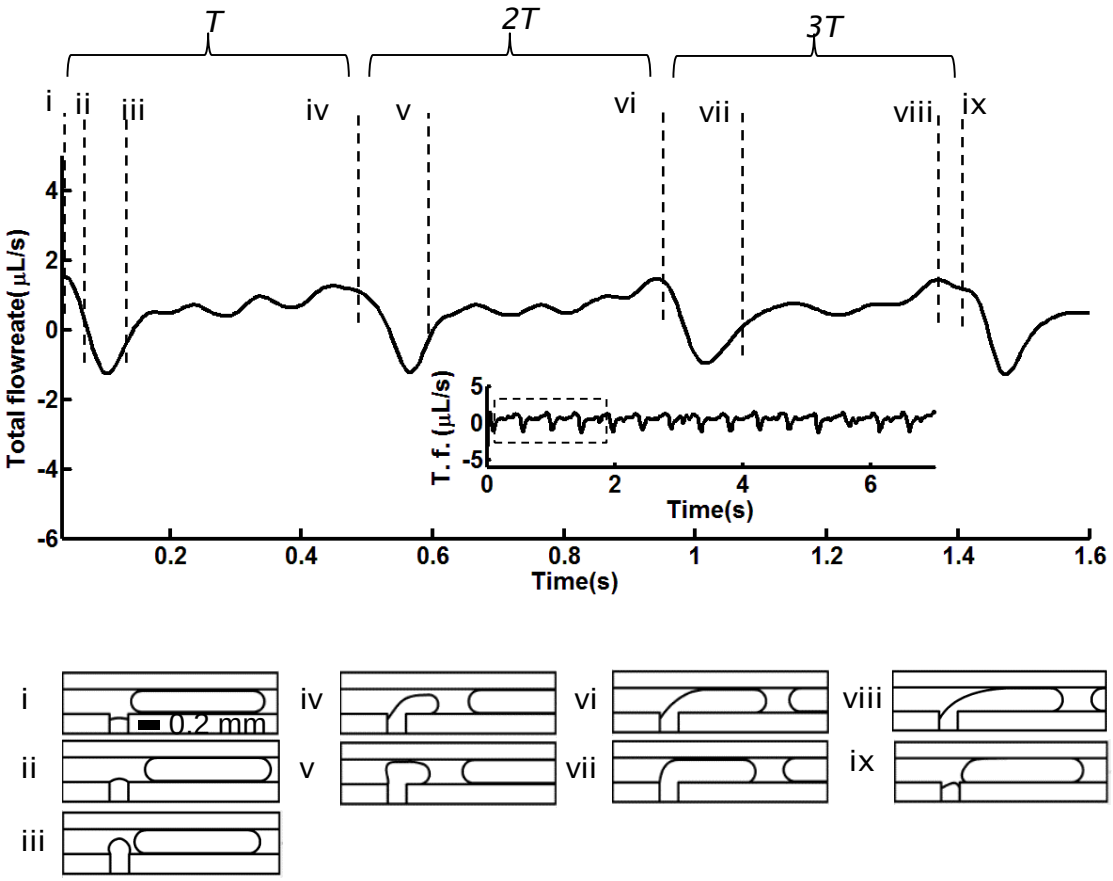

Figure 5.18 The processes of droplet break-up in irregular generation which require multiple periods. Three periods (*3*X*T*) were needed to complete the generation of one droplet. In moment (i), the aqueous tip is starting to go into the main channel. In moment (ii) and moment (iii), the tip was growing while the complete droplet was moving backwards due to the pulsation of the combination flow rate. In moment (iv), the tip was thinned and attempted to be squeezed off. This squeeze-off fails in the first period. From moment (iv) to moment (viii), the processes were repeated as those in the first period. In the last stage, the tip was finally squeezed off.

For a particular T-junction with wider main channel, the processes of break-up in this irregular generation were consistently observed even though rotation frequency was varied. However, the number of periods required to accomplish the generation of one droplet, change with pumping frequency. Figure 5.19 (A) presents the results which showed this trend in the demonstration of irregular generation: increasing the rotation frequency will decrease the sizes of droplets. There were identified six regions according to the size of droplets according to a series of pulsation frequencies from 0.5 Hz to 4.2 Hz. In region (a), the size of each droplets was around 0.207 μL with a polydispersity of 1.16 %. Such a region is termed a *stable region* because there was only one unique droplet size. The rotation frequency was ranging from 0.5 Hz to 0.75 Hz. It was observed that one complete generation of droplet needs 5 duty periods. Region (b) had two unique droplet sizes ~0.207 μL and ~0.163 μL, which was termed an *unstable region*. It was observed that this unstable phenomenon arose from the merging between the preformed droplets and the new aqueous tips, as shown in Figure 5.20. Region (c) had one unique droplet size, 0.163 μL. Region (d) had two unique droplet sizes, ~0.166 μL and ~0.130 μL, with rotation frequency 3~3.4 Hz. Region (e) had one unique droplet size 0.13 μL with generation frequency, 1.5 Hz. Region (f) was unstable region with two unique sizes ~0.129 μL and ~0.094 μL. Region (g) was stable region with a polydispersity of 7.74 %.

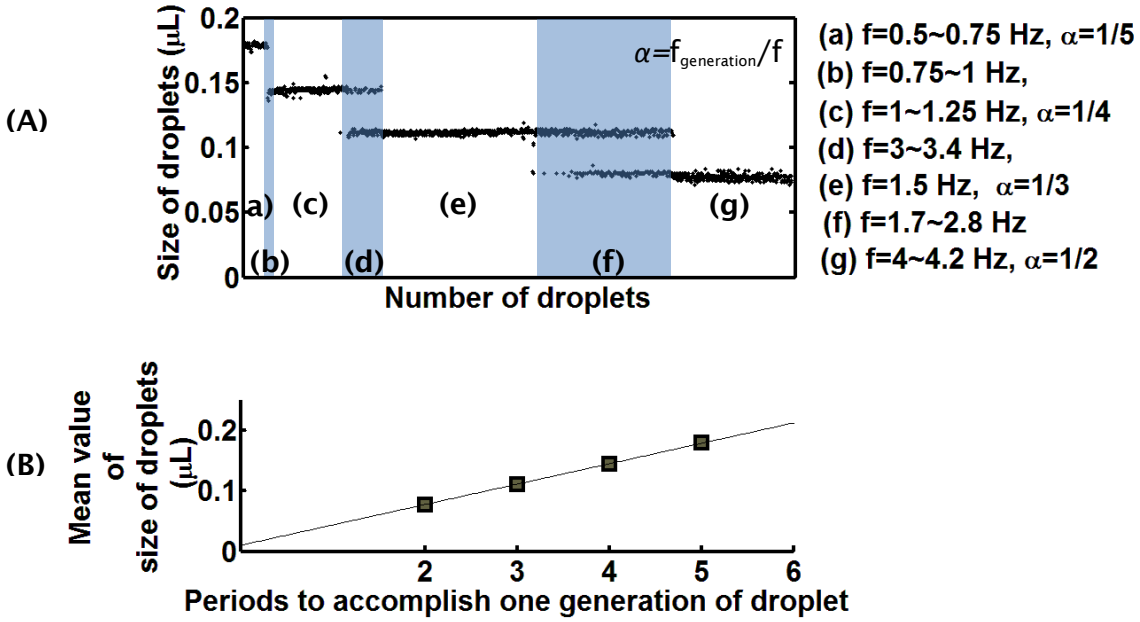

Figure 5.19 Sizes of droplets in irregular generation. (A) Sizes of individual droplets with different generating frequencies. (B) Quantified mean droplet sizes against time.

Figure 5.19 (B) quantified the mean values of the sizes of droplets in the stable regions. The mean value was linearly proportional to the number of duty periods which were need to accomplish one complete generation of droplets. The increment was ~ 0.037 μL, which indicates that the volume of aqueous phase compartmentalised between pitches is ~ 0.037 μL/period. Compared with the mean size of droplets in the generation with pitch 5.5 mm and aqueous phase tubing 0.13 mm in Figure 5.15, which was 0.074 μL, there was 50% difference. This difference may come from different compression of the cassettes where tight compress will bring smaller compartmentalised volume and looser compression will bring a bigger compartmentalised volume. It was observed that big pulsation tends to occur with higher frequencies, which can help the break-up of droplets in **stage 6** which is related to the flowrate change of the aqueous phase.

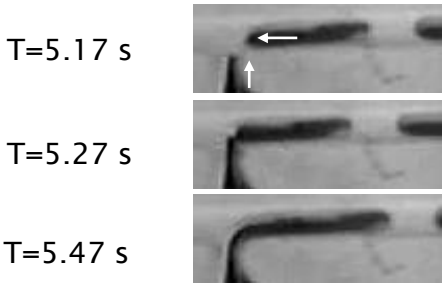

Figure 5.20 Snapshots of coalescence between the tip of aqueous phase and the formal droplet. The abrupt change of surface of the interface of the tip and the formal ensured low coverage of the surfactant, which would favor the coalescence.

5.4.3.3. Summary of this section

In this section, droplet generation is characterised under different combinations. The calibration results show that in regular generation, the size of droplets did not change with flowrates or generation frequencies and merely depends on the volume which the pump can deliver in one period. To understand the mechanisms of this generation scheme, the processes of break-up of droplets was analysed. There are 6 stages identified in the processes of break-up. The analysis shows that the crucial movement of break-up of droplets is in **Stage 5** and **Stage 6**.

5.4.4. Intermittent generation of droplets

Intermittent generation of droplets can be realised by simultaneously turn on the pump. In this section, the control of generation was manually operated by triggering and terminating the power of the pump. To achieve this function, two factors should be considered: (a) the compliance effects in the system which could affect the accuracy of dosing; (b) the stages of generating droplets during which stage 5 and stage 6 dominate the break-up of droplets. These two factors determine the moments when the pump is turned on and off. Here, the turn-on was performed in the beginning of the generation (**stage 1**) and the turn off was performed in the end of the generation (**stage 6**).

Figure 5.21 presents the results of the sizes of droplets in the intermittent generation. The black plot showed the local total flow rate of fluids after the T-junction. It was observed that the flow rate was almost 0 when the pump was terminated off. By controlling the duration during which the power is off, the reaction time could be controlled. The grey plot showed the sizes of the droplets. The mean value of sizes of droplets was 0.1362 μL with a polydispersity of 5.38 %, which showed that the size of droplets had highly uniform value. The generation of droplets is always in-phased with the pulsation. A video is shown in video 5.4.

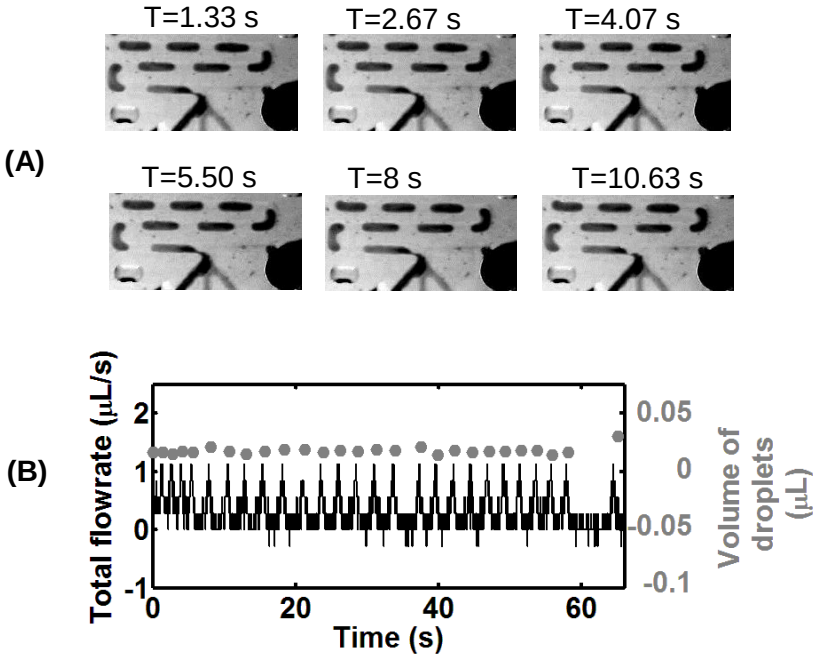

Figure 5.21 (A) An example of 6 droplets in intermittent generation. The brightness contrast has been tuned for better observation. (B) The plots of local total flow rate of fluids after the T-junction and the sizes of droplets. The mean value of sizes of droplets is 0.1362 μL with a polydispersity of 5.38 % which indicates the high uniformity of sizes.

5.4.5. Small Taylor dispersion

When sampling or detecting a continuous chemical signal in microfluidics, Taylor dispersion becomes an issue, especially for continuous microfluidics. An initial volume of fluid will be dispersed along the channel due to the velocity gradients from the centre of the channel to the channel walls. Therefore the peak of the signal get blurred along the channel. Applying droplets can effectively avoid Taylor dispersion in the fluidic system because the sample fluid is compartmentalised into discrete units and flow in sequence in the channel. As required in the design of in-situ sampling device (Figure 5.1), the sampling module should be placed close to the droplet generation module and thus Taylor dispersion can be minimised.

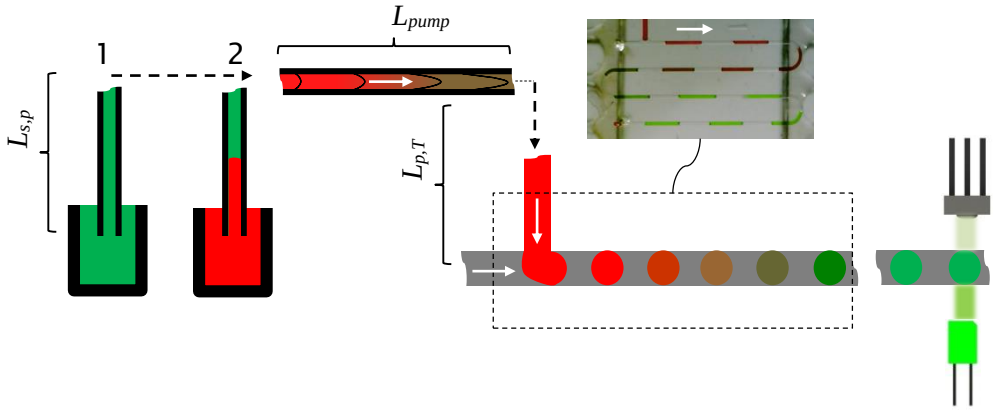

Figure 5.22 Experimental set-up to monitor Taylor dispersion from sampling point to T-junction. The distance that contributes to induce Taylor dispersion includes the distance ($L_{s,p}$) from sampling module to inlet of peristaltic pump, the distance (L_{pump}) inside peristaltic pump, the distance ($L_{p,T}$) from outlet of peristaltic pump to T-junction.

In this device, as shown in Figure 5.22, Taylor dispersion only exists before the generation module with three channel lengths, $L_{s,p}$ the distance from sampling point to the pump, L_{pump} the distance inside the pump, and $L_{p,T}$, the distance from outlet of the pump to the T-junction. Noticeably, the occlusion in between the pitches inside peristaltic pump can help to reduce the Taylor dispersion by disabling the communication between the adjacent occlusions.

Here, the low Taylor dispersion from this device was demonstrated by reducing $L_{s,p}$ and $L_{p,T}$. To realise that, the sample containers were placed directly to the inlet of peristaltic pumps and the T-junction chip was placed close to the outlet

of the pump. Red and green aqueous samples were sequentially introduced into the pump and the droplets generated were examined with the aforementioned colorimetric flow-cell (Chapter 4). The experimental set-up was schematically shown in Figure 5.22.

Figure 5.23 presents the detected colour in a sequence of droplets from green to red. It showed that the device needs ~12 droplets to change from one colour to another one. It is believed with further engineering to reduce $L_{s,p}$, L_{pump} and $L_{p,T}$, this number can be further decreased.

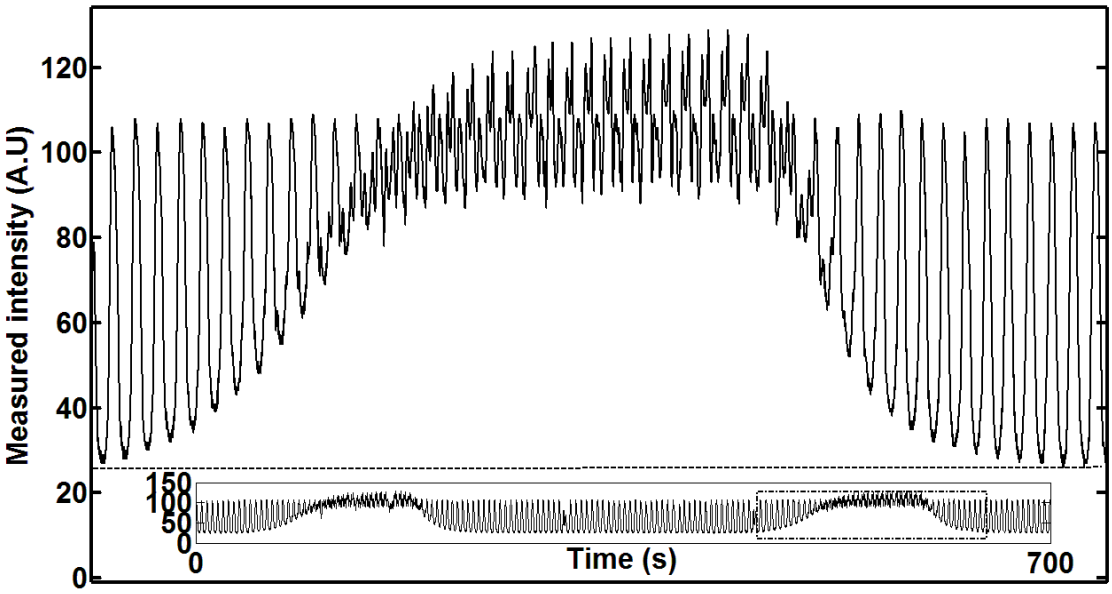

Figure 5.23 Measured intensity of the immediate sample changing. The enlarged plot shows the area highlighted in the inset plot.

5.4.6. A glucose assay as an example application

In this section, this device with multiple channels was used to demonstrate the detection of glucose with different concentrations, as a potential application of in-situ sampling.

In this application, two channels for aqueous phase were pumped with 0.13 mm I.D. tubing, and oil tubing of 0.25mm I.D. the screw shaft has a pitch of 7 mm. With this combination, the droplet size produced is about 60 nL. Glucose solution was pumped in one channel, glucose enzymatic reagent was pumped by in the other channel as shown in experimental set-up (Figure 5.24). Subsequently, the two streams were pumped into a T-junction and generated into droplets. The droplets were collected to a polyurethane tubing. The generation frequency was controlled to be 0.1 Hz in all of the tests. After ~10 minutes reaction time the reaction is complete the red droplets were examined by the flow cell.

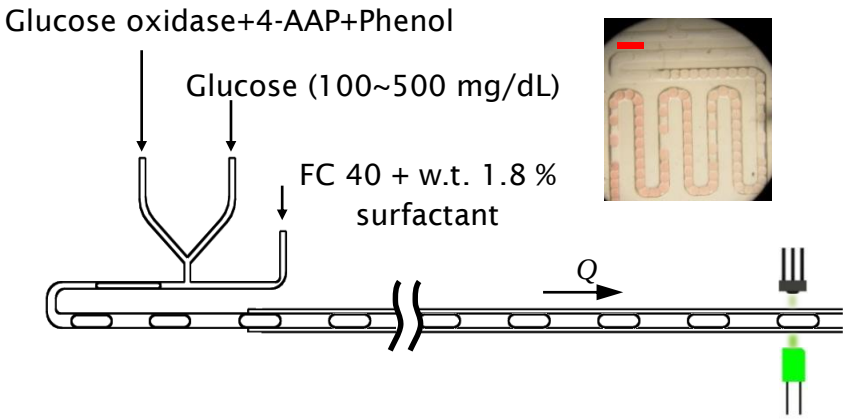

Figure 5.24 The design of chip for glucose reaction and detection and experimental set-up. At a generation frequency of 0.27 Hz, the channel was designed to ensure 10 min reaction time. The concentration of glucose is ranging from 100 mg/dL to 500 mg/dL. The inset picture shows an example of droplets of a concentration of 500 mg/dL stored in a chip. The scale bar is 1 mm.

Figure 5.25 presents the initial calibration on glucose samples with different concentrations, from 0 mg/dL to 600 mg/dL. There were at least 8 repeats of each concentration in the test as shown in Figure 5.25 (A). The measured light intensity tends to decrease with the increase of the concentrations. The quantified absorbance was plotted in Figure 5.25 (B). It showed that the absorbance is linearly proportional to the concentration of glucose.

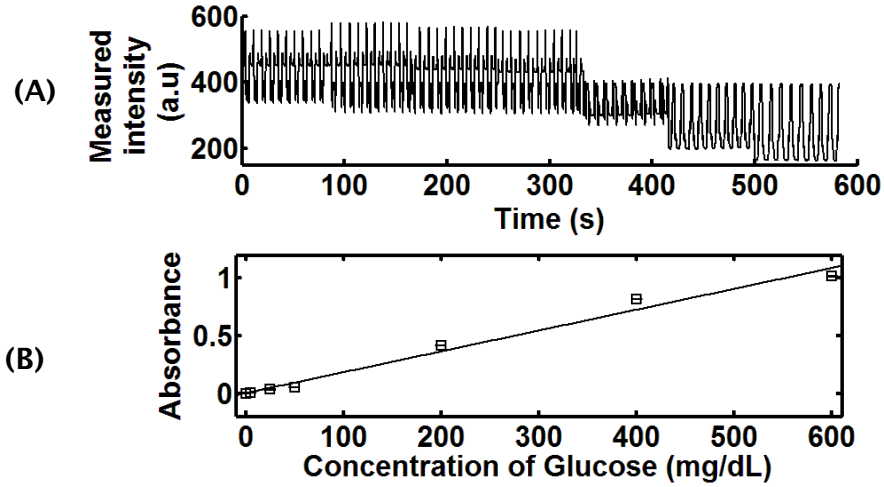

Figure 5.25 Calibration of glucose (0 mg/dL, 5 mg/dL, 25 mg/dL, 50 mg/dL 200 mg/dL, 400 mg/dL and 600 mg/dL). (A) The measured intensity for 5 different concentrations. Each concentration contains 3 repeat. From left to right, there are examined 0 mg/dL to 600 mg/dL. (B) Quantified absorbance. The concentration of glucose shows a linear relationship with the quantified absorbance.

5.4.7. Summary

This section has further developed a modified version of using multiple-channels of a peristaltic pump. This modified peristaltic pump is robust and is able to run continuously for about 2 hours to generate droplets. With this robust device, a systematic calibration of sizes of droplets has been performed. The detailed droplet generation processes were analysed. Some novel functions such as intermittent droplet generation have been demonstrated. Taylor dispersion is minimised in the system. It shows that only 12 droplets are needed to completely change from one sample to another sample. A glucose assay is used to provide an initial application of this in-situ sampling. With further engineering, it is believed that Taylor dispersion can be further reduced and more functions on droplet operation can be explored.

5.5. Multiplexed droplets generation

5.5.1. Introduction and designs

Flexibilities and versatilities of a device can strengthen its miniaturisation capability and thus a more convenient and integrated format can be achieved [17]. In this section, droplet generation from parallel channels with one single oil phase channel was investigated. Through this investigation, two extra functions are to be explored:

a. Whether the droplets can be generated in parallel with synchronised control format
b. Whether samples can be injected into the pre-formed droplets in the system.

Firstly, parallel operation of droplets is an issue in microfluidics. The successful exploration of the function in this system can provide an alternative method of parallel generation particularly for *in-situ* sampling. Secondly, injection of samples into droplets is a fundamental process to trigger reactions. Ismagilov *et al* group [18] has demonstrated the direct injection of reagents with T-junctions. The injecting volume of reagents is difficult to control as it only relies on the size of the preformed droplets. Abate et al [19] has developed a pico-injector to control injecting volume by controlling the injection pressure. The study with this device can provide an alternative method to solve that issue in droplet microfluidics, which can be further used in systems requiring multi-step reactions [18].

Here, microchips with the various distances between the parallel channels, L_d, was designed to achieve these two functions, as schematically shown in Figure 5.26 (A) for the droplet generation and the design of the chip shown in Figure 5.26 (B). The tubing and screw used in this study are: PVC tubing of I.D 0.13 mm for aqueous channel, PVC tubing of I.D 0.25 mm for oil channel and screw shaft with 7 mm pitch. W.t. 1%~1.8% homemade surfactant was added into the FC 40 oil.

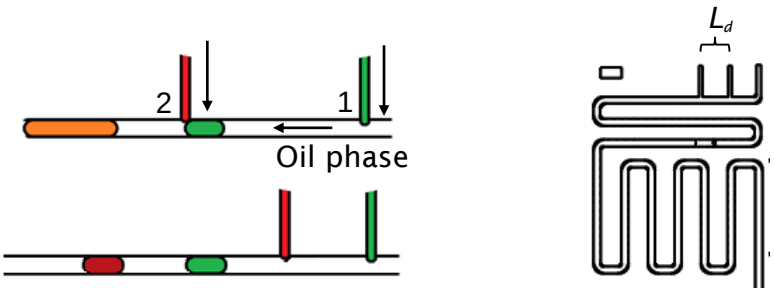

(A) **(B)**

Figure 5.26 The proposed scheme to inject reagents into the pre-formed droplets. (A) The heuristic sketch distinguishing from injections to parallel generations; (B) The design of the chip which contains two parallel channels**.** L_d is designed to be 1.41 mm, 2.66 mm and 3.00 mm.

5.5.2. Results and discussion

Figure 5.27 shows snapshots of the experiments. In the first design, the two aqueous channels have a distance of 1.41 mm (Figure 5.27 (A)). Firstly, a preformed droplet from channel 1 would cut the tip of aqueous phase from channel 2 into a daughter droplet. Secondly, the left aqueous phase from channel would be injected into the preformed droplet as the one period delivery of aqueous has not been completed in the first stage. Figure 5.28 (A) details the processes. As it is shown, at T=0.2 s, the tip of the green aqueous phase was attempting to block the main channel before the preformed droplet's arrival. As soon as the preformed droplet was touching the neck of the aqueous tip, at T=0.33 s, it would squeeze off the tip rather than merging. As a result, a daughter droplet was generated at T=0.4 s. After this, the aqueous phase from channel 2 was still growing to form a new tip, due to the strong flow rate during the period between T=0.4 s and T=0.8 s. The growing tip was blocking the main channel and was approaching the preformed red droplet. At T=0.8 s, the pulsation occurred which separated the new tip and the preformed red droplet. This abrupt separation helped the tip merging with the preformed droplet. This

phenomenon where decompression will favour coalescence of droplets has been observed, studied and understood [20, 21]. After this, the new merged regime became a long tip linked to the green reagent as shown at T=0.73 s, eventually the new tip was squeezed off (T=0.8 s) whose process was similar to those from stage IV to stage VI in Figure 5.16. The whole process makes generation into this format: *cut-injection,* which is unstable in the design with this distance, L_p=1.44 mm.

In the second design with L_p=2.66 mm (Figure 5.27 (B)), the first droplet is unstably generated and showed two sizes as indicated by the red arrow line, which may be explained by irregular generation. Different from the observation in the design with L_p=1.44 mm, the *cut-injection* format was not observed. However, dual generation of droplets in first channel directly lead the generation of droplets in the second channel as indicated by the red arrow line and formed a *small-big* format.

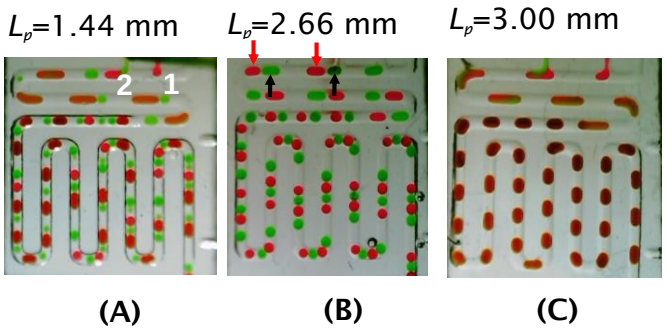

Figure 5.27 (A) Schematic of parallel T-junction chips for injection. (B) The snapshots of injection of reagent into the preformed droplet in the three different designs.

In the third design with L_p=3.00 mm (Figure 5.27 (C)), the injection of samples was successfully achieved. The processes of successful injection of aqueous samples from channel 2 into droplets were illustrated in Figure 5.28 (B). At T=0.53 s, the green reagent was dodging in the side channel while the red droplet was formed as marked by the black arrow. At T=0.73 s, the preformed droplet was crossing over the T-junction. Meanwhile, the tip of the aqueous sample 2 was growing to strike the body of the preformed droplet, which was different from that in the first design. The tip was subsequently merging with the preformed droplet as soon as they were touching with each other. The next processes were also similar to those in between stage 5 to stage 6 in Figure 5.17.

Compared with what was observed in the first design, it was concluded that the merging of the aqueous phase 2 with the preformed droplet can occur if the tip of sample 2 is able to strike main body of the preformed droplet. This can ensure successful injection even with w.t. 1.8% concentration surfactant. This difference is schematised in the sketch in Figure 5.28 (A, B). Figure 5.28 (C) presents the comparison of sizes between red droplets and the injected in the third design. The preformed droplets had a mean value of size with a polydispersity of 1.5 % which showed high uniformity. There were 6 unmerged droplets in the merged droplets. These unmerged droplets were due to that the tip of the reagent was slightly advanced, which may come from the perturbation from the environment. The success rate of injection was 95.5 %.

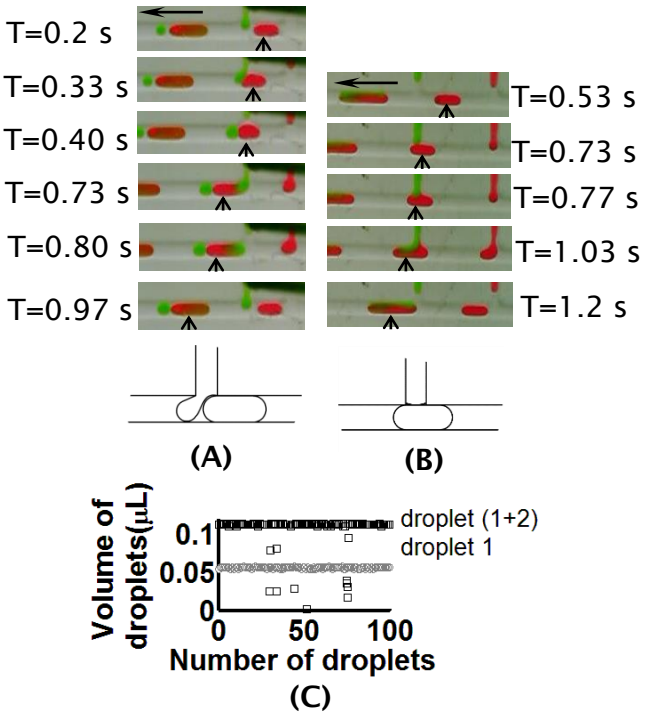

Figure 5.28 The detailed processes of droplets in parallel and quantified sizes of successful injection of aqueous sample 2. (A) Processes of droplets in the first design: cut-injection format. (B) Processes of droplets in the third design: successful injection. (C) Quantified sizes of successful injection in the third design.

From this investigation, it did not suggest to use this design to realise synchronised parallel generation of droplets and this function needs further investigation and further development. However, successful parallel injection of aqueous samples into the pre-formed droplets has been demonstrated with the third design. To ensure the injection, a non-trivial step to ensure that the injected

tip should be able to strike the main body of the preformed droplets, is necessary.

Based on this investigation, the three parallel channel design was further developed to realise complexed injection. There were two versions of designs: *upstream* design and *downstream* design, as shown in Figure 5.29 (i) (A~B). Figure 5.29 (iii) compares the droplet sizes between the droplet 1 and droplet (1+2+3) and shows 100 % injection rate. Both of the designs have successfully demonstrated the injection in a variety of conditions. Besides, air bubbles can also added into the system for certain applications. (see video 5.5_a, video 5.5_b and video 5.5_c for additions of samples into droplets in three parallel channels).

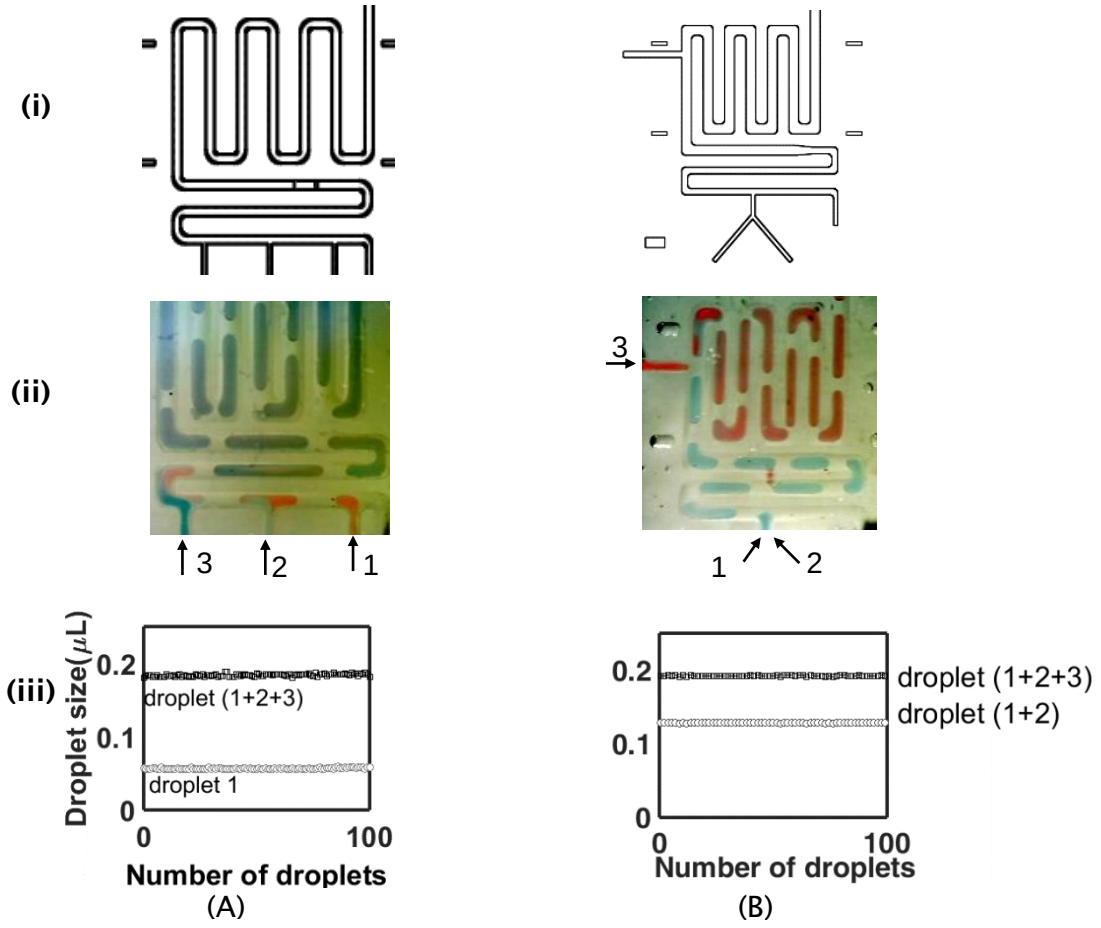

Figure 5.29 Additions of samples into droplets in three parallel channels. (A) Sequential injection (i) design of three parallel channels with 3.00 mm (ii) Snapshot of the chip. Left: w.t. 1.8 %. Right: w.t. 1%. (iii) Droplet size calibration (B) Injection in the downstream (i) design of three parallel channels; (ii) Snapshot of injection. (iii) Droplet size calibration.

5.5.3. Summary and future work

In this section, multiplexed droplet generation in parallel channels with the in-situ sampling device was investigated by varying the distance, L_p, between the parallel channels. It was observed that simultaneous droplet generation from parallel channels was difficult to realise which may be explained by the interference of flow-rate from channel 1 shifting the flow rate phase difference between channel 2 and the oil channel. To circumvent this problem, a modified design was suggested by incorporating two anti-phase systems in one pump, as shown in Figure 5.30. The other function, sequential injection of samples into pre-formed droplets can be easily achieved. With the key step that the tip of injecting stream shall be able to strike the main body of the preformed droplet. This demonstration might find further application in the realisation of multi-step reactions.

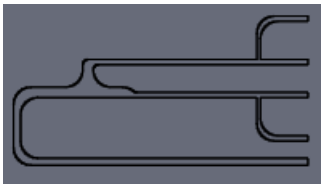

Figure 5.30 Modified design for independent parallel generation.

5.6. Conclusion and outlook

In this chapter, a novel droplet generation method was proposed to realise in-situ droplet sampling. A preliminary design was first designed and demonstrated. It was observed that droplet sizes do not rely on the flow rate or generation frequencies. This makes precise flowrate control superfluous. However, due to the limitation of the engineering processes, the early device cannot robustly work because of the high friction induced from peristaltic tubing and screw shaft.

A modified version of the device was designed which utilises a sandwich structure. Such device is able to achieve a long running time (at least 2 hours as tested). The size of droplets was systematically calibrated. The processes of

droplet break-up were observed and analysed. Other novel functions such as intermittent generation of droplets, sequential injection were successfully achieved, which can conveniently control the reaction time in the device or to be used in multiple step reactions. It was observed that the current device needs ~12 droplets to change a sample due to Taylor dispersion in the continuous fluidic part, this can be improved with further system miniaturisation. A glucose assay was demonstrated as an example application of this *in-situ* sampling device. It is believed that this *in-situ* droplet sampling method can find wide ranges of applications in environment monitoring, online healthcare and on-chip diagnosis, etc.

Reference list

1. Slaney, T.R., et al., *Push-Pull Perfusion Sampling with Segmented Flow for High Temporal and Spatial Resolution in Vivo Chemical Monitoring.* Analytical Chemistry, 2011. **83**(13): p. 5207-5213.

2. Chen, D., et al., *The chemistrode: A droplet-based microfluidic device for stimulation and recording with high temporal, spatial, and chemical resolution.* Proceedings of the National Academy of Sciences of the United States of America, 2008. **105**(44): p. 16843-16848.

3. Musteata, F.M., *Recent progress in in-vivo sampling and analysis.* Trac-Trends in Analytical Chemistry, 2013. **45**: p. 154-168.

4. Abate, A.R. and D.A. Weitz, *Syringe-vacuum microfluidics: A portable technique to create monodisperse emulsions.* Biomicrofluidics, 2011. **5**(1).

5. Gielen, F., et al., *Interfacing Microwells with Nanoliter Compartments: A Sampler Generating High-Resolution Concentration Gradients for Quantitative Biochemical Analyses in Droplets.* Analytical Chemistry, 2015. **87**(1): p. 624-632.

6. Rhie, W. and T. Higuchi, *Design and fabrication of a screw-driven multi-channel peristaltic pump for portable microfluidic devices.* Journal of Micromechanics and Microengineering, 2010. **20**(8).

7. Churski, K., et al., *Rapid screening of antibiotic toxicity in an automated microdroplet system.* Lab on a Chip, 2012. **12**(9): p. 1629-1637.

8. Guzowski, J., et al., *Automated high-throughput generation of droplets.* Lab on a Chip, 2011. **11**(21): p. 3593-3595.

9. Churski, K., J. Michalski, and P. Garstecki, *Droplet on demand system utilizing a computer controlled microvalve integrated into a stiff polymeric microfluidic device.* Lab on a Chip, 2010. **10**(4): p. 512-518.

10. van Steijn, V., et al., *Block-and-break generation of microdroplets with fixed volume.* Biomicrofluidics, 2013. **7**(2).

11. Korczyk, P.M., et al., *Microfluidic traps for hard-wired operations on droplets.* Lab on a Chip, 2013. **13**(20): p. 4096-4102.

12. Draper, M.C., et al., *Compartmentalization of Electrophoretically Separated Analytes in a Multiphase Microfluidic Platform.* Analytical Chemistry, 2012. **84**(13): p. 5801-5808.

13. Garstecki, P., et al., *Formation of droplets and bubbles in a microfluidic T-junction - scaling and mechanism of break-up.* Lab on a Chip, 2006. **6**(3): p. 437-446.

14. Christopher, G.F., et al., *Experimental observations of the squeezing-to-dripping transition in T-shaped microfluidic junctions.* Physical Review E, 2008. **78**(3).

15. van Steijn, V., M.T. Kreutzer, and C.R. Kleijn, *mu-PIV study of the formation of segmented flow in microfluidic T-junctions.* Chemical Engineering Science, 2007. **62**(24): p. 7505-7514.

16. De Menech, M., *Modeling of droplet breakup in a microfluidic T-shaped junction with a phase-field model.* Physical Review E, 2006. **73**(3).

17. Rakszewska, A., et al., *One drop at a time: toward droplet microfluidics as a versatile tool for single-cell analysis.* Npg Asia Materials, 2014. **6**.

18. Shestopalov, I., J.D. Tice, and R.F. Ismagilov, *Multi-step synthesis of nanoparticles performed on millisecond time scale in a microfluidic droplet-based system.* Lab on a Chip, 2004. **4**(4): p. 316-321.

19. Abate, A.R., et al., *High-throughput injection with microfluidics using picoinjectors.* Proceedings of the National Academy of Sciences of the United States of America, 2010. **107**(45): p. 19163-19166.

20. Lai, A., N. Bremond, and H.A. Stone, *Separation-driven coalescence of droplets: an analytical criterion for the approach to contact.* Journal of Fluid Mechanics, 2009. **632**: p. 97-107.

21. Bremond, N., A.R. Thiam, and J. Bibette, *Decompressing emulsion droplets favors coalescence.* Physical Review Letters, 2008. **100**(2).

6. Conclusion

In this thesis, new droplet sampling methods were introduced to solve the '*sample in*' problems in droplet microfluidics. These methods are based on engineering droplet generation method coupling with peristaltic pumping system.

Firstly, a platform capable of continuously generating and pumping droplets was proposed, engineered, and studied. The key parts of the platform are a linear aspiration droplet generator and a peristaltic pumping system. Fluidic dynamics has been investigated in details, especially the pulsating flow rate from peristaltic pump which can affect the generation of droplets, and integrities of droplets that can be affected during the pumping. It was found that the sizes of droplets can be affected by the pulsating flow rate when the frequency of droplet generation does not match that of the pulsatile flow. When pre-formed droplets are introduced into the peristaltic pump, the interties of droplets are challenged. To solve these two issues, a feedback control system was proposed and engineered to bring droplet generation into phase with the flow-rate pulsations of the peristaltic pump. With this feedback system, the polydispersity of the size of droplets was reduced from ~21 % to 6.1% and the trend of the size was stabilized. With proper adjustment of the phase difference between the droplet generation and the pumping pulsation, the droplets could be properly positioned in between the adjacent peristaltic pump rollers. In the study, it was found that the use of w.t. 1.8 % homemade surfactant/FC 40 oil can effectively improve the surface property of the inner surface of PVC tubing.

Secondly, a multiple channel system has been further developed to realise parallel operation and synchronisation of droplets. With this integrated platform, the synchronisation of droplets with different conditions, i.e. different droplet sizes and different flow rates, has been investigated and implemented. It was observed the quantified mean phase difference was generally smaller than 5% although the variable droplet sizes induce a phase change in the single channel. The investigation of the phase change of droplets in a single channel showed that droplets with a bigger size would be delayed while one with a smaller size would be advanced after they went through the peristaltic pump, which may be

caused by the strong pulsations in the movement of droplets with different sizes. A droplet merging chamber was fabricated and tested that could effectively trap and merge these synchronised droplets. Furthermore, the coalescence of droplets with multiple samples was also demonstrated. This shows that the integrated system could realise the function proposed which is to inject different samples into the reagents. Some interesting phenomena of coalescence of droplets before the merging chamber was observed. It was also observed that the introduction of air bubbles could help to regulate the coalescence of droplets in the merging chamber. For example, with an air bubble generated in the Y-junction, 2 droplets could be effectively merged by the merging chamber that was designed for 4 droplets. Moreover, the introduction of air bubbles could help specific reactions that requires oxygen. The phase difference between the merged droplets and the droplets in one of the three parallel channels was generally smaller than 5 %. These results suggested that further unit operations could be performed, such as injecting reagents into the merged droplets for multi-step reactions. Screening of glucose with different concentrations was carried out with a colorimetric detecting method. This platform successfully calibrated the concentration of the glucose samples and showed linear relation from in the measured absorbance against theoretical concentrations.

Finally, an in-situ droplet sampling device was successfully engineered. A preliminary design was first designed and demonstrated. It was observed that droplet sizes are not dependent on the flow rate or generation frequencies. This makes precise flowrate control superfluous. However, due to the limitation of the engineering processes, the early device could not robustly work because of the high friction induced from the peristaltic tubing and screw shaft. A modified version of the device was designed which utilises a sandwich structure. Such a device is able to achieve a long running time (at least 2 hours as tested). The size of droplets was systematically calibrated. The processes of droplet break-up were observed and analysed. Other novel functions such as intermittent generation of droplets and sequential injection were successfully achieved, which can conveniently control the reaction time in the device be used in multiple step reactions. It was observed that the current device needs ~12 droplets to change a sample due to Taylor dispersion in the continuous fluidic part, this can be improved with further system miniaturisation. A glucose assay was demonstrated as an example application of this *in-situ* sampling device. It

is believed that this *in-situ* droplet sampling method can find wide ranges of applications in areas such as environment monitoring, online healthcare and on-chip diagnosis.